Investigating ApoE4-Mediated Molecular Alterations in H4 Neuroglioma Cells of Alzheimer's Disease Using OrbiSIMS and LC-MS/MS.

Li Lu (Jennifer)

School of Pharmacy

University of Nottingham

UK

Thesis submitted to the University of Nottingham for the degree of Doctor of Philosophy

2025

ABSTRACT

Apolipoprotein E4 (ApoE4) is the significant risk gene for late-onset Alzheimer's disease (AD), which is not only associated with the AD pathological features, including amyloid-β deposition, phosphorylation of Tau proteins and neuroinflammation; but also involved with metabolism, neuron growth, and synaptic plasticity. Growing clinical evidence has revealed that dysfunction of systematic molecular alterations in the brain occurs even twenty years before the onset of AD pathological features. Multi-omics such as metabolomics and proteomics have been applied widely in identifying key disease-related molecular alteration and disease-progression-related changes. Despite recent advances in the development of analytical technologies, screening the whole profile of metabolites remains challenging, due to many classes of compounds with diverse chemical properties that would need different extraction processes.

In this study, we combined two omics (metabolomics and proteomics) to study the molecular alteration effected by ApoE4 in H4 neuroglioma cells. Typically, we first conducted metabolomics that uses Orbital trapping secondary ion mass spectrometry (OrbiSIMS) as a screening tool to gain a non-biased overview of metabolic alteration under ApoE4-carried neuroglioma cells. Sample preparation optimisation for H4 cells in OrbiSIMS analysis has been conducted under two conditions: freeze-dried and frozen-hydrated. The findings are subsequently followed by LC-MS/MS targeted metabolomics for further confirming specific metabolite classes. Then proteomics was also performed by using UHPLC-MS. Subsequentially, Gene ontology (GO) analysis has been applied to link the metabolomics and proteomics results.

The initial OrbiSIMS approach has shown the advantages of detecting large numbers of metabolites with minimal sample preparation, small sample size and a relatively rapid analysis time, allowing 192 putatively annotated metabolites detected in our

study. Overall, OrbiSIMS as screening tool then followed by LC-MS/MS is successfully developed to investigate cellular metabolomics, revealing the disruption of lipid metabolism (glycerophospholipids and sphingolipids) and amino acid metabolism. This includes alanine, aspartate, and glutamate metabolism, aminoacyl-tRNA biosynthesis, glutamine metabolism, and taurine and hypotaurine metabolism. Proteomics study further confirms the dysfunction of amino acids, tRNA aminoacylation metabolic processes, and reveals RNA splicing process affected by ApoE4. GO analysis suggests that nitrogen compounds, amino acids, tRNA aminoacylation metabolic processes play important roles in ApoE4 mediated molecular alterations in AD.

Declaration

I hereby declare that the data published in this thesis is the result of my own work at the University of Nottingham, UK. This thesis has been completed exclusively by me and has not previously been submitted for any other degree or qualification.

Covid Statement

The COVID-19 pandemic posed significant challenges during the completion of this PhD. Restrictions on laboratory access, delays in the supply chain for essential materials, and limited opportunities for in-person collaboration affected the timeline and scope of some experimental work. My PhD officially began in October 2020; however, due to the global pandemic crisis, I was unable to arrive in the UK until December 2020 because of limited flight availability and prohibitive costs during that period.

After arriving in the UK, universities and laboratories gradually reopened and resumed operations. During the first year, access to facilities was limited, and the global impact on supply chains caused significant delays in procuring consumables and laboratory equipment. These challenges necessitated the adoption of alternative strategies, such as virtual collaborations and extensive literature reviews, to maintain progress.

I would like to express my sincere gratitude to all individuals, institutions, and colleagues who demonstrated exceptional flexibility, support, and understanding during this unprecedented period. Their efforts and collaborative spirit were instrumental in overcoming the obstacles imposed by the pandemic and ensuring the successful completion of this study.

Acknowledgments

I would like to express my sincere gratitude to my supervisor, Dr. Zheying Zhu, for giving me the opportunity to work on this incredible project. Her guidance, constant support, and encouragement have not only facilitated my time in the lab but have also greatly contributed to my personal and professional growth. I am especially thankful for her availability and unwavering support during challenging times, and I will always remain grateful for the chance to work under her supervision. Zheying's encouragement to attend conferences and present our work has greatly improved my academic presentation skills and boosted my confidence in presenting and engaging in discussions with external researchers.

I would also like to thank my co-supervisors, Prof. Morgan Alexander and Dr. David Scurr, for their patience and invaluable guidance throughout this research project, particularly in the application of OrbiSIMS on H4 cells. Dr. David Scurr's expertise and passion for SIMS instrumentation inspired me to develop a profound interest in SIMS analysis, motivating me to learn more about its operation and functionality. I am deeply appreciative of his patience and willingness to explain complex concepts and guide me through this entire project. Similarly, I am grateful to Prof. Morgan Alexander for his wise and insightful ideas, as well as his detailed questions and thoughtful discussions during our monthly supervision meetings. Their critical thinking and constructive suggestions were instrumental in improving my research outcomes and helping me grow as a scientist. I also appreciate their support and understanding during periods when results were less favourable.

I would also like to extend my heartfelt gratitude to my internal assessor, Dr. Rian Griffiths, for her unwavering support and guidance throughout my PhD journey. Her assistance went beyond project-related advice, offering invaluable mental support and

encouragement that helped me build confidence in expressing myself. Her constructive feedback and motivation significantly boosted my confidence, particularly in delivering presentations, for which I am deeply thankful. I also appreciate Dr. Andrew Hook for taking over as my internal assessor during Rian's maternity leave and helping to coordinate and arrange my viva date.

A special thanks goes to Dr. Anna Kotowska for her guidance in OrbiSIMS data analysis and the execution of cryogenic OrbiSIMS experiments, as well as her valuable suggestions and feedback during the writing of this thesis.

I am also grateful to my lab mates in D35, particularly Valentine Anyanwu and Tejasvi Shivakumar, for their kindness and support when I first joined the lab. Their camaraderie and encouragement made the transition into this new environment much smoother.

I am thankful to all my group mates, Tiantian Li, Fatimah Qassadi, Carver Wong, Zhiwei Li, Yuhan Wang, and Napoleon Vrettos, for their support. Special thanks to Yonghui Lu for supporting me in OrbiSIMS data analysis during my first year.

I want to express my gratitude to my family for supporting me throughout this incredible journey. Thank you to my dad and mom for always being so kind and supportive of my education and for allowing me to explore different places around the world. A special mention to my friends Yu Hong, Xin Wang, and Yao Xie for keeping me encouraged despite the distance.

I would also like to thank my partner, Ed. Meeting you near the end of this journey, during such a stressful time, was truly a blessing. I deeply appreciate your unwavering support, encouragement, and the joy you bring to my life. Thank you for making every

day special and for being my source of strength through it all.

Finally, I wish to express my gratitude for the support provided by the Engineering and Physical Sciences Research Council (EPSRC) through the grant titled "3D OrbiSIMS: Label-free chemical imaging of materials, cells, and tissues" (EP/P029868/1). Additionally, I extend my thanks to both the Centre for Analytical Bioscience (CAB) and the Nanoscale and Microscale Research Centre (nmRC) at the University of Nottingham for their invaluable contributions to LC-MS metabolomics experiments and confocal microscopy analysis.

ABBREVIATIONS

ABC – ATP-Binding Cassette Transporters

AD – Alzheimer's Disease

APCI – Atmospheric-Pressure Chemical Ionisation

APP – Amyloid Precursor Protein

ApoE4 – Apolipoprotein E4

BACE1 – β-site Amyloid Precursor Protein Cleaving Enzyme 1

BBB – Blood-Brain Barrier

Bi – Bismuth

BMP – Bis(monoacylglycero)phosphate

CerP – Ceramide Phosphates

CL – Cardiolipin

CNS – Central Nervous System

CPA – Cyclic Phosphatidic Acid

CSF – Cerebrospinal Fluid

DBE – Double Bond Equivalence

DESI – Desorption Electrospray Ionisation

DG – Diacylglycerolipids

DLR – Low-Density Lipoprotein Receptor (should be LDLR?)

ESI – Electrospray Ionisation

FA – Fatty Acyls

FDR – False Discovery Rate

GABA – Gamma-Aminobutyric Acid

GCIB – Gas Cluster Ion Beam

GLUT3 – Glucose Transporter Type 3

GO – Gene Ontology

GWAS – Genome-Wide Association Studies

HDL – High-Density Lipoproteins

HDR – Homology-Directed Repair

Hex – Hexosylceramides

HexCer – Hexosylceramides

HILIC – Hydrophilic Interaction Chromatography

iPSC – Induced Pluripotent Stem Cells

KI – Knock-In

LAESI – Laser Ablation Electrospray Ionisation

LC-MS – Liquid Chromatography–Mass Spectrometry

LDL – Low-Density Lipoproteins

LDLR – Low-Density Lipoprotein Receptor

LESA – Liquid Extraction Surface Analysis

LN2 – Liquid Nitrogen

LMIG – Liquid Metal Ion Gun

LOAD – Late-onset AD

LPA – Lysophosphatidic Acid

LPC – Lysophosphatidylcholine

LPE – Lysophosphatidylethanolamine

LPI – Lysophosphatidylinositol

LRP1 – Low-Density Lipoprotein Receptor-Related Protein 1

LTQ – Linear Trap Quadrupole

LXR – Liver X Receptor

MALDI – Matrix-Assisted Laser Desorption/Ionisation

MAPT – Microtubule-Associated Protein Tau

MG – Monoacylglycerolipids

MRI – Magnetic Resonance Imaging

NHEJ – Non-Homologous End Joining

NMR – Nuclear Magnetic Resonance

OrbiSIMS – Orbitrap Secondary Ion Mass Spectrometry

PA – Phosphatidic Acid

PC – Phosphatidylcholine

PCA – Principal Component Analysis

PE – Phosphatidylethanolamine

PET – Positron Emission Tomography

PG – Phosphatidylglycerol

PI – Phosphatidylinositol

PLS-DA – Partial Least Squares Discriminant Analysis

PPAR – Peroxisome Proliferator-Activated Receptor

PS – Phosphatidylserine

PTM – Post-Translational Modification

RPLC – Reversed Phase Liquid Chromatography

SALDI – Surface-Assisted Laser Desorption/Ionisation

SNP – Single Nucleotide Polymorphism

SM – Sphingomyelin

SP – Sphingolipids

ST – Sulfatides

TAG – Triacylglycerols

TG – Triacylglycerolipids

TOF – Time of Flight

TREM2 – Triggering Receptor Expressed on Myeloid Cells 2

UHPLC – Ultra-High-Performance Liquid Chromatography

VIP – Variable Importance in Projection

Publication

1. **Lu, L.**, A.M. Kotowska, S. Kern, M. Fang, T.R. Rudd, M.R. Alexander, D.J. Scurr and Z. Zhu, *Metabolomic and Proteomic Analysis of ApoE4-Carrying H4 Neuroglioma Cells in Alzheimer's Disease Using OrbiSIMS and LC-MS/MS.* Anal. Chem. 2024, 96, 29, 11760-11770.
2. Li, T.; **Lu, L.**; Pember, E.; Li, X.; Zhang, B.; Zhu, Z. *New Insights into Neuroinflammation Involved in Pathogenic Mechanism of Alzheimer's Disease and Its Potential for Therapeutic Intervention.* Cells 2022, 11, 1925.

Conferences and Presentations

1. Alzheimer's Research UK 2022: Flash oral presentation on Early Careers Day: "Exploring the Role of Lipid Metabolism in Human H4 Neuroglioma Cells in Alzheimer's Disease – Advancing Metabolomics with 3D OrbiSIMS Technology."
2. Poster Prize Winner, AHPGR Conference 2023, School of Pharmacy, University of Nottingham.
3. Castle Award, YSA Competitions at UK Surface Analysis Forum 2023: Presentation on "Utilizing OrbiSIMS as an Alzheimer's Disease Screening Tool to Investigate ApoE4 Gene-Mediated Molecular Alterations in H4 Neuroglioma Cells."
4. Alzheimer's Association International Conference AAIC 2023: Poster session on Developing Topics.
5. SIMS Europe 2023, oral presentation: Using OrbiSIMS as an Alzheimer's disease screening tool to investigate ApoE4-mediated molecular alteration of H4 neuroglioma cells.

Contents

Chapter 1: Introduction

Apolipoprotein E4 (ApoE4) is the strongest genetic risk factor for late-onset Alzheimer's disease (AD), increasing the risk by 3 to 12 times in individuals carrying at least one ApoE4 allele [1]. Over the past 20 years, research has gradually unveiled the complex role of ApoE4 in AD. It is associated not only with standard pathological features such as amyloid-β deposition and tau protein phosphorylation but also plays a crucial role in mediating neuroinflammation, brain metabolism, neuron growth, and synaptic plasticity [2]. As a lipid transport protein, ApoE4 significantly affects brain metabolism, further impairing normal brain function and exacerbating pathological changes like amyloid deposition, tau phosphorylation, and neuroinflammation [3]. Notably, emerging clinical evidence suggests that systemic molecular alterations in the brain occur up to 20 years before the onset of AD's pathological features, underscoring the importance of monitoring molecular changes related to ApoE4.

Commonly used methods for metabolic/protein monitoring include LC-MS/MS for metabolomics and lipidomics, proteomics in liquid biopsy tests, as well as positron emission tomography (PET) scans to assess glucose consumption in the brain [4, 5]. However, most ApoE4-related research has primarily been conducted in animal models. A significant challenge arises from the differences between animal and human disease states and metabolic conditions, compounded by the complex environment of the human body, various disease states, and individual variability. Translating findings from animal studies to clinical settings is difficult due to the challenges in collecting precise human samples. While blood and urine samples are readily accessible and can reflect overall body metabolism, they do not provide sufficient information about specific tissue changes. Cerebrospinal fluid and human brain samples are more challenging to obtain but are critical for reflecting disease-related alterations. Therefore, an analytical method that requires a small sample size, minimal sample preparation, and allows for rapid analysis would provide valuable information and serve as a guide for further testing.

The first chapter begins with an introduction to Alzheimer’s disease (AD), highlighting the significance of ApoE4 in AD pathogenesis research. It outlines the

role of ApoE4 in the progression of the disease and its impact on the brain's molecular and cellular processes. Following this, the chapter introduces multi-omics approaches, including metabolomics and proteomics, and their application in AD research, demonstrating how these techniques provide deeper insights into the molecular alterations associated with the disease. The chapter then discusses the most used mass spectrometry-based analytical techniques for studying molecular changes in Alzheimer's disease, focusing on their ability to detect and quantify a wide range of metabolites and proteins. Finally, the chapter introduces OrbiSIMS, a state-of-the-art instrument that integrates mass spectrometry and imaging, and explores its potential applications and future perspectives in metabolomics research and the multi-omics field, highlighting its promise for advancing AD research and therapeutic development.

1.1 Alzheimer's disease

Dementia is a neurological disease characterised by the gradual decline in memory, reasoning, language skills, and the ability to perform daily tasks. There are 55.2 million people who have dementia worldwide according to World Health Organization (WHO) 2019 report. By 2030, the prevalence of dementia is predicted to double, and by 2050, it will triple [6]. In 2019, the number of women with dementia surpassed that of men globally, a trend expected to continue until 2050. Furthermore, the projected increase in dementia cases exhibits geographical heterogeneity, with lower growth rates in high-income Asia-Pacific and Western Europe, while North Africa, the Middle East, and eastern sub-Saharan Africa are anticipated to experience higher percentage changes [7]. From an economic perspective, the annual global cost of dementia was estimated at US $ 1.3 trillion for 55.2 million individuals affected by the condition. Nearly 50% of these costs are attributed to informal caregivers, such as family members and close friends. Additionally, 16% of the costs are direct medical expenses, while 34% are associated with direct social sector costs [8].Currently, there is no therapeutic method to cure dementia. While some treatments are available, they primarily delay the progression of the disease. Overall, dementia impacts not only the patients but also places a significant burden on families and society.

Alzheimer's disease is the most common type of dementia, accounting for 60-70% of all cases, affecting more than 50 million people worldwide, and is expected to rise by over 150 million cases by 2050 [9]. Other types of dementia include vascular dementia, Lewy body dementia, and frontotemporal dementia. Alzheimer's disease is characterised by abnormal protein deposits, forming amyloid plaques and tau tangles throughout the brain. In vascular dementia, cognitive decline results from inadequate blood flow, often due to blood clots or strokes [10]. Lewy body dementia involves abnormal deposits of α-synuclein proteins, which disrupt the brain's chemical messengers [11]. Frontotemporal dementia is marked by the accumulation of abnormal tau and TDP-43 proteins within neurons in the frontal and temporal lobes [12]. The frontal lobe is associated with movement, reasoning, behaviour, memory, and speech, while the temporal lobe is involved in language comprehension, behaviour, memory, and hearing.

In the human brain, the outermost layer is the cerebral cortex, characterised by numerous folds that increase surface area. It is divided into four lobes: frontal, parietal, temporal, and occipital [13], as shown in Figure 1.1. The frontal lobe is the largest and is responsible for personality, decision-making, judgement, and voluntary movement. It processes and integrates information from the environment, emotions, and memories to facilitate sophisticated decision-making [14]. The parietal lobe plays a crucial role in integrating sensory information, including touch, temperature, pressure, and pain [15]. The occipital lobe, located at the back of the brain, serves as the brain's visual processing centre [16]. The temporal lobe is involved in memory, emotion, and language comprehension. Information destined for long-term memory is funnelled through the entorhinal cortex of the temporal lobe and into the hippocampus, where memories are created [17, 18].

The entorhinal cortex acts as a bridge between the cerebral cortex and the hippocampus, directing various types of sensory input, such as auditory and visual information, into the hippocampus for memory consolidation [19]. Both the entorhinal cortex and hippocampus are highly susceptible to damage in the early stages of AD, leading to memory deterioration [20, 21]. Two other areas near the hippocampus, the amygdala and perirhinal cortex [22, 23], have also been implicated in early-stage AD.

As AD progresses, regions of the cerebral cortex associated with language, reasoning, and social behaviour, including the frontal, temporal, and parietal lobes, become increasingly affected.

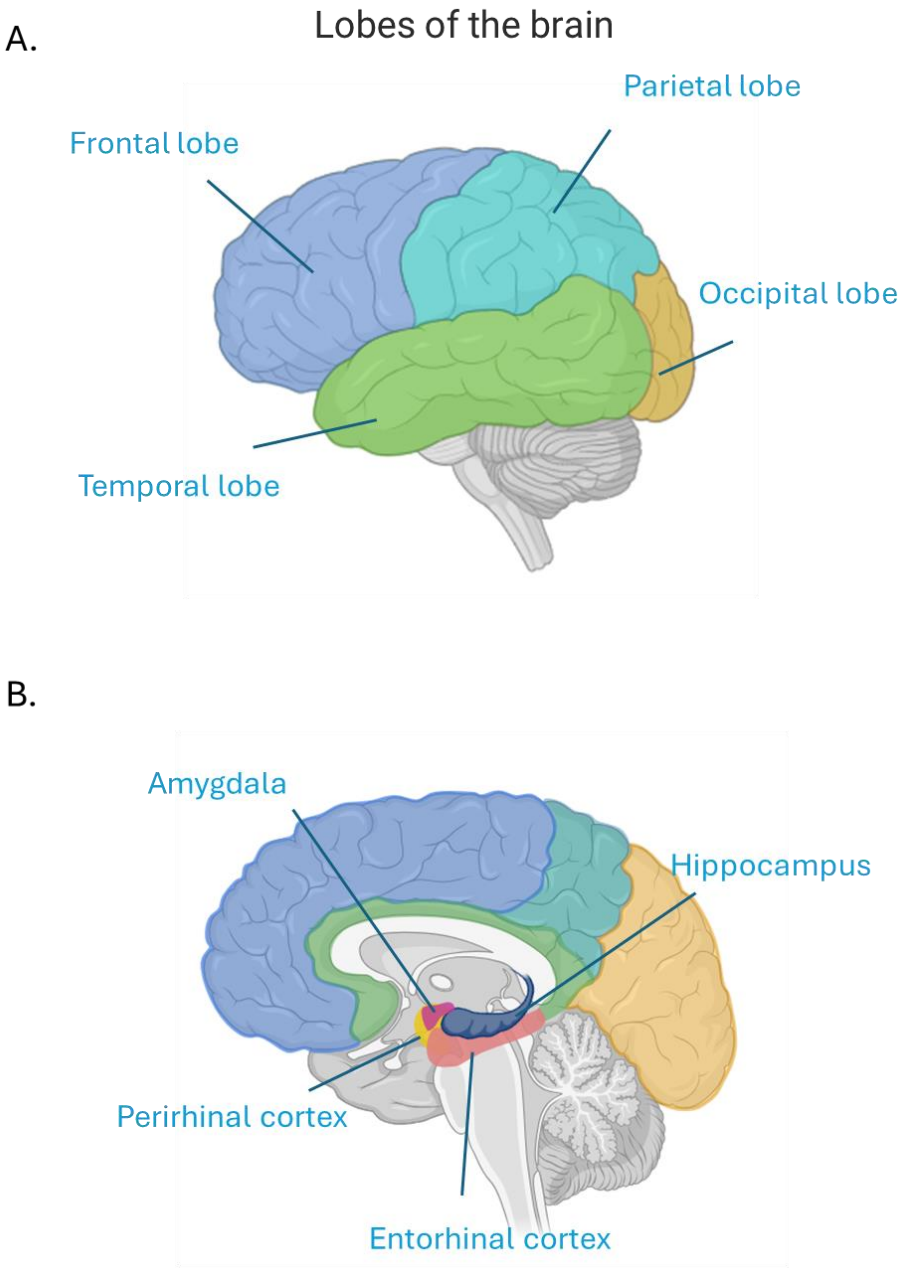

Figure 1.1. *An illustration of the four lobes of the cerebral cortex, along with a diagram showing the location of the hippocampus and the key areas nearby involved in memory. (The figure was created using BioRender.com, and refer the paper published by Raslau et al. [24])*

The majority of AD cases usually occur after the age of 65 termed as sporadic/late-onset AD (LOAD), while the cases occur before age 65 are extremely rare, accounting for less than 5% of all case and are described as early-onset AD (EOAD) [9]. In addition, genetically inherited Alzheimer's patients, who usually develop the disease before the age of 65 with more rapid rate of AD progression, constituting for only 1%-2% of all AD cases and are termed familial/autosomal dominant AD (ADAD). Most of ADAD attributed to amyloid precursor protein (APP) and presenilins1/2 (PSEN1/2) mutation which can lead to the increasing of Aβ42 and the death of neurons [25]. More than 90% of AD patients are LOAD that does not exhibit autosomal-dominant inheritance and associate with some genetic factors such as the Ɛ4 allele of the apolipoprotein E (APOE) [26, 27].

The early observations of Alzheimer's disease were made by Dr. Alois Alzheimer between 1902 and 1906 in a patient named Auguste Deter [28]. During the autopsy, he noted the presence of amyloid plaques, neurofibrillary tangles, loss of neurons, granulovacuolar degeneration, and changes in brain structure. These early findings laid the groundwork for understanding the pathological features of Alzheimer's disease and have been crucial for subsequent research into its mechanisms and potential treatments. Even though it has been more than 100 years now since Alois Alzheimer first found and described this disease, the amyloid plaques and neurofibrillary tangles are still the standard pathological diagnosis for AD. The observation of the form extracellular tau tangles and intracellular amyloid plaques are common in Alzheimer's disease patients' autopsy brain section (Figure 1.2).

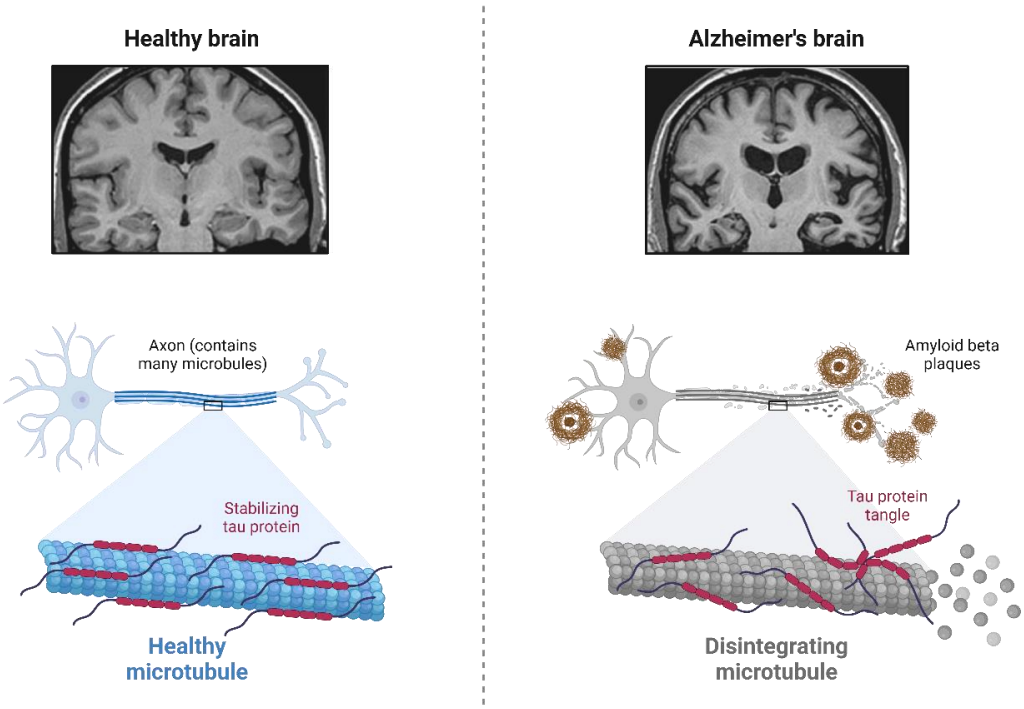

Figure 1. 2. *An illustration depicting brain atrophy in Alzheimer's patients and the two hallmark features of AD (The figure was created using BioRender.com.). The left graph illustrates a section of a healthy brain and neuron axons, where tau stabilises the axon structure, and no amyloid plaques are present. In contrast, the right graph depicts the brain of an Alzheimer's patient, showing characteristic brain atrophy. The neuron axons highlight the formation of extracellular amyloid-beta plaques and intracellular tau tangles, which are key features of Alzheimer's disease.*

Many drugs and therapeutics in clinical trials target these two pathologies, including reducing the Aβ production, increase the clearance of amyloid plaques, and inhibit the phosphorylation of tau [29]. However, the presence of Aβ and neurofibrillary tangles (NFTs) are not sufficient to fully explain the pathology of AD, indicating it as only one piece of the puzzle of AD [30]. The most impressing development in AD is the approval of aducanumab by the Food and Drug Administration (FDA) in June 2021, which is the first targeted therapy of AD and the first AD drug approved by the FDA since 2003 [31]. Aducanumab targets amyloid-β to alleviate AD symptoms. But there are still many controversies pointing to the inconspicuous effects of aducanumab in clinical trials. It does need more clinical data and market responses to supplement the

effects on AD. The exact mechanism of AD remains unclear and requires further investigation into its pathology.

With the development of genomics and genome-wide screening technologies, numerous gene mutations have been associated with LOAD. Genome-wide association studies (GWAS) have identified a wide range of genetic risk factors for LOAD, enhancing our understanding of the underlying pathophysiological processes such as ApoE4, TREM2, ADAM10 and PLD3 [32]. Among these, ApoE4 is recognised as the strongest risk gene factor, with individuals carrying ApoE4 alleles having up to 12-fold increased risk of developing AD compared to non-carriers. Understanding the role of ApoE4 may offer valuable insight into mechanisms driving Alzheimer's disease pathogenesis [33].

1.2 The strongest risk gene ApoE4 in late-onset AD

The human APOE gene is located on chromosome 19's long arm. Two nonsynonymous single nucleotide polymorphisms (SNPs) in exon 4 of chromosome 19 (rs429358 and rs7412) result in three isoforms including APOE2 (TGC/TGC), APOE3 (TGC/CGC), and APOE4 (CGC/CGC) that differ at amino acid residues 112 or 158 (APOE2 112Cys/158Cys, APOE3 112Cys/158Arg, and APOE4 112Arg/158Arg) [34]. The APOE2 variant has been shown improve AD symptoms and provide neuroprotective effects, while the presence of APOE4 increases the risk of Alzheimer's disease by 3 to 12 times [35]. The three polymorphic alleles of APOE - ε2, ε3 and ε4, have a worldwide frequency of 8.4%, 77.9% and 13.7%, respectively, whereas for ε4 allele the frequency is increased to ~40% in AD patients [36].

The APOE gene is transcribed and expressed as Apolipoprotein E (ApoE), consisting of 299 amino acids and having a molecular weight of approximately 34 kDa. It features two main functional regions: the receptor-binding region near amino acids 136-150 and the lipid-binding region within the carboxy-terminal domain (amino acids 244-272) as shown in Figure 1.3 It has been suggested that the movement of N – and C-terminal domains determines the accessibility of the receptor-binding region [37, 38].

However, in the lipid-bound form, the lipid-binding region directly interacts with lipid particles, causing the two domains to separate. This structural change enhances the accessibility of the receptor-binding region to receptors.

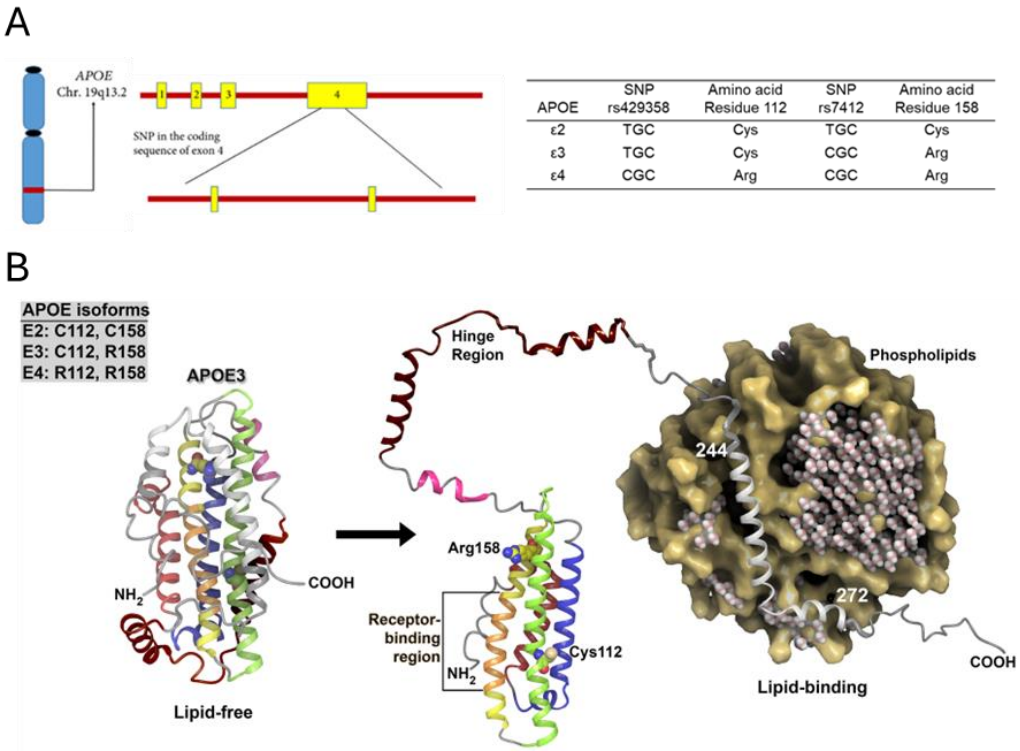

APOE	SNP rs429358	Amino acid Residue 112	SNP rs7412	Amino acid Residue 158
ε2	TGC	Cys	TGC	Cys
ε3	TGC	Cys	CGC	Arg
ε4	CGC	Arg	CGC	Arg

Figure 1. 3. *The genetic location of ApoE in chromosome 19 and the amino acid differences of three allelic variants of ApoE (ApoE2, ApoE3, ApoE4), the structure of Apolipoprotein E. Yamazaki et al. Nat Rev Neurol, (2019)*

The most prevalent receptors for ApoE are within the low-density lipoprotein receptor (LDLR) family, which includes LDLR and LDLR-related protein 1 (LRP1) [39]. Variations in amino acids at positions 112 and 158 significantly affect the structure and function of ApoE isoforms, influencing their capacity to bind lipids and receptors. Notably, ApoE3 and ApoE4 exhibit significantly stronger binding (50 times greater) to LDLR compared to ApoE2 [40]. ApoE4 shows a higher affinity for triglyceride-rich/larger very low-density lipoproteins (VLDL), whereas ApoE3 and ApoE2 predominantly bind to smaller phospholipid-rich high-density lipoproteins (HDL) [41]. LDLs transport insoluble lipids, such as cholesterol and triglycerides, from their site of synthesis in the liver to various organs and tissues throughout the body. In contrast,

HDLs facilitate the transport of lipids back to the liver, where they are metabolised into bile acids and subsequently excreted from the body. Due to these roles, elevated LDL levels are associated with a higher risk of cardiovascular disease, whereas higher HDL levels are generally considered beneficial for health.

1.2.1 ApoE in lipid metabolism

The importance and association between AD and lipids established on the finding of the genetic risk gene of ApoE, which is a crucial mediator on cholesterol and triglyceride metabolism [42]. ApoE is a lipid-binding protein used to deliver lipids including cholesterol, phospholipids, and triglycerides. ApoE is mainly expressed in the liver and brain and is secreted primarily in astrocytes in the brain followed by microglia. Additionally, ApoE is the most abundant lipoprotein in the central nervous system [43]. The transfer of lipids to ApoE to form lipoprotein particles is based on the cell surface ATP-binding cassette transporters ABCA1 and ABCG1. The ApoE4 lipoprotein particle is formed by the function of ABCA1 and ABCG1, which transport cellular biosynthetic cholesterol and lipids to bind with ApoE.

In the brain, ApoE is secreted by astrocytes, transporting cholesterol and lipids to near neurons via ApoE receptors, such LDLR family. Xiaohui *et al*. probed the role of ApoE in cholesterol, which shows that astrocytic ApoE reprogramming neuronal lipid metabolism, stabling the neuron metabolism balance [44]. In a study based on AD and frontotemporal dementia patients, the patients carrying ApoE4 showed more severe brain atrophy in disease-specific regions compared to noncarriers, indicating ApoE4 carriers are at greater risk for neurodegenerative disease clinical progression [45].

Multiple studies suggest the presence of ApoE4 with the accumulation of intracellular lipids (cholesterol, triacylglycerols (TAGs)) in human induced pluripotent stem cell (iPSC)-derived astrocytes and microglia, and oligodendrocytes. The accumulation of lipid in glia has been found to link to inflammatory responses then enhance the development of neurodegeneration disease. A study conducted in P301S tau transgenic mice found the expression of human ApoE4 significantly elevates the level of cholesteryl esters and lipids within microglia of P301S mice [46]. ApoE presents as two statues in the cell, lipidated ApoE, and free ApoE. The lipidation status of ApoE

has been shown the ability of lower Aβ production, while the unlipidated ApoE promotes amyloid plaques deposit [47]. These results show that lipid metabolism and lipid-related protein are important for AD, especially ApoE4-mediated AD progression, getting more information on lipids metabolism will deepen our knowledge of ApoE4 in AD.

ApoE4 is not only associated with lipid metabolism but is also recognised as the strongest genetic risk factor for AD. It has been strongly linked to multiple AD pathologies, including the formation of amyloid plaques and neurofibrillary tangles.

1.2.2 The effect of ApoE4 on AD pathologies

Amyloid pathology

Aβ is produced from cleavage of β-amyloid precursor protein (APP) by β-secretase and γ-secretase. After that Aβ peptides aggregate into Aβ oligomer, protofibrils and fibrils that are detectable in AD brain. Aβ42 has longer C-terminus resulting in the feature of hydrophobicity and are prone to aggregate into oligomers and fibrils. The amyloid cascade hypothesis has been proposed by Hardy and Higgins in 1992 [48], positing the deposition of Aβ initiates the AD pathogenesis, which leads to subsequent neurofibrillary tangles, neurons and synaptic loss, vascular damage, and cognitive impairment. ApoE4 binds less efficiently with Aβ compared with ApoE3, regulating its metabolism, clearance, aggregation, and deposition. Longitudinal cerebrospinal fluid (CSF), Magnetic Resonance Imaging (MRI) and Positron Emission Tomography (PET) imaging studies of preclinical stage of AD showed that amyloid deposition began at an earlier age of ApoE4 carriers comparing with E4 non-carriers before symptom onset [49]. Neuropathology studies of AD brain have found the correlation of ApoE4 and intraneuronal accumulation of Aβ, deposition of plaques in parenchyma, and formation of neurotoxic Aβ oligomers [50]. Aβ deposition in brain showed higher in those patients carrying at least an ApoE4 allele.

A growing body of evidence has shown that ApoE4 increase the risk of AD by influencing Aβ production and release in neurons, as well as its clearance in glial cells.

Also, it regulates the microglial response to amyloid plaques [51]. It has been shown to increase Aβ seeding and fibrillization, resulting in increased amyloid deposition, and to obstruct Aβ removal from the brain parenchyma by binding competitively to Aβ receptors on glial cells. Additionally, recent study applied AD transgenic neuron cells to investigate the interaction of ApoE with amyloid-beta, which showed the internalised ApoE interacts with Aβ proteins whereas the ApoE4 increase the levels of internalised amyloid protein in neurons [52]. Expressing ApoE4 in APP/PS1 mice increased Aβ pathology, which could be reversed by deleting LRP1, which suggests the increased Aβ by ApoE4 mediated by LRP1 [53]. Hashimoto *et al*. isolated endogenous ApoE from tris-buffered saline (TBS)-soluble fraction of human brain to examine the effect of it on Aβ oligomers. Their study demonstrated that ApoE4 increases the formation of Aβ oligomers [54]. Another study investigated the interaction of ApoE fragments with different forms of Aβ from post-mortem brains. The results indicate the Aβ 1-42 in heteromers of 18 are highly interact with ApoE fragments, especially in ApoE4 carriers [55]. In overall, ApoE4 associated amyloid pathology is via binding with Aβ proteins, promoting its oligomerisation, obstacle the release and clearance of Aβ from neurons.

Tau pathology

Tau is the major microtubule-associated protein (MAP) expressed in the neuron, plays the role in the microtubule assembly, stabilisation of neuronal axons, and regulation of microtubule transport [56]. Different from Aβ pathology, the phase of tau pathology correlates with the progression of cognitive reduction. On longitudinal and cross-sectional studies, tau- and amyloid- PET imaging, and structural MRI shows the presence of tau was a predictor of cognitive decline, whereas amyloid was a predictor of more severe tau-correlated cognitive impairment [57]. Interestingly, cognitive impairment in AD brain is only found when tau seeds spread from the entorhinal cortex into the neocortex. It suggests tau is highly correlated with cognitive decline observed in AD patients. The direct effect of ApoE4 on tau pathology or tau-mediated neurodegeneration is less certain, however, ApoE4 has been reported strongly influence and exacerbate tau pathology by activating microglial [53, 58, 59].

ApoE4 carriers demonstrate greater rates of disease progression from the symptomatic

AD individuals who have Aβ and tau-pathology positive. A P301S tau transgenic mice study found that ApoE4 worsens tau pathology, resulting in increased microgliosis and increased neuroinflammatory cytokine production [60]. In addition, another study on tauopathy mouse model found ApoE regulates neurodegeneration predominantly by modulation microglial activation [61]. Furthermore, ApoE4 have been found that may disrupt the blood-brain barrier function and impede Aβ/tau degradation by failing to bind to LRP1 expressed on cells effectively [62].

Except for the two major hallmarks of AD, amyloid plaques and neurofibrils, another area of AD research, innate immunity, has experienced much intense investigation in recent years [63]. Microglia and astrocytes are the most important immune cells. The neural functions of the cerebral microglial are remodelling synapses, clearing debris, and supporting trophic factors for neurons. Astrocytes are considered as supporting cells that provide trophic support for neurons and can eliminate neuronal toxicity [64].Increasing evidence has demonstrated the prolonged neuroinflammation results from the chronic glial activation, inducing neuronal damage and death in AD brain [65]. Activated microglia produce reactive oxygen species (ROS) and nitric oxide (NO), which can injure and kill neurons. Additionally, stressed neurons may release death signals and subsequently be phagocytosed by activated microglial cells. Moreover, activated microglia can crosstalk with astrocytes which involves the upregulation of inflammatory mediators and neurotoxic substances that damage neurons, coupled with a reduction in trophic support function. Compared to ApoE3, the expression of ApoE4 in the microglia of a mouse model results in cognitive impairment and reduces the number of microglia surrounding amyloid-β plaques by impairing lipid metabolism [66].

Additionally, ApoE4 has been strongly linked to vascular impairment and the breakdown of the blood-brain barrier (BBB). A recent study investigated the mechanism of ApoE4 in vascular damage was independently with amyloid-beta and was via cyclophilin A-matrix metalloproreinase-9 BBB-degrading pathway [67]. In addition, the impairment of synaptic integrity and alteration of the gut microbiota has been reported associated with ApoE4 [68-70]. Supplementation with short-term antibiotics in tauopathy mice model (P301S) reduced tau pathology and

neurodegeneration in ApoE4 carrier mice, suggesting potential therapeutic approaches for treating conditions in the presence of ApoE4.

The exact function of ApoE lipoproteins in brain cells—and how ApoE4 alters this function—remains incompletely understood. Figure 1.4 summarises current findings on the relationship between ApoE and amyloid-β (Aβ) pathology. In the brain, ApoE is primarily secreted by astrocytes, where it binds to lipids via ABCA1 to form lipoproteins. These lipoproteins can then bind to soluble Aβ, which is released from neurons. The resulting ApoE–Aβ complexes interact with lipoprotein receptors such as LRP1 and LDLR on microglia, astrocytes, and cells of the blood-brain barrier (BBB), facilitating Aβ clearance.

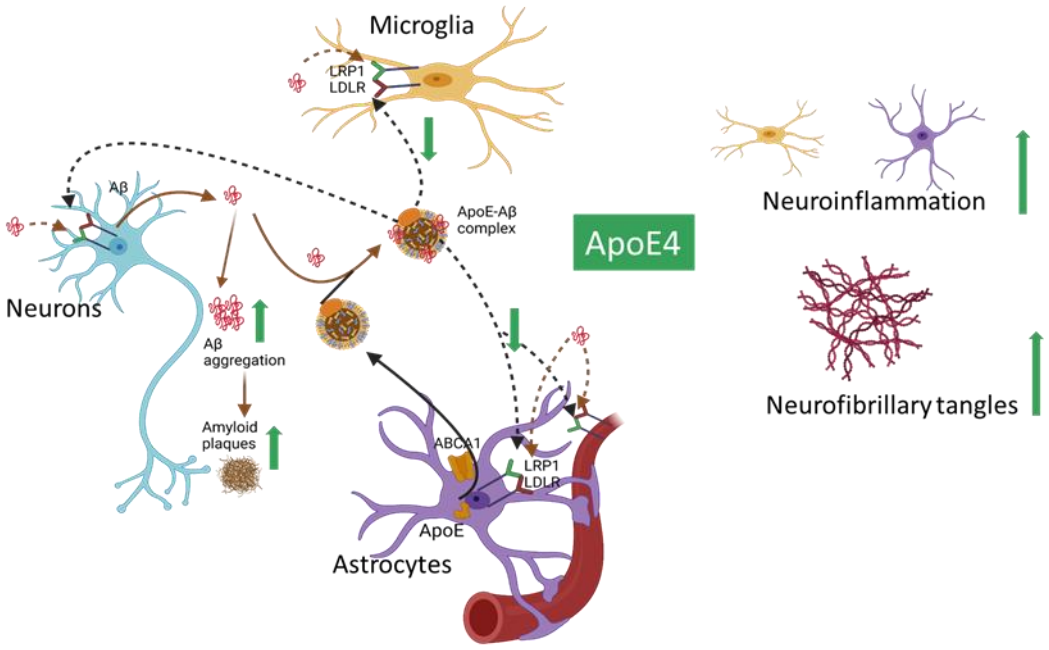

Figure 1. 4. *The role of ApoE in amyloid-β transport and clearance in brain cells, and the impact of ApoE4 on Alzheimer's disease pathogenesis*

In the presence of the ApoE4 isoform, the binding affinity between ApoE and Aβ is reduced, leading to increased Aβ aggregation and plaque formation. ApoE4 has also been shown to impair Aβ clearance mechanisms, further exacerbating amyloid pathology. In addition, increasing evidence points to ApoE4's strong association with neuroinflammation and the formation of neurofibrillary tangles, both key features of Alzheimer's disease. These findings indicate that ApoE4 contributes to multiple

aspects of AD pathology, shaped by the complex cellular environment of the brain. A deeper understanding of ApoE4's effects across different brain cell types may support the development of more effective therapeutic strategies for individuals carrying the ApoE4 allele.

1.2.3 The therapeutic strategies targeting ApoE

Several clinical studies using animal models and human-derived stem cell models have been conducted to investigate ApoE-associated therapies, highlighting the significant potential of targeting ApoE in AD treatment. For example, selective removal of astrocytic ApoE4 showed the strong protection on tau-mediated neurodegeneration in P301S mice model [71]. In 2019, a phase 1 trial of gene-therapy approach began, aiming to evaluate the tolerable dose of LX1001 in AD patients who carry two ApoE4 alleles and were diagnosed with mild cognitive impairment to moderate dementia. LX1001 is a gene therapy method using AAVrh.10 hApoE2-HA vector to deliver an ApoE2 expression cassette, which have been found increasing brain expression of ApoE2, and decreased Aβ levels and amyloid deposition in mice models [72-74]. Jackson *et al*. reported a gene therapy by exposing APP/PS1 mouse brain to ApoE2, leading to the reduction of Aβ plaque deposition, synaptic loss, and microglial activation [75]. The phase I clinical trial of LX1001 is set to end in April 2024, a five-year follow up to assess safety and biomarkers will run until 2028.

Bexarotene Targeting on lipids associated receptor is found to have the ability to reduce neurodegeneration. A study suggests the effect of liver-X receptor (LXR) agonist GW3965 on reduction of tau pathology and glial inflammation and synaptic deficits in ApoE4 carrying P301S mice [46]. The neuroprotection of LXR agonist is mediated by ATP binding cassette transporter A1 (Abca1), therefore, overexpression of Abca1 in the brain of ApoE4 mice reduces lipid accumulation in microglia and ameliorates tau pathology, and synapse loss.

Peroxisome proliferator-activated receptors (PPARs) are nuclear receptors which mediate the expression of lipid genes including APOE and ABCA1. Rosiglitazone, a

PPAR-γ agonist, demonstrated memory improvement in mouse AD models but showed no significant effect in clinical trials. Modulating the lipidation of ApoE such as targeting ABCA1 has been shown the benefits for reducing AD pathologies. Those therapeutic approaches are still in preclinical stage, more work needs to be done.

Therapies targeting the gut microbiota have been proposed as a potential approach to alleviate and slow the progression of AD. Studies using AD mouse models have shown that AD amyloidosis is exacerbated when gut microbiota from AD mice are transferred into germ-free mice [76]. GV-917, a marine-derived oligosaccharide, has been studied for its effects in reducing amyloid plaques and inhibiting neuroinflammation [77-79]. Most recently, Bosch *et al*. reported the effects of GV-971 on gut microbiota, Aβ, and microglia activation in the APPPS1-21 mice model [80]. Their results demonstrated that GV-971 reduced amyloid plaques and neuroinflammation by altering gut microbiota and microglia, highlighting the essential role of microbiota-microglia-amyloid axis. Although several recent studies have suggested that ApoE isoforms differentially affect the gut microbiota [69, 81], it remains unknown whether the effect of GV-971 on AD improvement involves ApoE isoforms.

1.3 Multi-Omics Application for ApoE4-Associated pathogenesis mechanisms in AD

For such complicated pathological mechanisms of ApoE4 in Alzheimer's disease, growing evidence supports the concept of multi-omics in identifying key disease-related molecular alteration and disease-progression-related changes [82, 83]. Multi-omics approaches encompass genomics, transcriptomics, proteomics, and metabolomics, each focusing on a specific target: genes, RNA, proteins, or small metabolites, respectively.

Genomics, often using genome-wide association studies (GWAS), is widely applied to identify genetic differences between AD patients and healthy individuals, aiming to uncover genetic risk factors for AD. In addition to ApoE4, which is the strongest risk gene for AD, other genes such as TREM2, SORL2, ABCA7, ABCA1, and ADAM10

are also highly associated with an increased risk of AD [32, 84]. For the past few decades, transcriptomics and proteomics have been applied widely in neurodegenerative disease to investigate gene expression and help explain phenotypes of diseases. Giuseppe *et al.* applied multi-omics methods, which includes single-nucleus RNA-sequencing, phosphoproteome and proteome analysis, to study the effect of ApoE4 on mice blood-brain barrier and synaptic dysfunction [85]. They found that the strong association of early disruption of BBB transcriptome in ApoE4 knock-in mice compared with ApoE3, and dysregulation in protein signalling networks in brain endothelium, as well as transcription and RNA splicing suggestive of DNA damage in pericytes.

Multi-omics studies that combine transcriptome and proteomics analyses offer a comprehensive view of ApoE4-related molecular mechanisms; however, gene expression levels often show poor correlation with protein levels in AD brain tissue due to the complexity and variability of translation process. Therefore, genomics or transcriptomics do not provide a complete map of pathogenic changes in AD, and much recent research applied metabolomics technology as a complement tool to get a whole better view on disease-related molecular alteration. This section will explore the application of metabolomics and proteomics in investigating ApoE4-related mechanisms in Alzheimer's disease. Key analytical tools commonly employed in these studies will be reviewed, along with a discussion of current challenges in multi-omics.

1.3.1 Metabolomics

Metabolomics is a powerful approach, a large-scale study of small molecules includes: sugars, lipids, amino acids, fatty acids *et al* [86], unlike other “omics” measurements, metabolites and their concentrations directly represent the underlying metabolic activity and condition of the cell [87]. Thus, metabolomics refers to the complete set of metabolites within a cell, tissue, or biological sample at a given time point, and it best depicts the molecular phenotype [88]. Analytical platforms such as mass spectrometry (MS) and nuclear magnetic resonance (NMR) spectroscopy are the cornerstone techniques in metabolomics. MS, often coupled with separation methods like liquid chromatography (LC-MS) or gas chromatography (GC-MS), provides high sensitivity and specificity for detecting a wide range of metabolites. NMR

spectroscopy, while less sensitive, offers unparalleled reproducibility and the ability to analyse metabolites in a non-destructive manner.

According to the latest release of the Human Metabolome Database (HMDB 5.0), the number of metabolite entries specific to humans has increased to 217,920 compounds [89]. Due to the complexity and vast number of metabolites, there is currently no standardised system for their categorisation. Common classification methods include grouping metabolites based on their involvement in specific pathways, such as amino acid metabolism, lipid metabolism, the tricarboxylic acid (TCA) cycle, and glycolysis. Another approach is to classify them based on their chemical characteristics, such as organic acids, amino acids, lipids, sugars, vitamins, and nucleic acids.

In this thesis, metabolites are classified based on the KEGG Compound Database, which provides a framework for categorising molecules by their structural and functional properties. Amino acids (AAs) are a class of compounds characterised by a central carbon atom bonded to an amino group ($–NH_2$), a carboxyl group (–COOH), a hydrogen atom, and a distinctive side chain that defines their specific chemical behaviour. AAs are essential in numerous biological processes, serving as the building blocks of proteins and contributing to cellular structure, function, and signalling. They also participate in a wide range of metabolic pathways critical to physiological regulation [90]. Carbohydrates comprise a broad group of metabolites containing carbon (C), hydrogen (H), and oxygen (O), and are involved in key metabolic pathways such as glycolysis and the tricarboxylic acid (TCA) cycle. Nucleotide metabolism-related metabolites typically contain carbon, hydrogen, oxygen, nitrogen, and phosphorus (C, H, O, N, P), and play essential roles in energy transfer, genetic information storage, and signalling [91]. Another major class of metabolites is lipids, which will be discussed on the following page. In addition to endogenous metabolites produced or metabolised within the host organism, metabolites can also originate from external sources, such as microorganisms, dietary intake, and other exogenous factors. The biological functions of metabolites include energy production and storage, cell signalling, serving as intermediates in the biosynthesis of essential biological macromolecules, and acting as end-product waste that can influence cellular function

[92]. Metabolites are well known to act as co-substrates in regulating protein post-translational modifications (PTMs). Key metabolites such as ATP, acetyl-CoA, and NAD^+ play critical roles in histone PTMs [93]. Increasing evidence suggests that the regulation of immunity is linked to PTMs mediated by lipids, amino acids, and polyamines, which alter enzyme activity and disrupt protein-protein interactions [94]. Additionally, lipids like fatty acids and phospholipids serve not only as building blocks for cell membranes but also as crucial interactors with membrane proteins, facilitating various protein transport processes and functions [95, 96]. Protein lipidation is a type of post-translational modification in which lipid moieties are covalently attached to proteins. This modification alters the hydrophobicity and conformation of the protein, leading to changes in its functions and interactions with other ligands or proteins.

Lipids were considered a subset of metabolites, and in the coming era of precision medicine, the biomedical community has shifted its focus to lipids in a big manner, accounting for lipids as a substantial fraction of all metabolites. In addition, in the last five years, rising interest has attracted a new generation of scientists who see lipids in a new light, as a component of a larger big data picture. The enormous development of lipidomic is due to the advances in analytical tools of mass spectrometry, which led us to gain a depth understanding of lipids in AD pathogenesis [97].

Based on the classification system proposed by Fahy *et al.* (2005) [98], lipids are categorised into eight major classes: fatty acyls, glycerolipids, glycerophospholipids, sphingolipids, sterol lipids, prenol lipids, saccharolipids, and polyketides [99]. Example structures for each lipid class are presented in Figure 1.5. This classification system has been widely accepted and is used internationally in lipidomics research. Fatty acyls (FAs) are a diverse group of molecules synthesised through the chain elongation of an acetyl-CoA primer with malonyl-CoA (or methymalonyl-CoA) units. They may include cyclic structures or substitutions with heteroatoms such as oxygen, nitrogen, sulfur or halogens. The simplest fatty acyls are straight-chain saturated fatty acids with a terminal carboxylic acid group - palmitic acids (FA 16:0) being a common example. Derivatives include branched-chain fatty acids, heteroatom-containing fatty acids, and fatty acids with three to six-membered cyclic or heterocyclic rings.

Glycerolipids consist of mono-, di, and tri-substituted glycerols, with triglycerides (TAG) being the most well-known example. Glycerophospholipids, closely related to glycerolipids, are distinguished by the presence of a polar head group at the sn-3 position of the glycerol backbone in eukaryotes (or sn-1 position in archaebacteria). Common head groups include choline, ethanolamine, inositol, serine and glycerol, forming phosphatidylcholine (PC), phosphatidylethanolamine (PE), phosphatidylinositol (PI), phosphatidylserine (PS) and phosphatidylglycerol (PG), respectively.

Sphingolipids (SP) are a complex group of compounds that featuring a common structure: a sphingoid base backbone, which is synthesised *de novo* from serine and a long-chain fatty acyl-CoA. This backbone is further modified to produce ceramides, phosphosphingolipids, glycosphingolipids, and other derivatives. Sterol lipids are characterised by fused four-ring core structure that forms the basis of compounds like cholesterol and steroid hormones. Prenol lipids are derived from five-carbon isoprene units, such as 2E,6R-dolichol (shown in Figure 1.5). These lipids are biosynthesised through the condensation of isopentenyl diphosphate and dimethylallyl diphosphate. Saccharolipids are a class of compounds in which fatty acids are directly linked to a sugar backbone, forming lipid structures that incorporate carbohydrate-derived components. Polyketides are synthesised through the polymerisation and successive condensation of simple carboxylic acid units, and are typically produced by bacteria, fungi, and plants. These compounds are structurally diverse and include many bioactive natural products.

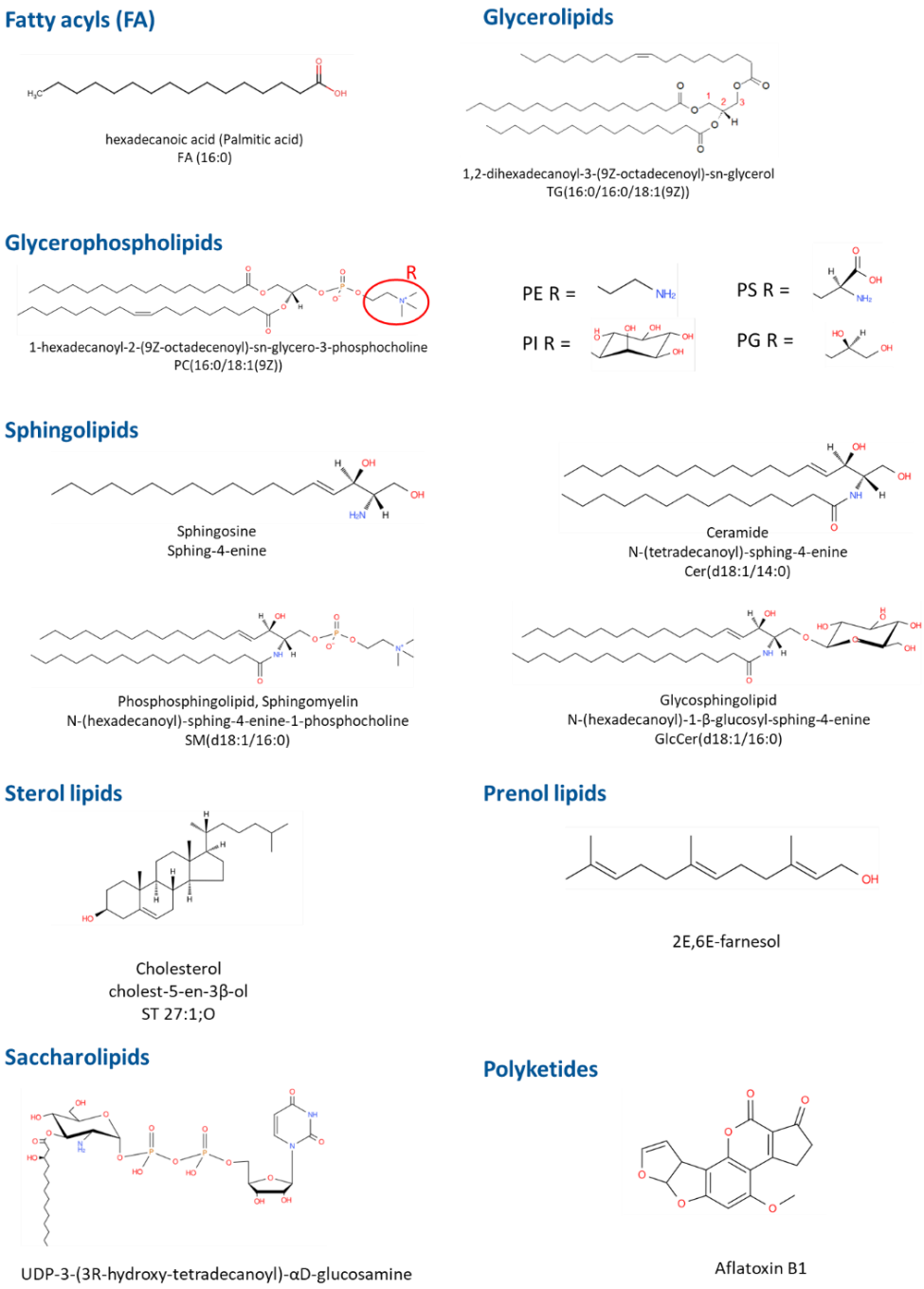

Figure 1.5. Example lipid structures representing eight major lipid classes: fatty acyls, glycerolipids, glycerophospholipids, sphingolipids, sterol lipids, prenol lipids, saccharolipids, and polyketides.

Lipid nomenclature has been standardised by the International Union of Pure and Applied Chemistry and the International Union of Biochemistry and Molecular Biology Commission on Biochemical Nomenclature [98, 99]. Fatty acids are numbered starting from the carbon atom of the carboxyl group and unsaturation is indicated by the number of double bonds. For example, palmitic acid is denoted as C16:0. The stereospecific numbering (sn) system is used to describe the position of fatty acid chains in glycerolipids and glycerophospholipids. The E/Z system (rather than trans/cis) defines the geometry of double bonds, while the R/S system (rather than α/β or D/L) is used to describe stereochemistry. Abbreviations for glycerophospholipids - such as PC, PE, PI, and PS—refer to molecules with one or two radyl side chains. The structures of these side chains are indicated within parentheses using the format Headgroup (sn-1/sn-2). For example, PC (16:0/18:1(9Z)) represents a phosphatidylcholine with a 16:0 fatty acid at sn-1 and an 18:1(9Z) fatty acid at sn-2. These molecules typically exhibit R stereochemistry at the C2 position of the glycerol backbone, with the headgroup attached at the sn-3 position. Similarly, the abbreviations TG (triacylglycerolipids), DG (diacylglycerolipids), and MG (monoacylglycerolipids) refer to glycerolipids containing one to three side chains, denoted in the format Headgroup (sn-1/sn-2/sn-3). An alkyl ether linkage is indicated by the prefix 'O-', while a (1Z)-alkenyl ether species is indicated by the prefix 'P-'—for example, DG (O-16:0/18:1(9Z)/0:0). In cases where the regiochemistry and stereochemistry of the side chains are unknown, simplified notations such as PI 38:3 are used. Here, the numbers refer to the total number of carbon atoms and double bonds across all side chains.

Lipid is an essential component of the cell that modulate membrane stability, transmit cellular signal and stabilize synapsis. About 50 % weight of the dry brain is lipids, also the brain is the richest lipid organ except for adipose tissue. Clinical trials show that adipose inclusion was formed in the AD brain [100]. Increasing evidence shows that the dysfunction of lipids pathways, lipids raft alteration, and lipid peroxidation, is associated with Alzheimer’s disease pathogenesis, including impaired synaptic plasticity, increased amyloid plaques, and p-tau [101]. First, lipid modulates the transportation and proteolytic activity of membrane proteins include APP, BACE1 (β-site amyloid precursor protein cleaving enzyme 1), presenilins, and ApoE. Second, the

markers of AD, Aβ and tau protein exert the neuronal injury primarily by disrupting membrane structure. Third, lipids may modulate the neuropathology of Aβ and tau. Much attention has been focused on cholesterol metabolism in AD, besides, other lipids, such as sphingolipids, phospholipids, and fatty acids, also are important in AD progression [102]. Cholesterol- and sphingolipid-enriched micromembrane environment (lipid rafts) was approved that able to decrease BACE1 and γ-secretase activity that resulting in the reduction of Aβ [102]. Lipids rafts are the two-layer membrane with a combination of cholesterol, sphingolipids, and fatty acid. The outer layer is constituted by PC and sphingomyelin, the inner layer is PS, PE, and PI.

Metabolomics methodologies are broadly classified into two types: untargeted and targeted metabolomics. Untargeted metabolomics aims to detect and include as many molecules or metabolites as possible in a sample, without prior knowledge of their identity [103]. The resulting datasets are often complex, requiring computational tools for metabolite identification and data interpretation. Targeted metabolomics, on the other hand, is conducted based on prior knowledge [104]. Extraction and analysis methods are specifically optimised for a particular class of metabolites or a metabolic pathway of interest. Compared to untargeted approaches, targeted metabolomics offers higher detection sensitivity and selectivity.

1.3.2 Metabolomics Advances Applied in AD

Over the past decades, metabolomic studies found that systematic metabolism dysfunction occurs for up to 20 years before the onset of AD pathological features, such as decreased glucose metabolism and increased level of total tau in the cerebrospinal fluid [105]. Several metabolomics studies in both animal models and humans have been conducted to monitor metabolic changes associated with the progression of AD [106, 107]. These studies highlight metabolomics as a promising tool for early disease diagnosis and for advancing research into the mechanisms of AD. Decreased glucose metabolism in the brains of AD patients has been confirmed by multiple clinical studies using the Fluorodeoxyglucose positron emission tomography (FDG-PET) technique [108, 109]. In 2009, Purandare *et al*. carried out metabolomics to identify biomarkers in the serum of AD patients using GC-TOF-MS and UPLC-LTQ-Orbitrap [110]. Another study applied flow injection MS and LC-MS/MS to

investigate glucose and glycolytic amino acid-targeted metabolomics in postmortem human brain tissue. The results showed that higher glucose concentration, reduced glycolytic flux, and lower glucose transporter-3 (GLUT3) are related to the severity of AD pathology [111].

With the discovery of apolipoprotein E4 (ApoE4) as the major risk gene for LOAD, lipid homeostasis raises increasing interest in investigating the potential role of lipid metabolism in AD development [35]. A large amount of evidence suggests that the dysfunction of lipid metabolism pathways is associated with AD pathogenesis, leading to impaired synaptic plasticity, increased amyloid plaques, and hyperphosphorylated tau [112, 113]. Furthermore, ApoE4 affects energy metabolism by disturbing glucose uptake and biomolecular biosynthesis [114]. Lee *et al.* integrate single-cell RNA sequencing and metabolomics technologies to systematically characterise ApoE4's role in microglial response, found that ApoE4 microglial displays the disruption of aerobic glycolysis and lipid metabolism pathway [115]. A study of targeted LC-MS/MS metabolomics showed that ApoE4 disturbed neuron-astrocyte coupling of fatty acid metabolism and inhibited astrocytic ApoE4 impeding the progression of tau-mediated neurodegeneration [116]. ApoE4 has been found not only relation to the function of neuron, astrocyte and microglia [117], but also impairs the myelination of oligodendrocytes via cholesterol dysregulation [118]. A multi-omics study combining single-cell transcriptomics profiling and lipidomic analysis of post-mortem human brains, conducted by Blanchard *et al*. [118], revealed abnormal cholesterol deposition in oligodendrocytes. Oligodendrocytes are a type of cell in the central nervous system responsible for producing the myelin sheath, which insulates nerve fibres and enhances the electrical activity of neurons.

The impact of ApoE4 on lipid signatures varies regionally, as demonstrated by a lipidomic study conducted on 14–15-month-old APOE3/3, APOE3/4, and APOE4/4 targeted replacement mice [119]. The results revealed that the entorhinal cortex is more susceptible to ApoE4 expression compared to the primary visual cortex, showing a decrease in diacylglycerol levels and an increase in ceramide and glycosylated sphingolipids. An increasing number of metabolomics studies on ApoE4 have highlighted its impact on glucose and lipid metabolism across various central nervous

system (CNS) cell types, as well as its differing effects in distinct brain regions. This suggests that ApoE4 may play diverse roles depending on the cell type and brain region. These findings underscore the need for more comprehensive metabolomics studies to fully understand the role of ApoE4 in AD and to advance therapeutic development for ApoE4-related AD. Several studies investigating ApoE4 are mostly based on the transgenic animal model [120]. Although human iPSC (induced pluripotent stem cells)-derived neural stem cells were applied in the recent preclinical studies to investigate the potential mechanism of ApoE4 [68], however, the lack of sensitive and efficient metabolomics screen platforms has limited the ability to simultaneously study the dozens of different metabolites that may be affected in the presence of ApoE4, resulting in ignorance of other related metabolites that may be involved in ApoE4 carriers.

1.3.3 Proteomics

Proteomics, like metabolomics and lipidomics, is a branch of 'omics' science that investigates the interactions, functions, and structures of proteins on a large scale. Proteomics is typically categorised into three types: expression proteomics, which quantitatively and qualitatively studies protein expression to identify differences between disease and control conditions; functional proteomics, which examines protein-protein interactions to elucidate cellular signalling pathways; and structural proteomics, which uses techniques like NMR spectroscopy and X-ray crystallography to determine the 3D structure of proteins.

Mass spectrometry (MS), particularly LC-MS/MS, is the most widely used tool in expression and functional proteomics [121]. This approach is applied through two primary workflows: bottom-up and top-down proteomics. In the bottom-up approach, proteins are digested into peptides (e.g., with trypsin), separated via liquid chromatography, and then analysed by MS to identify sequences and post-translational modifications. Conversely, the top-down method analyses intact proteins directly, preserving post-translational modifications and other structural features, although it can be less effective for low-solubility proteins. Both methods rely on measuring the mass-to-charge ratio of peptides or proteins and computational tools to decode amino

acid sequences and modification sites. In addition to these workflows, modern proteomics techniques have advanced to decipher not only protein sequences but also their 3D structures and protein-protein interactions, offering deeper insights into cellular processes and disease mechanisms.

Mass spectrometry-based proteomics has been widely applied in Alzheimer's disease research, utilising samples such as cerebral spinal fluid, serum, brain tissue, and patient-derived neuron cells [122]. Proteomics has been increasingly employed in Alzheimer's disease pathogenesis research, encompassing studies ranging from cellular pathology investigations to clinical biomarker characterization for the development of early Alzheimer's disease diagnosis and the differentiation of various types of the disease. A proteomics study by Yun Ju *et al*. suggests that the combined analysis of proteins in the brain, cerebral spinal fluid, and plasma could identify markers for sporadic and genetic forms of Alzheimer's disease [122]. Another cerebrospinal fluid proteomic study investigated proteins correlated with autosomal dominant AD and found that SMOC1 and SPON1 proteins were elevated in AD cerebrospinal fluid nearly 30 years before the onset of symptoms [123]. In addition, an integrated proteomics study conducted by Lenora Higginbotham *et al*. found that five protein panels, including synaptic, metabolic, glial-enrich myelination and immunity panels, could serve as cerebrospinal fluid biomarkers in asymptomatic and symptomatic Alzheimer's disease [124].

1.4 The advanced analytical methodologies apply for studying molecular alteration in Alzheimer's disease

Mass spectrometry (MS)-based analytical techniques are among the most widely used methods for investigating molecular alterations. A general mass spectrometry system comprises four key components: a sample inlet, an ion source, a mass analyser, and a mass detector, as illustrated in Figure 1.6. This figure also includes the setup for tandem mass spectrometry (MS/MS). In standard MS, a single mass analyser is used to separate ions based on their mass-to-charge (m/z) ratio. In contrast, MS/MS typically involves two mass analysers. The first mass analyser (MS1) selects and filters precursor ions within a defined m/z range. These selected ions are then transferred to a collision cell, where they undergo fragmentation, commonly via collision-induced dissociation (CID). The resulting fragment (product) ions are subsequently analysed by the second mass analyser (MS2), allowing for enhanced structural elucidation and improved specificity in complex mixtures.

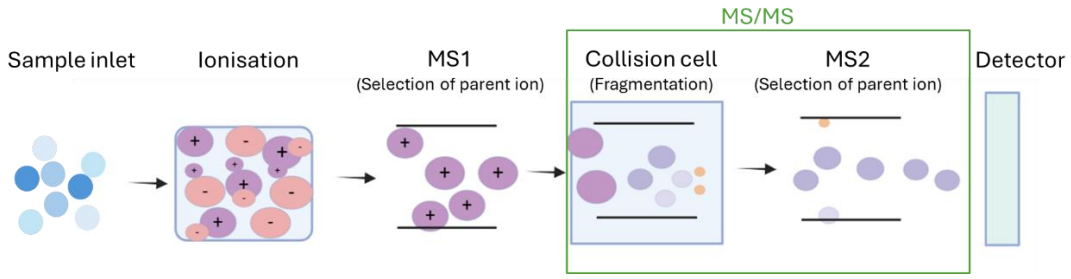

***Figure 1.6**. Basic components of a mass spectrometry instrument, including the sample inlet, ion source, mass analyser, and detector.*

For detecting molecular alterations affected by various disease conditions or treatments, the common approach can be divided into detecting small molecules, such as metabolites and lipids, and large molecules, such as proteins, DNA, and RNA. For high-throughput detection of small molecules as mentioned previous, the most common methods are liquid chromatography or gas chromatography coupled with tandem mass spectrometry (LC-MS/MS or GC-MS/MS), which are known as metabolomics and lipidomics studies, depending on the chemical properties of the extracted metabolites [125]. GC-MS is suitable for analysing volatile and semi-

volatile metabolites, while non-volatile substances require derivatisation before GC-MS detection. Currently, LC-MS/MS is the most widely used tool for metabolomics, as it does not require complex derivatisation during sample preparation, and enables the analysis of a wide variety of small molecules [126]. Similar to metabolomics, LC-MS/MS is also one of the most commonly used techniques in proteomics studies. However, it requires more complex sample preparation methods for protein extraction and digestion compared to other techniques.

1.4.1 Liquid-chromatography mass spectrometry

LC-MS is a highly sensitive and specific tool for the separation and identification of compounds [127]. It combines liquid chromatography (LC) to separate chemical species with high-resolution mass spectrometry (MS), which provides accurate molecular weight information for compound annotation and identification. The separation of molecules is based on their affinity for the mobile and stationary phases. The most used LC methods are reversed-phase liquid chromatography (RPLC) and hydrophilic interaction liquid chromatography (HILIC) [128]. RPLC employs hydrophobic stationary phases, such as C18, with a hydrophilic mobile phase, making it ideal for separating polar and medium-polar metabolites. In contrast, HILIC uses a hydrophilic stationary phase combined with a mobile phase containing a high concentration of organic solvent, allowing for the retention and separation of hydrophilic compounds in the sample.

The workflow of LC-MS/MS metabolomics could be summarised in four steps: sample preparation, separation and detection of metabolites, and data analysis [129]. Biological samples are quenched immediately to arrest metabolism, preventing stress-responsive metabolites produced from the sample preparation process. Next, extraction and enrichment are conducted for depleting proteins and other matrices to concentrate metabolites within samples. The mixed metabolites are then separated by the LC system, where the sample components are separated based on their interactions with the mobile and stationary phases. After separation, the liquid metabolites flow out from the LC column, are desolvated into the gas phase, and are then introduced into the mass spectrometer. For detection in a mass analyser, molecules or metabolites must first be charged through ionisation. Most LC-MS-based metabolomics studies

utilise electrospray ionisation (ESI) [130, 131], a widely used technique due to its compatibility with a broad range of metabolites. However, for metabolites that do not ionise efficiently with ESI, atmospheric-pressure chemical ionisation (APCI) serves as an alternative method, providing improved ionisation for less polar or non-polar compounds [132, 133].

It is generally accepted that metabolite quenching methods and extraction processes can cause the loss of metabolites [128, 134]. Furthermore, a large amount of sample material is required, typically at least 10 mg of tissue or 1 million cells, for LC-MS/MS-based metabolomics. Different sample extraction systems and solvents are required for various metabolites, such as methanol/water for polar and isopropanol/chloroform for non-polar metabolites, and the destructive structure of biological samples during processing may result in an incomplete metabolic profile [135]. Mostly, destructive sample preparation makes it unable to get the localisation of species in samples. Therefore, a method capable of detecting multiple metabolite species and mapping their localisation within biological samples could provide further insights into the effects of ApoE4 across different cell types. For the first time, we propose adopting the state-of-the-art Orbitrap Secondary Ion Mass Spectrometry (OrbiSIMS) as a metabolomics screening tool to address this issue.

OrbiSIMS is a hybrid SIMS instrument originally developed for metabolomics and drug delivery studies in biological samples, including single-cell analysis. It combines the high mass resolution of an Orbitrap MS with the low mass resolution but high imaging speed of a ToF MS. In the next section (1.5), the principles and structure of SIMS and OrbiSIMS will be introduced, along with a discussion of the different ionisation mechanisms of SIMS compared to other commonly used ionisation methods in LC-MS/MS.

1.4.2 Orbitrap Secondary ion mass spectrometry (OrbiSIMS)

Secondary ion mass spectrometry (SIMS) is a highly sensitive analytical technique capable of describing the chemical composition and distribution of a sample's surface, near surface, or bulk regions. It utilises various primary ion sources to impact the surface, generating secondary ions (positively charged and negatively charged ions),

neutrals and radicals through a collision cascade. Then these generated secondary ions are extracted and analysed by a mass analyser [136]. Positively charged ions are produced through protonation, while negatively charged ions are generated via deprotonation. The process also includes fragments or ions formed by rearrangement and the loss of neutral fragments. There are general two modes of SIMS analysis: static SIMS and dynamic SIMS, distinguished by the extent of damage to the sample surface caused by the primary ions [137, 138]. Static SIMS collects and analyses only the surface of sample, focusing on the top monolayer using a low primary ion dose. In contract, dynamic SIMS employs a higher energy ion beam that exceeds the 'static' limit, resulting in surface damage. This mode is used for depth profiling, allowing the collection of information from beneath the surface.

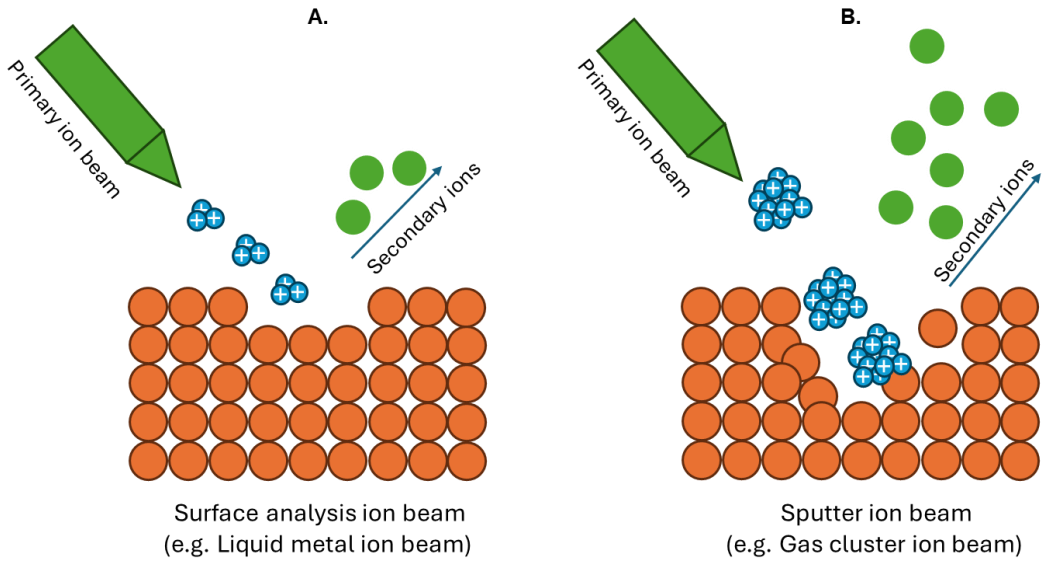

Figure 1.7. *The schematic illustrates the formation of secondary ions from a primary ion beam bombardment on the surface of samples: A) an example of a surface analysis ion beam, such as LMIG, and B) a sputter ion beam, such as GCIB.*

Commonly used SIMS Ion sources

Various primary ions are used in SIMS, including monatomic ions, small cluster ion beams (such as Ar^+, Cs^+, Au_3^+, Bi^+, Bi_3^+), as well as cluster ion beams like C_{60}^+, and larger clusters like GCIB Ar_{1000}^+. These primary ions have energy levels ranging from 5 to 40 keV. Early-stage SIMS analysis used monoatomic ion beams with high energy will cause the damage of organic and biological samples, therefore it is suitable for more hard inorganic sample analysis. To expand the application of SIMS biological samples, many cluster ion beams has been developed with lower energy such as C_{60}^+, Ar_n^+, $(H_2O)_n^+$ and $(CO_2)_n^+$ [136].

Liquid metal ion gun (LMIG) and gas cluster ion gun (GCIB) are the most used ion beam for SIMS instrument. Bismuth (Bi) is the most commonly used liquid metal ion gun (LMIG) due to its high sensitivity for surface analysis, achieving spatial resolutions of up to 100 nm in biological samples [139]. The small spot size (< 100 nm) of liquid metal ion beam makes it ideal for high-resolution imaging analysis, however, the small, high-energy ions can penetrate the surface cause sub-surface damage as well as producing considerable fragmentation, making depth profiling unreliable.

Argon is the most widely used gas cluster ion beam (GCIB) for the analysis of organic and biological materials because of its ability to produce larger fragment ions. The size of Argon gas clusters ranges from 1,000 to 6,000, depending on the goals of the analysis [140]. Gas cluster ion beam has the feature of high-energy (1-70 keV) and large spot size (1.2-250 um), making it ideal for sputtering organic matter with less fragmentation. The argon gas cluster ion beam is the most used GCIB in SIMS, due to its inert gas feature that forms clusters easily. The larger spot size of GCIB allows the distribution of ion energy across all constituent atoms/molecules, resulting in a very gentle sputtering effect and almost no damage to layers underneath. GCIB is also commonly used as a sputter ion beam and is frequently coupled with Bismuth LMIG for 3D imaging of biological samples.

In 2013, a novel water cluster ion beam was reported by the Vickerman group, demonstrating higher signals for protonated ions when using $(H_2O)_n^+$ ions, which produce larger fragments. The use of water clusters has been shown to enhance lipid

signals in brain tissue sections from a mouse model of Alzheimer's disease [141].

Ionisation

The ionisation process in SIMS involves bombarding the sample surface with primary ions to generate secondary ions. The energy of these primary ions ranges from 5 to 40 keV, which is significantly higher than that of traditional ionisation methods in mass spectrometry, such as electrospray ionisation, typically operating in the range of tens to hundreds of eV [142]. This traditional method is widely used in LC-MS/MS for metabolomics and proteomics studies.

As a result, the spectra produced in SIMS not only include ions typically generated by traditional ionisation methods, such as protonated and deprotonated ions in both polarities, but also a variety of other fragments that may arise from the breakage of molecular ions, ion rearrangements, recombination, and more [143]. Additionally, the intensity of fragment ions is often greater than that of molecular ions, and the choice of primary ions used can significantly influence both the formation and intensity of these fragments.

Besides the energy of the primary ions, another crucial factor impacting ionisation—particularly in the analysis of biological samples—is the matrix effect [144]. Since ionisation in SIMS occurs at the sample surface, the surface environment significantly affects the electron exchange process, influencing the formation and efficiency of secondary ions. These factors contribute to the challenges of applying SIMS in quantitative analysis, as the ion intensity within a sample is not necessarily proportional to its concentration.

Mass analyser in SIMS

Time-of-flight (ToF) mass spectrometry is the most employed mass analyser in SIMS. In ToF-SIMS instruments, pulsed primary ion beams bombard the surface of the samples, generating secondary ions. Subsequently, a pulsed extractor voltage is applied to extract these secondary ions into the mass detector. All extracted ions are accelerated forward with the same kinetic energy. Although all the ions possess the same energy, they exhibit different velocities due to variations in mass, resulting in separation based on the mass-to-charge ratio. Smaller ions travel faster and reach the

detector more quickly than larger ions.

Time of flight is the most widely used mass analyser in SIMS imaging analysis, due to its high-speed imaging ability, high spatial resolution, and good mass resolution. The application of ToF-SIMS extends from engineering, materials analysis to biological samples analysis [136, 145]. However, the limited mass resolving power and mass accuracy of ToF-SIMS restrict its application in biomedical research. This limitation arises because a large number of organic molecules within biological samples share similar elements, such as carbon (C), hydrogen (H), oxygen (O), nitrogen (N), phosphorus (P), and sulfur (S), making it challenging to accurately differentiate between them. As a result, the ability of ToF-SIMS to identify and quantify specific biomolecules in complex biological systems is constrained. To fill this gap of SIMS, a hybrid SIMS instrument - OrbiSIMS has been introduced by combining the high mass resolution of Orbitrap MS with the high-speed imaging of ToF MS (mass resolution >240,000 and 11,000 amu for the Orbitrap and the ToF, respectively) [146]. Orbitrap mass spectrometry separates ions based on their oscillation frequencies in an electric field [147]. When ions enter the Orbitrap, they are captured through electrodynamic squeezing. Once captured, the ions oscillate around a central electrode and between two outer electrodes. Different ions oscillate at distinct frequencies, which are then converted into a mass spectrum by an image current detector. For example, Figure 1.8 shows a comparison between ToF-SIMS and OrbiSIMS spectra. A peak in the ToF-SIMS spectrum may represent multiple peaks or ions that cannot be separated due to similar mass-to-charge ratios.

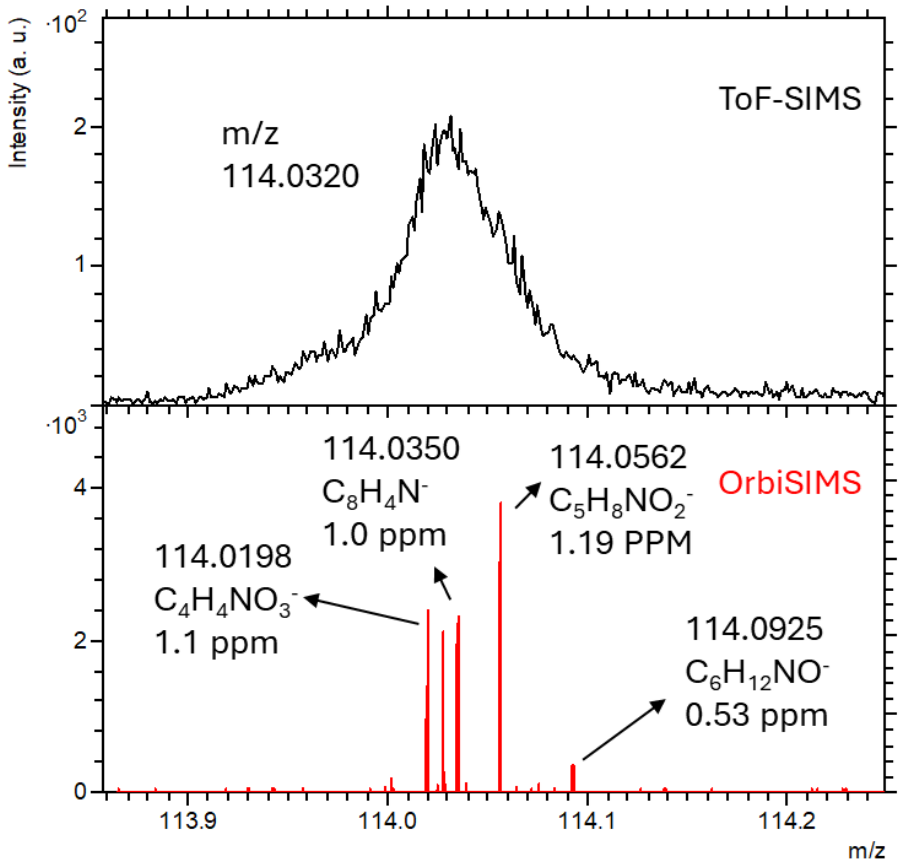

Figure 1.8. *A comparison example of ToF-SIMS and OrbiSIMS spectrum. For the peak m/z 114.0320 in ToF-SIMS data, it corresponds to multiple ions in OrbiSIMS spectrum. The ToF-SIMS spectrum was collected using the ToF-SIMS V instrument equipped with a 25 keV Bi_3^+ liquid metal ion gun (LMIG) for surface imaging analysis of test tissue homogenate samples. Subsequently, the OrbiSIMS depth profile analysis was performed on the same sample using a gas cluster ion beam (GCIB) with 20 keV Ar_{3000}^+ argon clusters and a 20 µm beam.*

OrbiSIMS integrates both ToF and Orbitrap analysers, with both sharing the same SIMS extraction optics, as illustrated in Figure 1.9a [146]. After extraction, ions can be directed into either the ToF or Orbitrap analyser by switching an electrostatic 90-degree deflector. For ions to be selected by the Orbitrap, they must possess an appropriate voltage and lower kinetic energy than what results from SIMS ionisation. Therefore, the sample target voltage and the collision cell gas pressure in the transfer system are key parameters for optimising OrbiSIMS. A methodology guide indicates that the optimum intensity for different chemistries requires specific sample target

voltages and collision cell gas pressures [148]. This suggests that by optimising these parameters for each targeted ion, it may be possible to enhance the signal for low-abundance ions. Furthermore, this approach could facilitate the differentiation of isobaric ions that have different structures but share the same mass-to-charge ratio. However, the relationship between these two parameters and the chemical structure remains unclear, necessitating further research to elucidate it.

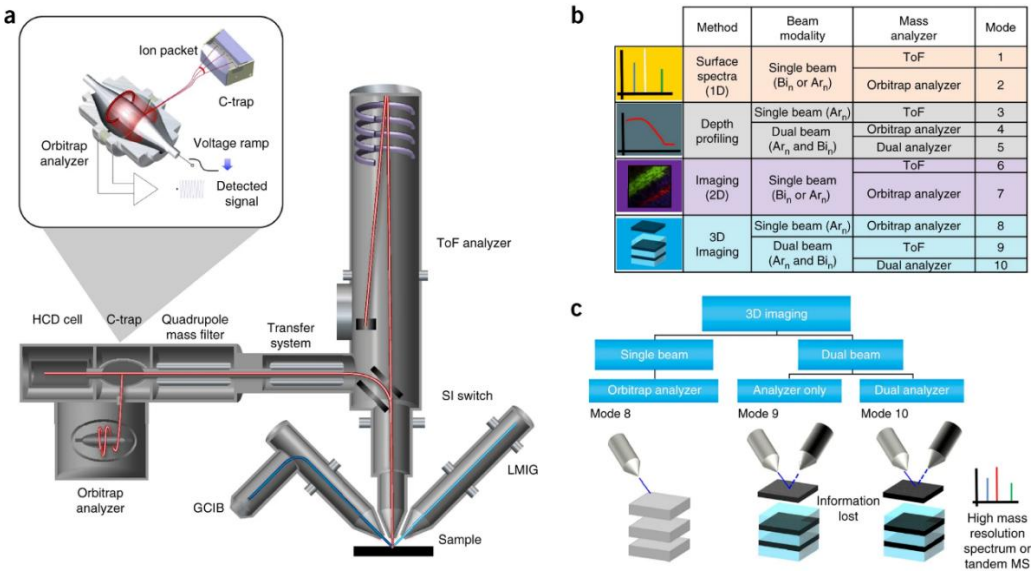

Figure 1. 9. *The schematic of OrbiSIMS.*

Passarelli, M., Pirkl, A., Moellers, R. et al. Nature Methods 14, 1175-1183 (2017).

With the development of the OrbiSIMS technique, label-free biomedical imaging can be conducted which allows us to detect multiple molecules (metabolites, lipids, peptides) from cells, tumours, and brain tissues, as well as get the localisation of them [146, 149, 150]. The figure below shows the schematic of 3D OrbiSIMS and the 10 modes of analysis methods by applying dual ion beam and dual analyser. For example, surface spectra analysis uses GCIB or bismuth liquid metal ion gun (Bi LMIG) compatible with ToF or Orbitrap analyser. And depth profiling by using GCIB with ToF or Orbitrap analyser.

In the present study, mode 4 was employed to perform depth profiling g of ApoE4-carrying H4 neuroglioma cells, using GCIB coupled with an Orbitrap mass analyser. This approach allowed us to characterise both the chemical metabolic alterations and vertical depth information.

Sample requirements

High vacuum conditions are essential for SIMS to minimise collisions between secondary ions and gas molecules, thereby enhancing signal-to-noise ratio and preserving sample surface integrity by preventing oxidation and contamination. Additionally, a high vacuum ensures that secondary ions are neither scattered nor neutralised by gas molecules during their transit [151].

Due to the requirement for ultra-high vacuum conditions in SIMS instruments, analysed samples need to be dehydrated before being placed in the OrbiSIMS instrument, or they can be frozen and analysed in a frozen-hydrated condition [152]. The most used methods for biological samples, such as tissue sections and cell samples, are freeze-drying and frozen hydration. For cell samples, a typical approach in LC-MS/MS metabolomics to halt metabolic activity is to use cold organic solvents, such as methanol or acetonitrile, to quench the cells, followed by cold solvent extraction. In SIMS analysis, cells are plunged into liquid nitrogen to freeze and stop metabolism before being transferred to a freeze dryer to remove any remaining water, or they can be kept in a frozen condition for analysis in a frozen-hydrated state.

Freeze-drying is the most widely used method for SIMS analysis due to its accessibility and lower cost compared to the frozen hydration approach, which requires longer cooling times and consumes a significant amount of liquid nitrogen. Recently, advancements in cryogenic SIMS have led to the integration of a Leica Vacuum Transfer system with the OrbiSIMS, enabling samples to be frozen and transferred to the instrument under vacuum conditions. Cryo-OrbiSIMS has been developed for analysing the molecular characteristics of bacterial biofilms and skin [153, 154]. Studies on biofilms have shown enhanced signal intensity for polar metabolites in frozen-hydrated samples, with significant increases also observed in skin samples, particularly for higher mass species. However, it remains unclear whether cryogenic sample preparation benefits all molecules or only specific species. Additionally, the frozen-hydrated method for cell samples has not yet been fully established.

Additionally, another sample preparation step is required for biological samples before freezing them: the removal of salt ions that may affect SIMS ionisation. Ammonium

formate has been reported to inhibit unwanted salt ions and enhance ion signal analysis [155]. A procedure involving washing cells with ammonium formate, followed by plunge-freezing in liquid nitrogen and freeze-drying, has been applied in studies on macrophages [149] and NR8383 cells [146].

Therefore, in the first chapter of this thesis, we conduct both sample preparation methods—freeze-drying and frozen hydration—to explore the most effective approach for H4 cells.

Data analysis challenge of OrbiSIMS

As mentioned in Chapter 1.5.2 on ionisation, the higher energy of the primary ion beam used in SIMS results in a complex spectrum that includes both molecular ions and fragments, which may form from ion rearrangements and recombination. Previous SIMS data assignments have primarily relied on ions validated and published by other researchers or on the analysis of standard samples. The formation of secondary ions in OrbiSIMS complicates ion assignment and data interpretation, making it challenging to manually assign possible chemical formulas. However, advances in data analysis software and machine learning have made the analysis of extensive OrbiSIMS datasets feasible. Edney *et al*. reported a chemical formula prediction program, simsMFP, which can assign and filter SIMS dataset based on their chemical composition [156]. SimsMFP uses the chemical formula prediction algorithms by matching accurate *m/z* values followed by heuristic filtering, as reported by Kind and Fiehn [157]. As well as provide the information the double bond equivalence (DBE) which will help to further category the chemistry. DBE is related to the degree of unsaturation from a predicted molecular formula by calculating the ratio of elements such as C, H, N, P and halogen atoms as indicated in figure 1.10. The DBE is contributed by a double bond or a ring system, and a benzene structure has DBE 4 due to 3 double bonds and a ring system.

A.

$$DBE = 1 + N_C + \left(\frac{N_N}{2} + \frac{N_P}{2}\right) - \left(\frac{N_H}{2} + \frac{N_X}{2}\right)$$

N_C = the number of carbon, N_H = the number of hydrogen, N_N = the number of nitrogen, N_P = number of phosphorus, N_X = number of halogen atoms (Br, Cl, I and F)

B.

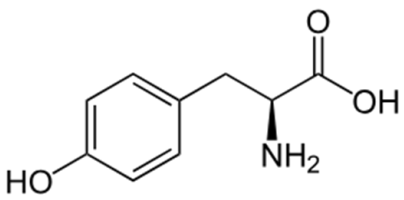

Tyrosine

$C_9H_{11}NO_3$

DBE = 5

C.

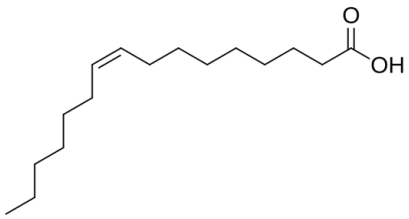

Palmitoleic acid (FA 16:1)

$C_{16}H_{30}O_2$

DBE = 2

Figure 1.10. *Illustration of double bond equivalence (DBE) value. A) The equation of calculating the DBE value, as reported by Edney et al [156]. B) An example of the DBE value for tyrosine, which is contributed by a benzene structure and a C=O from the carboxylic acid functional group. C) Palmitoleic acid, also known as fatty acid 16:1, has a DBE of 2, contributed by a C=C and a C=O.*

A key aspect of OrbiSIMS data analysis is that a deeper understanding of the chemical composition of samples allows for more accurate and quicker identification of molecules. The high mass accuracy of the Orbitrap can assign and annotate the chemical formulas of ions with a mass deviation within 2 ppm. Despite this high mass accuracy, it remains challenging to determine the unique chemical composition of each ion, necessitating additional algorithms to filter out uncorrelated assignments.

The application of OrbiSIMS in biological samples

OrbiSIMS has been applied for metabolomics analysis characterised by the high-resolution power of Orbitrap (> 240,000 at *m/z* 200) and high spatial resolution (< 200 nm) of TOF mass spectrometry [158]. Passarelli *et al.* imaged neurotransmitters in the mouse hippocampus section and putatively annotated 127 lipid species by 3D OrbiSIMS, which demonstrated the diverse component of the hippocampus and

different localisation of neurotransmitters in the brain section. OrbiSIMS has also been applied to investigate the drug distribution and cellular response of rat alveolar macrophage cells at the single cellular level [158]. The application of OrbiSIMS in brain tumour metabolomics was reported by Joris *et al.* key metabolites and related pathways of tumour relapse were identified from formalin-fixed paraffin-embedded tissue microarray samples [159]. Recently, the single-cell *in situ* metabolic analysis of 3D OrbiSIMS has been used for characterising macrophage subsets, leading to understanding the phenotype and immune response of different macrophage subsets M0, M1, and M2 [160]. Moreover, OrbiSIMS has been used in 3D hydrogel models for identifying biomarkers of aggressive Group 3 and SHH medulloblastoma [161]. Except for the application of OrbiSIMS in metabolomics, application on protein identification was proved by *de novo* peptide sequencing of 16 example proteins [162].

OrbiSIMS-based metabolomics provides an important platform for *in situ* metabolic analysis of tissue and cells with characteristics of minimal sample preparation (only need washing step and freeze-dried step), small sample size (minimum as single cell and hundreds of cells to get the enough signal), and rapid analysis time (a few minutes depend on the analysis mode), to increase the possibility of probing the functions of risk genes in different cell types. In addition, the imaging and depth profiling ability of SIMS enabling the localisation of molecules visualised in cellular level. Based on our established ApoE4-expressing H4 neuroglioma cells, the current work aims to perform OrbiSIMS depth profiling analysis for metabolic profiling and explore the underlying metabolic pathways involved in the ApoE4-carried AD cellular model.

1.5 Thesis aim

The aim of this project is to investigate ApoE4-mediated molecular alterations in H4 neuroglioma cells using OrbiSIMS and LC-MS/MS. For the metabolomics study, the screening capability of OrbiSIMS has been utilised and explored, leveraging its ability to detect a wide range of molecules in small samples with minimal preparation and reduced sample destruction compared to the standard LC-MS/MS method. To evaluate OrbiSIMS as a metabolomics tool, complementary LC-MS/MS metabolomics will be employed to validate its results. This project represents the first attempt to integrate and compare LC-MS/MS data with OrbiSIMS findings, showcasing the robust biological screening capabilities of OrbiSIMS for studying gene mutation-related disease states.

For the proteomics study, the LC-MS/MS technique has been applied to investigate the effects of ApoE4 on protein expression levels. Pathway and functional analysis tools will also be employed to integrate and interpret metabolomics results alongside proteomics data, providing a comprehensive understanding of ApoE4-mediated molecular changes.

Regarding OrbiSIMS sample preparation, two approaches for H4 neuroglioma cells—freeze-drying and frozen hydration—will be evaluated for SIMS analysis. The approach yielding a higher lipid signal will be selected to study the impact of ApoE4, given its role in lipid transport within cells. Subsequently, an ApoE4-overexpressing H4 cell model will be established and analysed using OrbiSIMS.

Chapter 2: Frozen hydrated vs freeze-dried analysis of H4 neuroglioma cells by OrbiSIMS

2.1 Chapter aims

To establish and evaluate the potential of OrbiSIMS for studying metabolomics in H4 neuroglioma cells, a proof-of-concept study was conducted, and two sample preparation methods for H4 cells were evaluated. As mentioned in Section 1.4.2 on sample requirements for OrbiSIMS, high vacuum conditions are crucial for ensuring the accuracy, sensitivity, and longevity of SIMS instrumentation. Consequently, specific sample preparation methods are required for biological samples to preserve their native structure as much as possible.

The most common approach is to fix samples chemically or cryogenically, followed by drying to remove residual water from the sample. Freeze-drying is the most widely used method for preparing biological samples, such as tissues or cells, due to its shorter preparation time, lower instrument, and laboratory requirements, and cost-effectiveness. The procedure involves plunge freezing in liquid nitrogen, followed by drying in a freeze dryer. A single-cell metabolic profiling study of macrophages using OrbiSIMS employed a freeze-drying approach to prepare macrophage cells [149]. This enabled differentiation of the metabolic signatures of various macrophage subsets from the OrbiSIMS data. However, there are concerns that drying protocols may lead to molecular redistribution and loss of information about volatile molecules during the drying process [149, 163].

Alternatively, the frozen-hydrated method has been applied in SIMS analysis, as it can preserve the native state of biological structures and has been shown to increase ion yields for polar molecules such as amino acids and peptides [164]. The cryogenic OrbiSIMS is equipped with a closed-loop liquid nitrogen circulation cooling system, which allows the load lock and main chamber to cool to -180 °C for extended periods, enabling the analysis of samples under cryogenic conditions. However, this process comes at the cost of significantly reduced analysis throughput.

To freeze samples and transfer them in vacuum conditions, a cryogenic vacuum transfer system has been introduced (the Leica EM-VCT 500), freezing samples at a consistent temperature (around -140 °C) and a pressure of 2.0 x 10^{-1} mbar [153, 165]. Newell *et al.* demonstrated that the cryogenic OrbiSIMS technique enhances the detection of a range of various biomolecules, including semi-volatiles in human fingerprints, plant leaves and Drosophila samples [165]. Zhang *et al.* analysed bacterial biofilms in a frozen hydrated state and observed a 10,000-fold increase in signal intensity for polar biomolecules, such as amino acids [153]. These findings strongly suggest that cryo-OrbiSIMS can effectively detect and image diverse types of biological samples in their native state with enhanced signal intensity. However, no studies have yet compared freeze-dried and frozen hydrated sample preparations in mammalian cells using OrbiSIMS, and it remains unclear whether cryogenic sample preparation benefits all molecules or only specific species. Additionally, given the high costs and longer analysis times associated with cryogenic OrbiSIMS, a comparison between freeze-dried and frozen-hydrated sample preparation methods for each sample type is recommended, before proceeding with further analysis.

This chapter presents a comparison of the efficacy of two sample preparation methodologies—freeze-drying and frozen hydration—for the analysis of H4 cells using OrbiSIMS. The aim is to expand knowledge in this field, particularly concerning the analysis of lipids and amino acids. Lipids have been identified as the most common secondary ions detected in OrbiSIMS analysis, while amino acids are suggested to exhibit a significant signal increase in frozen hydrated conditions [149, 153].

2.2 Methods

2.2.1 Cell sample preparation for OrbiSIMS

Neuroglioma cells H4 (ATCC® HTB-148TM) were obtained from the American Type Culture Collection (ATCC) and grown at 37 °C with 5 % CO_2 in Dulbecco's Modified Eagle's Medium supplemented with 10 % fetal bovine serum and 1 % penicillin-streptomycin. The H4 neuroglioma cells were seeded on glass slides merged in a complete culture medium for 24 h. After cells were adhered to glass slides, the media was discarded, and cells were washed three times using 150 mM ammonium formate solution.

Freeze dried H4: The freeze-dried sample preparation method is demonstrated in Figures 2.1A and B. The slides were frozen in liquid nitrogen and dried in a freeze-dryer for 48 hours. The cell slides were subsequently placed in a sealed container and stored at -80 ℃ until OrbiSIMS analysis. Prior to analysis, the sample slides were stabilised at room temperature for 1 hour, then were loaded into the OrbiSIMS instrument.

Frozen hydrated H4: The frozen hydrated sample preparation method is demonstrated in Figures 2.1A and C. Due to the size limitation of the cryo sample stage, the cell culture chamber slide needs to be cut into a 2 cm x 2 cm size. Three slides were subsequently sterilised and coated with poly-L-lysine. H4 neuroglioma cells have been growth for 24 hours on a pre-cut 8-well chamber slide for 24 h. Prior to OrbiSIMS analysis, the culture medium was removed, and the adherent cells were washed three times using a 150 mM ammonium formate solution to remove excess buffer containing salts. Then a pre-cut slide was attached onto a cryogenic sample stage with OCT. The metal sample stage was plunged freezing in liquid nitrogen by using Leica VCT system (below -140 °C), then transferred into pre-cooled OrbiSIMS system (below -140 °C) for depth profile analysis.

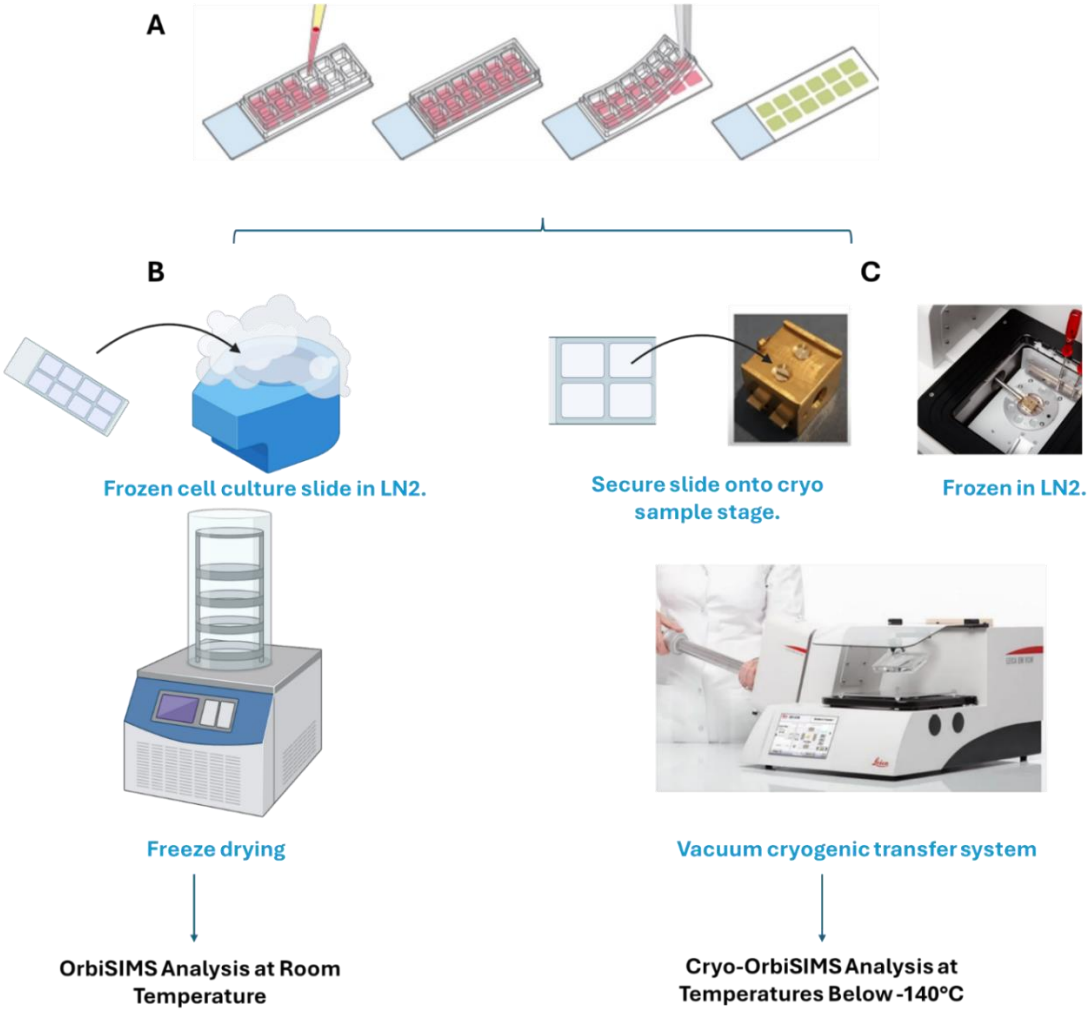

Figure 2. 1. *A workflow detailing the sample preparation for freeze drying and cryogenic OrbiSIMS analysis of H4 cells. A) H4 cells were plated and grown on a chamber slide with complete cell culture medium for 24 h, followed by removing medium and washing three times with ammonium formate. The chamber was removed before freezing the cells in liquid nitrogen (LN_2). B) Freeze drying process: The cell culture slide was plunge-frozen by using tweezers to immerse it into LN_2, then placed into a freeze dryer to dry at a temperature below -140 °C for 48 h. The freeze-dried H4 cells were then transferred to the OrbiSIMS instrument for analysis at room temperature. C) Frozen hydrated samples preparation process: The pre-cut slide was secured and fixed onto a cyro sample stage with OCT, then frozen with LN_2 in Leica VCT system. The frozen hydrated H4 cells were transferred into the VCT arm under vacuum conditions and subsequently attached to the pre-cooled OrbiSIMS instrument (below -140 °C) for further analysis.*

2.2.2 OrbiSIMS experimental methods

OrbiSIMS analysis was performed on a Hybrid SIMS instrument from IONTOF GmbH (Münster, Germany). The Orbitrap analyser was calibrated using silver clusters of a silver sample plate, following the method described by Passarelli *et al.* [158]. For calibration, liquid metal ion gun with Bi_3^+ clusters as primary ion species were used in spectrometry mode together with the ThermoFisher Tune software. For the subsequent measurements the following parameters were employed. The gas cluster ion beam (GCIB) was used with 20 keV Ar_{3000}^+ argon clusters with 20 µm beam diameter as primary ion source for sputtering of cell samples. Mass spectra were recorded in full-MS scan in the range of *m/z* 75 - 1125 in negative polarity.

For freeze dried condition, samples were analysed at room temperature across a 300 × 300 µm² area using random raster mode with crater size 384.6 × 384.6 µm² and mass resolving power of 240,000 at *m/z* 200. Cycle time was set to 200 µs and duty cycle to 4.4 %. Ar_{3000}^+ primary ion clusters were used with a target current of approximately 200 pA with charge compensation performed using a low energy (21 eV) electron flood gun. Argon gas flooding was utilised as well to aid with charge compensation, which led to a pressure of 9.0×10^{-7} mbar in the main chamber. Maximum injection time was set to 500 ms. The OrbiSIMS collision cell pressure was set to 6.15×10^{-2} mbar, and the target potential was set at -278 V during the duration of the experiment. Three separative areas were analysed on each sample, and each measurement lasted 300 scans.

For cryo-OrbiSIMS analysis, a liquid nitrogen circulation cooling system was used to cool the load lock and main chamber to at least -140 °C before transferring samples into OrbiSIMS instruments. All measurement set up parameters are the same as the parameters applied in room temperature OrbiSIMS analysis. The OrbiSIMS collision cell pressure was set to 5.6×10^{-2} mbar, and the target potential was set at -151 V. Three separative areas were analysed on each sample, and each measurement lasted 300 scans.

2.2.3 Data analysis and identification and annotation of metabolites

OrbiSIMS data acquisition and analysis were performed using SurfaceLab7 (IONTOF GmbH). Firstly, a peak search was performed on each raw data, a minimum counts threshold 3000 was set by visual inspection of the spectra that distinguished it from a noise peak. Ions extracted from the spectrum are assigned by applying elemental restrictions with mass deviation < 2 ppm for ions > *m/z* 95 and 5 ppm for ions < *m/z* 95 for molecular formula prediction. Which is conducted by using software simsMFP (SimsMFP is a Matlab-based script developed by Edney *et al. [156]*, especially for chemical filtering of the OrbiSIMS dataset): Lipid search (C_{1-230}, H_{3-130}, N_{0-2}, O_{0-20}, P_{0-2}, S_{0-1}), other amino acids search (C_{3-30}, H_{1-40}, N_{0-10}, O_{0-25}, S_{0-2}). Subsequentially, matching the chemical formula with LIPID MAPS (https://www.lipidmaps.org/databases/lmsd/overview).

A LipidMaps assignment script was used for lipid identification, incorporating 35,784 lipids from the Lipid Maps database. Those include FA, ST, CAR, LPA, LPC, LPE, LPI, BMP, Hex, PG, PC, PE, PS, DG, TG, HexCer, CerP, for example, *m/z* 255.2332 was assigned the chemical formula $C_{16}H_{31}O_2^-$, with a mass deviation of 0.96 ppm. This formula corresponds to the deprotonated ion of FA 16:0. In contrast, *m/z* 288.5239 was assigned the predicted formula $C_{45}H_{75}NO_8P^-$ (mass deviation: 0.41 ppm), which could correspond to several isobaric lipid species, including PC 37:7, PC O-37:8;O, PE 40:7, or PE O-40:8;O.

Statistical analysis

Intensity of each ion normalised to total ion intensity was used for Scatter plot and *t*-test analysis. For the *t*-tests, the ion intensity was considered to be significantly different between freeze dried and frozen hydrated samples with adjusted *p*-value <=0.05 and a fold change of >=2. Volcano plot was used to visualize the *t*-test analyses.

2.3 Results and Discussion

2.3.1. Freeze-Dried and Frozen-Hydrated Sample Preparation of H4 Neuroglioma Cells

As shown in Figure 2.1, H4 neuroglioma cells were plated and grown on a chamber slide for 24 hours to allow adherence to the slide. The medium was then removed, and the cell surface was washed three times with ammonium formate to eliminate salts from the culture medium and prevent interference from salt ions. The samples were then plunge-frozen in liquid nitrogen, followed by preparation using both freeze-drying and frozen-hydrated approaches to preserve intracellular water. The freeze-dried samples were analysed by OrbiSIMS at room temperature, while the frozen-hydrated samples were analysed by cryogenic OrbiSIMS at temperatures below -140 °C.

OrbiSIMS analysis at room temperature was conducted without a cooling system. The samples were loaded into the instrument's load lock, where the pressure was pumped down to below 5×10^{-6} mbar before being transferred to the main analysis chamber, which operated at a pressure of approximately 7×10^{-9} mbar. For cryogenic OrbiSIMS measurements, a closed-loop liquid nitrogen circulation cooling system was activated in advance to lower the temperature of the main chamber and load lock to below -140 °C. The H4 samples were then frozen and transferred using the Leica EM VCT500, which allowed the samples to be stored and transported under low-temperature (below -140 °C) and vacuum conditions (2×10^{-1} mbar). Throughout the transfer and cryogenic OrbiSIMS procedures, the temperatures of the VCT and the instrument were carefully monitored to prevent sample melting due to temperature increases. If a rise in temperature was detected, the liquid nitrogen (LN_2) reservoir was refilled to maintain the required low temperatures.

2.3.2. Lipid ions show higher signal intensity in freeze-dried H4 cells compared to frozen-hydrated H4 cells.

The OrbiSIMS data acquired for freeze-dried and frozen hydrated H4 cells are shown as inverted overlaid spectra in Figures 2.2 A and B for *m/z* = 100 – 500 and 500 – 1000 respectively. These two datasets show the different ion yield under different sample preparations, especially for the ions in the region of *m/z* 500 - 850. This indicates that the secondary ions produced from H4 cells are affected by the retention of water. The molecular or chemical changes might also be impacted under frozen hydrated conditions compared to freeze-dried cells.

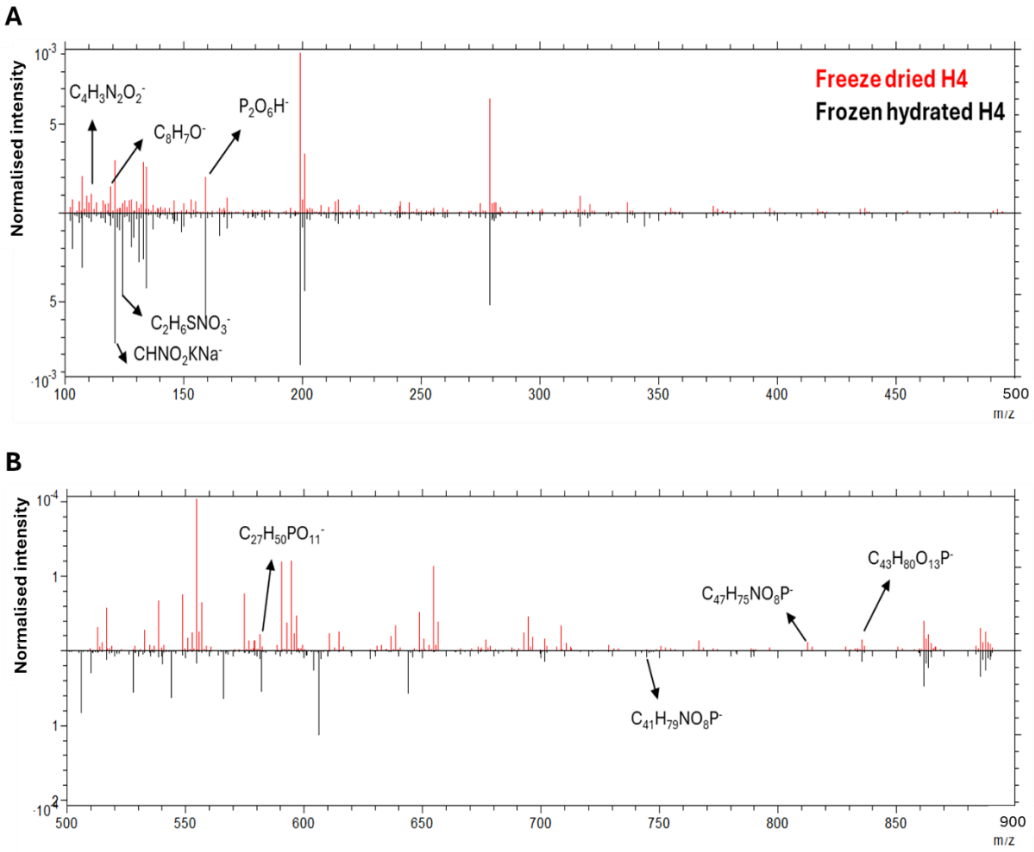

***Figure 2.2**. Inverted overlaid OrbiSIMS spectra for freeze dried H4 and frozen hydrated H4 cells. A) The overlaid OrbiSIMS spectra at the mass range of m/z 100-500. The accurate mass and mass deviation of assigned ions are as follows: $C_4H_3N_2O_2^-$ (m/z 111.0201, 0.5 ppm), $C_8H_7O^-$ (m/z 119.0502, 0.0 ppm), $CHNO_2KNa^-$ (m/z 120.9527, -0.5 ppm), $C_2H_6SNO_3^-$ (m/z 124.0074, -0.1 ppm), $P_2O_6H^-$ (m/z 158.9254, 0.0 ppm). B) The overlaid OrbiSIMS spectra at the mass range of m/z*

500-900. The accurate mass and mass deviation of assigned ions are as follows: $C_{27}H_{50}PO_{11}^-$ (m/z 581.3099, 0.4 ppm), $C_{41}H_{79}NO_8P^-$ (m/z 744.5555, 0.8 ppm), $C_{47}H_{75}NO_8P^-$ (m/z 812.5231, -0.6 ppm), $C_{43}H_{80}O_{13}P^-$ (m/z 835.5343, 0.1 ppm).

To further investigate the species changes between these two sample preparation methods for H4 cells, the accurate mass value of each peak was exported. Next, a chemical filtering method, the SIMS-Molecular Formula Prediction tool (simsMFP) (for a detailed introduction to simsMFP, please refer to Section 1.4.2 on Data Analysis of OrbiSIMS), was used to predict the chemical formulae of each secondary ion. This tool calculates possible chemical formulas based on elemental restrictions, enabling the categorisation of various chemistries. Here, lipid and amino acid chemistries were selected to evaluate the freeze-drying and frozen-hydration sample preparation methods for H4 cells.

Fatty acids are composed of a hydrocarbon chain with one terminal carboxyl group (COOH). *De novo* biosynthesis of phospholipids begins with the combination of glycerol-3-phosphate with fatty acid chains (as shown in Figure 2.3 A), followed by linking hydrophilic lipid head groups such as serine, ethanolamine, glycerol, inositol, and choline to generate phosphatidylserine (PS), phosphatidylethanolamine (PE), phosphatidylglycerol (PG), phosphatidylinositol (PI) and phosphatidylcholine (PC) (Figure 2.3) [166, 167]. According to the unique chemical structure of lipids, as shown in Figure 2.3, fatty acids contain only carbon, hydrogen, and oxygen, with two oxygen atoms due to the carboxyl group. When fatty acid chains link with glycerol-3-phosphate to form phosphoglycerolipids, an additional phosphorus atom and four oxygen atoms are introduced. Therefore, based on the characteristics of these compounds, elemental restrictions can be applied for chemical filtering of possible assignments. For example, saturated fatty acids (FA *n*:0) are assigned as $C_nH_{2n-1}O_2^-$, while unsaturated fatty acids (FA *n*:x) are $C_nH_{2n-2x-1}O_2^-$. Glycerophospholipids like PC, PE and PS contain the elements CHNOP, while PI and PG only contain CHOP.

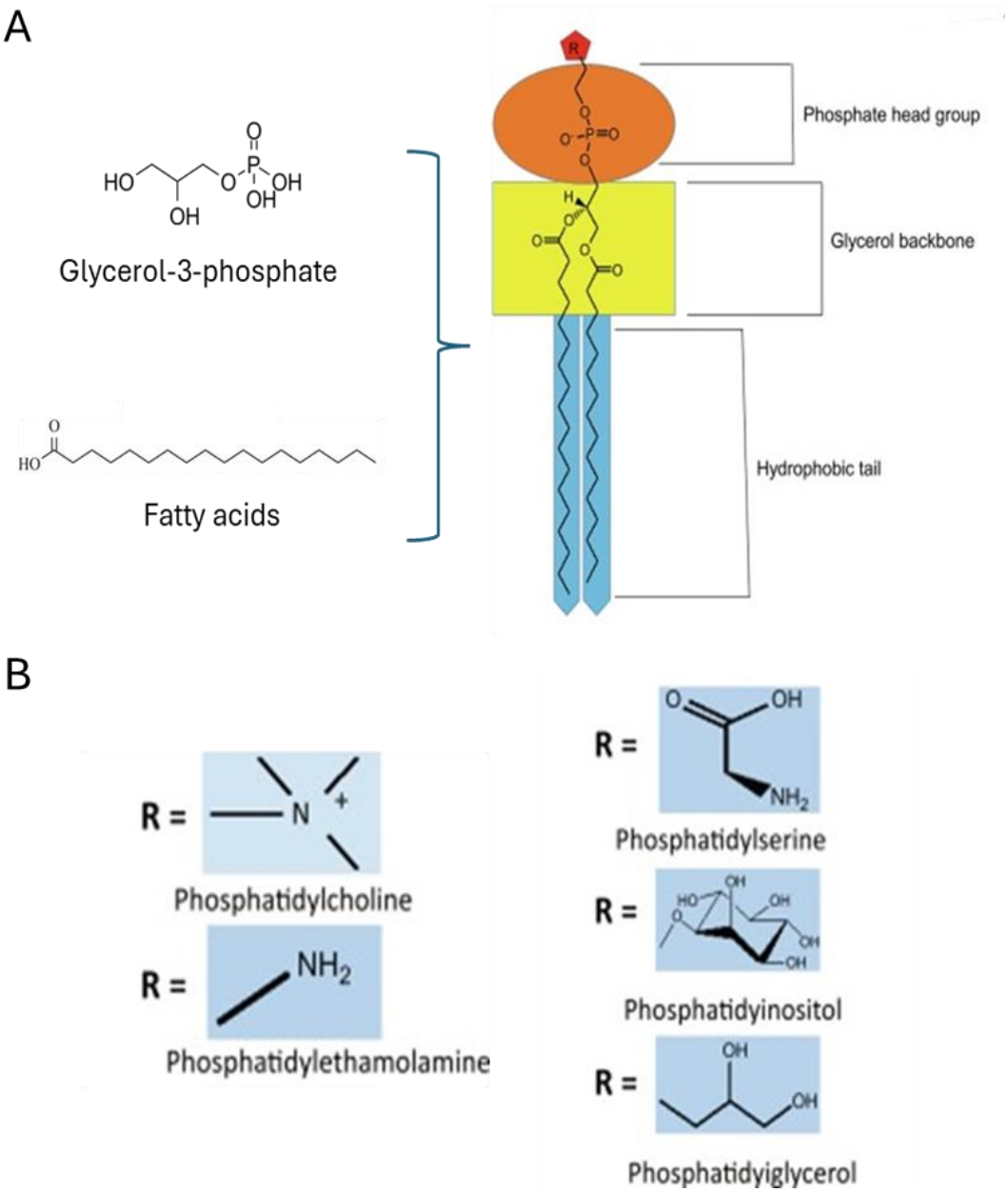

Figure 2.3. *The structure of glycerophospholipids [168]: A) The biosynthesis of glycerophospholipids begins with glycerol as the backbone, which is then linked to fatty acid chains to form the hydrophobic tail and a hydrophilic phosphate head group. B) The phosphate head group is further linked to choline, ethanolamine, serine, inositol, or glycerol.*

The elemental restriction applied for general lipid filtering are: C_{1-230}, H_{3-130}, N_{0-2}, O_{0-20}, P_{0-2}, S_{0-1}. These were selected based on the LipidMaps database to cover all reasonable lipid chemical formulas within the mass range of *m/z* 75-1200, while also limiting the analysis time in the simsMFP program, as broader elemental restrictions increase the required processing time. This enabled the assignment of lipid peaks with a mass deviation of < 2 ppm for *m/z* > 95 and < 5 ppm for *m/z* < 95. By applying elemental restrictions for lipid filtering, a peak list consisting of 2,566 ions generated 2,214 predicted formulas. The assigned chemical formulas were then matched with the LipidMaps database to search for lipid assignments, resulting in the identification of a total of 99 lipids from freeze-dried and frozen hydrated H4 cells. Table 2.1 below lists the details about the accurate mass and assigned lipid names. The annotated lipid ions listed in Table 2.1 all correspond to deprotonated ions $[M-H]^-$.

For OrbiSIMS secondary ions, only chemical formula can be assigned by calculating accurate mass. However, due to the complexity of lipid structures, specific lipid assignments cannot be achieved based solely on MS data. For example, for *m/z* 673.4823, the assigned formula is $C_{37}H_{70}O_8P^-$ which could correspond to any lipid from LPA 34:2;O/LPG O-31:3/PA 34:1/PA O-34:2;O.

Table 2.1. The peak list of lipids assigned in H4 cells.

Mass	Assignment	Formula	Deviation (ppm)
227.2019	FA 14:0 $[M-H]^-$	$C_{14}H_{27}O_2^-$	1.08
241.2177	FA 15:0 $[M-H]^-$	$C_{15}H_{29}O_2^-$	1.64
253.2177	FA 16:1 $[M-H]^-$	$C_{16}H_{29}O_2^-$	1.56
301.2174	FA 20:5/ST 20:2;O2 $[M-H]^-$	$C_{20}H_{29}O_2^-$	0.32
255.2332	FA 16:0 $[M-H]^-$	$C_{16}H_{31}O_2^-$	0.96
267.2334	FA 17:1 $[M-H]^-$	$C_{17}H_{31}O_2^-$	1.67
279.2331	FA 18:2 $[M-H]^-$	$C_{18}H_{31}O_2^-$	0.52
303.2332	FA 20:4/ST 20:1;O2 $[M-H]^-$	$C_{20}H_{31}O_2^-$	0.81
327.2330	FA 22:6/ST 22:3;O2 $[M-H]^-$	$C_{22}H_{31}O_2^-$	0.14
269.2491	FA 17:0 $[M-H]^-$	$C_{17}H_{33}O_2^-$	1.84
281.2490	FA 18:1 $[M-H]^-$	$C_{18}H_{33}O_2^-$	1.41

305.2489	FA 20:3/ST 20:0;O2 [M-H]$^-$	$C_{20}H_{33}O_2^-$	0.97
329.2488	FA 22:5/ST 22:2;O2 [M-H]$^-$	$C_{22}H_{33}O_2^-$	0.60
392.2292	CAR 11:0;O4 [M-H]$^-$	$C_{18}H_{34}NO_8^-$	0.53
389.2100	LPA O-16:3 [M-H]$^-$	$C_{19}H_{34}O_6P^-$	0.39
283.2646	FA 18:0 [M-H]$^-$	$C_{18}H_{35}O_2^-$	1.22
295.2645	FA 19:1 [M-H]$^-$	$C_{19}H_{35}O_2^-$	0.83
307.2645	FA 20:2 [M-H]$^-$	$C_{20}H_{35}O_2^-$	0.80
331.2647	FA 22:4/ST 22:1;O2 [M-H]$^-$	$C_{22}H_{35}O_2^-$	1.35
391.2261	LPA O-16:2 [M-H]$^-$	$C_{19}H_{36}O_6P^-$	1.53
418.2450	CAR 13:1;O4 [M-H]$^-$	$C_{20}H_{36}NO_8^-$	0.85
309.2803	FA 20:1 [M-H]$^-$	$C_{20}H_{37}O_2^-$	1.28
409.2366	LPA 16:0/LPA O-16:1;O [M-H]$^-$	$C_{19}H_{38}O_7P^-$	1.31
420.2607	CAR 13:0;O4 [M-H]$^-$	$C_{20}H_{38}NO_8^-$	0.97
417.2414	LPA O-18:3 [M-H]$^-$	$C_{21}H_{38}O_6P^-$	0.60
419.2574	LPA O-18:2 [M-H]$^-$	$C_{21}H_{40}O_6P^-$	1.43
435.2519	LPA 18:1/LPA O-18:2;O [M-H]$^-$	$C_{21}H_{40}O_7P^-$	0.43
437.2678	LPA 18:0/LPA O-18:1;O [M-H]$^-$	$C_{21}H_{42}O_7P^-$	1.00
436.2838	LPC O-13:1/LPE O-16:1 [M-H]$^-$	$C_{21}H_{43}NO_6P^-$	1.03
597.3059	ST 28:6;O3;GlCA/ST 28:7;O4;Hex [M-H]$^-$	$C_{34}H_{45}O_9^-$	-1.69
553.2790	BMP 19:1;O/LPI O-16:2 [M-H]$^-$	$C_{25}H_{46}O_{11}P^-$	1.22
579.2946	BMP 21:2;O/LPI O-18:3/PG 21:2;O [M-H]$^-$	$C_{27}H_{48}O_{11}P^-$	1.08
581.3107	BMP 21:1;O/LPI O-18:2/PG 21:1;O [M-H]$^-$	$C_{27}H_{50}O_{11}P^-$	1.85
599.3211	LPI 18:0/LPI O-18:1;O [M-H]$^-$	$C_{27}H_{52}O_{12}P^-$	1.52
699.4980	DG 43:11/DG O-43:12;O/TG O-43:11 [M-H]$^-$	$C_{46}H_{67}O_5^-$	-2.00
674.4854	HexCer 30:1;O4 [M-H]$^-$	$C_{36}H_{68}NO_{10}^-$	0.78
701.5140	DG 43:10/DG O-43:11;O/TG O-43:10 [M-H]$^-$	$C_{46}H_{69}O_5^-$	-1.50
673.4823	LPA 34:2;O/LPG O-31:3/PA 34:1/PA O-34:2;O [M-H]$^-$	$C_{37}H_{70}O_8P^-$	1.37

747.5198	DG 44:10;O2/TG 44:9;O/TG O-44:10;O2 $[M-H]^-$	$C_{47}H_{71}O_7^-$	-0.98
868.4769	PS 42:11;O $[M-H]^-$	$C_{48}H_{71}NO_{11}P^-$	-0.14
702.5165	HexCer 32:1;O4 $[M-H]^-$	$C_{38}H_{72}NO_{10}^-$	0.47
699.4980	LPG O-33:4/PA 36:2/PA O-36:3;O $[M-H]^-$	$C_{39}H_{72}O_8P^-$	1.39
850.4794	Hex2Cer 29:3;O6 $[M-H]^-$	$C_{41}H_{72}NO_{17}^-$	-1.38
834.5063	PE 44:12 $[M-H]^-$	$C_{49}H_{73}NO_8P^-$	-1.95
701.5140	LPG O-33:3/PA 36:1/PA O-36:2;O $[M-H]^-$	$C_{39}H_{74}O_8P^-$	1.88
852.4781	SHexCer 35:3;O6 $[M-H]^-$	$C_{41}H_{74}NO_{15}S^-$	-0.43
872.5002	Hex2Cer 32:5;O5 $[M-H]^-$	$C_{44}H_{74}NO_{16}^-$	-1.28
788.5239	PC 37:7/PC O-37:8;O/PE 40:7/PE O-40:8;O $[M-H]^-$	$C_{45}H_{75}NO_8P^-$	0.41
812.5234	PC 39:9/PC O-39:10;O/PE 42:9/PE O-42:10;O $[M-H]^-$	$C_{47}H_{75}NO_8P^-$	-0.22
830.4949	SHexCer 33:0;O6 $[M-H]^-$	$C_{39}H_{76}NO_{15}S^-$	0.94
834.5225	Hex2Cer 30:2;O4 $[M-H]^-$	$C_{42}H_{76}NO_{15}^-$	0.54
774.5520	HexCer 39:6;O3 $[M-H]^-$	$C_{45}H_{76}NO_9^-$	-0.72
790.5471	HexCer 39:6;O4 $[M-H]^-$	$C_{45}H_{76}NO_{10}^-$	-0.47
814.5085	PI-Cer 33:0;O5 $[M-H]^-$	$C_{39}H_{77}NO_{14}P^-$	-0.27
710.5496	CerP 41:3;O2/LPC O-33:4 $[M-H]^-$	$C_{41}H_{77}NO_6P^-$	0.28
774.5289	CerP 41:3;O6/PS 35:1/PS O-35:2;O $[M-H]^-$	$C_{41}H_{77}NO_{10}P^-$	-0.21
712.5727	CAR 34:1;O4/HexCer 35:1;O2 $[M-H]^-$	$C_{41}H_{78}NO_8^-$	-0.83
836.5384	Hex2Cer 30:1;O4 $[M-H]^-$	$C_{42}H_{78}NO_{15}^-$	0.84
833.5190	LPI 34:3;O/PI 34:2/PI O-34:3;O $[M-H]^-$	$C_{43}H_{78}O_{13}P^-$	0.53
860.5388	Hex2Cer 32:3;O4 $[M-H]^-$	$C_{44}H_{78}NO_{15}^-$	1.28
857.5202	PI 36:4/PI O-36:5;O $[M-H]^-$	$C_{45}H_{78}O_{13}P^-$	1.92
884.5377	Hex2Cer 34:5;O4 $[M-H]^-$	$C_{46}H_{78}NO_{15}^-$	0.00

744.5563	CerP 41:2;O4/LPC 33:2;O/PC 33:1/PC O-33:2;O/PE 36:1/PE O-36:2;O [M-H]$^-$	$C_{41}H_{79}NO_8P^-$	1.91
756.5561	CerP 42:3;O4/LPC 34:3;O/PC 34:2/PC O-34:3;O/PE 37:2/PE O-37:3;O [M-H]$^-$	$C_{42}H_{79}NO_8P^-$	1.61
788.5448	CerP 42:3;O6/PS 36:1/PS O-36:2;O [M-H]$^-$	$C_{42}H_{79}NO_{10}P^-$	0.12
730.5838	HexCer 35:0;O3 [M-H]$^-$	$C_{41}H_{80}NO_9^-$	-0.08
835.5344	LPI 34:2;O/PI 34:1/PI O-34:2;O [M-H]$^-$	$C_{43}H_{80}O_{13}P^-$	0.23
862.5544	Hex2Cer 32:2;O4 [M-H]$^-$	$C_{44}H_{80}NO_{15}^-$	1.22
859.5353	PI 36:3/PI O-36:4;O [M-H]$^-$	$C_{45}H_{80}O_{13}P^-$	1.27
886.5549	Hex2Cer 34:4;O4 [M-H]$^-$	$C_{46}H_{80}NO_{15}^-$	1.75
883.5344	PI 38:5/PI O-38:6;O [M-H]$^-$	$C_{47}H_{80}O_{13}P^-$	0.22
758.5698	CerP 42:2;O4/LPC 34:2;O/PC 34:1/PC O-34:2;O/PE 37:1/PE O-37:2;O [M-H]$^-$	$C_{42}H_{81}NO_8P^-$	-0.96
864.5702	Hex2Cer 32:1;O4 [M-H]$^-$	$C_{44}H_{82}NO_{15}^-$	1.39
861.5508	PI 36:2/PI O-36:3;O [M-H]$^-$	$C_{45}H_{82}O_{13}P^-$	1.10
873.5507	PI 37:3/PI O-37:4;O [M-H]$^-$	$C_{46}H_{82}O_{13}P^-$	0.97
888.5700	Hex2Cer 34:3;O4 [M-H]$^-$	$C_{46}H_{82}NO_{15}^-$	1.13
885.5516	PI 38:4/PI O-38:5;O [M-H]$^-$	$C_{47}H_{82}O_{13}P^-$	1.97
832.5931	HexCer 42:6;O4 [M-H]$^-$	$C_{48}H_{82}NO_{10}^-$	-1.59
912.5708	Hex2Cer 36:5;O4 [M-H]$^-$	$C_{48}H_{82}NO_{15}^-$	1.97
909.5510	PI 40:6/PI O-40:7;O [M-H]$^-$	$C_{49}H_{82}O_{13}P^-$	1.26
865.5739	PA 49:10/PA O-49:11;O [M-H]$^-$	$C_{52}H_{82}O_8P^-$	-1.59
863.5665	PI 36:1/PI O-36:2;O [M-H]$^-$	$C_{45}H_{84}O_{13}P^-$	1.15
875.5670	PI 37:2/PI O-37:3;O [M-H]$^-$	$C_{46}H_{84}O_{13}P^-$	1.71
890.5849	Hex2Cer 34:2;O4 [M-H]$^-$	$C_{46}H_{84}NO_{15}^-$	0.28
887.5669	PI 38:3/PI O-38:4;O [M-H]$^-$	$C_{47}H_{84}O_{13}P^-$	1.57
914.5861	Hex2Cer 36:4;O4 [M-H]$^-$	$C_{48}H_{84}NO_{15}^-$	1.59
912.5708	SHexCer 39:1;O6 [M-H]$^-$	$C_{45}H_{86}NO_{15}S^-$	-1.72

860.6117	Hex2Cer 34:1;O2[M-H]$^-$	$C_{46}H_{86}NO_{13}^-$	1.43
889.5819	PI 38:2/PI O-38:3;O [M-H]$^-$	$C_{47}H_{86}O_{13}P^-$	0.84
901.5828	PI 39:3/PI O-39:4;O [M-H]$^-$	$C_{48}H_{86}O_{13}P^-$	1.82
832.6060	CerP 45:2;O6/PS 39:0/PS O-39:1;O [M-H]$^-$	$C_{45}H_{87}NO_{10}P^-$	-1.57
710.6833	Cer 48:4;O [M-H]$^-$	$C_{48}H_{88}NO_2^-$	1.75
712.6968	Cer 48:3;O [M-H]$^-$	$C_{48}H_{90}NO_2^-$	-1.27
1063.6910	Hex(2)-HexNAC-Cer 34:1;O2/Hex-HexNAC-Cer 34:1;O2 [M-H]$^-$	$C_{54}H_{99}N_2O_{18}^-$	1.09
1064.6942	PS 56:11;O [M-H]$^-$	$C_{62}H_{99}NO_{11}P^-$	-1.81

Following lipid assignments, the normalised intensity of lipids was plotted with freeze-dried samples on the x-axis and frozen hydrated samples on the y-axis (as shown in Figure 2.4A). The plots in the blue area indicate higher intensity in the frozen-hydrated condition, while those in the orange area show higher intensity in the freeze-dried condition. In Figure 2,4A, more lipid plots are scattered in the orange area, suggesting that these lipids are more intense in the freeze-dried condition. To further explore the statistical differences between the two conditions, three replicates for each group were analysed. A t-test was performed, and the results, along with the fold change of lipids in the freeze-dried compared to the frozen hydrated state, were visualised using a volcano plot created with MetaboAnalyst [169]. In the comparison of freeze dried H4 and frozen hydrated H4, the majority of lipids have higher intensity in the freeze-dried samples. The volcano plot shows that 45 out of 99 (45.5%) total assigned lipids exhibited a statistically significant increase in freeze-dried H4 cells. This indicates that freeze-dried sample preparation of H4 cells is optimal for lipid detection in OrbiSIMS compared to frozen hydrated method.

Given the importance of ApoE4 in lipid transport and metabolism, the freeze-dried sample preparation, which shows higher lipid signals, is better suited for studying the effects of ApoE4 on lipid metabolism in H4 neuroglioma cells compared to the frozen-hydrated condition. However, aside from the effects on lipid ions, it remains unclear whether freeze-dried and frozen-hydrated preparations affect other types of molecules in H4 cells. Therefore, an evaluation of additional molecules, beyond lipid ions, is

necessary to assess these two approaches in H4 neuroglioma cells.

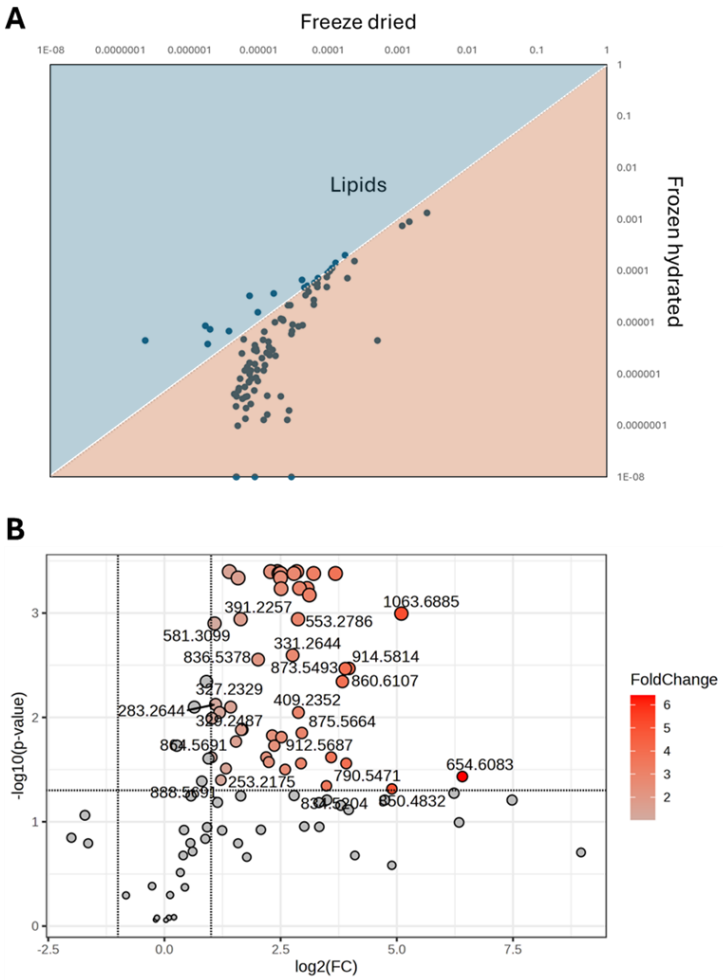

Figure 2.4. The comparison of lipid intensity in freeze-dried H4 cells versus samples in frozen hydrated conditions (freeze-dried/frozen hydrated). *The normalized intensity by total ion counts was used for all OrbiSIMS data analysis. A) The normalized intensity of assigned lipids in freeze-dried H4 sample 1 and frozen hydrated H4 sample 1 were plotted as a scatter plot. The plots spread in the upper left (blue area) indicate the lipids with higher signals in frozen hydration. Those located in the lower right (orange area) indicate lipids with higher signals in the freeze-dried state. B) The volcano plot was used to visualize the statistical analysis of the comparison of lipid intensity in freeze-dried and frozen hydrated H4 samples (n=3). Each circle was labelled with the accurate mass for assigned lipids. The fold change in lipid intensity is presented as the ratio between freeze-dried and frozen-hydrated conditions. The lipids with a fold change above 2 and an adjusted p-value below 0.05 were labelled in red, with the degree of red colour corresponding to the fold change, as indicated by the scale bar on the right side of Figure 2.4.B.*

The depth profile pattern of lipid ions in both conditions was assessed in Figure 2.5. The low intensity of lipids throughout the entire depth profiling analysis was consistent with the comparison analysis mentioned above in Figure 2.4. High concentrations of lipids were observed on the surface of freeze-dried H4 cell samples, consistent with the high lipid signals typically detected under freeze-dried conditions. This observation aligns with the biodistribution of lipids, which are enriched in the cell membrane. In contrast, frozen-hydrated samples showed almost no significant depth profile patterns, consistent with the lower lipid signals observed in frozen-hydration conditions (Figure 2.5.B).

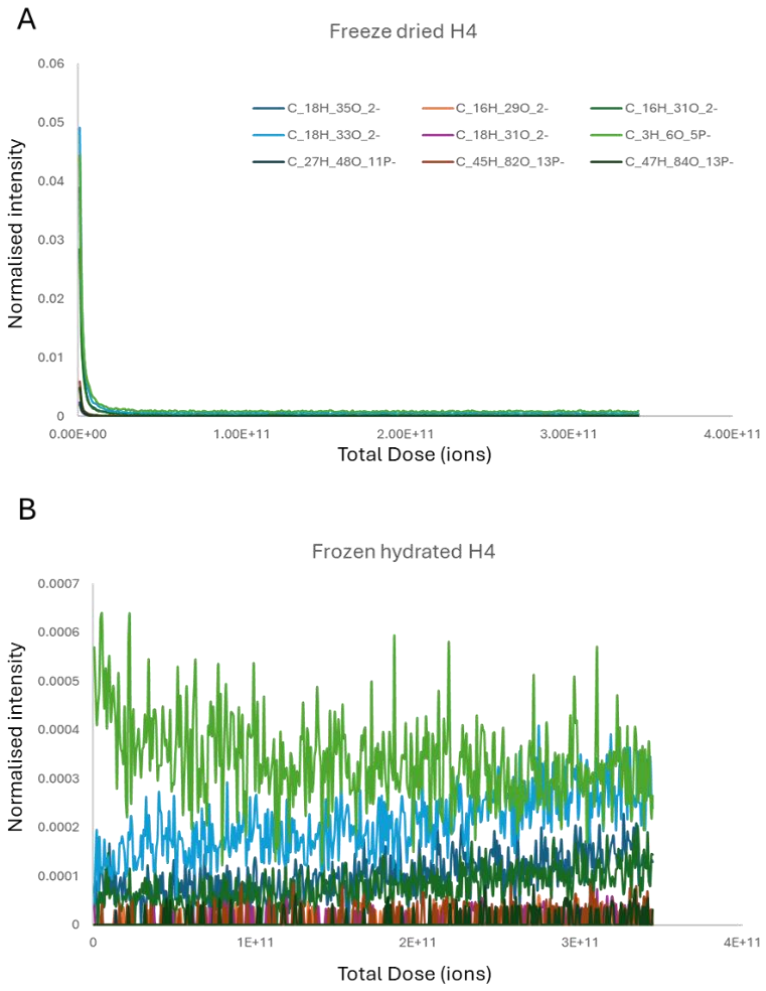

Figure 2.5. The depth profiling of lipid ions in freeze-dried H4 cells (A) and samples in frozen hydrated conditions (B). *The x-axis is labelled as "total dose," indicating the primary ion dose used to sputter or remove the surface material. The y-axis shows the normalized intensity by total ion counts.*

2.3.3 Amino acid ions do not show significant differences between freeze-dried and frozen-hydrated H4 cells.

Table 2.2 below displays the abbreviations of the amino acids used in the following section.

Table 2.2 The abbreviation of amino acids.

Abbreviation	Abbreviation	Amino acid name
Ala	A	Alanine
Arg	R	Arginine
Asn	N	Asparagine
Asp	D	Aspartic acid
Cys	C	Cysteine
Gln	Q	Glutamine
Glu	E	Glutamic acid
Gly	G	Glycine
His	H	Histidine
Ile	I	Isoleucine
Leu	L	Leucine
Lys	K	Lysine
Met	M	Methionine
Phe	F	Phenylalanine
Pro	P	Proline
Pyl	O	Pyrrolysine
Ser	S	Serine
Sec	U	Selenocysteine
Thr	T	Threonine
Trp	W	Tryptophan
Tyr	Y	Tyrosine
Val	V	Valine

In addition, 97 amino acid-related ions were also assigned, and Table 2.3 shows the details about the amino acids and their fragments. The assignment of amino acids and their fragments was based on the structure and molecular ions of amino acids, as well

as the reference database from the ToF-SIMS amino acid reference spectra by Kawacki *et al.* [170, 171]. This table provides an unprecedented level of detail regarding the amino acid fragments present by OrbiSIMS in H4 neuroglioma cells. As shown in Table 2.3, the analysis detected not only the deprotonated molecular ions for each amino acid but also their corresponding fragmented ions. As described in Section 2.3.2, deprotonated ions of lipids ($[M-H]^-$) were primarily observed, along with $[M-H]^-$ adducts of amino acids, as detailed in Table 2.3. Water-loss fragments were also annotated; for example, ions related to aspartate (D) include 132.0304 ($[M-H]^-$, $C_4H_6NO_4^-$) and 114.0197 ($[M-H-H_2O]^-$, $C_4H_4NO_3^-$). The formation of these fragments may result from the loss of neutral molecules, such as H_2O, during ionisation or potentially due to the freeze-dried sample preparation, which could enhance water loss from analytes. Although the exact fragmentation patterns and ionisation mechanisms of OrbiSIMS remain unclear, the data presented here could provide valuable insights for further elucidation. Additional reference sample tests are recommended to better understand the ionisation behaviour of OrbiSIMS.

For example, the OrbiSIMS ions associated with the amino acid glutamine (Q) were detected and assigned as follows: *m/z* 145.0618, $C_5H_9N_2O_3^-$, $Q[M-H]^-$; *m/z* 127.0513, $C_5H_7N_2O_2^-$, $Q[M-H-H_2O]^-$; *m/z* 82.0296, $C_4H_4NO^-$, $Q[M-H-NH_3-CO_2-H_2]^-$; and another small fragment at *m/z* 99.0564, $C_4H_7N_2O^-$. Table 2.3 provides a detailed overview of amino acids, and their related fragments identified during OrbiSIMS measurements. This represents the first instance of amino acid-related ions being mapped in mammalian H4 neuroglioma cells. The findings demonstrate that OrbiSIMS is capable of detecting multiple amino acid ions, and that fragmentation occurs during secondary ion formation. This highlights the need to account for fragmentation effects in future SIMS analyses.

Due to the similar structure of amino acids, some secondary ions in the low mass range are shared by multiple amino acids. For example, *m/z* 86.0245 ($C_3H_4NO_2^-$) could be a fragment produced from alanine, cysteine, leucine, lysine, and serine. The plot Figure 2.6A of amino acids shows that some of them have higher signals in freeze-dried conditions, while others have higher signals in frozen hydrated conditions. The volcano plot in Figure 2.6B further indicated that the intensity of 29 out of 97 (29.9%)

amino acid fragments is statistically significantly more intense in frozen hydrated conditions, while 36 (37.1%) are statistically significantly more intense in freeze-dried samples. Overall, amino acids comparison of H4 cells in cryogenic condition and in freeze-dried condition did not reveal strong ionisation enhancements.

Fatty acids C16:1 and C16:0 were detected only in frozen hydrated conditions from previous cryo-OrbiSIMS analysis in human latent fingerprint samples [165], but not in the room temperature analysis. However, in our results, cryogenic sample analysis did not improve the lipid ion intensity, which suggests that the cryogenic analysis is not always beneficial for all types of samples and method evaluation, and development is suggested to conduct for the samples that have not been studied in cryogenic OrbiSIMS.

Another cryo-OrbiSIMS study performed on a bacterial biofilm sample [153], which is a type of sample consisting of about 90% water. A total of 87 compounds were annotated from the biofilm sample, including 85 polar compounds (nucleobases, amino acids, and alkyl quinolones) and 2 lipids. Almost all these 87 ions showed enhanced intensity in the frozen hydrated state compared to the freeze-dried biofilm. However, in this biofilm study, only 2 annotated lipids were compared, and biofilm is a type of biological sample that contains high water, which cannot be directly extrapolated to other biological samples. Conclusive results that clearly indicate emerging trends cannot be determined, given the limited research conducted in cryo-OrbiSIMS. Therefore, we suggest that sample preparation method development is needed for different types of samples to be analysed by either room temperature OrbiSIMS or cryo-OrbiSIMS.

Combining the lipid and amino acid results, frozen hydration did not yield significant ionisation of amino acids in H4 cells, whereas the freeze-dried condition significantly enhanced the lipid signal. Consequently, freeze-dried sample preparation has been selected as the optimal method for subsequent OrbiSIMS analysis of H4 cells.

Table 2.3. The peak list of amino acids assigned in H4 cells

Mass	Description	Assignment	Mass Deviation (ppm)
88.0402	A[M-H]-, D	$C_3H_6NO_2^-$	-1.9759
86.0245	A, C, O, L, K, S[M-H-H2O]-	$C_3H_4NO_2^-$	-2.4012
131.0826	R[M-H-CH2N2]-, Ornithine[M-H]-	$C_5H_{11}N_2O_2^-$	-0.1159
156.0779	R[M-H-NH3]-	$C_6H_{10}N_3O_2^-$	0.2553
158.0936	R	$C_6H_{12}N_3O_2^-$	0.3679
113.0357	N[M-H-H2O]-, D[M-OH+NH2-H-H2O]-*	$C_4H_5N_2O_2^-$	0.6320
114.0197	N[M-H-NH3]-, D[M-H-H2O]-	$C_4H_4NO_3^-$	0.2306
131.0462	N[M-H]-	$C_4H_7N_2O_3^-$	-0.0817
98.0247	D, M, N[M-H-NH3-O]-	$C_4H_4NO_2^-$	-0.3590
115.0037	D[M-H-NH3]-	$C_4H_3O_4^-$	0.1261
117.0192	D	$C_4H_5O_4^-$	-1.3884
132.0304	D[M-H]-	$C_4H_6NO_4^-$	1.2708
85.0293	E, V	$C_4H_5O_2^-$	-2.7082
100.0404	E, I, M[M-H-CH3SH]-, V, T[M-H-H2O]-	$C_4H_6NO_2^-$	-0.1607
102.0561	E[M-H-CO2]-	$C_4H_8NO_2^-$	-0.0220
128.0353	E[M-H-H2O]-, Q[M-H-NH3]-, O	$C_5H_6NO_3^-$	0.1676
146.0459	E[M-H]-	$C_5H_8NO_4^-$	-0.0096
82.0296	Q[M-H-NH3-CO2-H2]-, O, E[M-H-H20-CO2-H2]-	$C_4H_4NO^-$	-2.9981
99.0564	Q	$C_4H_7N_2O^-$	-0.2422
145.0618	Q[M-H]-	$C_5H_9N_2O_3^-$	-0.1225
80.0377	H[M-H-C2H4NO2]-	$C_4H_4N_2^-$	-3.5906
81.0456	H[M-H-C2H3NO2]-	$C_4H_5N_2^-$	-3.3029
93.0457	H[M-H-NH3-CO2]-	$C_5H_5N_2^-$	-1.0467
104.0254	H	$C_5H_2N_3^-$	0.2491
108.0568	H[M-H-CH2O2]-	$C_5H_6N_3^-$	0.5014
137.0356	H	$C_6H_5N_2O_2^-$	-0.1789
154.0622	H[M-H]-	$C_6H_8N_3O_2^-$	0.0693
99.0087	O	$C_4H_3O_3^-$	-0.2283
110.0248	O	$C_5H_4NO_2^-$	0.4396
130.0510	O[M-H]-	$C_5H_8NO_3^-$	-0.1193
114.0561	I, L, P[M-H]-	$C_5H_8NO_2^-$	0.1790
128.0717	I, L, K	$C_6H_{10}NO_2^-$	0.1792

130.0873	I/L[M-H]-, K	$C_6H_{12}NO_2^-$	-0.1465
145.0982	K[M-H]-	$C_6H_{13}N_2O_2^-$	-0.2525
91.0552	F[M-H-C2H3NO2]-	$C_7H_7^-$	-1.4441
97.0083	F	C_8H^-	-0.2854
103.0554	F[M-H-NH3-CO2]-	$C_8H_7^-$	1.1557
118.0663	F[M-H-CH2O2]-	$C_8H_8N^-$	0.4619
147.0452	F	$C_9H_7O_2^-$	0.0986
164.0717	F[M-H]-	$C_9H_{10}NO_2^-$	0.2077
112.0405	O[M-H-H2O]-, P	$C_5H_6NO_2^-$	0.5549
87.0086	S	$C_3H_3O_3^-$	-2.3018
104.0354	S[M-H]-	$C_3H_6NO_3^-$	1.0068
118.0509	T[M-H]-	$C_4H_8NO_3^-$	-0.3057
108.0455	W	$C_6H_6NO^-$	0.5073
116.0506	W[M-H-C3H5NO2]-	$C_8H_6N^-$	0.3411
136.0533	W	$C_8H_8O_2^-$	2.4015
142.0662	W[M-H-NH3-CO2]-	$C_{10}H_8N^-$	-0.3237
157.0771	W	$C_{10}H_9N_2^-$	-0.2129
203.0827	W[M-H]-	$C_{11}H_{11}N_2O_2^-$	0.7090
93.0345	Y[M-H-NH3-CO2-C2H2]-	$C_6H_5O^-$	-1.0168
119.0502	Y[M-H-NH3-CO2]-	$C_8H_7O^-$	0.0358
134.0611	Y[M-H-CH2O2]-	$C_8H_8NO^-$	0.0438
163.0401	Y[M-H-NH3]-	$C_9H_7O_3^-$	-0.0824
180.0667	Y[M-H]-	$C_9H_{10}NO_3^-$	0.2503
116.0717	V[M-H]-	$C_5H_{10}NO_2^-$	0.1656
102.9860	C	$C_3H_3SO_2^-$	0.7006
221.0054	E[M-OH+NH2-H-CO2]-*	$C_6H_9N_2O_3S_2^-$	-2.7119
102.0019	C[M-H-H2O]-	$C_3H_4SNO^-$	-0.2241
127.0513	Q[M-H-H2O]-	$C_5H_7N_2O_2^-$	0.0767
136.0516	H[M-H-H2O]-	$C_6H_6N_3O^-$	-0.2595
112.0768	I/L[M-H-H2O]-	$C_6H_{10}NO^-$	0.5447
127.0877	K[M-H-H2O]-	$C_6H_{11}N_2O^-$	0.0540
146.0611	F[M-H-H2O]-	$C_9H_8NO^-$	-0.0625
96.0454	P[M-H-H2O]-	$C_5H_6NO^-$	-0.5016
185.0721	W[M-H-H2O]-	$C_{11}H_9N_2O^-$	0.1453
162.0561	Y[M-H-H2O]-	$C_9H_8NO_2^-$	0.1569
98.0611	V[M-H-H2O]-	$C_5H_8NO^-$	-0.3313
113.0721	Ornithine[M-H-H2O]-, P[M-OH+NH2-H]-*	$C_5H_9N_2O^-$	0.6005
124.0074	Taurine[M-H]-	$C_2H_6SNO_3^-$	-0.1321

129.0584	W(NL)	$C_9H_7N^-$	0.2225
106.0425	Y[M-H-NH3-CO2-CH]-	$C_7H_6O^-$	0.3984
96.0091	D[M-H-2H2O]-, N[M-H-NH3-H2O]-	$C_4H_2NO_2^-$	-0.5151
84.0453	E[M-H-H2O-CO2]-, Q[M-H-NH3-CO2]-	$C_4H_6NO^-$	-2.6867
101.0720	E[M-OH+NH2-H-CO2]-, Q[M-H-CO2]-	$C_4H_9N_2O^-$	-0.0746
109.0408	Q[M-H-2H2O]-	$C_5H_5N_2O^-$	0.3604
163.0877	F[M-OH+NH2-H]-*	$C_9H_{11}N_2O^-$	0.2366
110.0724	H[M-H-CO2]-	$C_5H_8N_3^-$	0.4481
118.0411	H[M-H-2H2O]-	$C_6H_4N_3^-$	0.4551
153.0782	H[M-OH+NH2-H]-*	$C_6H_9N_4O^-$	0.3140
82.0660	I/L[M-H-CH2O2-H2]-	$C_5H_8N^-$	-2.9739
129.1034	I/L[M-OH+NH2-H]-*	$C_6H_{13}N_2O^-$	0.2178
97.0771	K[M-H-CH2O2-H2]-	$C_5H_9N_2^-$	-0.4565
144.1142	K[M-OH+NH2-H]-*	$C_6H_{14}N_3O^-$	-0.2131
95.0250	N[M-H-2H2O]-	$C_4H_3N_2O^-$	-0.7458
130.0622	N[M-OH+NH2-H]-*	$C_4H_8N_3O_2^-$	-0.1597
112.0880	R[M-H-NH3-CO2]-	$C_5H_{10}N_3^-$	0.2334
130.0986	R[M-OH+NH2-H-CH2N2]-*	$C_5H_{12}N_3O^-$	-0.1554
115.0877	V[M-OH+NH2-H]-	$C_5H_{11}N_2O^-$	0.2730
130.0662	W[M-H-C2H3NO2]-	$C_9H_8N^-$	-0.2105
159.0928	W[M-H-CO2]-	$C_{10}H_{11}N_2^-$	0.0471
186.0561	W[M-H-NH3]-	$C_{11}H_8NO_2^-$	0.1681
202.0988	W[M-OH+NH2-H]-*	$C_{11}H_{12}N_3O^-$	0.8747
107.0503	Y[M-H-NH3-C2O2]-	$C_7H_7O^-$	0.4057
133.0533	Y[M-H-CH3O2]-	$C_8H_7NO^-$	0.0028
136.0768	Y[M-H-CO2]-	$C_8H_{10}NO^-$	-0.1372
179.0826	Y[M-OH+NH2-H]-*	$C_9H_{11}N_2O_2^-$	0.2280

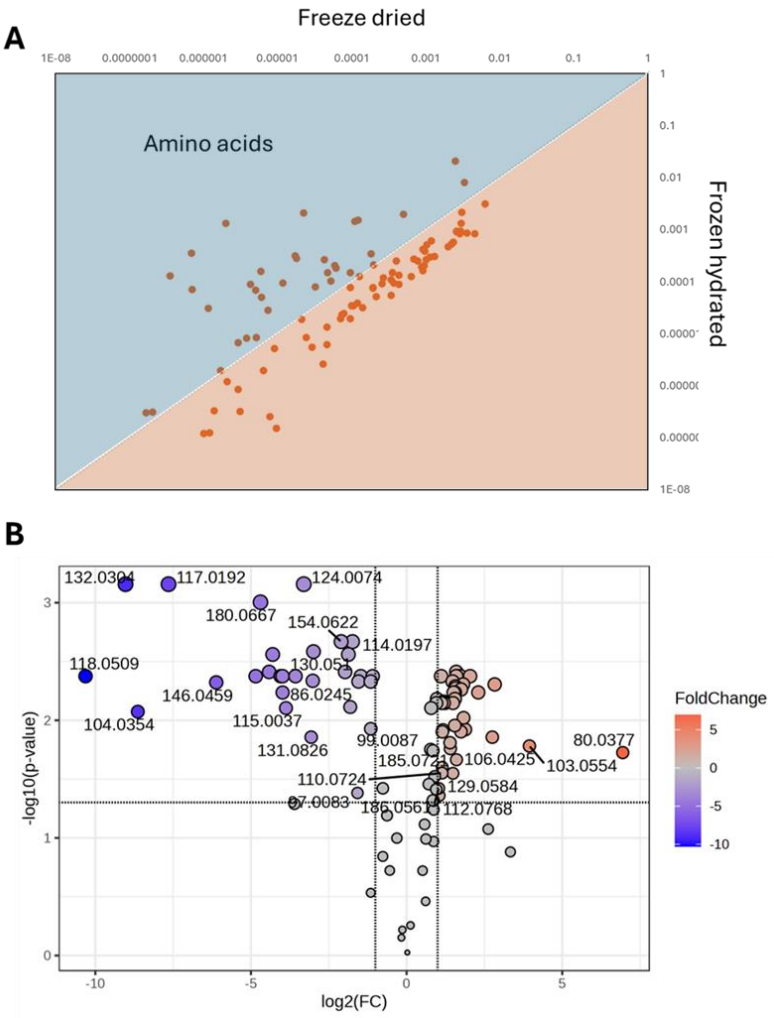

Figure 2.6. The comparison of amino acids (AAs) intensity in freeze dried H4 cells versus samples in frozen hydrated conditions (freeze-dried/frozen hydrated). *The normalized intensity by total ion counts was used for all OrbiSIMS data analysis.* ***A)*** *The normalized intensity of assigned AAs in freeze-dried H4 sample 1 and frozen hydrated H4 sample 1 were plotted as a scatter plot. The plots spread in the upper left above the grey dotted line indicate amino acids with higher signals in frozen hydration. Those located in the lower right below the grey dotted line indicate AAs with higher signals in the freeze-dried state.* ***B)*** *The volcano plot was used to visualize the statistical analysis of the comparison of AAs intensity in freeze-dried and frozen hydrated H4 samples (n=3). Each circle was labelled with the accurate mass for assigned amino acids. The fold change in amino acid intensity is presented as the ratio between freeze-dried and frozen-hydrated conditions. The AAs with a fold change > 2 or < -2 and an adjusted p-value below 0.05 were labelled in red or purple, with the degree of red/purple corresponding to the fold change, as indicated by the scale bar on the right side of Figure 2.6.B.*

2.4 Conclusions

Additionally, when considering frozen-hydrated analysis, sample throughput, time, and expense must be factored into the experimental design. Firstly, due to the limitations of the cryo stage size (around 2 x 2 cm), only 1-4 samples can be loaded at a time, depending on sample size, which limits daily sample throughput. Secondly, frozen-hydrated sample preparation requires 2-3 hours for preparation and instrument setup, compared to freeze-dried analysis. This includes refilling the LN_2 tank and pre-cooling the OrbiSIMS instrument and Leica VCT transfer system. Thirdly, the cost for frozen-hydrated measurements is higher than for freeze-dried conditions, due to the consumption of LN_2 and the use of the vacuum cryogenic transfer system. Typically, a filled 80-liter LN_2 tank will only support up to two days of cryogenic OrbiSIMS work. Overall, these three factors should be carefully considered when discussing and designing frozen-hydrated OrbiSIMS measurements.

In our study, although some amino acids have higher intensity in frozen hydrated samples, most lipid signals are reduced in frozen hydrated conditions. These lipid signals are the primary metabolites of interest related to APOE, as it is a lipid transport protein. Additionally, sample preparation for cryogenic conditions may introduce ice, which complicates the spectrum and requires longer sample preparation time as well as higher costs. The results demonstrate that the freeze-dried sample preparation protocol is advantageous for investigating the role of ApoE4 in H4 neuroglioma cells. Therefore, freeze-dried sample preparation for OrbiSIMS is used for the following experiments.

Chapter 3: Establishment of ApoE4-carrying H4 neuroglioma cells

3.1 Chapter aims

This chapter aims to develop ApoE4-carrying H4 cells for further OrbiSIMS analysis to investigate the metabolic effects of ApoE4 in H4 neuroglioma cells. Firstly, the genotype of ApoE in H4 neuroglioma cells needs to be assessed using sequencing methods to determine which ApoE isoforms are present in the cells, as there is no published information indicating the ApoE isoform expressed in H4 neuroglioma cells, nor is this specified in the purchased safety data sheet from the American Type Culture Collection (ATCC). Based on the ApoE isoforms expressed in H4 neuroglioma cells, the gRNA will be designed to specifically target the ApoE sequence, followed by the insertion of the ApoE4 donor DNA to replace the targeted sequence. To create H4 neuroglioma cells carrying ApoE4, the CRISPR-Cas9 gene-editing tool was used to cut the ApoE sequence and deliver the gRNA and donor DNA into wild-type H4 cells, resulting in the introduction of the ApoE4 isoform.

CRISPR-Cas9 is an immune response mechanism in the bacteria immune system, which uses guide RNA (gRNA) and Cas9 complex to cleave viral DNA for protection. CRISPR-Cas9 system consists of the Cas9 nuclease and guide RNA (crRNA, tracrRNA), which has a 20-nt sequence that directs Cas9 to the DNA of interest, preceded by the 5'-NGG PAM (protospacer adjacent motif) [172]. The Cas9 nuclease cuts the gene of interest based on the gRNA sequences, inducing DNA double-stranded breaks (DSBs). In response to DNA damage, organisms activate two pathways for DNA repair: non-homologous end joining (NHEJ) and the homology-directed repair (HDR). The genome prefers repairing DNA using the NHEJ pathway, which involves insertions and deletions, resulting in gene knock-out. However, in the presence of donor DNA (sharing homology sequences with the targeted gene), HDR is activated, allowing specific DNA to be inserted into the DSB.

It has been published that HDR efficiency is much lower than NHEJ, with cells predominantly using the NHEJ pathway to repair DNA breaks rather than the HDR

pathway [173]. As a result, only a small proportion of cells will incorporate the donor DNA. To increase the efficacy of the ApoE4 knock-in (KI), the fluorescent tagged transfection method and monoclonal dilution method [174] could be employed to select the KI cell line before conducting further analysis.

In this study, a donor DNA containing the ApoE4 gene was designed to activate the HDR pathway. Due to the low efficiency of HDR-mediated ApoE4 knock-in, monoclonal culture was used to select ApoE4 KI cell clones. The levels of tau phosphorylation at sites 199 and 396, ApoE4 protein, and gene sequencing were used to evaluate the ApoE4- carrying H4 cells.

3.2 Methods

3.2.1 Reagents

Dulbecco's Modified Eagle's Medium-high glucose (D6429, Sigma life science), Fetal bovine serum (F7524, Sigma life science), Penicillin-Streptomycin (P4333, Sigma life science), 0.25 % Trypsin-EDTA (25200-056, Gibco), Phosphate Buffered Saline (10010-015, Gibco), RIPA lysis buffer (89900, Thermo scientific), Halt Protease Inhibitor Cocktail (87786, Thermo Scientific), Halt Phosphatase Inhibitor Cocktail (78420, Thermo Scientific), Coomassie (Bradford) protein assay kit (23200, Thermo Fisher Scientific), Lipofectamine CRISPRMAX Transfection Reagent (MAN0014545, Thermo Fisher Scientific), Invitrogen TrueCut Cas9 Protein v2 (A36497, Thermo Fisher Scientific), Tris Buffered Saline (TBS), 10× solution (10776834, Fisher bioreagents), 10× Tris/Glycine/SDS Buffer (1610732, Bio rad), Trans-Blot Turbo 5×Transfer Buffer (10026938), 4× Laemmli sample buffer (1610747, Bio rad), Precision Plus protein dual colour standards (1610374, Bio rad), Mini-Protean TGX Gels (4569035, Bio-Rad), Pierce ECL western blotting substrate (32106, Thermo Scientific).

3.2.2 Cell culture and ApoE4 knock-in neuroglioma cell by Crispr-cas9

Neuroglioma cells H4 (ATCC® HTB-148TM) were obtained from the American Type Culture Collection (ATCC) and grown at 37 °C with 5 % CO_2 in Dulbecco's Modified Eagle's Medium supplemented with 10 % fetal bovine serum and 1 % penicillin-streptomycin. H4 cells were passaged at a 1:4 ratio using 0.25 % Trypsin-EDTA (for about 2min) when reaching approximately 80-90% confluency. All experiments were performed using cells between passages 5-20. The cells were resuspended in a cryopreservation medium (complete culture medium supplemented with 5 % DMSO) for cryopreservation.

To start with the ApoE4 gene knock-in (KI) process, gRNA is firstly designed according to the target sequence, following the Invitrogen TrueDesign Genome Editor platform that designs gRNA and Donor DNA

(https://apps.thermofisher.com/apps/genome-editing-portal/). The gRNA and donor DNA sequences of the ApoE4 gene are shown in Table 2.1.

Table 2. 1. *The sequences of gRNA and donor DNA for ApoE4 gene*

Reagents	Sequences
gRNA	G*G*A*GGACGUGUGCGGCCGCC + modified scaffold
Donor DNA	OECAGGCCCGGCTGGGCGCGGACATGGAGGACGTGCGCGGCCGCCTG GTGCAGTACCGCGGCGAGGTGCAGGCCAZEC

The cells are seeded as 4×10^5/well in a 6-well plate before transfection so that they are 50 % confluent on the day of transfection. On the day of transfection, the manufacturer's guide is followed for gene editing (Table 2.2).

On the day of transfection, prepare Tube 1 and Tube 2 as described in the table, incubate Tube 2 for 1min at RT, then add Tube 2 into Tube1 and mix well by pipetting. After incubating for 10min at RT, the transfection mixture is added to cells and incubated at 37 ℃, 5 % CO_2 for 2 days. Finally, the transfected samples are used for further analysis and monoclonal culture.

Table 2. 2. *The gene-editing protocol and medium used in ApoE4 knock-in experiment*

Tube 1: Reagent	6-well	Tube 2: Reagent	6-well
Opti-MEM™ I Medium	125 μL	Opti-MEM™ I Medium	125 μL
TrueCut™ Cas9 Protein v2	6.26 μL (6250 ng/37.5 pmol)	Lipofectamine™ CRISPRMAX™ Reagent	7.5 μL
gRNA(10μM)	3.75 μL (1200 ng/37.5 pmol)		
Donor DNA	10.2 μL (2500 ng)		
Lipofectamine™ Cas9 PLUS Reagent	12.5 μL		

3.2.3 Isolating a monoclonal cell population by limiting dilution

After transfection, the cells are isolated by trypsin and the concentration of cells is quantified by a hemocytometer. The cell suspension is further diluted at a concentration of 5 cells/mL, and 100 μL of the 5 cells/mL suspension is transferred into each well of the 96-well plate and incubated for 7-14 days. Once the cells reach 80 % confluence, the cells are transferred and expanded to 12-well plates and 6-well plates. The expanded cells are used to perform Western blot to screen for lines with the highest ApoE4 expression.

3.2.4 Protein extraction and Western blot

Proteins in cells were extracted using RIPA lysis buffer containing Halt Protease Inhibitor Cocktail and Halt Phosphatase Inhibitor Cocktail. The protein concentration was determined and normalized to the protein concentration of 2.5 μg/ μL for each cell lysate, an equal volume of 4X Laemmli sample buffer was added in. Cell lysate in sample buffer was then boiled at 100 ℃ for 5 min to reduce and denature proteins in samples. 20 μg of total protein of each sample was loaded into each well of SDS-PAGE gel (12 %), along with a molecular weight marker. The gel was run for 30 min at 80V, followed by 120 V for 60 min. Proteins in the gel were transferred to the PVDF membrane at 2.5 A, 25 V for 3 min in the Bio-Rad turbo system. The membrane was blocked for 1 h at room temperature using blocking buffer (5 % BSA). The PVDF membrane was incubated with APOE4 antibody (1:1000 dilution) in blocking buffer overnight at 4 ℃. After incubating overnight with primary antibody, the membrane was washed three times with TBST for 10 min each. The membrane was incubated with secondary antibody in blocking buffer at RT for 1 h and then washed three times with TBST for 10 min each. The secondary antibody in membrane was detected by Chemiluminescent solution using GelDoc. Information of the primary and secondary antibodies is as follows: β-actin (sigma, 1:1000), ApoE4 (1:1000), anti-rabbit IgG (A6154 sigma, 1:5000), anti-mouse IgG (A4416 sigma, 1:4000).

3.2.5 Total tau and pTau (S199, S396) quantification

The total tau and phosphorylation of tau on serine 199 and 396 were quantified using ELISA kits (RAB1085, Sigma-Aldrich; KHB7041, KHB7031, Thermo Fisher Scientific) according to the manufacturer's instructions. Briefly, 50 µL of sample and 50 µL of standard diluent buffer was added into each well of the antibody-coated plate and tap gently on side of the plate to mix. Incubate 2 hours at room temperature then wash wells 4 times with wash buffer. Add 100µL of Hu Tau (pS199 or pS396) detection antibody solution into each well and incubate 1 h (pS199) or 2 h (pS396) at RT. After 4 times washing, add 100 µL anti-rabbit IgG HRP solution into each well and incubate for 30 min at RT. After washing, add 100 µL stabilized chromogen to each well for incubating 30 min at RT in the dark. Finally, add 100 µL stop solution and read the absorbance at 450 nm within 2 h after adding the stop solution.

3.2.6 DNA isolation and Sanger sequence analysis

Cells are grown in a 6-well plate for 24 h before DNA isolation, after aspirating with culture medium and being washed twice by PBS, 1 ml DNAzol Reagent (Invitrogen™, 10503027) is added into each well. The cells are lysed by gently pipetting after being transferred into new Eppendorf tubes. DNA from cell lysate is precipitated by adding 500 µL pure ethanol, mixed by inversion, and stored at room temperature for 3 min. DNA quickly becomes visible, then the supernatant is aspirated. DNA precipitate is washed twice with 1 ml of 75 % ethanol. DNA is air-dried for 15 s after removing ethanol. DNA is then dissolved in 300 µL of 8 mM NaOH. DNA in NaOH solution is stable for more than one year at -20 °C.

The PCR products for sequencing are generated using Q5 High-Fidelity DNA polymerase (NEB, M0491), followed by the manufacturer’s guidance. Forward primer for PCR (F-CCTCCCACTGTGCGACACCCTCC) and reverse primer (R-GTCCGGCTGCCCATCTCCTCCAT) were obtained from Invitrogen. PCR product length is ~532 bp. PCR products were sent to the DNA sequencing facility of the University of Nottingham for Sanger sequence analysis.

3.2.7 Statistical analysis

Data were analysed using GraphPad Prism and are expressed as the mean ± standard deviation (SD). Statistical significance of differences was evaluated using Student's t-test and $p<0.05$ was considered statistically significant.

3.3 Results and Discussion

3.3.1 CRISPR-Cas9 transfection

Firstly, the ApoE genotype of wild-type H4 neuroglioma cells was assessed using the Sanger sequencing method. The results showed that the ApoE genotype of H4 neuroglioma cells is ApoE3 (Figure 3.1). Figure 3.1A displays the single nucleotide polymorphism (SNP) site rs429358, which determines the expression of amino acid residue 112 in the ApoE protein, while SNP rs7412 (Figure 3.1B) controls the expression of amino acid residue 158. The codon TGC corresponds to cysteine, and CGC corresponds to arginine. Based on the sequencing data shown in Figure 3.1, the presence of TGC (rs429358) and CGC (rs7412) in wild-type H4 cells indicates that only ApoE3 is expressed.

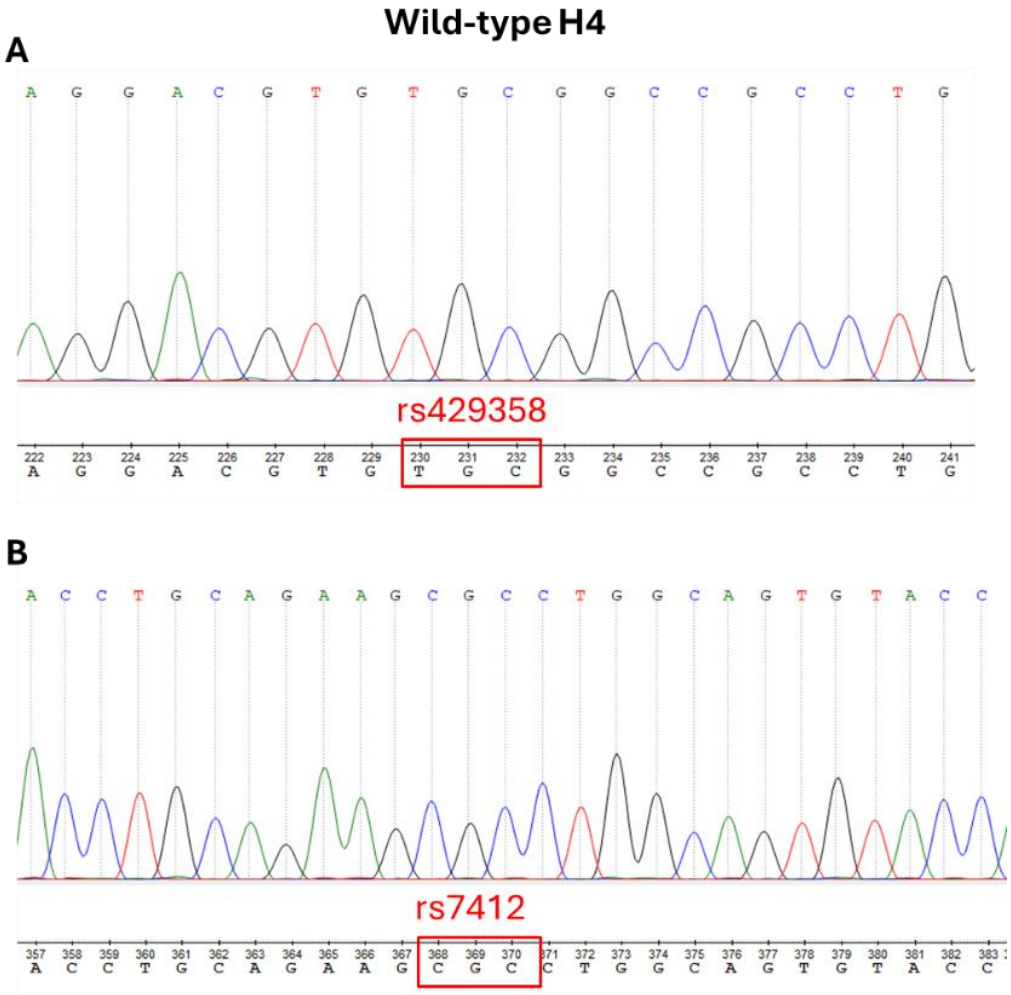

Figure 3.1. *The ApoE genotype of wild-type H4 cells detected by Sanger sequencing method. The ApoE isoforms are identified by the SNPs rs429358 and rs7412: ApoE2 (rs429358 TGC/rs7412 TGC), ApoE3 (TGC/CGC), and ApoE4 (CGC/CGC).* A) The DNA sequence of SNP rs429358 in the ApoE genome is TGC; B) The DNA sequence of SNP rs7412 is CGC. Therefore, the genotype of ApoE in wild-type H4 neuroglioma cells is ApoE3 (TGC/CGC).

ApoE is predominantly expressed by astrocytes and microglia in the brain, with APOE3 being the most abundantly expressed isoform in the human body compared to APOE2 and APOE4. To investigate the mechanism of ApoE4 in Alzheimer's disease, H4 neuroglioma cells were chosen as the cellular model. This immortalised cell line offers several advantages, including lower cost, ease of culture, and established use in Alzheimer's disease research. H4 cells have been widely utilised as a model system to explore mechanisms related to Alzheimer's disease pathogenesis [175, 176]. In this model, ApoE3 was mutated into ApoE4 by substituting a thymine (T) with a cytosine (C) at the rs429358 locus, resulting in a cysteine-to-arginine substitution (Figure 3.2A).

In terms of the knock-in mechanism, the gRNA is designed according to the target sequence. Then designed gRNA is combined with the Cas9 protein, and the gRNA-Cas9 complex is transfected into the cell using a lipofectamine reagent. When the DNA is cleaved by Cas9, two pathways can occur (Figure 3.2B): non-homologous end joining (NHEJ), which is the preferred pathway when using CRISPR-Cas9 to generate a genetic knockout, and HDR. In HDR, a donor DNA template that shares homology with the targeted area can induce HDR, resulting in the knock-in of the APOE4 sequence.

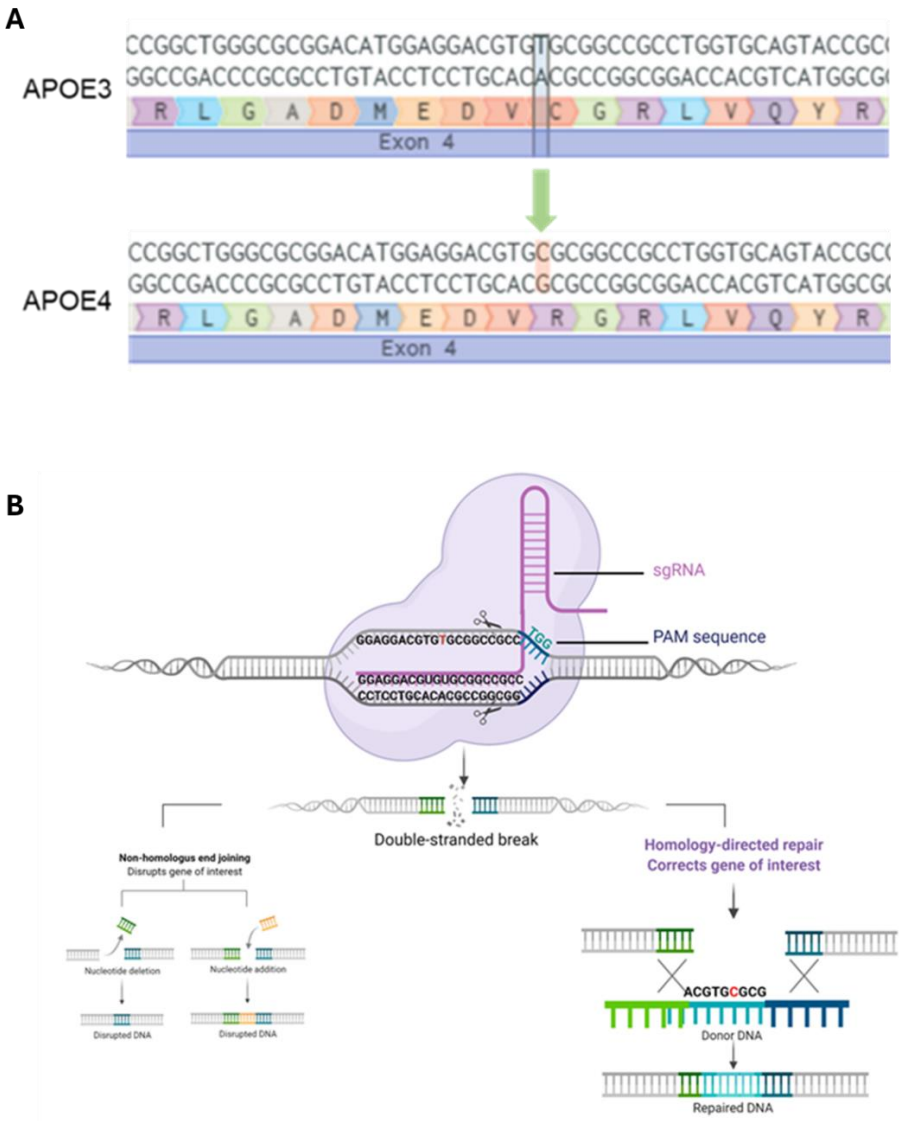

Figure 3. 2. *The principle of SNP mutation and gene-editing by CRISPR-Cas9. A) The illustration of the SNP mutation from ApoE3 to ApoE4 by altering the rs429358 sequence from TGC to CGC. B) The designed gRNA sequence and the pathways of non-homologous end joining (NHEJ) and homology-directed repair (HDR) used in cell repair mechanisms.*

After adding the transfection reagent into the cell culture medium as mentioned in Table 2.2, the cells were cultured for three days. Then, the cells were collected, and proteins were extracted for Western blot and phosphorylation tau tests. The cell passage collected directly after transfection was named passage 1 (P1), and subsequent passages were named as passage 2 (P2). ApoE4 expression was tested by Western

blotting. After transfection, ApoE4 levels decreased compared to the non-transfected group (Figure 3.3). These results indicate that the depletion of ApoE leads to a low level of ApoE4.

However, the Western blotting imaging showed the presence of ApoE4 in wild-type H4 control cells, which is controversial given that the Sanger sequencing results demonstrated only ApoE3 in control H4 cells. One possible reason could be the non-specificity of the ApoE4 antibody, which may have been bound to ApoE3. Therefore, another evaluation method was needed, and the level of tau phosphorylation was examined. The presence of ApoE4 is related to hyperphosphorylation of Tau, so p-tau was detected using the ELISA kit.

According to the literature, serine phosphorylation sites 199 and 396 were chosen [177]. The levels of pS199 and pS396 in passage 1 cells after transfection decreased significantly compared to the control group (Figure 3.4A). The relative concentration level of pS199 in transfected cells (0.40 ± 0.02) decreased by approximately 2.5 times compared to control cells (1.00 ± 0.06). The reduction of pS396 in transfected cells (0.18 ± 0.02) was about 5.5 times compared to the control (1.00 ± 0.07).

When the transfected cell line was passaged to passage 2 (Figure 3.4B), the levels of pS199 and pS396 also decreased. The level of pS199 (0.72 ± 0.03) reduced by approximately 1.38 times compared to the control level (1.00 ± 0.03), while pS396 (0.68 ± 0.04) in transfected cells decreased by approximately 1.5 times compared to the control H4 cells (1.00 ± 0.03). However, the decreased fold change of pS199 and pS396 in passage 2 transfected cells compared to control H4 cells decreased from 2.5 to 1.38 times and from 5.5 to 1.5 times, respectively. These results indicate that the efficiency of knock-in is very low, resulting mostly in ApoE knock-out, which leads to decreased ApoE4 and p-Tau levels.

Additionally, the transfection efficiency reduces over passage time. In conclusion, the gRNA and Cas9 protein effectively guided and cut the targeted gene, resulting in stable ApoE knock-out cell lines. However, the knock-in efficiency is very low, necessitating further optimisation of selection methods.

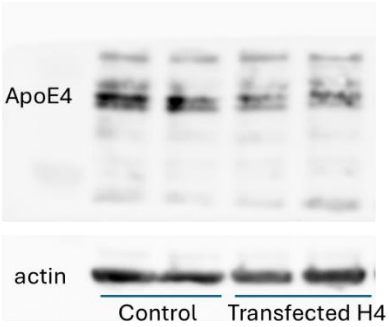

Figure 3.3. *The western blotting image of ApoE4 (34 kDa) and actin (42 kDa) in control H4 and transfected H4 cells.*

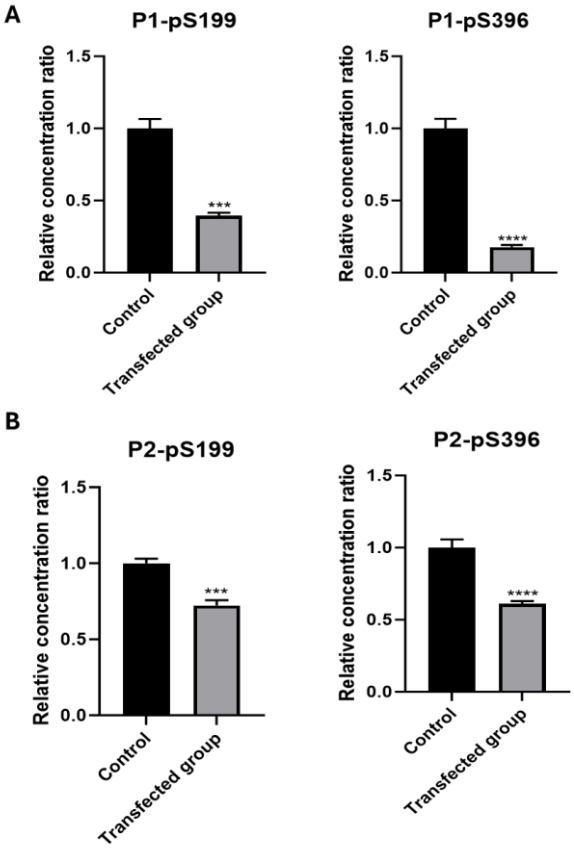

Figure 3.4. *The hyperphosphorylation of tau protein level analysis between transfected group and control group. A) Relative concentration ratio of hyperphosphorylation pS199 and pS396 tau after transfection in passage 1 of cells. B) Relative concentration ratio of hyperphosphorylation pS396 tau after transfection in passage 2 of cells. Data are expressed as the mean ± SD (n=3). *** p < 0.001; **** p < 0.0001.*

3.3.2 Monoclonal culture of transfected H4 cells

After transfecting by CRISPR Cas9, to select the most effective transfection cell being knock in of ApoE4, the limiting dilution method is used for selecting and expanding from single cell. Figure 3.5 shows the western blotting results for selecting monoclonal cell population with the highest or lowest transgene expression. 42 monoclonal cell pools were collected, lots of cell populations are ApoE4 low expression, for example, cell line 7 decreased 5 times compared with the no-transfected group (Figure 3.5 A). While there are 4 pools of ApoE4 over-expression (19, 22, 23, 36) (Figure 3.5 C, D), among them cell line 36 is most significantly ApoE4 over-expression represent more than 2 times compared with the control group (Figure 3.5 D). Therefore, cell line 36 was used to further analysis as ApoE4 knock-in group.

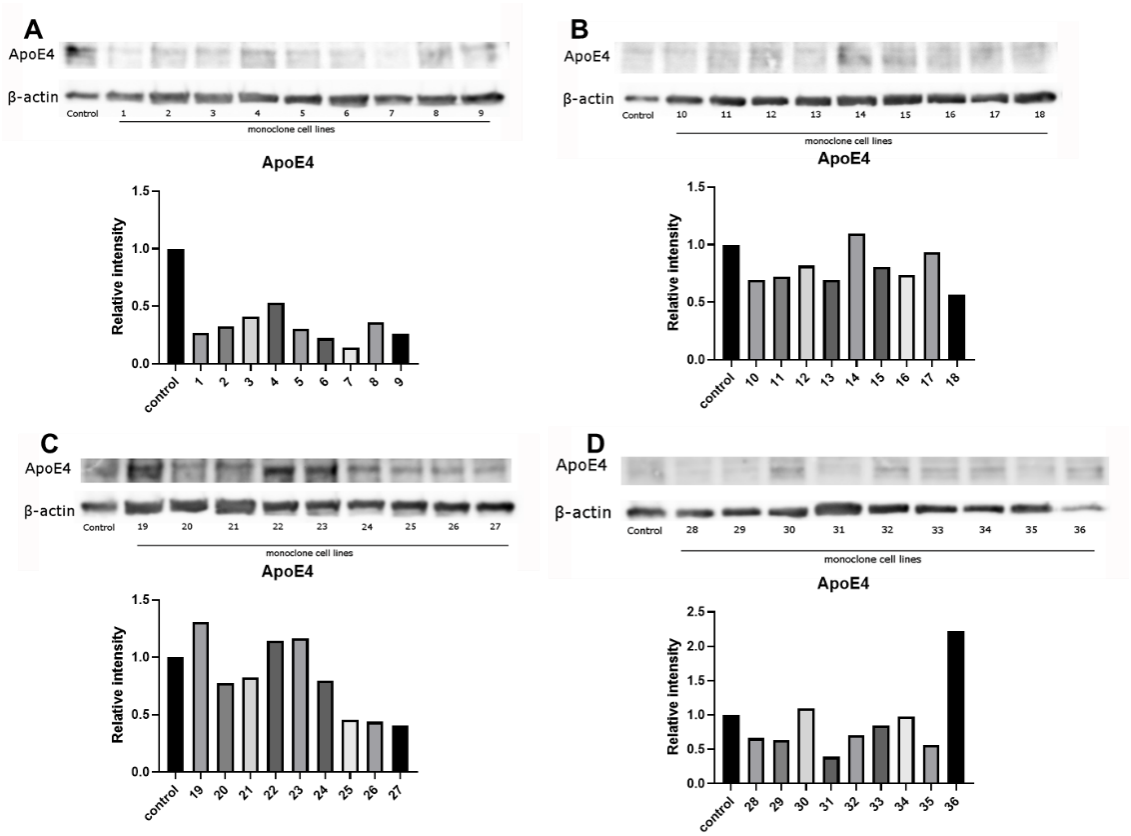

Figure 3.5. *The ApoE4 expression in monoclonal cell populations (1-36) of the gene-editing group by limiting dilution. A) The western blotting analysis and relative comparison of ApoE4 expression in 1-9 monoclonal pools with the control group. B) The western blotting analysis and relative comparison of ApoE4 expression in 10-18*

monoclonal pools with the control group. C) The western blotting analysis and relative comparison of ApoE4 expression in 19-27 monoclonal pools with the control group. D) The western blotting analysis and relative comparison of ApoE4 expression in 28-36 monoclonal pools with the control group.

Cell line 36 has been further expanded and passaged for validation (Figure 3.6). Compared with control H4 cells, the high expression of ApoE4 and the increase in pS199 levels (Figure 3.6 A & B) suggest the most significant ApoE4 overexpression in cell line 36. The pS199 in ApoE4 KI cell line 36 (1.48 ± 0.07) increased by approximately 1.48 times compared to the control (1.00 ± 0.02), and pS396 (2.53 ± 0.53) increased by 2.53 times compared to the control (1.00 ± 0.13). Furthermore, the Sanger sequencing result indicated that the TGC site of wild-type H4 has been changed to CGC, showing the successful ApoE4 knock-in of cell line 36 (Figure 3.6C). Therefore, cell line 36 was used for further analysis as the ApoE4 knock-in group.

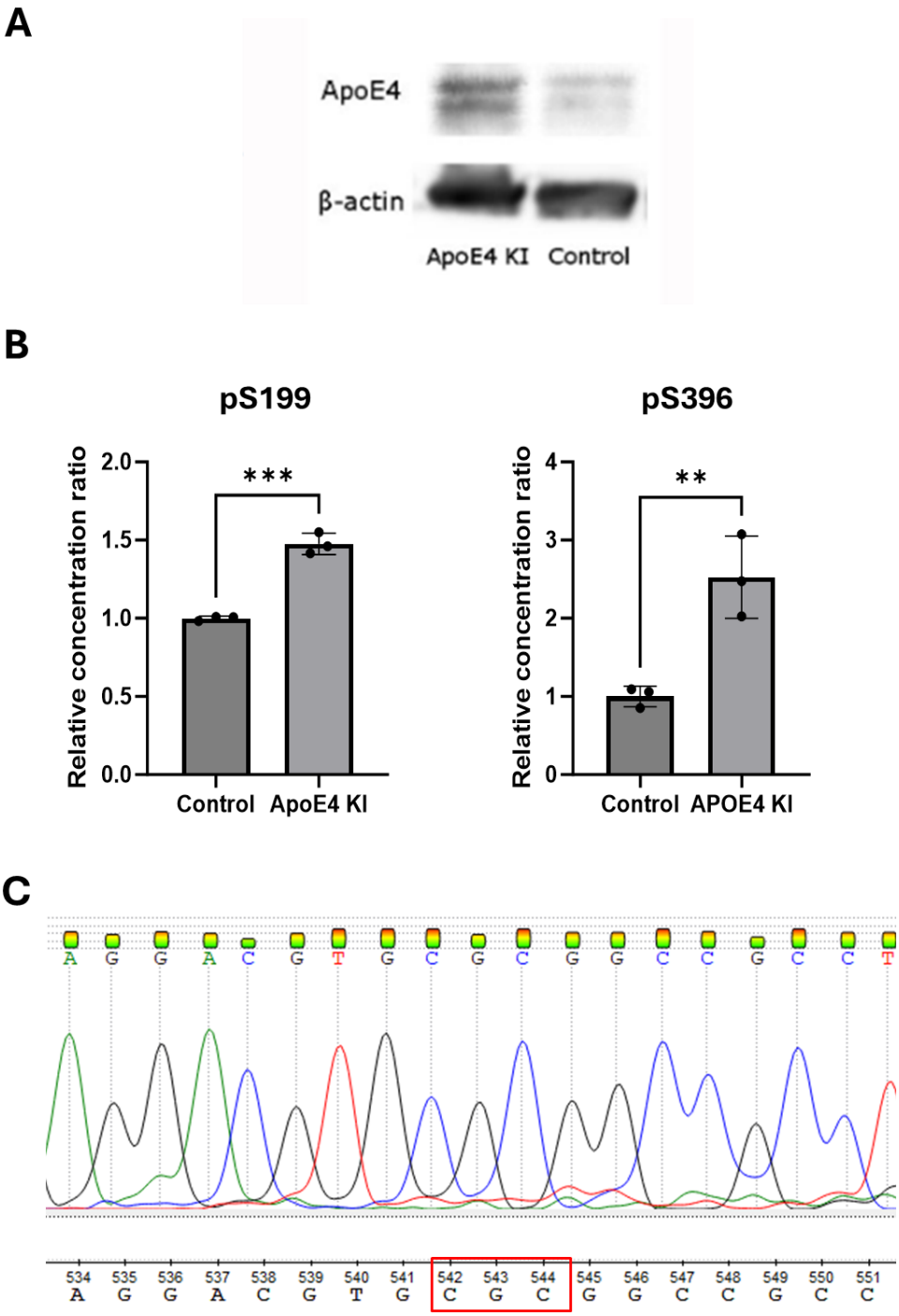

Figure 3.6. *Validation of ApoE4 KI cell line 36.* ***A)*** *The ApoE4 expression in monoclonal cell line 36.* ***B)*** *The pS199 and pS396 level were tested in control H4 cells compared to ApoE4 KI cell line 36.* ***C)*** *The Sanger sequence results of ApoE4 KI cell line indicate the TGC site of wild-type H4 has been changed to CGC.*

In this study, we used CRISPR-Cas9 gene-editing tools to manipulate the ApoE allelic variants in astrocytes to research the mechanism of ApoE4 in AD. To increase the low efficiency of ApoE4 knock-in, transfected cells have been selected by the limiting dilution monoclonal method. Then the ApoE4 over-expression cell line was selected for further analysis. Compared with the control group, the hyperphosphorylated tau of pS199 increased in ApoE4 over-expression group. Therefore, ApoE4-carried neuroglioma H4 cells were generated using CRISPR/Cas9 gene-editing technology and selected by monoclonal culturing. Two groups of H4 cells, Control and ApoE4-carrying, are applied as cell models for further metabolomic and proteomic studies.

A potential problem with this ApoE4 KI model is the lack of clinical relevance because H4 cells, being immobilized, cannot fully represent the actual impact of ApoE4 on the human brain. The brain involves many cell types, including neurons, astrocytes, and microglia, and cell-cell communication plays a significant role in AD. Therefore, it is necessary to apply this model to other types of cells and co-culture systems to fully understand the ApoE4 mechanism in AD.

3.4 Conclusions

This chapter explored the ApoE4 knock-in (KI) method in H4 neuroglioma cells using the CRISPR-Cas9 transfection approach, coupled with monoclonal cell culture to select KI cell lines. For the first time, the ApoE genotype of wild-type H4 neuroglioma cells was assessed, revealing that only the ApoE3 isoform is expressed. This finding expands the potential application of H4 neuroglioma cells in ApoE4-related pathogenesis studies.

The significant reduction in ApoE4 levels and phosphorylated tau levels indicated successful targeting and cleavage of the DNA sequence near the rs429358 site. However, this study also highlighted the low efficiency of the gene knock-in process, as demonstrated by reduced ApoE protein levels and decreased phosphorylated tau levels after transfection without any selection method. To overcome this limitation, monoclonal selection was employed to identify and isolate ApoE4 knock-in H4 cell lines, providing a more reliable model for further studies. The significantly increased levels of pS199 and pS396, along with Sanger sequencing results, confirm the successful selection and evaluation of the ApoE4 knock-in cell line.

However, limitations remain with the gene-editing method used in this chapter. The CRISPR-Cas9 system is often associated with off-target or mis-target effects, which may result in Cas9 cleaving unintended sites in the DNA outside of rs429358. This possibility raises concerns about unintended genetic alterations and highlights the need for whole-genome sequencing of H4 cells to identify and evaluate any off-target effects.

Chapter 4: A Novel Approach to Investigate ApoE4-Mediated Metabolic Alterations in H4 Neuroglioma Cells Using OrbiSIMS

4.1. Chapter aims

This chapter aims to explore the possibility of using OrbiSIMS as a multi-omics tool. This will be assessed in two stage process: firstly, by identifying the classes of metabolites/lipids that OrbiSIMS can detect in H4 cells, and secondly, by determining whether OrbiSIMS data can successfully differentiate the molecular differences between H4 control cells and ApoE4 knock-in cells.

The sample preparation methods presented in Chapter 2 describe the benefits of freeze-dried sample preparation for H4 cells, particularly for achieving higher lipid signals in OrbiSIMS, in comparison with cryo-OrbiSIMS. Apolipoprotein E4 is an important lipid transport protein that plays a crucial role in lipid metabolism. To investigate ApoE4-related molecular changes in H4 cells, freeze-drying OrbiSIMS analysis was selected as the preferred method of analysis, because it provides a stronger lipid signal, as mentioned in Chapter 2. The ApoE4 KI H4 cell model presented in Chapter 3, along with wild-type H4 cells, were freeze-dried and analysed by OrbiSIMS at room temperature.

Due to the complexity of the OrbiSIMS spectra, simsMFP was applied for ion assignment. The predicted chemical formulas obtained from simsMFP were matched with LipidMaps and the Human Metabolome Database (HMDB) to annotate the metabolite categories and names. Multivariate analysis, specifically principal component analysis (PCA), will be used to distinguish the metabolite profiles between wild type/control H4 cells and ApoE4 KI cells. For significant statistical analysis, a t-test and VIP values will be used to select and identify the most significantly changed metabolites in ApoE4 KI cells compared to H4 control cells. Furthermore, the

metabolic pathways, in which these significant metabolites are mostly enriched, will be analysed using pathway/enrichment analysis in MetaboAnalyst.

4.2 Methods

4.2.1 Freeze dried sample preparation and OrbiSIMS measurement

The non-transfected cells and transfected cells were seeded on glass slides merged in a complete culture medium for 24 h. The freeze died sample preparation has been mentioned in Chapter 2, method 2.2.1.

The measurement set up of OrbiSIMS at room temperature has been mentioned in Chapter 2, method 2.2.2.

4.2.2 Data analysis and identification and annotation of metabolites

The OrbiSIMS is operated by software provided by SurfaceLab7 (IONTOF, Germany). First, we performed a peak search on each raw data, a minimum counts threshold 5000 was set by visual inspection of the spectra that distinguished it from a noise peak. Ions extracted from the spectrum are assigned by applying elemental restrictions with mass deviation < 2.5 ppm for ions > *m/z* 95 and 5 ppm for ions < *m/z* 95 for molecular formula prediction. Which is conducted by using software simsMFP (SimsMFP is a Matlab-based script developed by Max *et al. [156]*, especially for chemical filtering of the OrbiSIMS dataset): Lipid search (C_{1-230}, H_{3-130}, N_{0-2}, O_{0-20}, P_{0-2}, S_{0-1}), other energy related metabolism (C_{3-30}, H_{1-40}, N_{0-10}, O_{0-25}, P_{0-3}, S_{0-1}). Subsequentially, matching the chemical formula with LIPID MAPS (https://www.lipidmaps.org/databases/lmsd/overview) and HMDB database (https://hmdb.ca/spectra/ms/search).

Data were analysed using GraphPad Prism and expressed as the mean ± standard deviation (SD). The statistically significant difference of the metabolites between control and ApoE4 KI group was evaluated using Student's t-test and PLS-DA. FDR-

adjusted *p*-value <0.05 combined with VIP >1 was considered as statistical significance.

4.2.3 Pathway and enrichment analysis

Pathway and enrichment analysis are performed using Metaboanalyst web-based software (https://www.metaboanalyst.ca/). Lipid enrichment is based on 35 super and 464 main chemical class metabolite sets or lipid sets, with containing at least 2 entries to match the metabolite set library.

4.2.4 HCS LipidTOX^{TM} green neutral lipid stain

H4 cells were plated at a density of 5×10^5/well in a 6-well plate with 50 μg/mL poly-D-lysine coated 1$^{\#}$ coverslips. After incubation at 37 °C with 5 % CO_2 for 24 h, cells were fixed by 4 % formaldehyde for 30 min at RT. Cells were washed with PBS buffer 3 times and then incubate with 1× LipidTOX neutral lipid stain for 30 min. NucBlue DAPI stain was incubated with cells for 5 min before imaging. After cells have been stained with Lipid and DAPI dyes, coverslips were picked up and gently mounted by using Fluoromount^{TM} Aqueous Mounting Medium (Sigma, F4680) on the glass slides. Allow fluoromount to dry for 30-45 min at RT, then the stained samples were imaged using Confocal microscope from the Nanoscale and Microscale Research Centre of University of Nottingham. For LipidTox staining, an excitation wavelength of 498 nm and an emission wavelength of 507 nm were used. For imaging DAPI, excitation/emission (Ex/Em) wavelengths of 353 nm and 465 nm were utilised.

4.3 Results and Discussion

4.3.1 OrbiSIMS metabolites assignment by simsMFP

After ApoE4-KI and control H4 cells were grown on the chamber slide for 24 hours, they were freeze-dried under vacuum conditions, followed by OrbiSIMS depth profiling analysis in negative polarity. Example spectra from one of the H4 control samples and ApoE4 KI samples are presented in Figure 4.1 as overlaid spectra. Some parts of the control spectrum overlapped with the ApoE4 KI spectrum, while some peaks were not visible in the ApoE4 KI spectrum, especially in the mass range *m/z* 400-700. This might relate to lipid ions, as suggested by the results in Chapter 2, indicating that the peaks in this mass range are likely assigned to lipid species.

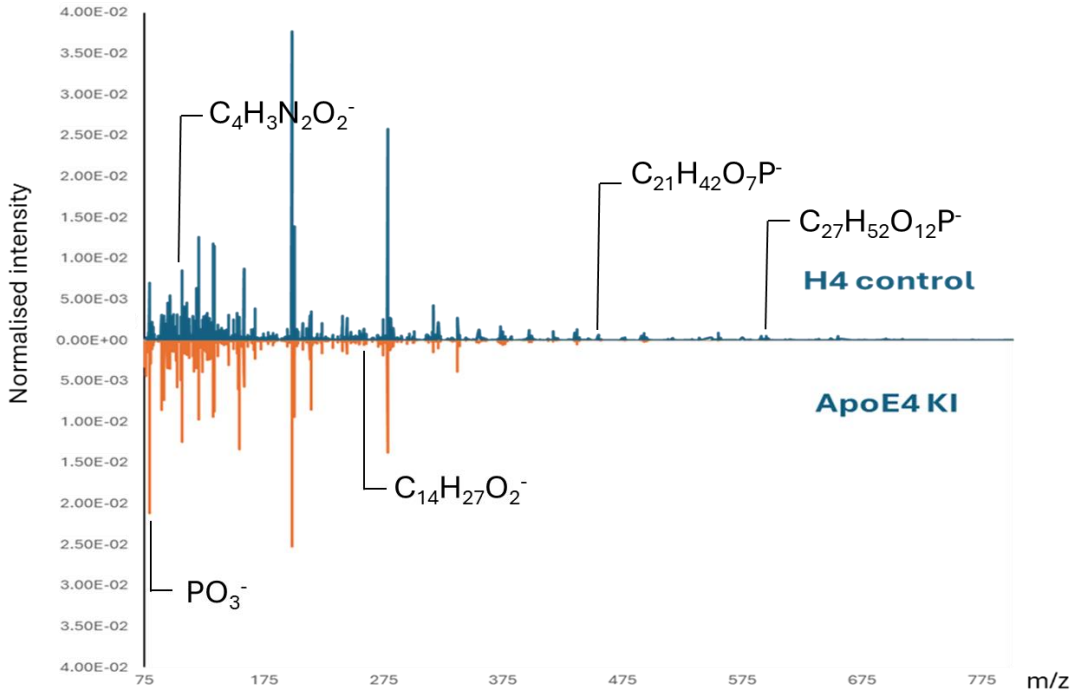

Figure 4.1. *The overlayed spectra of H4 control and ApoE4 KI OrbiSIMS dataset. The x-axis is the m/z value, y-axis is presented as normalised intensity.*

Next, the simsMFP was used to assign the ions from both control and ApoE4 KI samples as discussed in Chapter 2. All ions from each dataset were generated and extracted by searching peaks that can differentia them with noise peaks. Finally, 192 putatively annotated metabolites have been detected from H4 control and ApoE4-KI groups using the OrbiSIMS by assigning chemical formula using simsMFP software [156] (Lipid search (C_{1-230}, H_{3-130}, N_{0-2}, O_{0-20}, P_{0-2}, S_{0-1}), other energy related metabolism (C_{3-30}, H_{1-40}, N_{0-10}, O_{0-25}, P_{0-3}, S_{0-1})), followed by matching with LipidMaps and HMDB databases (Table 4.1.). These 192 putatively annotated metabolites are classified into nine groups based on their major chemical classes and involvement in metabolism pathways, including lipids, amino acids and derivatives, carbohydrates and carbohydrate conjugates, carboxylic/dicarboxylic acids and derivatives, purines nucleotides and purine derivatives, pyridines and derivatives, pyrimidines and pyrimidine derivatives, neurotransmitters, and other organic compounds. The numbers of each class of annotated metabolites are presented in Table 4.2. Notably, lipids constitute a substantial portion of these metabolites, a finding that is supported by the inherent capability of SIMS to analyse intact lipids effectively.

Table 4. 1. *The peak list of annotated metabolites in OrbiSIMS analysis.*

Metabolites	**Deviation**	**Accurate peak mass**	**Formula**	**Metabolites**	**Deviation**	**Accurate peak mass**	**Formula**
myo-Inositol [M-H]⁻	0.5	179.0563	$C_6H_{11}O_6^-$	LPG O-33:4/PA 36:2/PA O-36:3;O [M-H]⁻	0.4	699.4973	$C_{39}H_{72}O_8P^-$
Lactate [M-H]⁻	-2.0	89.0246	$C_3H_5O_3^-$	LPA 32:1;O/LPG O-29:2/PA 32:0/PA O-32:1;O/DG 39:9/DG O-39:10;O/TG O-39:9 [M-H]⁻	0.7	647.4662	$C_{35}H_{68}O_8P^-$
1-Aminocyclopropane	-0.2	100.0404	$C_4H_6NO_2^-$	PA 38:1/PA O-	0.6	729.544	$C_{41}H_{78}O_8P^-$

-1-carboxylate [M-H]$^-$				38:2;O [M-H]$^-$		4	
Alanine [M-H]$^-$	-2.0	88.0402	$C_3H_6NO_2^-$	PA 38:3/PA O-38:4;O/DG 45:12/TG O-45:12 [M-H]$^-$	1.3	725.5134	$C_{41}H_{74}O_8P^-$
Asparagine [M-H]$^-$	-0.1	131.0465	$C_4H_7N_2O_3^-$	PA 38:4/PA O-38:5;O [M-H]$^-$	-0.7	723.4965	$C_{41}H_{72}O_8P^-$
Glutamate [M-H]$^-$	0.0	146.0461	$C_5H_8NO_4^-$	CerP 39:1;O4/LPC 31:1;O/LPE 34:1;O/LPS O-33:1/PC 31:0/PC O-31:1;O/PE 34:0/PE O-34:1;O [M-H]$^-$	0.7	718.5398	$C_{39}H_{77}NO_8P^-$
Glutamine [M-H]$^-$	-0.1	145.0620	$C_5H_9N_2O_3^-$	CerP 39:2;O4/LPC 31:2;O/LPE 34:2;O/LPS O-33:2/PC 31:1/PC O-31:2;O/PE 34:1/PE O-34:2;O [M-H]$^-$	0.4	716.5239	$C_{39}H_{75}NO_8P^-$
Histidine [M-H]$^-$	0.1	154.0622	$C_6H_8N_3O_2^-$	CerP 41:2;O4/LPC 33:2;O/PC 33:1/PC O-33:2;O/PE 36:1/PE O-36:2;O [M-H]$^-$	0.8	744.5555	$C_{41}H_{79}NO_8P^-$
Leucine/isoleucine [M-H]$^-$	-0.1	130.0873	$C_6H_{12}NO_2^-$	CerP 41:3;O4/LPC 33:3;O/PC 33:2/PC O-33:3;O/PE 36:2/PE O-	1.7	742.5405	$C_{41}H_{77}NO_8P^-$

				36:3;O [M-H]$^-$			
Lysine [M-H]$^-$	-0.3	145.0982	$C_6H_{13}N_2O_2^-$	CerP 42:2;O4/LPC 34:2;O/PC 34:1/PC O-34:2;O/PE 37:1/PE O-37:2;O [M-H]$^-$	-2	758.5690	$C_{42}H_{81}NO_8P^-$
Ornithine [M-H]$^-$	-0.1	131.0826	$C_5H_{11}N_2O_2^-$	CerP 42:3;O4/LPC 34:3;O/PC 34:2/PC O-34:3;O/PE 37:2/PE O-37:3;O [M-H]$^-$	1.3	756.5559	$C_{42}H_{79}NO_8P^-$
Proline [M-H]$^-$	0.2	114.0561	$C_5H_8NO_2^-$	PE(38:3)/HexCer 37:3;O4 [M-H]$^-$	13	768.5649	$C_{43}H_{79}NO_8P^-$
Taurine [M-H]$^-$	-0.1	124.0076	$C_2H_6NO_3S^-$	CerP 43:5;O4/PC 35:4/PC O-35:5;O/PE 38:4/PE O-38:5;O [M-H]$^-$	2.2	766.5409	$C_{43}H_{77}NO_8P^-$
Tryptophan [M-H]$^-$	0.7	203.0828	$C_{11}H_{11}N_2O_2^-$	PC 37:7/PC O-37:8;O/PE 40:7/PE O-40:8;O [M-H]$^-$	-0.6	788.5231	$C_{45}H_{75}NO_8P^-$
Tyrosine [M-H]$^-$	0.3	180.0668	$C_9H_{10}NO_3^-$	PC 39:9/PC O-39:10;O/PE 42:9/PE O-42:10;O [M-H]$^-$	-0.6	812.5231	$C_{47}H_{75}NO_8P^-$
Valine [M-H]$^-$	0.2	118.0861	$C_5H_{10}NO_2^-$	CerP 39:2;O3/LPC 31:2/LPC O-31:3;O/LPE 34:2/LPE O-34:3;O/PC O-	0.5	700.5290	$C_{39}H_{75}NO_7P^-$

				31:2/PE O-34:2/ PE(P-34:1) [M-H]–			
Aspartate [M-H]–	1.3	132.0305	$C_4H_6NO_4^-$	PE(P-36:1) [M-H]–	3.4	728.5624	$C_{41}H_{79}NO_7P^-$
Acetylglycine [M-H]–	0.3	116.0353	$C_4H_6NO_3^-$	CerP 43:3;O3/PC O-35:3/PE O-38:3/ PE(P-38:2) [M-H]–	1.8	754.5770	$C_{43}H_{81}NO_7P^-$
1-Methyl-histidine [M-H]–	0.0	168.0779	$C_7H_{10}N_3O_2^-$	CerP 43:6;O3/PC O-35:6/PE O-38:6/ PE(P-38:5) [M-H]–	2.1	748.5303	$C_{43}H_{75}NO_7P^-$
C16 taurine [M-H]–	0.6	362.2373	$C_{18}H_{36}NO_4S^-$	PE(P-40:6)/HexCer 39:6;O3 [M-H]–	9.3	774.5515	$C_{45}H_{77}NO_7P^-$
C18:1 taurine [M-H]–	-0.5	388.2525	$C_{20}H_{38}NO_4S^-$	BMP 34:1/LPG 34:2;O/PG 34:1/PG O-34:2;O [M-H]–	0.3	747.5184	$C_{40}H_{76}O_{10}P^-$
Cysteate [M-H]–	1.7	167.9974	$C_3H_6NO_5S^-$	DG 46:10;O2/TG 46:9;O/TG O-46:10;O2/PG 36:1/PG O-36:2;O [M-H]–	1.5	775.5507	$C_{42}H_{80}O_{10}P^-$
Glutathione [M-H]–	0.5	306.0766	$C_{10}H_{16}N_3O_6S^-$	PG 36:2/PG O-36:3;O [M-H]–	0.5	773.5342	$C_{42}H_{78}O_{10}P^-$
Homocysteic acid [M-H]–	1.8	182.0132	$C_4H_8NO_5S^-$	Phosphocholine-CH3 [M-H]–	-0.1	168.0431	$C_4H_{11}NO_4P^-$
Kynurenine [M-H]–	0.4	207.0776	$C_{10}H_{11}N_2O_3^-$	PI head group [M-H]–	0.8	241.0121	$C_6H_{10}PO_8^-$

N-Acetylhistidine [M-H]⁻	0.3	196.0728	$C_8H_{10}N_3O_3^-$	LPI 32:1;O/PI 32:0/PI O-32:1;O [M-H]⁻	0.4	809.5188	$C_{41}H_{78}O_{13}P^-$
Phenylalanine [M-H]⁻	0.2	164.0719	$C_9H_{10}NO_2^-$	LPI 32:2;O/PI 32:1/PI O-32:2;O [M-H]⁻	-0.4	807.5026	$C_{41}H_{76}O_{13}P^-$
Pyroglutamic acid [M-H]⁻	0.2	128.0356	$C_5H_6NO_3^-$	LPI 34:2;O/PI 34:1/PI O-34:2;O [M-H]⁻	0.1	835.5343	$C_{43}H_{80}O_{13}P^-$
N-Acetylaspartate [M-H]⁻	1.0	174.0409	$C_6H_8NO_5^-$	LPI 34:3;O/PI 34:2/PI O-34:3;O [M-H]⁻	-0.2	833.5184	$C_{43}H_{78}O_{13}P^-$
4-Aminobenzoate [M-H]⁻	-0.3	136.0404	$C_7H_6NO_2^-$	PI 35:1/PI O-35:2;O [M-H]⁻	0.2	849.5500	$C_{44}H_{82}O_{13}P^-$
Benzoate [M-H]⁻	0.1	121.0295	$C_7H_5O_2^-$	PI 35:2/PI O-35:3;O [M-H]⁻	0.2	847.5344	$C_{44}H_{80}O_{13}P^-$
Hippurate [M-H]⁻	0.4	178.0512	$C_9H_8NO_3^-$	PI 36:1/PI O-36:2;O [M-H]⁻	0.3	863.5657	$C_{45}H_{84}O_{13}P^-$
Dimethylbenzimidazole [M-H]⁻	-0.2	145.0771	$C_9H_9N_2^-$	PI 36:2/PI O-36:3;O [M-H]⁻	0.3	861.5501	$C_{45}H_{82}O_{13}P^-$
Glucose 6-phosphate [M-H]⁻	0.6	259.0226	$C_6H_{12}O_9P^-$	PI 36:3/PI O-36:4;O [M-H]⁻	0.8	859.5349	$C_{45}H_{80}O_{13}P^-$
Glyceraldehyde 3-phosphate [M-H]⁻	0.8	168.9909	$C_3H_6O_6P^-$	PI 36:4/PI O-36:5;O [M-H]⁻	0.7	857.5191	$C_{45}H_{78}O_{13}P^-$
5-phospho-α-D-ribose 1-diphosphate, [M-H-H20]-	0.7	370.9340	$C_5H_{10}P_3O_{13}^-$	PI 37:1/PI O-37:2;O [M-H]⁻	1.5	877.5825	$C_{46}H_{86}O_{13}P^-$

Glucosamine 6-phosphate, [M-H-H2O]-	0.6	240.0281	$C_6H_{11}PNO_7^-$	PI 37:2/PI O-37:3;O [M-H]$^-$	1.2	875.5666	$C_{46}H_{84}O_{13}P^-$
X5P/R5P [M-H-H20]-	0.5	211.0014	$C_5H_8PO_7^-$	PI 37:3/PI O-37:4;O [M-H]$^-$	-0.7	873.5492	$C_{46}H_{82}O_{13}P^-$
N-Acetyl-glucosamine 1-phosphate [M-H]$^-$	0.8	300.0492	$C_8H_{15}NO_9P^-$	PI 37:4/PI O-37:5;O [M-H]$^-$	-1.7	871.5327	$C_{46}H_{80}O_{13}P^-$
5-Aminolevulinate [M-H]$^-$	-0.1	130.0512	$C_5H_9NO_3^-$	PI 38:1/PI O-38:2;O [M-H]$^-$	1.5	891.5981	$C_{47}H_{88}O_{13}P^-$
Creatine [M-H]$^-$	-0.2	130.0622	$C_4H_8N_3O_2^-$	PI 38:2/PI O-38:3;O [M-H]$^-$	0.2	889.5813	$C_{47}H_{86}O_{13}P^-$
Creatinine [M-H]$^-$	0.6	112.0517	$C_4H_6N_3O^-$	PI 38:3/PI O-38:4;O [M-H]$^-$	0.4	887.5659	$C_{47}H_{84}O_{13}P^-$
Fumarate [M-H]$^-$	0.1	115.0040	$C_4H_3O_4^-$	PI 38:4/PI O-38:5;O [M-H]$^-$	0.2	885.5501	$C_{47}H_{82}O_{13}P^-$
Succinate [M-H]$^-$	2.0	117.0196	$C_4H_5O_4^-$	PI 38:5/PI O-38:6;O [M-H]$^-$	0.2	883.5343	$C_{47}H_{80}O_{13}P^-$
2-Oxobutanoate [M-H]$^-$	-0.3	101.0247	$C_4H_6O_3^-$	PI 38:6/PI O-38:7;O [M-H]$^-$	-0.7	881.5179	$C_{47}H_{78}O_{13}P^-$
Glycerol 3-phosphate [M-H]$^-$	0.3	171.0067	$C_3H_8O_6P^-$	PI 39:3/PI O-39:4;O [M-H]$^-$	0.2	901.5813	$C_{48}H_{-86}O_{13}P^-$
Itaconate [M-H]$^-$	0.2	129.0194	$C_5H_5O_4^-$	PI 39:4/PI O-39:5;O [M-H]$^-$	0.3	899.5658	$C_{48}H_{84}O_{13}P^-$
CAR 13:0;O4 [M-H]$^-$	0.1	420.2603	$C_{20}H_{38}NO_8^-$	PI 40:2/PI O-40:3;O [M-H]$^-$	1.4	917.6137	$C_{49}H_{90}O_{13}P^-$

CerP(21:0)/LPC O-13:1/LPE O-16:1 [M-H]$^-$	-0.1	436.2833	$C_{21}H_{43}NO_6P^-$	PI 40:3/PI O-40:4;O [M-H]$^-$	0.3	915.5971	$C_{49}H_{88}O_{13}P^-$
Cholesterol Sulfate [M-H]$^-$	-0.5	465.3042	$C_{27}H_{45}O_4S^-$	PI 40:4/PI O-40:5;O [M-H]$^-$	0.5	913.5816	$C_{49}H_{86}O_{13}P^-$
CL(78:9) [M-2H]$^{2-}$	-1.4	764.5169	$C_{87}H_{150}O_{17}P_2^-$	PI 40:5/PI O-40:6;O [M-H]$^-$	0.7	911.5661	$C_{49}H_{84}O_{13}P^-$
CPA(16:0)/ LPA O-16:2 [M-H]$^-$	0.5	391.2257	$C_{19}H_{36}O_6P^-$	PI 40:6/PI O-40:7;O [M-H]$^-$	0.1	909.5499	$C_{49}H_{82}O_{13}P^-$
CPA(18:0)/LPA O-18:2 [M-H]$^-$	0.5	419.2570	$C_{21}H_{40}O_6P^-$	PI 40:7/PI O-40:8;O [M-H]$^-$	0.5	907.5347	$C_{49}H_{80}O_{13}P^-$
CPA(18:1)/LPA O-18:3 [M-H]$^-$	0.5	417.2414	$C_{21}H_{38}O_6P^-$	PI(P-36:0)/PI O-36:1/TG 49:9;O3 [M-H]$^-$	0.9	849.5870	$C_{45}H_{86}O_{12}P^-$
FA(14:0) [M-H]$^-$	0.4	227.2019	$C_{14}H_{27}O_2^-$	PI(P-36:3)/PI O-36:4/TG 49:12;O3 [M-H]$^-$	2.3	843.5413	$C_{45}H_{80}O_{12}P^-$
FA(15:0) [M-H]$^-$	1.0	241.2175	$C_{15}H_{29}O_2^-$	POV-PG/BMP 21:1;O/LPI O-18:2/PG 21:1;O [M-H]$^-$	0.4	581.3099	$C_{27}H_{50}O_{11}P^-$
FA(16:0) [M-H]$^-$	0.9	255.2332	$C_{16}H_{31}O_2^-$	CerP 40:3;O6/LPS 34:2;O/PS 34:1/PS O-34:2;O [M-H]$^-$	0.1	760.5135	$C_{40}H_{75}NO_{10}P^-$
FA(16:1) [M-H]$^-$	0.8	253.2175	$C_{16}H_{29}O_2^-$	CerP 41:3;O6/PS 35:1/PS O-35:2;O [M-H]$^-$	-1.3	774.5281	$C_{41}H_{77}NO_{10}P^-$

FA(17:0) [M-H]–	0.9	269.2488	$C_{17}H_{33}O_2^-$	CerP 42:3;O6/PS 36:1/PS O-36:2;O [M-H]–	0	788.5447	$C_{42}H_{79}NO_{10}P^-$
FA(17:1) [M-H]–	0.8	267.2332	$C_{17}H_{31}O_2^-$	CerP 42:4;O6/PS 36:2/PS O-36:3;O [M-H]–	0.9	786.5297	$C_{42}H_{77}NO_{10}P^-$
FA(18:0) [M-H]–	0.6	283.2642	$C_{18}H_{35}O_2^-$	PS(39:3) [M-H]–	5.3	826.5647	$C_{45}H_{81}NO_{10}P^-$
FA(18:1) [M-H]–	0.5	281.2486	$C_{18}H_{33}O_2^-$	CerP 42:3;O5/PC 34:2;O/PE 37:2;O/PS O-36:2/PS(P-36:1) [M-H]–	-1.1	772.5489	$C_{42}H_{79}NO_9P^-$
FA(18:2) [M-H]–	0.4	279.2331	$C_{18}H_{31}O_2^-$	CerP 44:5;O5/PC 36:4;O/PE 39:4;O/PS O-38:4/ PS(P-38:3) [M-H]–	0.1	796.5499	$C_{44}H_{79}NO_9P^-$
FA(20:0) [M-H]–	0.9	311.2957	$C_{20}H_{40}O_2^-$	PE-Cer 36:1;O2/SM 33:1;O2 [M-H]–	0.4	687.5449	$C_{38}H_{76}N_2O_6P^-$
FA(20:1) [M-H]–	0.3	309.2800	$C_{20}H_{37}O_2^-$	Dopamine [M-H]–	0	152.0717	$C_8H_{10}NO_2^-$
FA(20:2) [M-H]–	0.3	307.2643	$C_{20}H_{35}O_2^-$	GABA [M-H]–	0	102.0563	$C_4H_8NO_2^-$
FA 20:3/ST 20:0;O2 [M-H]–	0.3	305.2487	$C_{20}H_{33}O_2^-$	Serotonin [M-H]–	0.1	175.0877	$C_{10}H_{11}N_2O^-$
FA 20:4/ST 20:1;O2 [M-H]–	0.3	303.2330	$C_{20}H_{31}O_2^-$	Acetylphosphate [M-H]–	0	138.9802	$C_2H_4O_5P^-$

FA 20:5/ST 20:2;O2 [M-H]⁻	0.0	301.2173	$C_{20}H_{29}O_2^-$	L-Histidinol [M-H]⁻	0	140.0829	$C_6H_{10}N_3O^-$
FA(22:0) [M-H]⁻	-0.8	339.3266	$C_{22}H_{43}O_2^-$	Phenylpyruvic acid [M-H]⁻	-0.1	163.0401	$C_9H_7O_3^-$
FA(22:1) [M-H]⁻	0.0	337.3112	$C_{22}H_{41}O_2^-$	Adenosine [M-H]⁻	1.7	266.0894	$C_{10}H_{12}N_5O_4^-$
FA(22:2) [M-H]⁻	0.0	335.2956	$C_{22}H_{39}O_2^-$	Guanosine [M-H]⁻	0.7	282.0846	$C_{10}H_{12}N_5O_5^-$
FA 22:3/ST 22:0;O2 [M-H]⁻	0.0	333.2799	$C_{22}H_{37}O_2^-$	ADP [M-H]⁻	0.8	426.0225	$C_{10}H_{14}N_5O_{10}P_2^-$
FA 22:4/ST 22:1;O2 [M-H]⁻	0.4	331.2644	$C_{22}H_{35}O_2^-$	AMP [M-H]⁻	0.3	346.0559	$C_{10}H_{13}N_5O_7P^-$
FA 22:5/ST 22:2;O2 [M-H]⁻	0.2	329.2487	$C_{22}H_{33}O_2^-$	cAMP [M-H]⁻	0.7	328.0460	$C_{10}H_{11}N_5O_6P^-$
FA 22:6/ST 22:3;O2 [M-H]⁻	0.0	327.2329	$C_{22}H_{31}O_2^-$	GMP Guanosine monophosphate [M-H]⁻	0.7	362.0510	$C_{10}H_{13}N_5O_8P^-$
FA(24:0) [M-H]⁻	-0.6	367.3579	$C_{24}H_{47}O_2^-$	Adenine [M-H]⁻	0.2	134.0472	$C_5H_4N_5^-$
FA(24:1) [M-H]⁻	-0.3	365.3424	$C_{24}H_{45}O_2^-$	Guanine [M-H]⁻	-0.2	150.0421	$C_5H_4N_5O^-$
PA head group [M-H]⁻	0.0	152.9958	$C_3H_6O_5P^-$	Hypoxanthine [M-H]⁻	0.2	135.0313	$C_5H_3N_4O^-$
Hex2Cer30:1;O4 [M-H]⁻	0.1	836.5378	$C_{42}H_{78}NO_{15}^-$	Purine [M-H]⁻	0	119.0363	$C_5H_3N_4^-$

Hex2Cer32:1;O4 [M-H]⁻	0.1	864.5691	$C_{44}H_{82}NO_{15}^-$	Xanthine [M-H]⁻	-0.1	151.0261	$C_5H_3N_4O_2^-$
Hex2Cer32:2;O4 [M-H]⁻	0.1	862.5534	$C_{44}H_{80}NO_{15}^-$	6-Methylnicotinamide [M-H]⁻	0.2	135.0564	$C_7H_7N_2O^-$
Hex2Cer34:4;O4 [M-H]⁻	0.0	886.5534	$C_{46}H_{80}NO_{15}^-$	Pyridoxine [M-H]⁻	-0.1	168.0666	$C_8H_{10}NO_3^-$
HexCer32:1;O4 [M-H]⁻	0.4	702.5165	$C_{38}H_{72}NO_{10}^-$	Pyridoxal [M-H]⁻	0	166.0510	$C_8H_8NO_3^-$
LdMePE(16:0)/LPC 15:0/LPC O-15:1;O/LPE 18:0/LPE O-18:1;O [M-H]⁻	0.2	480.3097	$C_{23}H_{47}O_7NP^-$	Nicotinamide [M-H]⁻	0.1	121.0407	$C_6H_5N_2O^-$
LPA(16:0) /LPA O-16:1;O [M-H]⁻	0.3	409.2362	$C_{19}H_{38}O_7P^-$	Cytidine [M-H]⁻	1.7	242.0787	$C_9H_{12}N_3O_5^-$
LPA(18:0) /LPA O-18:1;O [M-H]⁻	0.1	437.2674	$C_{21}H_{42}O_7P^-$	Uridine [M-H]⁻	1.4	243.0626	$C_9H_{11}N_2O_6^-$
LPE(P-18:0)/LPC O-15:1/LPE O-18:1 [M-H]⁻	0.0	464.3147	$C_{23}H_{47}O_6NP^-$	Cytidine monophosphate [M-H]⁻	0.1	322.0446	$C_9H_{13}N_3O_8P^-$
LPI(16:0)/LPI O-16:1;O [M-H]⁻	0.5	571.2891	$C_{25}H_{48}O_{12}P^-$	dCMP [M-H]⁻	0.6	306.0498	$C_9H_{13}N_3O_7P^-$
LPI(18:0)/LPI O-18:1;O [M-H]⁻	0.6	599.3205	$C_{27}H_{52}O_{12}P^-$	dUMP [M-H]⁻	1.5	307.0341	$C_9H_{12}N_2O_8P^-$
Oleamide/SPB 18:2;O [M-H]⁻	0.5	280.2646	$C_{18}H_{34}NO^-$	UDP-N-acetylglucosamine [M-H]⁻	0.2	606.0748	$C_{17}H_{26}N_3O_{17}P_2^-$

LPA 32:2;O/LPG O-29:3/PA 32:1/PA O-32:2;O [M-H]$^-$	0.0	645.4500	$C_{35}H_{66}O_8P^-$	Uridine 5'-monophosphate [M-H]$^-$	0.1	323.0286	$C_9H_{12}N_2O_9P^-$
LPA 34:2;O/LPG O-31:3/PA 34:1/PA O-34:2;O [M-H]$^-$	0.4	673.4816	$C_{37}H_{70}O_8P^-$	Cytosine [M-H]$^-$	0.4	110.0360	$C_4H_4N_3O^-$
LPA 34:3;O/LPG O-31:4/PA 34:2/PA O-34:3;O/DG 41:11/TG O-41:11 [M-H]$^-$	1.3	671.4666	$C_{37}H_{68}O_8P^-$	Methylcytosine [M-H]$^-$	-0.2	124.0516	$C_5H_6N_3O^-$
LPG O-33:3/PA 36:1/PA O-36:2;O [M-H]$^-$	0.6	701.5131	$C_{39}H_{74}O_8P^-$	Thymine [M-H]$^-$	-0.1	125.0356	$C_5H_5N_2O_2^-$
				Uracil [M-H]$^-$	0.5	111.0203	$C_4H_3N_2O_2^-$

Table 4. 2. *The classification of annotated metabolites detected from ApoE4 KI and wild-type H4 cells by OrbiSIMS.*

Classification of metabolites	**Number of metabolites (192)**
Lipids	115 (86 ions have multiple assignment)
Amino acids and derivatives	27
Carbohydrates and carbohydrate conjugates	6
Carboxylic/Dicarboxylic acids and derivatives	5
Purines nucleotides and purine derivatives	11
Pyridines and derivatives	4
Pyrimidines and pyrimidine derivatives	11
Neurotransmitters	3
Other organic compounds	10

Due to the presence of isomeric ions in the OrbiSIMS spectrum, some ions were assigned to multiple lipid species that share the same chemical composition but have distinct arrangements of atoms in space (stereochemistry). For example, the ion at *m/z* 766.5409 was assigned the chemical formula $C_{43}H_{77}NO_8P^-$ with a mass deviation of less than 2 ppm by simsMFP. This ion matched with five possible lipids in the LipidMaps database (CerP 43:5;O4, PC 35:4, PC O-35:5;O, PE 38:4, PE O-38:5;O).

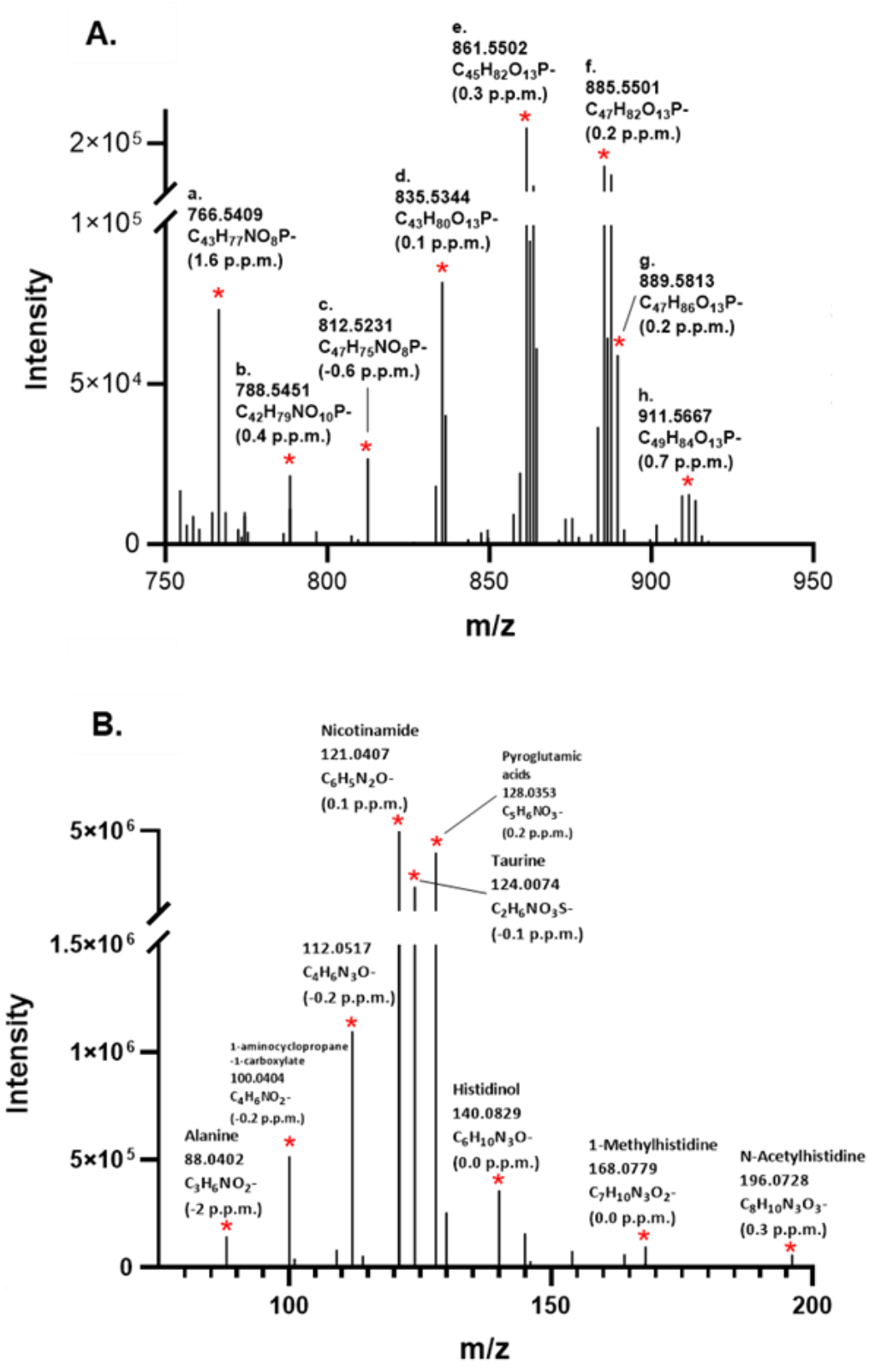
A.
e.
861.5502
C45H82O13P-
(0.3 p.p.m.)
f.
885.5501
C47H82O13P-
(0.2 p.p.m.)
d.
835.5344
C43H80O13P-
(0.1 p.p.m.)
a.
766.5409
C43H77NO8P-
(1.6 p.p.m.)
g.
889.5813
C47H86O13P-
(0.2 p.p.m.)
c.
812.5231
C47H75NO8P-
(-0.6 p.p.m.)
b.
788.5451
C42H79NO10P-
(0.4 p.p.m.)
h.
911.5667
C49H84O13P-
(0.7 p.p.m.)
2×10^5
1×10^5
5×10^4
0
Intensity
750
800
850
900
950
m/z
B.
Nicotinamide
121.0407
C6H5N2O-
(0.1 p.p.m.)
Pyroglutamic
acids
128.0353
C5H6NO3-
(0.2 p.p.m.)
Taurine
124.0074
C2H6NO3S-
(-0.1 p.p.m.)
5×10^6
1.5×10^6
112.0517
C4H6N3O-
(-0.2 p.p.m.)
1×10^6
1-aminocyclopropane
-1-carboxylate
100.0404
C4H6NO2-
(-0.2 p.p.m.)
Histidinol
140.0829
C6H10N3O-
(0.0 p.p.m.)
5×10^5
Alanine
88.0402
C3H6NO2-
(-2 p.p.m.)
1-Methylhistidine
168.0779
C7H10N3O2-
(0.0 p.p.m.)
N-Acetylhistidine
196.0728
C8H10N3O3-
(0.3 p.p.m.)
0
Intensity
100
150
200
m/z

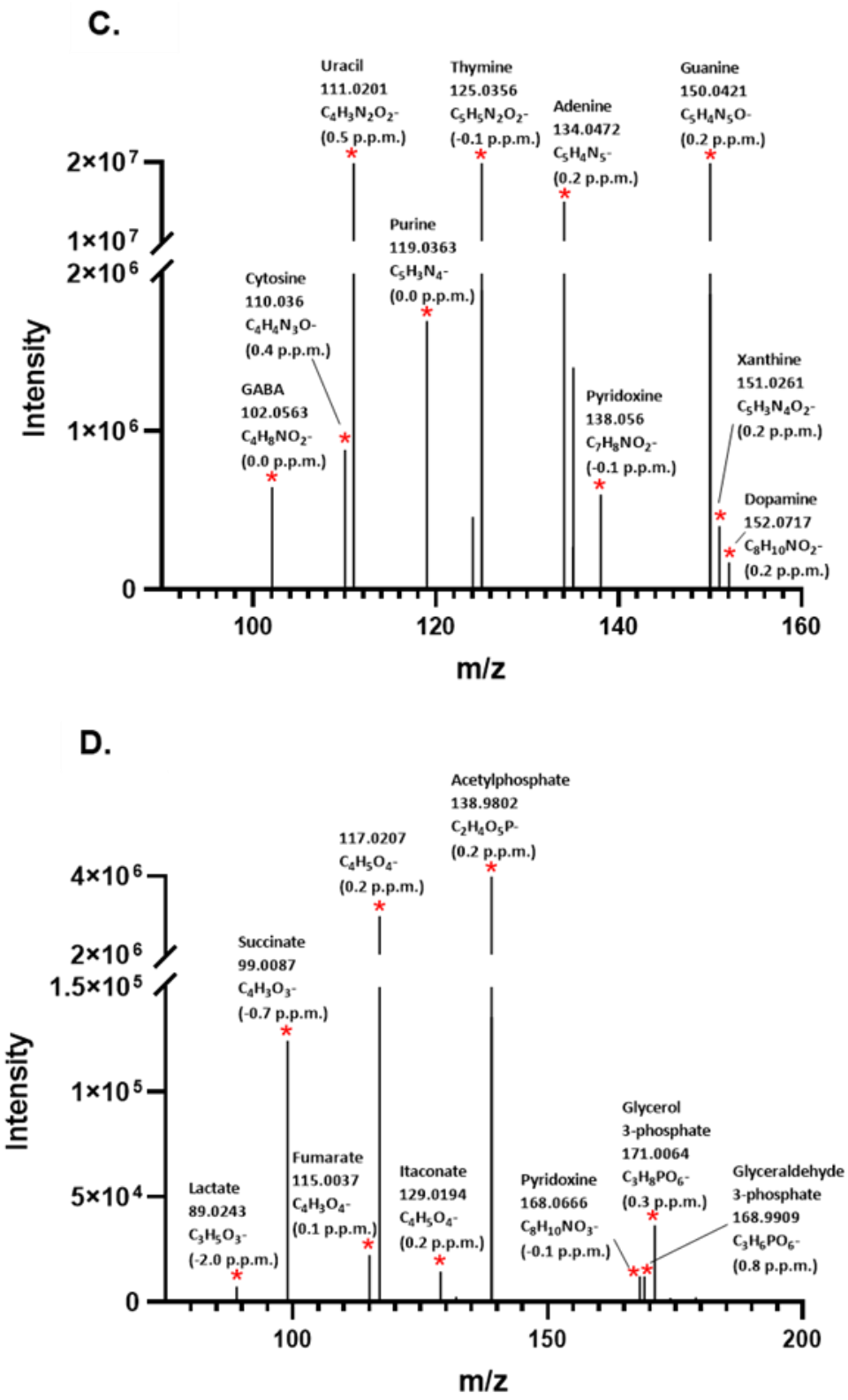

Figure 4. 2. *Example ions spectrum assignment of H4 cells. OrbiSIMS spectra for the control H4 cell sample with putative assignments for (A) lipids (only one*

assignment labelled for each lipid ion in this figure), (B) amino acids and amino acid derivatives, (C) neurotransmitters and nucleic acids and (D) carbohydrates, carboxylic acids and other organic acids. Full assignment for Figure 1b: PE 38:4(CerP 43:5;O4/PC 35:4/PC O-35:5;O/ PE O-38:5;O); PS 36:1(CerP 42:3;O6/ PS O-36:2;O); PE 42:9(PC 39:9/PC O-39:10;O/ PE O-42:10;O); PI 34:1(LPI 34:2;O/ PI O-34:2;O); PI 36:2(PI O-36:3;O); PI 38:4(PI O-38:5;O); PI 38:2(PI O-38:3;O); PI 40:5(PI O-40:6;O).

Figure 4.2A shows the assignment of a targeted series of lipid ions that were detected from H4 control and ApoE4-KI groups, including putatively annotated lipids such as $C_{43}H_{77}NO_8P^-$ (CerP 43:5;O4/PC 35:4/PC O-35:5;O/PE 38:4/PE O-38:5;O, *m/z* 766.5409), $C_{42}H_{79}NO_{10}P^-$ (CerP 42:3;O6/PS 36:1/PS O-36:2;O, *m/z* 788.5451), $C_{45}H_{82}O_{13}P^-$ (PI 36:2/PI O-36:3;O , *m/z* 861.5502). Overall, 115 lipids (86 ions have multiple assignment) have been annotated from H4 wild-type and ApoE4-KI cells, including the main eleven classes (FA, PA, PE, PS, PG, PI, SM, CL, CPA, CerP, HexCer) which also were mainly detected from a recent study of single-cell macrophage metabolomics using OrbiSIMS [160].

In the OrbiSIMS analysis of H4 control and ApoE4 knock-in (KI) cells, various amino acids and their derivatives were detected, including asparagine, glutamine, and taurine (Figure 4.2B). Neurotransmitters such as GABA and dopamine, along with pyrimidines and their derivatives (cytosine, thymine, uracil) and purines and their derivatives (guanine, adenine, hypoxanthine), were also identified in this study (Figure 4.2C). These findings align with previous work by Passarelli *et al*. [158, 160]. However, purine and xanthine, which were undetected in earlier studies, were successfully identified here. Additionally, Figure 4.2D highlights ions assigned to carbohydrates (glyceraldehyde 3-phosphate), carboxylic acids (fumarate), and other organic acids (lactate), which were also not detected in prior research. These findings demonstrate the extended molecular coverage achieved in this study.

The freeze-dried OrbiSIMS method for H4 cells successfully detects a wide range of metabolites, including polar metabolites such as amino acids and nucleic acids, as well as lipids. This highlights the potential and effectiveness of OrbiSIMS as a powerful metabolomics screening tool, capable of providing detailed molecular insights with

minimal sample preparation and without the need for extensive chemical modification. The ability to detect both polar and non-polar compounds further strengthens its application in metabolic profiling and biomarker discovery. Additionally, the depth profiles of selected secondary ions are depicted in Figure 4.3, which offers insights into the distinct localisation or enrichment patterns of molecules within the cells. Notably, the lipid ions shown in Figure 4.3A exhibit a higher concentration on the cell surface, with intensity gradually decreasing as analysis depth increases. This pattern aligns well with the high lipid content at the cell membrane. Similarly, amino acids exhibit the same trend as lipids, suggesting an enrichment of membrane-bound proteins. In contrast, ions related to nucleic acids display varying depth profiling trends.

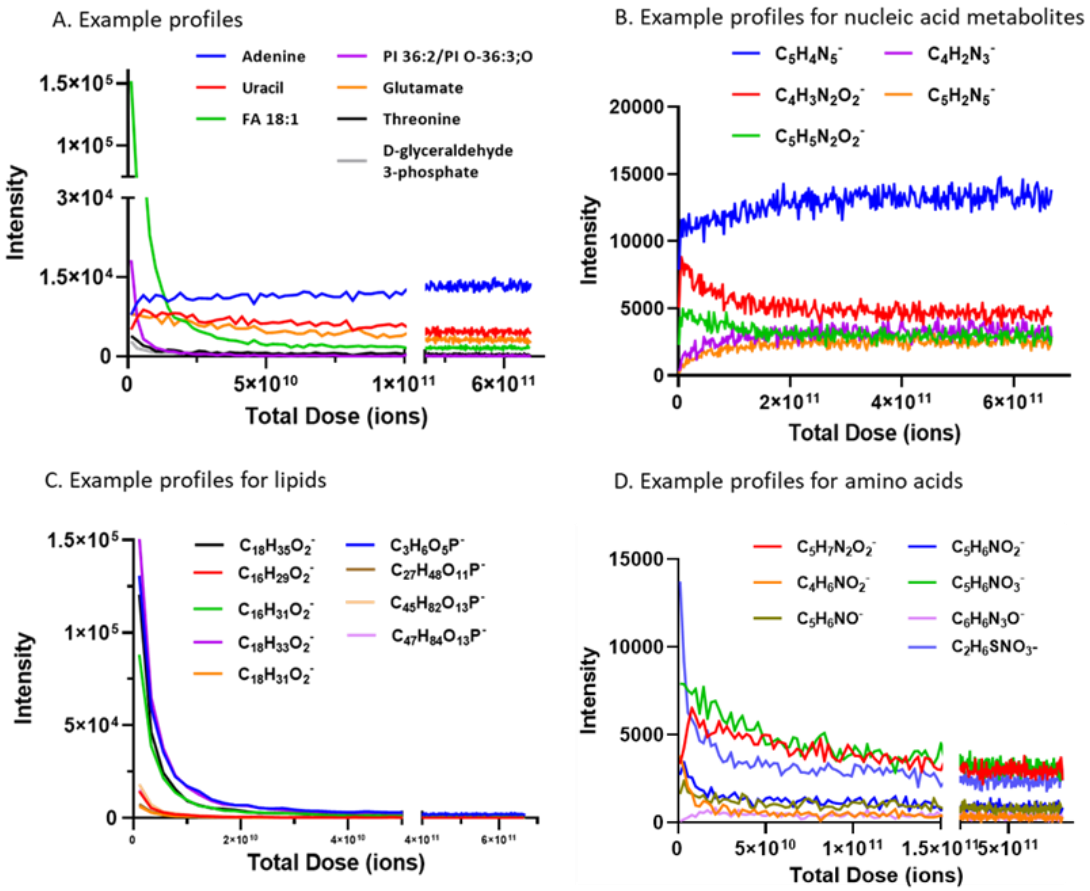

Figure 4.3. *The example profiles of metabolites assigned from H4 neuroglioma cells by using OrbiSIMS. It shows the unique depth profile of each compound class, such as lipids, the major components of membrane, which are highly enriched in the surface of cells.*

Surface mass spectrometry techniques such as MALDI (Matrix-Assisted Laser Desorption/Ionisation) are widely used for biological sample analysis, but require optimisation of sample preparation, including matrix application. LAESI (Laser Ablation Electrospray Ionisation) relies on water-rich samples, while DESI (Desorption Electrospray Ionisation) and LESA (Liquid Extraction Surface Analysis) are less commonly applied to cells and tissues due to their relatively low spatial resolution. In contrast, OrbiSIMS offers label-free analysis without the need for matrix or solvent-based preparation, enabling the detection of small sample amounts without interference from buffers or matrices. Beyond label-free metabolite detection and depth profiling, OrbiSIMS also allows for high-resolution metabolite imaging in cellular studies. Using OrbiSIMS imaging techniques, Linke *et al.* identified a novel metabolite biomarker (fumarate) associated with an aggressive medulloblastoma subgroup intermediate and also observed both intra- and inter-nodular heterogeneity [150]. These capabilities make OrbiSIMS particularly powerful for studying brain diseases at the cellular level, offering significant advantages over other surface mass spectrometry techniques in mainly three aspects including label-free, only minimal sample preparation and spatial resolution.

MALDI enables high spatial resolution imaging and is widely used for large biomolecules, but it requires matrix application, which can lead to background noise and complicate small molecule analysis. DESI operates under ambient conditions and allows direct analysis of tissue surfaces, but it typically suffers from low spatial resolution (around 50–200 μm) and solvent spreading, which can affect spatial accuracy. LESA enables targeted extraction of analytes from specific surface regions, making it useful for selective analysis, but it lacks spatial resolution (typically > 500 μm) and requires relatively large sampling areas.

In contrast, OrbiSIMS combines the high mass accuracy and resolving power of an Orbitrap mass analyser with secondary ion mass spectrometry. It offers label-free imaging with a spatial resolution as fine as 2 μm, enabling detailed molecular mapping at subcellular levels. Although OrbiSIMS imaging was not applied in this study, its high spatial resolution and depth profiling capabilities make it an excellent tool for investigating complex brain cell environments. Future research on the ApoE4 risk

gene and its molecular consequences in neurodegenerative disease could greatly benefit from the application of this technique.

Overall, metabolic screening of H4 cells using OrbiSIMS allows us to obtain a wide range of chemical classes *in situ*, covering polar metabolites and low polar lipids. The advantages of OrbiSIMS as a screening tool include the need for only a small amount of sample to collect enough signal, quick analysis time, and minimal sample preparation.

4.3.2 Multivariate analysis distinguishes control H4 cells and ApoE4 KI cells based on OrbiSIMS-annotated metabolites

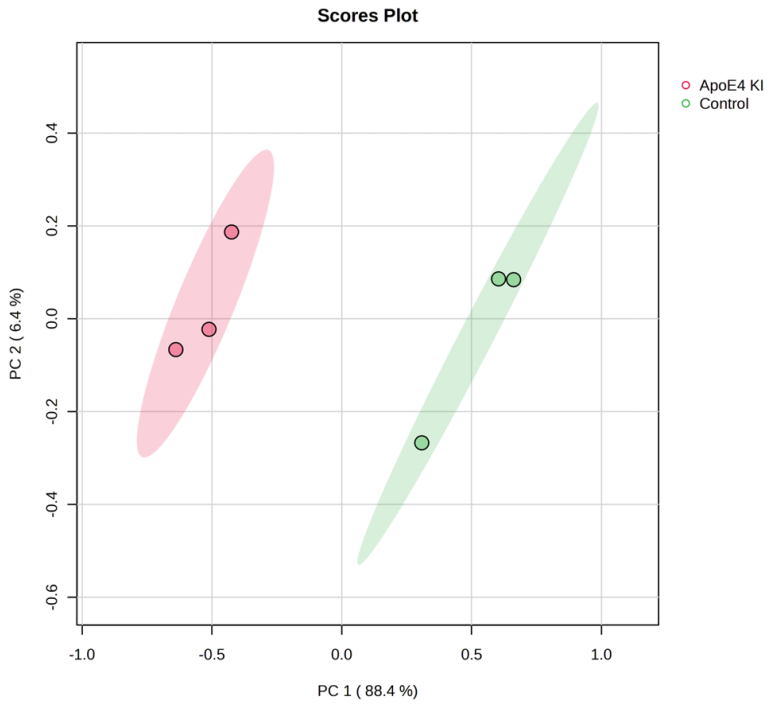

Figure 4.4. *PCA score plot of H4 control samples and ApoE4 KI samples. [PERMANOVA] F-value: 30.893; R-squared: 0.88536; p-value (based on 999 permutations): 0.1. PCA was performed on pareto scaled data.*

To further evaluate the screening tool capability of OrbiSIMS, multivariate analysis was performed to test whether OrbiSIMS data can distinguish the metabolic changes

between control and ApoE4 KI cells. Principal component analysis (PCA) based on 192 annotated datasets was performed and is presented in Figure 4.4. The ApoE4 KI samples are clearly separated from the control samples, with the main component PC1 explaining 88.4 % of the variance between control and ApoE4 KI cells. The R-squared value of this PCA model is 0.88536, indicating that the PCA is a good fit for the actual dataset. These PCA results provide evidence that the OrbiSIMS dataset can differentiate control samples from ApoE4 KI samples.

To further explore the ApoE4-related metabolic profile, PLS-DA (Partial least squares discriminant analysis) of all ions from ApoE4 KI was used for discriminative analysis compared with Control cells. The scores plot in Figure 4.5A shows the divergence in metabolic profiling between the control and ApoE4-expressing cells. The features with VIP (variable importance for projection) > 1 plus FDR (false discovery rate) adjusted *p*-value < 0.05 were considered statistically significant. From this analysis, we obtained 35 metabolic signatures (Table 4.3.) for further pathway analysis and their relative intensities are shown in Figures 4.5B and 4.5C. In which 26 out of 35 are lipids and have statistically less abundance in the ApoE4-carried cells (Figure 3.3a). Moreover, those lipids were mainly enriched in two classes of glycerophospholipids (glycerophosphoethanolamines, glycerolphosphoinositols) by metabolite set enrichment analysis, indicating the disruption of the glycerophospholipid pathway by ApoE4 (Figure 3.3b).

Table 4.3*. The peak list of significant features in OrbiSIMS*

Feature	**Accurate mass**	**Formula**	**FDR**	**VIP**
Alanine	90.05489	$C_3H_7NO_2$	0.001168	1.0242
Succinate	117.0196	$C_4H_6O_4$	0.001368	1.1278
Valine	118.0860	$C_5H_{11}NO_2$	0.000765	1.0213
Taurine	124.0075	$C_2H_7NO_3S$	0.00597	1.0231
Methylcytosine	124.0516	$C_5H_6N_3O^-$	0.0008	1.0228
Aspartate	132.0304	$C_4H_7NO_4$	0.005173	1.1645
Creatine	132.0765	$C_4H_9N_3O_2$	0.002327	1.1287
L-Histidinol	140.0829	$C_6H_{10}N_3O^-$	0.001411	1.1308
Glutamate	146.0460	$C_5H_9NO_4$	0.002434	1.1162
LPA 32:2;O/LPG O-29:3/PA 32:1/PA O-32:2;O	645.4500	$C_{35}H_{66}O_8P^-$	0.009797	1.3917

LPA 34:2;O/LPG O-31:3/PA 34:1/PA O-34:2;O	673.4816	$C_{37}H_{70}O_8P$-	0.021659	1.0075
PE-Cer 36:1;O2/SM 33:1;O2	687.5449	$C_{38}H_{76}N_2O_6P^-$	0.000994	1.2395
CerP 39:2;O4/LPC 31:2;O/LPE 34:2;O/LPS O-33:2/PC 31:1/PC O-31:2;O/PE 34:1/PE O-34:2;O	716.5239	$C_{39}H_{75}NO_8P^-$	0.006462	1.1123
BMP 34:1/LPG 34:2;O/PG 34:1/PG O-34:2;O	747.5184	$C_{40}H_{76}O_{10}P^-$	0.006266	1.0287
CerP 43:6;O3/PC O-35:6/PE O-38:6/ PE(P-38:5)	748.5303	$C_{43}H_{75}NO_7P^-$	0.029789	1.4563
CerP 43:3;O3/PC O-35:3/PE O-38:3/ PE(P-38:2)	754.5770	$C_{43}H_{81}NO_7P^-$	0.002326	1.5094
CerP 42:3;O4/LPC 34:3;O/PC 34:2/PC O-34:3;O/PE 37:2/PE O-37:3;O	756.5559	$C_{42}H_{79}O_8NP^-$	0.001956	1.6763
CerP 42:2;O4/LPC 34:2;O/PC 34:1/PC O-34:2;O/PE 37:1/PE O-37:2;O	758.5690	$C_{42}H_{81}O_8NP^-$	0.009101	1.5345
CerP 40:3;O6/LPS 34:2;O/PS 34:1/PS O-34:2;O	760.5135	$C_{40}H_{75}O_{10}NP^-$	0.006746	1.1989
CL(78:9) $[M-2H]^{2-}$	764.5169	$C_{87}H_{150}O_{17}P_2^-$	0.018211	2.1490
CerP 43:5;O4/PC 35:4/PC O-35:5;O/PE 38:4/PE O-38:5;O	766.5409	$C_{43}H_{77}NO_8P^-$	0.004197	2.1336
PE(38:3)/HexCer 37:3;O4	768.5649	$C_{43}H_{79}O_8NP^-$	0.003316	1.5664
CerP 42:3;O5/PC 34:2;O/PE 37:2;O/PS O-36:2/PS(P-36:1)	772.5489	$C_{42}H_{79}O_9NP^-$	0.003612	1.7160
CerP 41:3;O6/PS 35:1/PS O-35:2;O	774.5281	$C_{41}H_{77}O_{10}NP^-$	0.011201	1.7778
PE(P-40:6)/HexCer 39:6;O3	774.5515	$C_{45}H_{77}O_7NP^-$	0.001559	1.4745

DG 46:10;O2/TG 46:9;O/TG O-46:10;O2/PG 36:1/PG O-36:2;O	775.5507	$C_{42}H_{80}O_{10}P^-$	0.049386	1.2227
CerP 42:4;O6/PS 36:2/PS O-36:3;O	786.5297	$C_{42}H_{77}NO_{10}P^-$	0.008293	1.2742
PC 37:7/PC O-37:8;O/PE 40:7/PE O-40:8;O	788.5231	$C_{45}H_{75}O_8NP^-$	0.005007	1.6742
PC 39:9/PC O-39:10;O/PE 42:9/PE O-42:10;O	812.5231	$C_{47}H_{75}NO_8P^-$	0.010054	1.7771
PI 36:3/PI O-36:4;O	859.5349	$C_{45}H_{80}O_{13}P^-$	0.022609	1.0812
PI 37:3/PI O-37:4;O	873.5492	$C_{46}H_{82}O_{13}P^-$	0.006905	1.2638
PI 38:3/PI O-38:4;O	887.5659	$C_{47}H_{84}O_{13}P^-$	0.005864	1.0319
PI 38:2/PI O-38:3;O	889.5813	$C_{47}H_{86}O_{13}P^-$	0.039471	1.1953
PI 39:4/PI O-39:5;O	899.5658	$C_{48}H_{84}O_{13}P^-$	0.00597	1.0172
PI 39:3/PI O-39:4;O	901.5813	$C_{48}H_{86}O_{13}P^-$	0.03287	1.0457

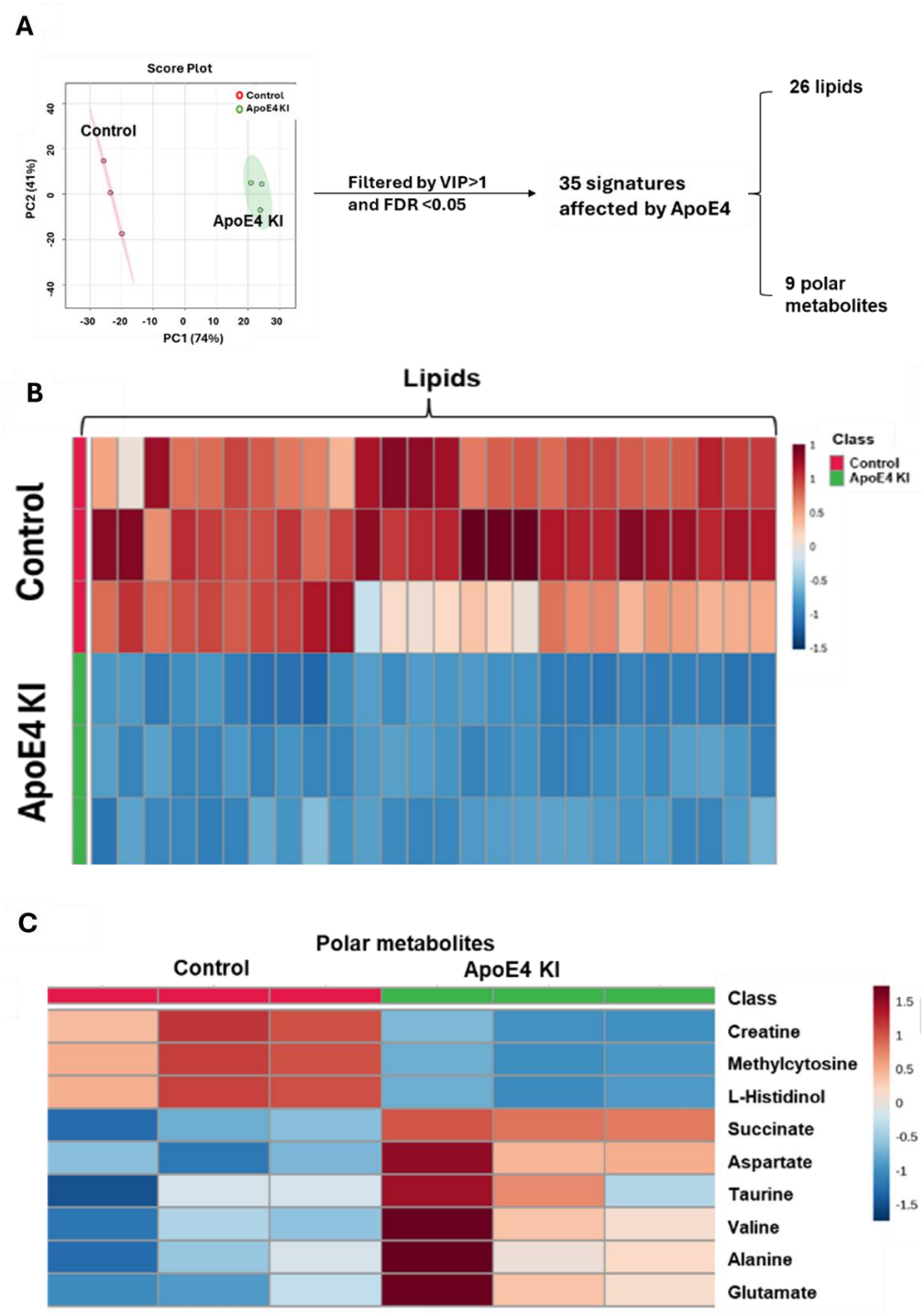

Figure 4.5. *Metabolomics analysis of OrbiSIMS. (A) Score plot of PLS-DA of OrbiSIMS data, following the lipid classification and pathway analysis for 35 significant metabolites. (B) Heatmap of 26 lipid signatures between Control and ApoE4 KI group. (C) Heatmap of 9 signatures between Control and ApoE4 KI group. (e) The pathway analysis of 9 out of 35 signatures except for 26 lipids.*

In addition, the rest of the 9 features vary differently between control and ApoE4 KI cells, and are mostly enriched in alanine, aspartate, and glutamate metabolism (Figure 4.6), suggesting the metabolic disorders of these three amino acids. Besides, aminoacyl-tRNA biosynthesis, glutamine metabolism and taurine and hypotaurine metabolism also have been affected by ApoE4. Levels of alanine, aspartate, and glutamate all increase in the ApoE4 KI group, which partially contrasts with other metabolomics studies showing their low concentrations in AD patients [178].

Glutamate is one of the excitatory neurotransmitters in the human brain and plays a crucial role in multiple cerebral functions such as memory, cognition, and motor behaviour [179]. A low level of glutamate has been detected in the aged human brain and AD patients, indicating the vital role of glutamate as a biomarker of brain functions. Moreover, the disruption of glutamate metabolism is associated with neuronal loss and synaptic damage. Aside from glutamate, the level of aspartate in AD patients' brains was decreased compared with the normal brain in previous studies [180].

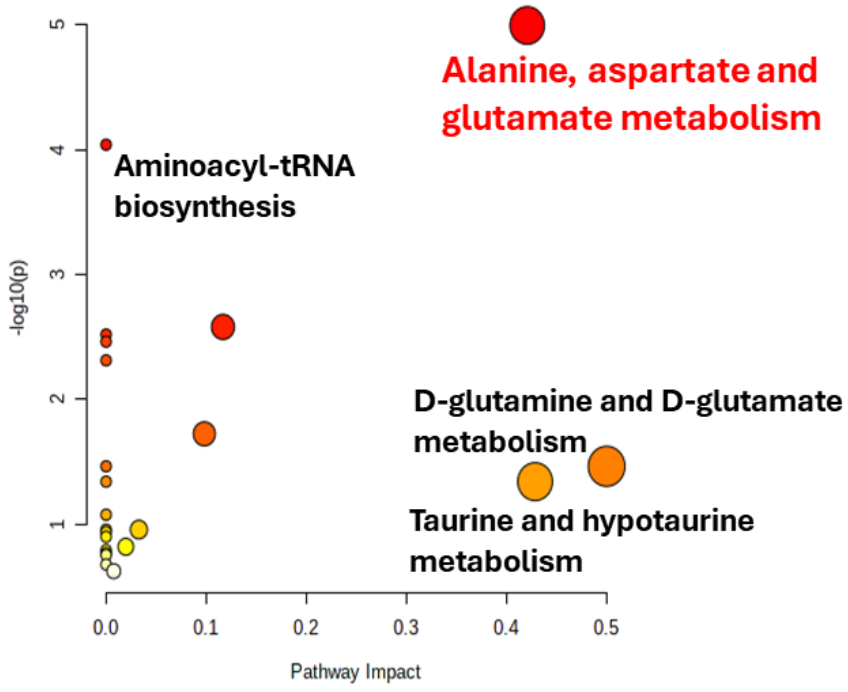

Figure 4.6. *The pathway analysis of 9 out of 35 signatures except for 26 lipids.*

Aspartate has many biochemical roles, donating amino groups to the urea cycle, participating in gluconeogenesis, as well as stimulating NMDA (N-methyl-D-aspartate) receptors which play a crucial role in synaptic modification [181]. Besides, the level of alanine during the development of AD is controversial due to the different functions of D and L-alanine. Higher D-alanine levels were associated with more behavioural symptoms, and the content of D-alanine in white and grey matter tissues of the Alzheimer's brain is significantly higher than in normal brains [182, 183]. However, total alanine content in Alzheimer's gray matter have shown a very significant decrease compared with normal tissues [182]. In mammals, alanine is used to make proteins, convert glucose into energy, and repair muscle tissue [184]. In terms of depth profiling analysis of OrbiSIMS that was used in our study, D and L enantiomers of alanine could not be differentiated therefore the alanine level is supposed to be lower in ApoE4-carried H4 cells.

4.3.3 Lipid Reduction Induced by ApoE4 in H4 Cells Validated Using LipidTOX Staining

To validate the alteration of lipids by ApoE4, cells were stained with LipidTOX neutral lipid dye which significantly dropped lipid droplets in the ApoE4 KI group (Figure 4.7). The results are consistent with the low ability of ApoE4 in transporting lipids and cholesterol, resulting in dysfunction of the intracellular lipid state which is associated with increased amyloid plaques and tau phosphorylation of AD [185, 186].

Besides, ApoE presents as two statues in the cell, lipidated ApoE, and free ApoE. The lipidation status of ApoE has shown its ability to lower Aβ production, while unlipidated ApoE promotes the formation of amyloid plaques [187]. A recent AD brain-based study found that the lower level of lipidated ApoE lipoprotein in the E4 carrier impacts Aβ binding to microglia and subsequently affects microglia clearance in response to Aβ [117]. Our results further support the hypothesis that ApoE4 triggers metabolic disorders of AD by affecting the abundance of glycerophospholipids.

Based on the results obtained from OrbiSIMS data and LipidTOX staining, the lipid

content within the cells has been detected and validated. This reduction in lipid levels might be attributed to three possible reasons: (1) lipid biosynthesis is affected by ApoE4; (2) the transport and absorption of lipids from the culture medium are inhibited by ApoE4, or ApoE4 is less efficient at lipid transport compared to ApoE3; and (3) the clearance or elimination of lipids is accelerated by ApoE4.

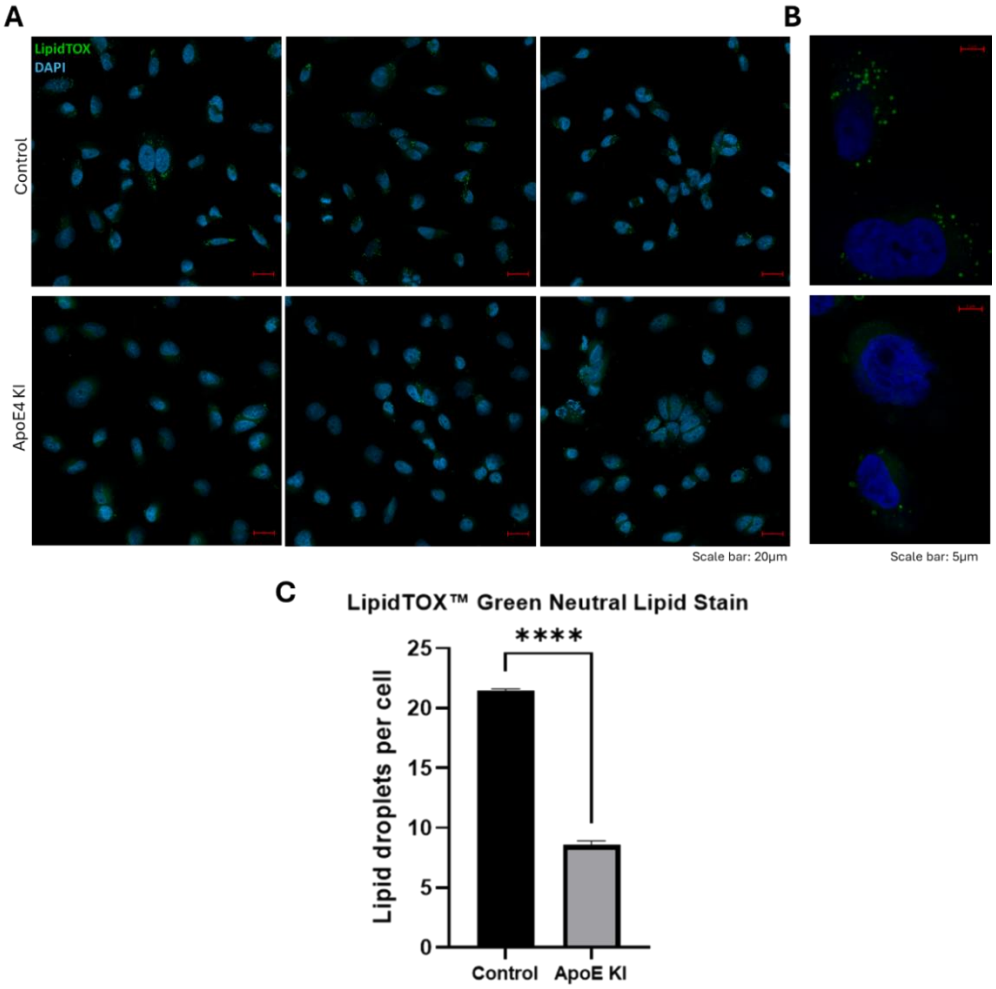

Figure 4.7. *Validation of Lipid Changes by LipidTOX Neutral Lipid Staining. A) The fluorescence image of LipidTOX Green Neutral Lipid Stain in control samples and ApoE4 KI samples (n=3). The nuclei were stained by DAPI, shown as blue colour. Scale bar: 20 μm. B) The fluorescence images with a scale bar of 5 μm. C) The statistical analysis of lipid changes in the control group compared to the ApoE4 KI group. The average number of lipid droplets per cell was calculated using ImageJ software. Data are expressed as the mean ± SD (n=3). *** $p < 0.001$; **** $p < 0.0001$.*

4.4 Conclusion

The results presented in this chapter demonstrate that OrbiSIMS can effectively detect a broad range of metabolites and lipids, offering a rapid and efficient approach for screening metabolic profiles in the context of the ApoE4 risk gene. Multivariate analysis revealed distinct metabolic differences between ApoE4 KI cells and control cells, with pathway analysis highlighting significant alterations in metabolic pathways. To validate the lipid changes observed in OrbiSIMS data, lipid fluorescent staining confirmed a reduction in lipid droplets, aligning with the OrbiSIMS findings.

However, the observed alterations in amino acids (alanine, aspartate, and glutamate) in ApoE4 cells did not fully match results from other studies, suggesting that further experimental methods may be required to confirm these findings. Despite this, OrbiSIMS presents notable advantages over conventional LC-MS/MS techniques, by eliminating the need for time-consuming sample preparation; and enabling the simultaneous analysis of both polar metabolites and lipids, without requiring specific extraction or separation solvents. Whilst OrbiSIMS simplifies the analysis process, it is important to account for the higher ionisation energy and fragmentation patterns inherent to this technique when interpreting data, particularly as they can affect the accuracy of metabolite identification.

Chapter 5: Polar metabolomics analysis using LC-MS/MS and comparative analysis with OrbiSIMS data.

5.1 Chapter aims

The results presented and explored in Chapter 4 elucidate the merits of OrbiSIMS as an effective multi-omics screening tool (polar metabolomics and lipidomics). OrbiSIMS can detect a wide range of metabolites and lipids, including both polar and non-polar compounds. Key advantages of using OrbiSIMS include minimal sample preparation, in combination with the need for a smaller number of cells. For example, only 400-500 cells were used in the OrbiSIMS analysis described in Chapter 4. However, due to the ionisation mechanism of OrbiSIMS not being fully understood, other validation approaches are needed to further confirm and evaluate OrbiSIMS results. The lipid results were evaluated using a lipid staining method in Chapter 4, which confirmed that the lipid detection from OrbiSIMS can reflect the actual changes in lipids affected by ApoE4.

For the lower mass range of metabolites, such as amino acids carboxylic/ dicarboxylic acids and carbohydrates, which might be fragments of other molecules, further investigation is needed. To explore amino acid alterations caused by the ApoE4 knock-in, standard polar metabolomics using the hydrophilic interaction chromatography (HILIC) LC-MS/MS method will be applied and discussed in this chapter. For the first time, the comparison of OrbiSIMS and LC-MS/MS results will be discussed in two aspects: the commonly detected metabolites and the alteration changes of the metabolites by both approaches.

5.2 Methods

5.2.1 Cell sample preparation for LC-MS/MS

The control and ApoE4 KI H4 cells were separately seeded in 25 cm² flasks at a concentration of 1×10^6 cells per flask and incubated for 24 hours. After incubation, the media was removed, and the cells were briefly washed with PBS at 37 °C. 500 µL cold methanol (- 40 ℃) was added to simultaneously quench the metabolism and extract the intracellular metabolites. Cells were scraped and vortexed vigorously for 1h on ice and centrifuged at 19,273 × g for 10 minutes at 4 ℃. Supernatants were transferred into new tubes and evaporated using the Jouan Centrifugal Evaporator. The remaining residue was reconstituted in 70 µL of methanol (4 ℃) and centrifuged at 19,273 × g for 10 min at 4 ℃. 50-70 µL of the extract was transferred into an amber HPLC vial with a glass insert, labelled, and used for LC-MS/MS analysis. 10 µL of each sample was collected and mixed as a pooled QC for untargeted analysis and MS/MS analysis to check the performance of the analytical system.

Drift in measured response, retention time, and mass calibration is a common issue in LC-MS instruments due to sample contact with multiple platform components and fluctuations in temperature, pressure, or instrument performance. Implementing a QC strategy is essential in LC-MS metabolomics to ensure reliable, reproducible, and high-quality data [188, 189]. QC serves several critical purposes: 1. Equilibrating the Analytical Platform: Ensures the system is stable and provides consistent data output. 2. Assessing Technical Precision: Evaluates the reproducibility of each analytical test. 3. Facilitating Signal Correction: Provides data for correcting signal drift within and across analytical tests.

5.2.2 LC-MS/MS analysis

LC-MS/MS analysis was performed using Q-Exactive Plus mass spectrometer equipped with a Dionex U3000 UHPLC system. Samples for metabolomics (10 µL, 4 °C) were separated and eluted through a ZIC-pHILIC column (4.6 × 150 mm, 5 µm particle size, Merck SeQuant, Darmstadt, Germany) at an HPLC flow rate of 300 µL min^{-1} and a temperature of 45 ℃. The gradients started with 20 % A (20 mM

ammonium carbonate in water) and 80 % of B (acetonitrile) and increased to 95 % A over 15 min, then the composition was returned to its initial conditions in 2 min, and the column was re-equilibrated for 7 min. The MS instrumentation was set as ESI^+ and ESI^- switching acquisition modes for profiling samples and in data-dependent MS/MS for identification of QC samples. Details of MS parameters were shown as follows: spray voltage at 4.5 kV (ESI^+) and -3.5 (ESI^-), the capillary voltage at 20 V (ESI^+) and −15 V (ESI^-). The sheath, auxiliary, and sweep gas flow rates were 40, 5, and 1 (arbitrary unit), respectively, for both modes. Capillary and heater temperatures were maintained at 275 °C and 150 °C, respectively. Data were acquired for LC-MS profiling with a resolution of 70,000 from *m/z* 70–1050. Top 5 dd MS/MS was performed on the QC sample ($n = 3$) at a resolution of 17,500 and stepped normalised collision energy (NEC) of 20, 30, and 40.

The cellular samples of the control group and ApoE4 KI group were randomized and analysed in a single LC-MS analytical run with the mixtures of authentic standards and reagent blanks. Pooled QC ($n = 4$) was injected at the beginning of the analysis to condition the column and after every 3–5 samples ($n = 6$) to check the stability, robustness, repeatability, and performance of the analytical system.

5.2.3 Data analysis and identification and annotation of metabolites

The LC-MS/MS data were pre-processed for untargeted metabolomics, univariate analysis, and metabolite identification using Compound Discoverer 3.3. Subsequently, principal component analysis (PCA) and partial least squares-discriminant analysis (PLS-DA) are processed using SIMCA P. Metabolite identification is performed using Compound Discoverer 3.3 software by matching retention time of detected peaks with the authentic standards, MS/MS fragmentation with mzCloud database and accurate masses with human metabolites in BioCyc database (https://biocyc.org/?sid=biocyc14-3922769627). Retention time ranges from 0.5 min to 15 min (RT tolerance at 0.5 min), the mass range is 70-1050 *m/z,* and mass tolerance ≤ 5 ppm is used for peak picking and identification. The confidence of identified metabolites is classified into four levels according to the classification rules of the metabolomics standard initiative [190]. Level 1 confidence in metabolite identification requires two or more properties of an authentic chemical standard (e.g., accurate mass,

retention time, and MS/MS spectra) to be compared with analyte data acquired under the same conditions (laboratory and analytical methods). Matching with standards is not required for Level 2 and Level 3 identifications. Level 2 confidence is based on matching accurate mass, retention time, and MS/MS data with an online spectral database or external laboratory database. Level 3 refers to putatively characterised compound class, while all unknown compounds are classified as Level 4.

Data were analysed using GraphPad Prism and expressed as the mean ± standard deviation (SD). The statistically significant difference of the metabolites between control and ApoE4 KI group was evaluated using Student's t-test and PLS-DA analysis. FDR-adjusted p-value < 0.05 combined with VIP > 1 was considered as statistical significance.

5.3 Results and Discussion

5.3.1 LC-MS/MS polar metabolomics analysis

HILIC is preferred in metabolomics for its superior retention of polar metabolites compared to reversed-phase liquid chromatography. The HILIC LC-MS/MS methodology includes extracting intracellular metabolic pools using methanol and separating molecules using the HILIC LC condition (Figure 5.1.). ESI ionisation was used in LC-MS/MS analysis, the soft ionization of ESI makes little fragmentation of analyte molecules.

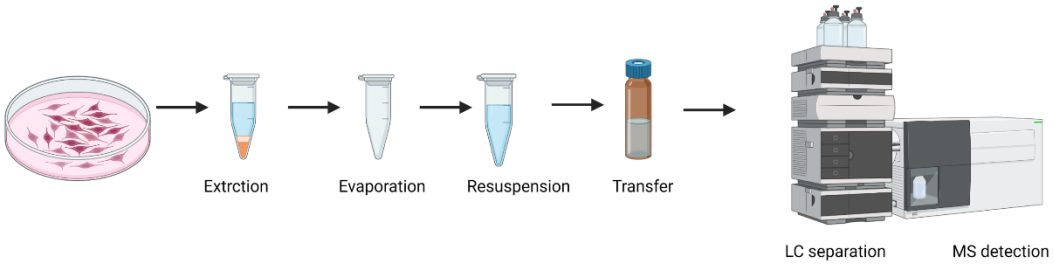

Figure 5.1. *The workflow for LC-MS/MS polar metabolomics analysis includes the extraction of polar metabolites using cold methanol, evaporation, and resuspension to concentrate the metabolites. This is followed by LC separation and mass spectrometry analysis.*

Two groups of H4 cells were used in this chapter — control and ApoE4 knock-in — paralleling our OrbiSIMS studies. The cells, plated at a concentration of 1×10^6 in a 25 cm² flask, were cultured for 24 hours, then extracted using cold methanol, followed by HILIC separation and mass spectrometry detection. In total, 1095 features were commonly detected from both groups and used for identification. The ions were identified based on our lab-based standards database through accurate mass matching and MS/MS data, allowing us to detect numerous polar metabolites, including many amino acids.

The identification process adhered to the confidence levels suggested by the Metabolomics Standards Initiative [190]. It suggests four confidence levels based on accurate mass, retention time, and MS/MS information:

- **Level 1: Identified compounds**. A metabolite is considered identified when two or more orthogonal properties of the analyte – such as retention time, accurate mass, and MS/MS fragmentation patters – match those of authentic standards samples. These standards must be analysed under identical laboratory conditions using the same analytical methods.

- **Level 2: Putatively annotated compounds**. A metabolite is considered putatively annotated when its identification is based on matching spectral data—such as accurate mass, retention time, and MS/MS value - with entries in online spectral databases or external laboratory data.

- **Level 3: Putatively characterised compound classes.** The chemical class of an analyte or metabolite is identified based on spectral similarity to known compound of a chemical class. For example, when only the accurate mass matches with an online mass database or external laboratory data, the compound is classified as Level 3.

Level 4: Unknown compounds. After applying confidence criteria, 121 metabolites were identified with high confidence (Levels 1 and 2) based on MSI levels of identification (Table 5.1.). These include amino acids and derivatives, lipids, carboxylic/dicarboxylic acids, carbohydrates, purines, pyridines, pyrimidines, and other organic acids (Table 5.2).

Table 5. 1. *The classification of annotated metabolites detected from H4 cells by LC-MS.*

Classification of metabolites	Number of metabolites (121)
Lipids	22
Amino acids and AA derivatives	25
Carbohydrates and carbohydrate conjugates	10
Carboxylic/Dicarboxylic acids and derivatives	20
Purines nucleotides and purine derivatives	6
Pyridines and derivatives	4
Pyrimidines and pyrimidine derivatives	5
Nucleosides, nucleotides, and analogues	4
Neurotransmitters	1
Other organic compounds	24

Table 5.2. *The peak list of identified metabolites (Level 1, 2) in LC-MS analysis.*

Metabolites	Classification	Accurate mass	Formula
myo-Inositol	Alcohols and polyols	179.0563	$C_6H_{12}O_6$
Lactate	Alpha hydroxy acids and derivatives	89.0246	$C_3H_6O_3$
1-Aminocyclopropane-1-carboxylate	Amino acids	84.0443	$C_4H_7NO_2$
Alanine	Amino acids	90.0549	$C_3H_7NO_2$
Asparagine	Amino acids	131.0465	$C_4H_8N_2O_3$
Aspartate	Amino acids	132.0305	$C_4H_7NO_4$
Glutamate	Amino acids	146.0461	$C_5H_9NO_4$
Glutamine	Amino acids	145.0620	$C_5H_{10}N_2O_3$
Histidine	Amino acids	156.0767	$C_6H_9N_3O_2$
Lysine	Amino acids	147.1127	$C_6H_{14}N_2O_2$
Proline	Amino acids	116.0704	$C_5H_9NO_2$

Taurine	Amino acids	124.0076	$C_2H_7NO_3S$
Tryptophan	Amino acids	203.0828	$C_{11}H_{12}N_2O_2$
Tyrosine	Amino acids	180.0668	$C_9H_{11}NO_3$
Valine	Amino acids	118.0861	$C_5H_{11}NO_2$
Arginine	Amino acids	175.1188	$C_6H_{14}N_4O_2$
Glycine	Amino acids	76.0393	$C_2H_5NO_2$
Leucine	Amino acids	132.1017	$C_6H_{13}NO_2$
Serine	Amino acids	106.0498	$C_3H_7NO_3$
Threonine	Amino acids	120.0654	$C_4H_9NO_3$
1-Methyl-histidine	Amino acids derivatives	170.0922	$C_7H_{11}N_3O_2$
Cysteate	Amino acids derivatives	167.9974	$C_3H_7NO_5S$
Glutathione	Amino acids derivatives	306.0766	$C_{10}H_{17}N_3O_6S$
Kynurenine	Amino acids derivatives	207.0776	$C_{10}H_{12}N_2O_3$
N-Acetylaspartate	Amino acids derivatives	174.0409	$C_6H_9NO_5$
Phenylalanine	Amino acids derivatives	164.0719	$C_9H_{11}NO_2$
Pyroglutamic acid	Amino acids derivatives	128.0356	$C_5H_7NO_3$
4-Aminobenzoate	Benzenoids	138.0548	$C_7H_7NO_2$
Benzoate	Benzenoids	123.0439	$C_7H_6O_2$
Hippurate	Benzenoids	178.0512	$C_9H_9NO_3$
2-Ethylhexyl phthalate	Benzenoids	279.1587	$C_{16}H_{22}O_4$
homovanillate	Benzenoids	181.0508	$C_9H_{10}O_4$
N-(2-hydroxyphenyl)acetamide	Benzenoids	152.0705	$C_8H_9NO_2$

Erythrose 4-phosphate	Carbohydrates and carbohydrate conjugates	199.0015	$C_4H_9O_7P$
Fructose 6-phosphate	Carbohydrates and carbohydrate conjugates	259.0224	$C_6H_{13}O_9P$
Gluconic acid	Carbohydrates and carbohydrate conjugates	195.0511	$C_6H_{12}O_7$
Glucono 1,4-lactone	Carbohydrates and carbohydrate conjugates	214.1797	$C_{12}H_{20}O_2$
Glycerate	Carbohydrates and carbohydrate conjugates	105.0196	$C_3H_6O_4$
L-Threonic acid	Carbohydrates and carbohydrate conjugates	135.0302	$C_4H_8O_5$
Mannitol	Carbohydrates and carbohydrate conjugates	181.0716	$C_6H_{14}O_6$
N-Acetyl-D-glucosamine	Carbohydrates and carbohydrate conjugates	222.0969	$C_8H_{15}NO_6$
N-Acetylneuraminate	Carbohydrates and carbohydrate conjugates	308.0988	$C_{11}H_{19}NO_9$
Sucrose	Carbohydrates and carbohydrate conjugates	360.1493	$C_{12}H_{22}O_{11}$
5-Aminolevulinate	Carboxylic acids and derivatives	130.0512	$C_5H_9NO_3$
Creatine	Carboxylic acids and derivatives	132.0766	$C_4H_9N_3O_2$
Creatinine	Carboxylic acids and derivatives	114.0661	$C_4H_7N_3O$
2-Aminoadipate	Carboxylic acids and derivatives	162.0758	$C_6H_{11}NO_4$

Acetylcysteine	Carboxylic acids and derivatives	162.0233	$C_5H_9NO_3S$
Capryloylglycine	Carboxylic acids and derivatives	202.1434	$C_{10}H_{19}NO_3$
Citrate	Carboxylic acids and derivatives	191.0199	$C_6H_8O_7$
Cystathionine	Carboxylic acids and derivatives	223.0744	$C_7H_{14}N_2O_4S$
Glutarate	Carboxylic acids and derivatives	131.0352	$C_5H_8O_4$
Glutathione disulfide	Carboxylic acids and derivatives	613.1582	$C_{20}H_{32}N_6O_{12}S_2$
Guanidinoacetate	Carboxylic acids and derivatives	118.0610	$C_3H_7N_3O_2$
Methionine	Carboxylic acids and derivatives	148.0440	$C_5H_{11}NO_2S$
N-Acetylglutamine	Carboxylic acids and derivatives	189.0867	$C_7H_{12}N_2O_4$
N-Acetyl-L-glutamate	Carboxylic acids and derivatives	190.0708	C_7H_{11} NO_5
N-Acetyl-L-methionine	Carboxylic acids and derivatives	190.0545	$C_7H_{13}NO_3S$
N-Acetylornithine	Carboxylic acids and derivatives	175.1075	$C_7H_{14}N_2O_3$
N-Methyl-lysine	Carboxylic acids and derivatives	161.1284	$C_7H_{16}N_2O_2$
Phenylacetylglycine	Carboxylic acids and derivatives	192.0668	$C_{10}H_{11}NO_3$
Fumarate	Dicarboxylic acids and derivatives	115.0040	$C_4H_4O_4$
Succinate	Dicarboxylic acids and derivatives	117.0196	$C_4H_6O_4$
S-Adenosyl-L-homocysteine	Gamma butyrolactones	385.1280	$C_{14}H_{20}N_6O_5S$
Malate	Hydroxy acids and derivatives	133.0145	$C_4H_6O_5$
4-Coumarate	Hydroxycinnamic acids and derivatives	182.0811	$C_9H_8O_3$

5-Hydroxyindoleacetate	Indoles and derivatives	209.0918	$C_{10}H_9NO_3$
2-Oxobutanoate	Keto acids and derivatives	101.0247	$C_4H_6O_3$
Glycerol 3-phosphate	Lipids	171.0067	$C_3H_9O_6P$
Oleamide	Lipids	280.2646	$C_{18}H_{35}NO$
(5Z)-3-aminonon-5-enoic acid	Lipids	170.1189	$C_9H_{17}NO_2$
3-Hydroxy-3-methylglutaric acid	Lipids	161.0458	$C_6H_{10}O_5$
4-Trimethylammoniobutanoate	Lipids	146.1174	$C_7H_{15}NO_2$
Caprylic acid	Lipids	143.1079	$C_8H_{16}O_2$
Decanoic acid	Lipids	171.1392	$C_{10}H_{20}O_2$
Ethyl myristate	Lipids	255.2330	$C_{16}H_{32}O_2$
FA(14:0), Myristic acid	Lipids	227.2019	$C_{14}H_{28}O_2$
FA(18:0), Octadecanoic acid	Lipids	283.2642	$C_{18}H_{36}O_2$
FA(18:1), Oleic acid	Lipids	281.2486	$C_{18}H_{34}O_2$
FA(20:0), Arachidic acid	Lipids	311.2957	$C_{20}H_{40}O_2$
Glycero-3-Phosphocholine	Lipids	258.1096	$C_8H_{20}NO_6P$
Heptanoic acid	Lipids	129.0924	$C_7H_{14}O_2$
Hexadecanamide	Lipids	256.2629	$C_{16}H_{33}NO$
Hexanoic acid	Lipids	115.0767	$C_6H_{12}O_2$
Hexanoylcarnitine	Lipids	260.1850	$C_{13}H_{25}NO_4$
Leucinic acid	Lipids	131.0716	$C_6H_{12}O_3$
Nonanoic acid	Lipids	157.1235	$C_9H_{18}O_2$
O-Acetylcarnitine	Lipids	204.1228	$C_9H_{17}NO_4$
O-Butanoylcarnitine	Lipids	232.1539	$C_{11}H_{21}NO_4$
Propionylcarnitine	Lipids	218.1383	$C_{10}H_{19}NO_4$
GABA	Neurotransmitters	102.0563	$C_4H_9NO_2$
Inosine	Nucleosides, nucleotides, and analogues	269.0874	$C_{10}H_{12}N_4O_5$

Methylthioadenosine	Nucleosides, nucleotides, and analogues	298.0961	$C_{11}H_{15}N_5O_3S$
NAD+	Nucleosides, nucleotides, and analogues	664.1151	$C_{21}H_{27}N_7O_{14}P_2$
NADH	Nucleosides, nucleotides, and analogues	666.1309	$C_{21}H_{29}N_7O_{14}P_2$
2-Hydroxyglutarate	Organic acids and derivatives	147.0301	$C_5H_8O_5$
2-Oxoglutarate	Organic acids and derivatives	145.0145	$C_5H_6O_5$
3-Methyl-2-oxobutanoic acid	Organic acids and derivatives	115.0403	$C_5H_8O_3$
Hypotaurine	Organic acids and derivatives	110.0269	$C_2H_7NO_2S$
Phenolsulfonphthalein	Organic acids and derivatives	355.0626	$C_{19}H_{14}O_5S$
Carnitine	Organic nitrogen compounds	162.1122	$C_7H_{15}NO_3$
Choline	Organic nitrogen compounds	104.1068	$C_5H_{13}NO$
Choline phosphate	Organic nitrogen compounds	184.0731	$C_5H_{14}NO_4P$
Acetoin	Organic oxygen compounds	87.0453	$C_4H_8O_2$
Pantothenate	Organic oxygen compounds	220.1175	$C_9H_{17}NO_5$
methylglyoxal	Organooxygen compounds	71.0139	$C_3H_4O_2$
Adenosine	Purine nucleosides	268.1033	$C_{10}H_{13}N_5O_4$
cAMP	Purine nucleotides	328.0460	$C_{10}H_{12}N_5O_6P$
dGMP	Purine nucleotides	346.0554	$C_{10}H_{14}N_5O_7P$
Adenine	Purines and purine derivatives	136.0616	$C_5H_5N_5$
Hypoxanthine	Purines and purine derivatives	137.0456	$C_5H_4N_4O$

Xanthine	Purines and purine derivatives	151.0263	$C_5H_4N_4O_2$
6-Methylnicotinamide	Pyridines and derivatives	137.0708	$C_7H_8N_2O$
Pyridoxal	Pyridines and derivatives	168.0653	$C_8H_9NO_3$
Pyridoxine	Pyridines and derivatives	170.0809	$C_8H_{11}NO_3$
Nicotinamide	Pyridines and derivatives	123.0551	$C_6H_6N_2O$
UDP-N-acetylglucosamine	Pyrimidine nucleotides	606.0748	$C_{17}H_{27}N_3O_{17}P_2$
UDP-Glucose	Pyrimidine nucleotides	565.0482	$C_{15}H_{24}N_2O_{17}P_2$
Cytosine	Pyrimidines and pyrimidine derivatives	112.0504	$C_4H_5N_3O$
Uracil	Pyrimidines and pyrimidine derivatives	111.0203	$C_4H_4N_2O_2$
Thiamine	Pyrimidines and pyrimidine derivatives	265.1113	$C_{12}H_{16}N_4OS$

The PCA (Figure 5.2) based on 121 identified metabolites showed a clear separation of ApoE4 KI cells from control samples, with an R-squared value of 0.76 for the PCA model. PC1 explained 76.1% of the variance between control and ApoE4 KI samples, suggesting that PCA can differentiate the metabolomics changes between these groups. To determine which metabolites had significant changes affected by ApoE4, the VIP value from PLS-DA and the p-value from the t-test were used to select the most significant metabolites (VIP > 1 and FDR < 0.05). 34 metabolites were considered statistically significant with the condition of VIP > 1 and FDR value < 0.05 (Table 5.3.).

Notably, the levels of alanine, aspartate, and glutamate decreased in the presence of ApoE4, which aligns with observed clinical metabolomics alterations (Figure 5.3). This finding contrasts with the changes observed for alanine, aspartate, and glutamate

in the OrbiSIMS analysis presented in Chapter 4, where an increase in these three metabolites was detected in ApoE4 KI cells compared to control cells. The discrepancy between the LC-MS results and OrbiSIMS findings may stem from the fragmentation issues associated with OrbiSIMS when applied to biological samples. Since OrbiSIMS generates ion fragments with undefined and higher ionisation energy compared to LC-MS, the fragmentations could potentially alter the metabolite profiles, leading to differing results between the two techniques.

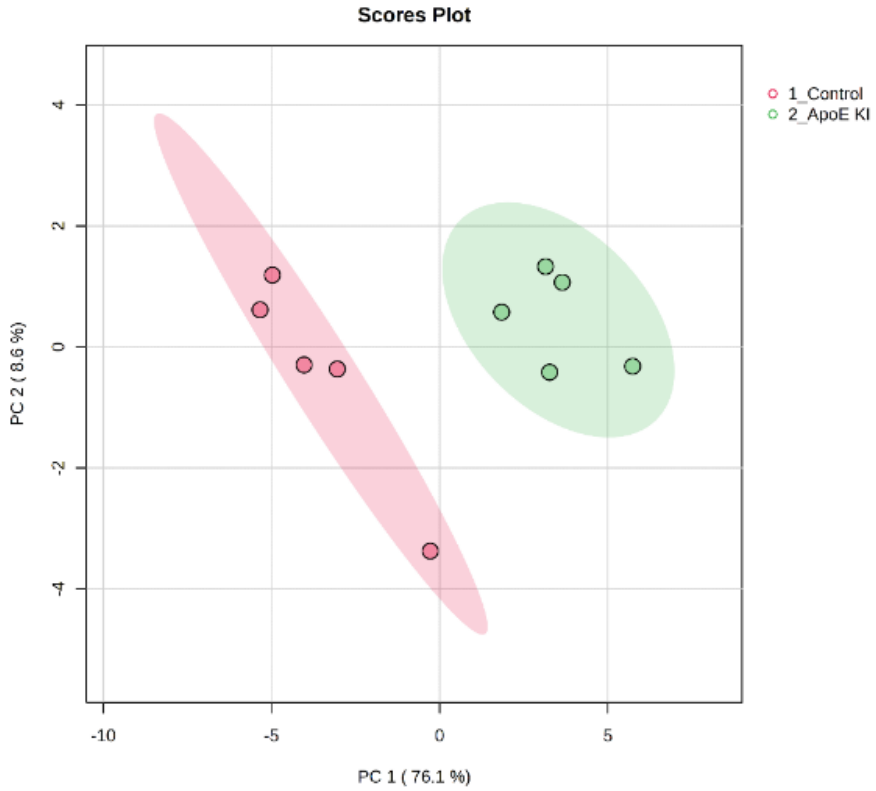

Figure 5.2. *PCA score plot of LC-MS/MS results from H4 control samples and ApoE4 KI samples. [PERMANOVA] F-value: 25.816; R-squared: 0.76342; p-value (based on 999 permutations): 0.006.*

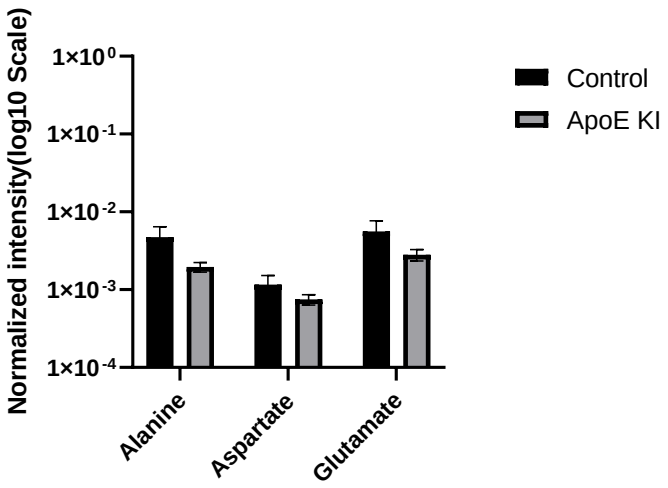

Figure 5.3. *The normalised intensity of alanine, aspartate, and glutamate detected in LC-MS/MS.*

The normalised intensity of the 34 signatures in the H4 control group was compared to the ApoE4 KI group, as shown in Figure 5.4. Statistical analysis of the normalised intensity revealed significant differences between the ApoE4 KI and control H4 cells. This indicates that the signatures selected through PLS-DA and t-test analysis effectively highlight the notable metabolic changes associated with ApoE4. These results demonstrate the power of these statistical methods in identifying and distinguishing key metabolites altered in response to ApoE4 expression.

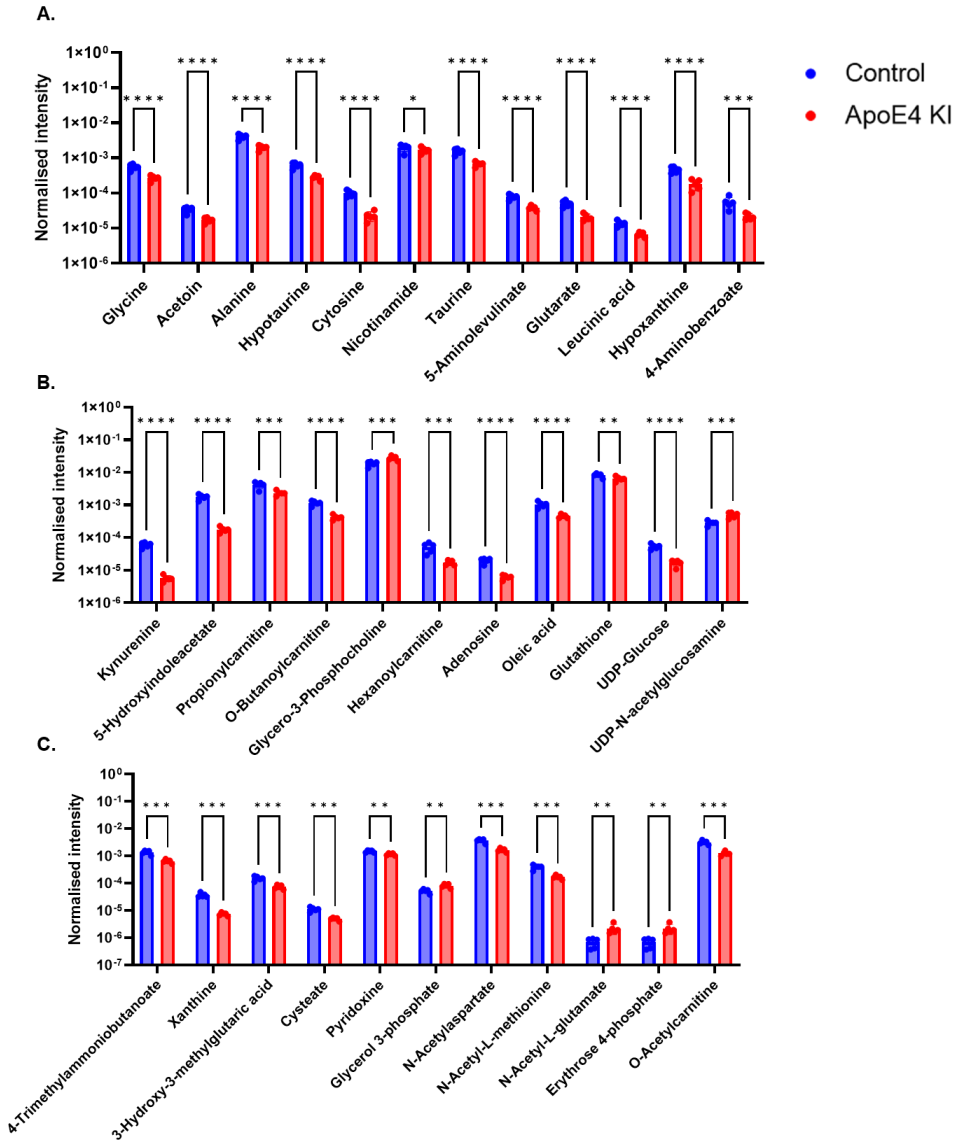

Figure 5.4. *The statistical analysis of significant metabolites in ApoE4 KI compared to control H4 cells. Data are expressed as the mean ± SD (n=3). * $p < 0.05$; ** $p < 0.01$; *** $p < 0.001$; **** $p < 0.0001$.*

Pathway analysis based on 34 features presented in Figure 5.5 indicates that the metabolism of taurine and hypotaurine is the most affected pathway by LC-MS/MS. Metabolites (cysteate, taurine, hypotaurine) involved in this pathway are down-regulated in ApoE4-expressing cells. Taurine has a neuromodulator role in brain development, and one of its intermediates is hypotaurine [191]. Moreover, cysteate is an amino acid generated by the oxidation of cysteine, which is employed in regulating major endogenous antioxidant molecules [192]. Overall, ApoE4 might impair

neuronal function and trigger the production of oxidant molecules by interrupting taurine and hypotaurine metabolism.

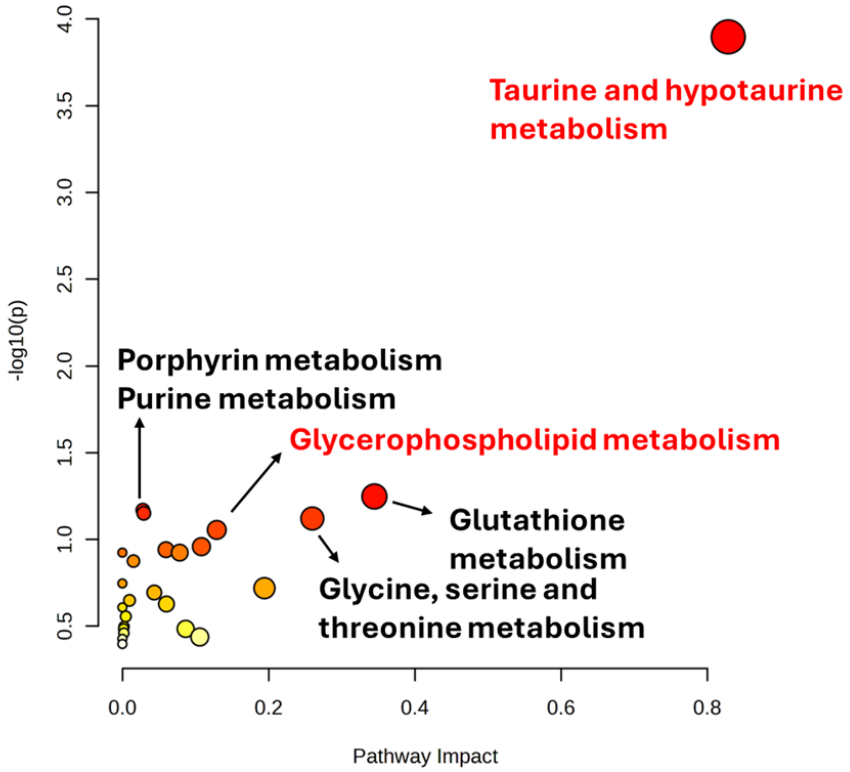

Figure 5. 5. *The pathway analysis of LC-MS/MS 34 signatures. Homo sapiens (KEGG) has been chosen as pathway library in pathway analysis. Scatter plot was chosen as visualization of pathway analysis results. Enrichment method is hypergeometric test, and relative-betweenness centrality as topology measure.*

Table 5.3. *The peak list of significant features in LC-MS/MS.*

Metabolites	Accurate mass	Formula	*p* value	q value
Glycine	76.03928	$C_2H_5NO_2$	0.000568	0.000064
Acetoin	87.04533	$C_4H_8O_2$	0.000553	0.000064
Alanine	90.05489	$C_3H_7NO_2$	0.000187	0.000038
Hypotaurine	110.0269	$C_2H_7NO_2S$	0.000188	0.000038

Cytosine	112.0504	$C_4H_5N_3O$	0.000039	0.000038
Nicotinamide	123.0551	$C_6H_6N_2O$	0.263967	0.026661
Taurine	124.0076	$C_2H_7NO_3S$	0.000168	0.000038
5-Aminolevulinate	130.0512	$C_5H_9NO_3$	0.000180	0.000038
Glutarate	131.0352	$C_5H_8O_4$	0.000387	0.000056
Leucinic acid	131.0716	$C_6H_{12}O_3$	0.000328	0.000055
Hypoxanthine	137.0456	$C_5H_4N_4O$	0.000444	0.000272
4-Aminobenzoate	138.0548	$C_7H_7NO_2$	0.008672	0.003285
4-Trimethylammoniobutanoate	146.1174	$C_7H_{15}NO_2$	0.000191	0.000193
Xanthine	151.0263	$C_5H_4N_4O_2$	0.000011	0.000034
3-Hydroxy-3-methylglutaric acid	161.0458	$C_6H_{10}O_5$	0.000449	0.000272
Cysteate	167.9974	$C_3H_7NO_5S$	0.000177	0.000193
Pyridoxine	170.0809	$C_8H_{11}NO_3$	0.003202	0.001386
Glycerol 3-phosphate	171.0067	$C_3H_9O_6P$	0.002903	0.001386
N-Acetylaspartate	174.0409	$C_6H_9NO_5$	0.000080	0.000041
N-Acetyl-L-methionine	190.0545	$C_7H_{13}NO_3S$	0.000175	0.000071
N-Acetyl-L-glutamate	190.0708	$C_7H_{11}NO_5$	0.006800	0.001717
Erythrose 4-phosphate	199.0015	$C_4H_9O_7P$	0.006800	0.001717
O-Acetylcarnitine	204.1228	$C_9H_{17}NO_4$	0.000063	0.000041
Kynurenine	207.0776	$C_{10}H_{12}N_2O_3$	0.000004	0.000005
5-Hydroxyindoleacetate	209.0918	$C_{10}H_9NO_3$	0.000005	0.000005
Propionylcarnitine	218.1383	$C_{10}H_{19}NO_4$	0.003991	0.001344
O-Butanoylcarnitine	232.1539	$C_{11}H_{21}NO_4$	0.000032	0.000041
Glycero-3-Phosphocholine	258.1096	$C_8H_{20}NO_6P$	0.005038	0.002181
Hexanoylcarnitine	260.185	$C_{13}H_{25}NO_4$	0.002581	0.001304
Adenosine	268.1033	$C_{10}H_{13}N_5O_4$	0.000029	0.000041

FA (18:1), Oleic acid	281.2486	$C_{18}H_{34}O_2$	0.000405	0.000306
Glutathione	306.0766	$C_{10}H_{17}N_3O_6S$	0.037915	0.014360
UDP-Glucose	565.0482	$C_{15}H_{24}N_2O_{17}P_2$	0.000040	0.000041
UDP-N-acetylglucosamine	606.0748	$C_{17}H_{27}N_3O_{17}P_2$	0.002182	0.001304

5.3.2 Comparative analysis of LC-MS/MS with OrbiSIMS

To evaluate the screening performance of OrbiSIMS in cellular metabolomics, we compared OrbiSIMS data with LC-MS/MS data to exploit how many metabolites were commonly detected in the two methods. The comparative analysis of OrbiSIMS and LC-MS/MS was based on all annotated metabolites. Firstly, the Venn Diagram in Figure 5.6 shows 50 metabolites commonly detected in both methods, mainly including major amino acids and amino acid derivatives. Moreover, the relative abundance of these molecules in LC-MS/MS and OrbiSIMS are presented in Figures 5.7a and b, respectively.

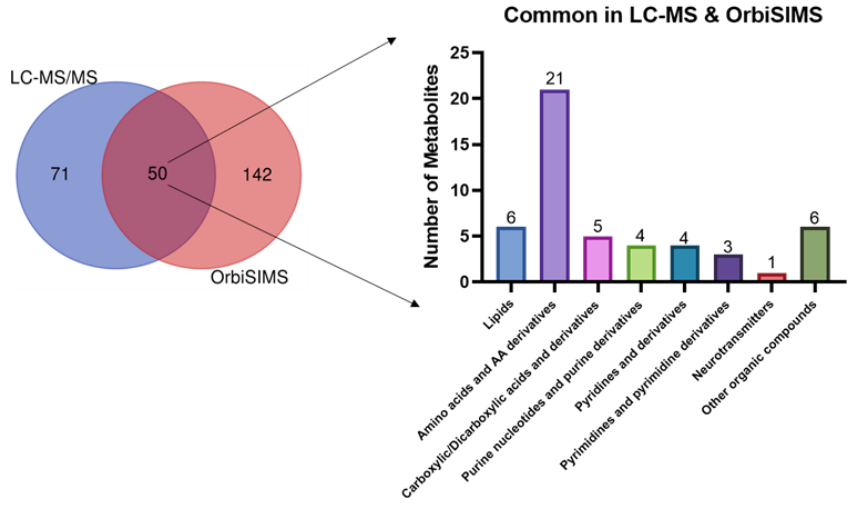

Figure 5. 6. *The overlap of metabolites detected from OrbiSIMS and LC-MS/MS. The Venn diagram of identified metabolites in LC-MS compared with putatively annotated metabolites in OrbiSIMS, in which fifty metabolites are commonly detected from both LC-MS and OrbiSIMS.*

Almost all features show the same trend between the control and ApoE4 KI groups. While there are six features that did not retain the same change between the two methodologies, including four amino acids and AA derivatives (green circled, alanine, glutamate, taurine, and aspartate), one lipid (glycerol 3-phosphate) and one carboxylic/dicarboxylic acid (fumarate). These six features ($m/z < 150$) not only play a role in energy metabolism and signal transduction, but also as metabolic intermediates. Therefore, they share a similar structure with other higher molecular weight analytes, resulting in annotated peaks that might contain the area of free analytes and fragments that are produced from other metabolites.

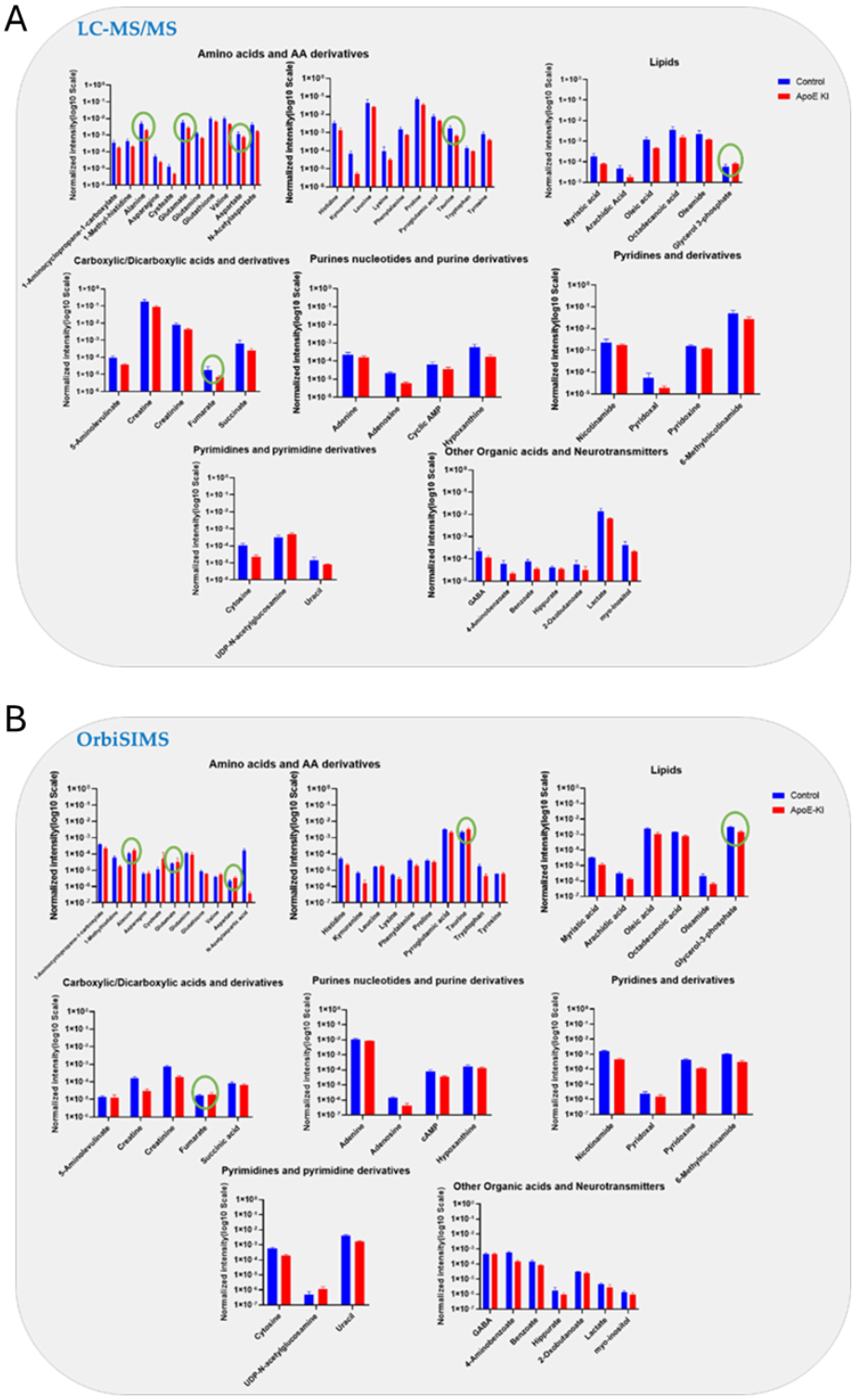

Figure 5. 7. *The relative abundance of common metabolites. (a) The bar chart shows the relative intensity of 50 metabolites commonly detected in the LC-MS/MS method between control group and ApoE4 KI group. (b) The bar chart shows the relative intensity of 50 metabolites commonly detected in the OrbiSIMS method between*

control group and ApoE4 KI group. All these data were normalized by total ion intensity and scaled by log10 in the bar chart. The green circled metabolites indicate the five features that did not retain the same change between the LC-MS/MS and OrbiSIMS methods.

The alanine deprotonated ion observed at *m/z* 88.0402 in the OrbiSIMS dataset is annotated as $C_3H_6NO_2^-$. However, this ion overlaps with a fragment derived from aspartate, as highlighted in Table 2.3 of Chapter 2, due to their shared amino acid backbone or structural similarity, as illustrated in Figure 5.8. A similar scenario is observed for glycerol 3-phosphate, which may originate from the fragmentation of lysophosphatidic acid. Lysophosphatidic acid, a key intermediate in lipid metabolism, is synthesised from glycerol 3-phosphate through the action of glycerol-3-phosphate acyltransferases (GPATs) and plays an essential role in various biological functions. This overlap indicates that the signal at *m/z* 88.0402 might not exclusively represent alanine but could also include contributions from aspartate fragmentation.

Such overlaps underscore the challenges in distinguishing certain metabolites in OrbiSIMS analysis, particularly when fragmentation patterns are not fully resolved. This reinforces the importance of complementary validation techniques, such as LC-MS/MS, to confirm the identity and levels of metabolites.

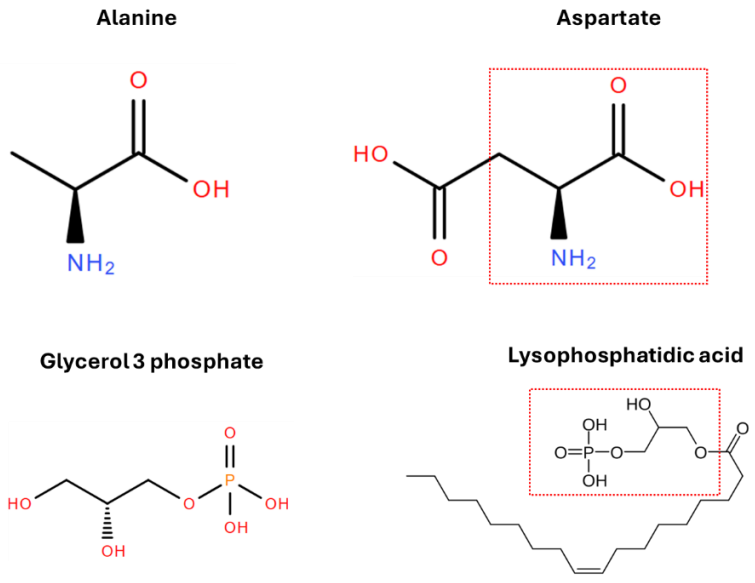

Figure 5.8. *The chemical structures of alanine, aspartate, and related metabolites*

(glycerol 3-phosphate and lysophosphatidic acid) highlighting their shared backbone or structural similarity. The red squared regions indicate potential fragmentations that may contribute to overlapping signals in OrbiSIMS analysis.

In conclusion of the metabolomics study mentioned above, metabolomic screening using OrbiSIMS demonstrated broad coverage in detecting various chemical classes, including polar and non-polar metabolites. This confirms the qualitative and semi-quantitative capabilities of OrbiSIMS. However, the production of small fragments hampers the quantitative ability of OrbiSIMS. Fragments produced from higher mass molecules might share the same chemical structure with some low mass molecules, making them mix, which is challenging to differentiate in the spectrum. Therefore, LC-MS/MS was applied to further confirm those lower mass range metabolites and complement the OrbiSIMS data. Combining both methods, the presence of ApoE4 in H4 cells significantly affected the lipid metabolism (glycerophospholipids and sphingolipids) and amino acid metabolism, including alanine, aspartate, and glutamate metabolism, aminoacyl-tRNA biosynthesis, glutamine metabolism, and taurine and hypotaurine metabolism.

5.4 Conclusion

The hard ionisation method used in OrbiSIMS raises key concerns, especially in relation to its application to biological and cellular samples due to extensive molecular fragmentation. The MS/MS capability of OrbiSIMS can assist in differentiating isobaric ions and provide detailed structural information. However, only ions with sufficient intensity—specifically, an intensity per shot greater than 0.5—can be selected for MS/MS analysis. Nevertheless, this study presents the first comparative analysis integrating LC-MS/MS and OrbiSIMS datasets in H4 neuroglioma cells. The high degree of overlap in features detected by these two techniques underscores the potential of OrbiSIMS in multi-omics studies, highlighting its value as a robust analytical tool despite the challenges associated with fragmentation. Further investigations into the fragmentation patterns of various metabolites in OrbiSIMS are necessary to enhance its applicability and reliability in biological research.

In addition, our study has identified clear guidance strongly advocating for the use of other analytical methods to complement and validate the OrbiSIMS results for further confirmation and to explore the metabolites of interest. However, the results observed as part of this study show that OrbiSIMS has been successfully applied to studying ApoE4-related metabolic and lipid changes, demonstrating its potential as metabolic screening tool. More comparative analyses and validation methods in various sample types are needed to further explore and solidify the applicability of OrbiSIMS in this field.

Chapter 6: Peptides assignment by OrbiSIMS and Proteomics analysis by LC-MS/MS

6.1 Chapter aims

The analysis process of OrbiSIMS involves sputtering the surface of cell samples using a primary ion beam, which ejects secondary ions that are subsequently transferred into a mass spectrometer for detection. During the sputtering process, all elements and molecular species on the surface or inside the H4 cells, including small metabolites such as amino acids, lipids, carbohydrates, and nucleic acids, as well as peptides and proteins—the major components of cells—are produced. Typically, standard protein characterisation requires enzyme digestion to break down large protein into small peptide chains prior to mass spectrometry. Kotowska *et al.* reported annotating 16 example proteins (up to 272 kDa) by de novo sequencing, applying this methodology to characterise a protein monolayer biochip, and conducting *in situ* depth profiling of proteins through human skin [162].

Aside from metabolomics application of OrbiSIMS, simsMFP allowed for filtration of peptide-related peaks from the OrbiSIMS dataset based on elemental composition. Although peptide assignment and protein identification have been reported by Kotowska and Max *et al.* [156, 162], this phenomenon in more complex cell samples has not been studied yet. In this chapter, the potential application of OrbiSIMS on proteomics study will be discussed by further analysing the freeze-dried data collected from Chapter 4. The elemental restriction especially for SIMS protein fragments will be used to filter out peptide-related peaks from control and ApoE4 KI samples. Furthermore, the standard proteomics approach by LC-MS/MS has been conducted and will be reviewed as part of this chapter.

6.2 Methods

6.2.1 Peptide related ions assigned by simsMFP

For peptide-related fragments assignment, simsMFP was also applied for chemical element filtering H4 dataset. Firstly, elemental restriction ($C_{4\text{-}100}$, $H_{8\text{-}200}$, $N_{0\text{-}20}$, $O_{0\text{-}20}$, $S_{0\text{-}1}$) and DBE value ($0.1667C_n < DBE < 0.6667C_n$) reported by Kotowska *et al.* were applied to filter out peptide-related peaks for negative ion mode [72]. Another constraint for restricting chemical formulas is element ratios of H/C, N/C, and O/C which are also based on protein fragments from 16 protein samples.

6.2.2 Sample Preparation for LC-MS proteomics

Cells were washed twice by PBS. Cell pellets were collected in microcentrifuge tubes by removing and discarding the supernatant through centrifugation at 16,615 × g for 5 min at 4 °C. Then cell pellets were incubated in lysis buffer (8M Urea, 4 % CHAPs in 30mM Tris buffer, pH = 8.5) for 30 min on ice, with vortexing at 10min intervals. Transfer the extract to microcentrifuge tubes and centrifuge at 16,615 × g for 10 min at 4 °C. Aliquot the clear lysate to clean microcentrifuge tubes. These samples are ready for assay. Lysates can be stored at -80 °C. Avoid multiple freezes/thaws.

A filter-aided sample preparation (FASP) method was used to generate enzymatic peptides, which means the protein denature, reduction, alkylation and trypsin digestion were performed on the membrane of a cartridge with a molecular weight cut-off (MWCO) of 10KDa (Vivacon 500, Sartorius).

25 μg of lysates were denatured and reduced using 200μL of 20 mM Tris (2-carboxyethyl) phosphine hydrochloride (TCEP)/8 M urea in 200 mM Triethylammonium bicarbonate (TEAB) buffer, pH 8.5. Alkylation was performed by adding 200 μL of 50 mM Iodoacetamide (IAA) in TEAB buffer. Trypsin digestion was carried out at 37 ℃ for 16 h with an enzyme: protein ratio of 1:25. Between steps, the samples were cleaned with TEAB buffer. Protein digests were eluted with 0.1 % TFA in H_2O, 0.1 % TFA in 50 % acetonitrile in H_2O and 0.1 % TFA in acetonitrile by centrifugation, the 3 fractions obtained were pooled and solvent was removed using

Eppendrof Concentrator Plus (Eppendrof).

6.2.3 Peptides Separation and Mass Spectrometric Data Acquisition

Tryptic peptides separation and mass spectrometric analysis was performed on an Vanquish™ Neo UHPLC System coupled with an Orbitrap Eclipse mass spectrometer (Thermo Fisher Scientific). The data were recorded using Xcalibur 4.4 software (Thermo Fisher Scientific).

After removing solvent, tryptic peptides were resuspended in 100 µL of 0.1 % trifluoroacetic acid in H_2O. For the chromatographic separation of peptides, 4 µL (1 µg) of resuspended solution was loaded on an Acclaim™ PepMap™ 100 C18 HPLC Column (500 mm, 75 µm i.d., 3 µm and 100 Å, Thermo Fisher Scientific). The column oven was set as 40 °C. Peptides were separated with a 120 min linear gradient from 5 % to 28 % buffer B (80 % acetonitrile in H_2O, 0.1 % formic acid), i.e., 95 % to 72 % buffer A (2 % acetonitrile in H_2O, 0.1 % formic acid) over 105 min, then to 40 % B over 15 min, finally to 95 % B over 10 min and kept at 95 % for 10 min, at a flow rate of 300 nL/min. The column was connected to an Thermo Easy-Spray capillary Emitter.

MS1 spectra were acquired in the Orbitrap (Resolution = 120,000, Scan range = 175 - 1800, RF Lens = 40%, AGC target = Standard and Maximum injection time mode = Auto). Charge states between 2 and 7 were required for MS2 analysis, and a 20 s dynamic exclusion window was used. Cycle time was set at 2 second.

MS2 fragmentation was performed in the ion trap with normalized HCD collision energy of 30 (Isolation mode = Quadrupole, isolation window = 1.6 Da, Auto scan range mode). MS2 spectra were acquired in the orbitrap (Resolution = 15,000, Maximum injection time = 35 ms, AGC target = 50,000, Normalised AGC target = 100% and Auto scan range).

Protein identification and label-free quantification were achieved using Proteome Discoverer, version 2.5 (Thermo Fisher Scientific). Raw files were searched against the Uniprot homo sapiens database (Swiss-Prot with isoforms) with the Sequest HT search algorithm and using modified standard processing and consensus workflows. The processing workflow included the mass recalibration node (spectrum files RC)

along with the standard spectrum selector, Minora Feature Detector, Sequest HT and Percolator nodes. The precursor mass tolerance was set to 10 ppm, and the fragment mass tolerance was set to 0.02 Da, with maximum number of missed cleavages set to 2. Carbamidomethylation of cysteine residues (+57.021 Da) was set as static modification, while the oxidation of methionine residues (+15.995 Da) and N-terminal protein modifications of Acetyl (+42.011 Da) were set as dynamic modifications. False discovery rate (FDR) tolerances in the Percolator node were set to 0.01 for high confidence and 0.05 for medium confidence. The final results were rescored with percolator and filtered to 1 % FDR.

The proteomics network and enrichment analysis were performed by using Cytoscape and StringApp according to the method reported by Nadezhda *et al* [193].

6.2.4 Gene Ontology Analysis for Metabolomics

To cover the relevant GO metabolic processes that were not mentioned by alternative pathway analysis approaches, IDSL.GOA (gene ontology analysis for metabolomics) is performed for a more comprehensive and accurate analysis of metabolite pathway data. (https://goa.idsl.site/goa/#/intro) Firstly, to perform IDSL.GOA analysis, we need to map the significant metabolites to KEGG ID which were used as input for IDSL.GOA by using the enrichment function in Metaboanalyst (https://genap.metaboanalyst.ca/MetaboAnalyst/upload/EnrichUploadView.xhtml) and the PubChem Identifier Exchange service (https://pubchem.ncbi.nlm.nih.gov/idexchange/idexchange.cgi).

6.3 Results and Discussion

6.3.1. Peptide fragments can be observed from H4 cells by OrbiSIMS

The dataset utilised for peptide assignment is the same as that obtained from the OrbiSIMS metabolomics analysis described in Chapter 4. Initially, peak search was performed on each raw data file requiring a minimum count of 5000, generating an ion peak list for each sample. Subsequently, simsMFP was used to predict and filter the ions based on elemental restrictions: ($C_{4\text{-}100}$, $H_{8\text{-}200}$, $N_{0\text{-}20}$, $O_{0\text{-}20}$, $S_{0\text{-}1}$). Next, we applied DBE value constraints ($0.1667C_n < DBE < 0.6667C_n$) and calculated N/C, O/C, H/C ratios in accordance with the manually assigned OrbiSIMS peptide fragments of 16 example proteins by Kotowska *et al.*, as depicted in Figure 6.1. The necessity to apply unique rules for OrbiSIMS peptide assignment arises from the distinct fragmentation patterns observed in OrbiSIMS compared to other proteomics databases, necessitating the development and application of an in-house database. Ultimately, the numbers of peptide fragments assigned from each of the H4 samples are detailed in Table 6.1.

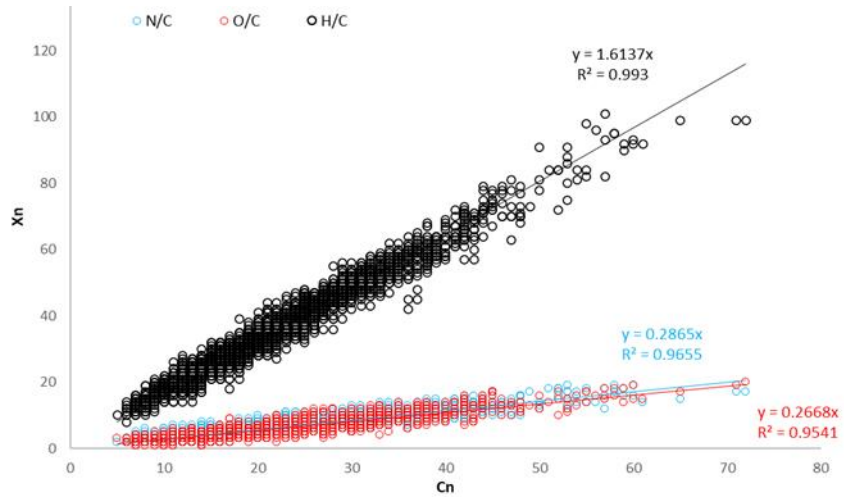

Figure 6. 1. *N, O, and H to C ratio of peptide-related ion peaks based on the 16 example proteins.*

Table 6. 1. *The number of peptide assignments after applying different chemical filtering restriction.*

Sample name	Control1	Control2	Control3	ApoE4 KI-1	ApoE4 KI-2	ApoE4 KI-3
Ion peaks	3012	3012	3012	6871	7091	6829
Elemental restriction	6793	6773	6823	6193	6851	7616
DBE and N, O, H to C ratio restriction	134	134	138	144	140	144

After applying all restrictions, more than 100 peptide assignments were found in each cell sample that are listed in Table S1 and S2. Venn diagram (Figure 6.2A) showed 90 peptide assignments commonly observed in the Control group, and 95 in the ApoE4 KI group. Venn analysis between 90 peptide fragments of Control and 95 of ApoE4 KI further revealed that 52 fragments are detected both from Control and ApoE4 KI. Moreover, we found the relative abundance of those 52 peptide assignments in ApoE4-carried cells much lower than those in control cells (Figure 6.2A). It might suggest that the protein biosynthesis might be inhibited by ApoE4. The defective protein synthesis of neurons by ApoE4 has been reported by Sarayu *et al.* which indicates an NMDA-mediated alteration of synaptic signalling in ApoE4 treatment [194]. Moreover, the detection of 38 unique peptide fragments in the control and 43 in ApoE4 suggests that some proteins are affected by ApoE4, possibly through changes in protein expression levels or modifications.

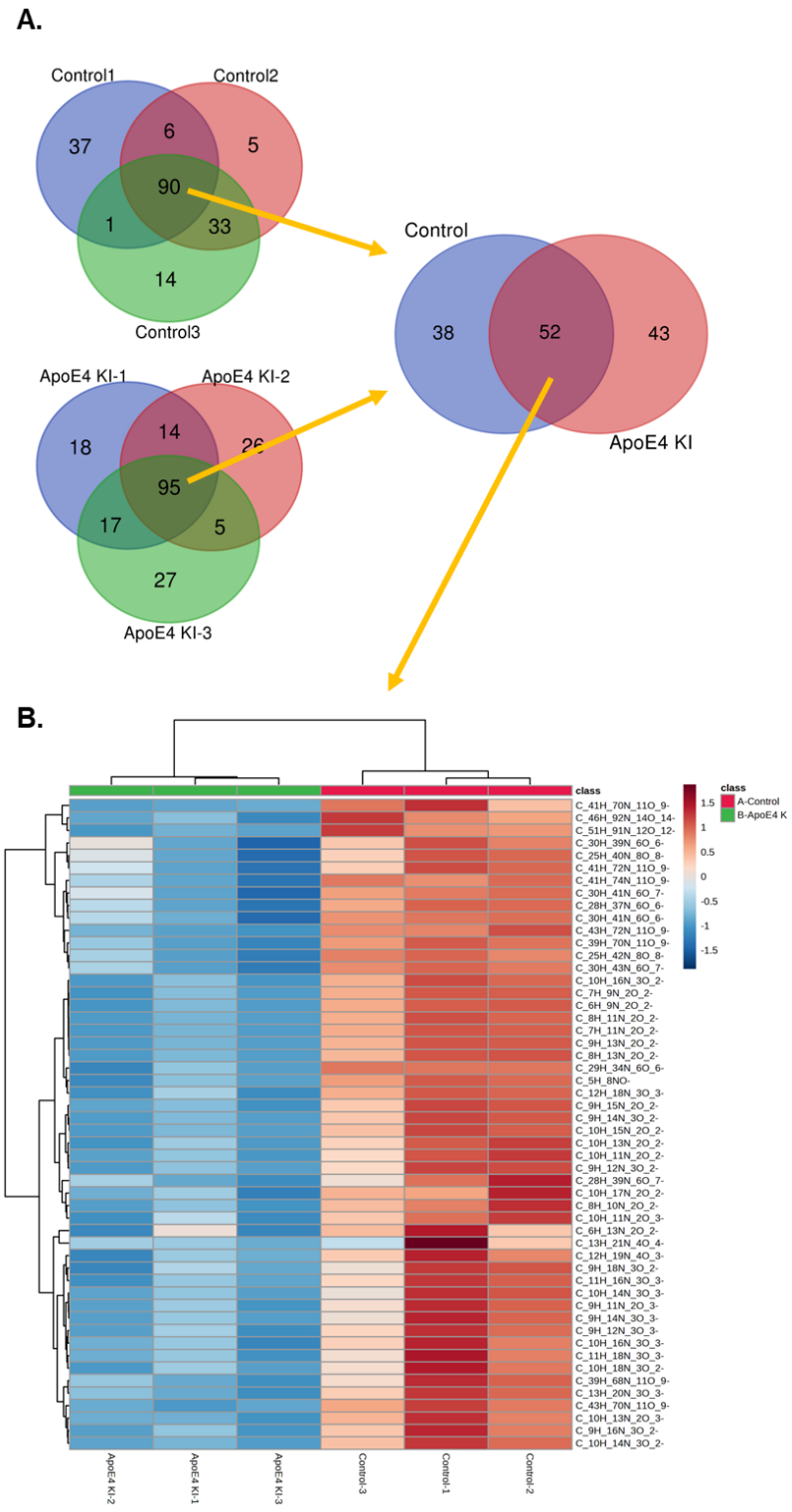

Figure 6. 2. *Peptide fragments from OrbiSIMS. The Venn diagram of peptide assignment from each of samples and assignments commonly detected from the control and ApoE4 KI groups. The heatmap of 52 common peptide fragments from the control and ApoE4 KI groups.*

6.3.2 Proteomics alteration affected by ApoE4 in H4 cells

The detection of peptides by using OrbiSIMS gives us a clue about the alteration of peptides from H4 cells which might indicate the ApoE4-mediated dysfunction of protein biosynthesis. However, due to the limited OrbiSIMS protein database we are not able to identify those peptides. In addition, to investigate the role of ApoE4 in protein level, proteomics was analysed on the Vanquish™ Neo UHPLC System coupled with Orbitrap Eclipse mass spectrometer.

By performing proteomics analysis, a total of 2925 proteins have been detected from two groups of samples. Based on the different expression levels of these proteins between ApoE4-carried and wild-type H4 cells, 1503 proteins have been selected by filtering the protein with ApoE4/control ratio of > 2 and < 0.5. Network building was performed using the STRING database by inputting these 1503 proteins, only 1458 protein IDs have been recognized by STRING protein database.

Starting with the list of 1458 proteins with significantly regulated features in the study, we first produce the corresponding STRING protein network in Cytoscape. Then, the log ratios of differentially expressed proteins between ApoE4-carried cells and wild-type H4 cells, can be visualised on the network nodes. Here, we use a blue-white-red colour gradient to highlight the nodes with low or high log ratios (Figure 6.3).

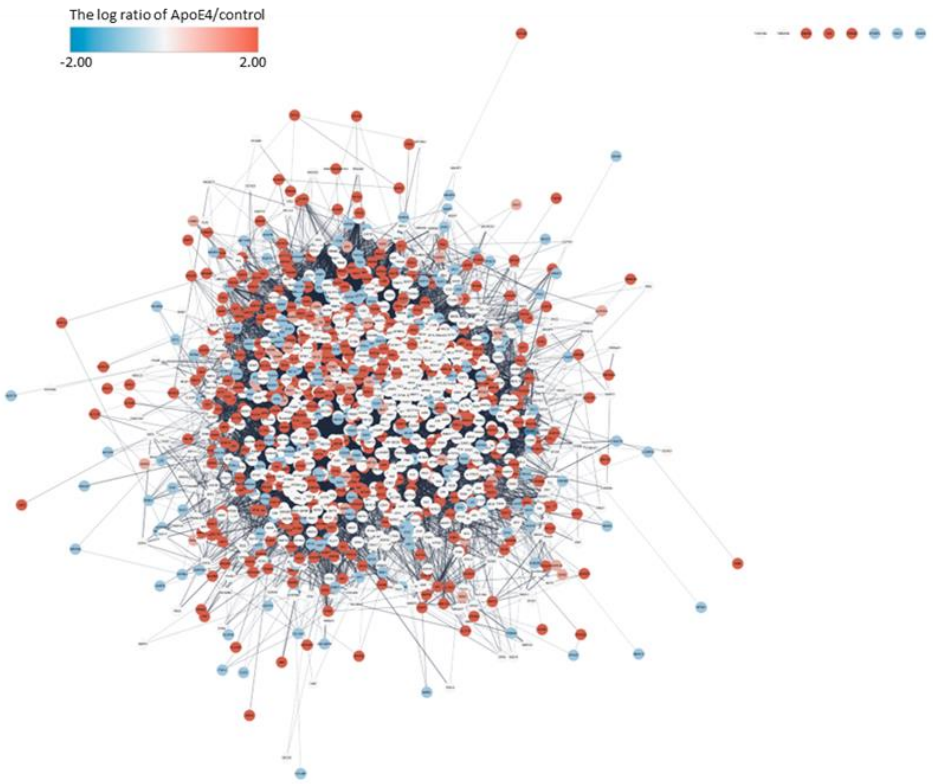

Figure 6. 3. *The protein network built by StringApp. The nodes (1458) present each protein, and edges (26953) present the interaction between proteins. Red nodes mean up-regulated proteins in the ApoE4-KI group compared with Control H4 cells. Blue nodes mean down-regulated proteins.*

Next, to functionally characterise these up or down-regulated proteins, stringApp was used to perform functional enrichment analysis. For 1161 up-regulated proteins (19864 interactions) affected by ApoE4, Markov clustering (MCL) algorithms have been performed to group the proteins in the network based on their interactions from STRING (inflation value: 4.0). After MCL simplification, only 1495 interactions within clusters are retained. Next, we only focused on the most cluster (101 proteins with 611 interactions) in the up-regulated protein network. To functionally characterize the cluster, we used stringApp to perform functional enrichment analysis, which resulted in a list of 96 statistically significant terms (FDR < 0.05) that span two categories: Gene Ontology (GO) Biological Process, and KEGG Pathways (listed in Table S3). Of these, the most significant GO biological processes were the

Organonitrogen compound biosynthetic process (Figure 6.4A), Cellular amino acid metabolic process, Mitochondrial gene expression, Nucleobase-containing compound metabolic process and tRNA processing suggesting by expressing ApoE4, the proteins that participate in metabolic processes of H4 cells have been up regulated. Besides, the KEGG pathways including aminoacyl-tRNA biosynthesis, biosynthesis of amino acids, alanine, aspartate and glutamate metabolism, fit well with previous metabolomics finding in this study that is consistent to dysfunction of aminoacyl-tRNA biosynthesis and amino acids affected by ApoE4.

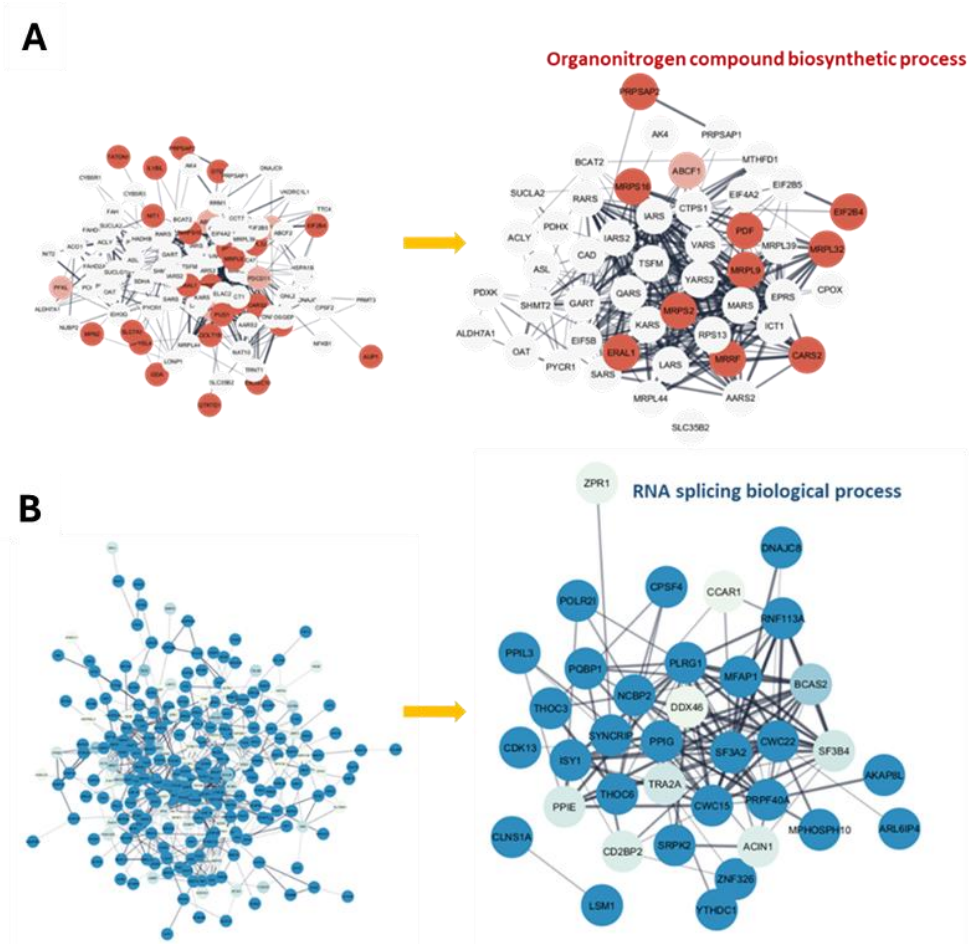

Figure 6. 4. *Clustered protein association network of up-regulated proteins (a) and down-regulated proteins (b), along with the proteins involved in their corresponding Gene Ontology (GO) biological processes. Log ratios between the ApoE4-carried group and the control group for each protein were mapped to the nodes using a blue-white-red gradient. Full details of those protein are listed in Supplementary Table S3 and S4.*

For 297 down-regulated proteins (715 interactions) affected by ApoE4, Markov clustering (MCL) algorithms have been performed to group the proteins in the network based on their interactions from STRING (inflation value: 4.0). After MCL simplification, we focused on the most cluster (255 proteins with 706 interactions) in the down-regulated protein network. In terms of down-regulated proteins after ApoE4 KI, the enrichment analysis resulted in a list of 69 (downregulated) statistical terms (Table S4). Of these, the two most significant GO biological processes were RNA splicing and RNA processing. The down-regulated enrichment pathways affected by ApoE4 fit well with the finding by Towfique *et al.* and Ping-Chung *et al* [195, 196] that the RNA splicing dysfunction is related to AD pathology. In addition, our KEGG pathways identified significant enrichment of spliceosome, endocytosis and RNA transport pathways. Our proteomics data supports the idea that ApoE4 is associated with the disruption of gene transcription and translation, however, the exact mechanism is not clear and needs to be further confirmed.

6.3.3 GO analysis of metabolomics and proteomics affected by ApoE4

Finally, to comprehensively interpret cross connection between proteomics data with metabolomics, we applied GO analysis for metabolomics as well. We built up metabolite datasets that were significantly different between the ApoE4 KI group and the control group from OrbiSIMS (35) and LC-MS (40), respectively. Out of this list, 15 (OrbiSIMS) and 28 (LC-MS) metabolites had KEGG identifiers available and were used as input for IDSL.GOA analysis [197]. The GO analysis for OrbiSIMS metabolomics suggested a total of 17 GO processes that were changed such as the cysteine, sulfur amino acid catabolic processes (Table S5), tRNA aminoacylation for mitochondrial protein were significantly affected by ApoE4. For LC-MS, 120 GO biological processes were affected by ApoE4 which involved pyridine-containing compound process, cysteine metabolic process, cellular amino acid biosynthesis process etc (Table S6). We found many overlapping metabolic processes from OrbiSIMS and LC-MS datasets, which are all involved in amino acid metabolism (Figure 6.5). Furthermore, by comparing GO analysis of metabolomics with proteomics GO analysis, cellular nitrogen compound metabolic process and tRNA

aminoacylation process are found commonly from both omics results. Overall, GO analysis of metabolomics by using IDSL.GOA provides more biological function information from metabolites study, as well as helps building the link between metabolomics and proteomics, overall suggesting that nitrogen compounds, amino acids, tRNA aminoacylation metabolic processes play important roles in ApoE4 mediated molecular alterations in AD.

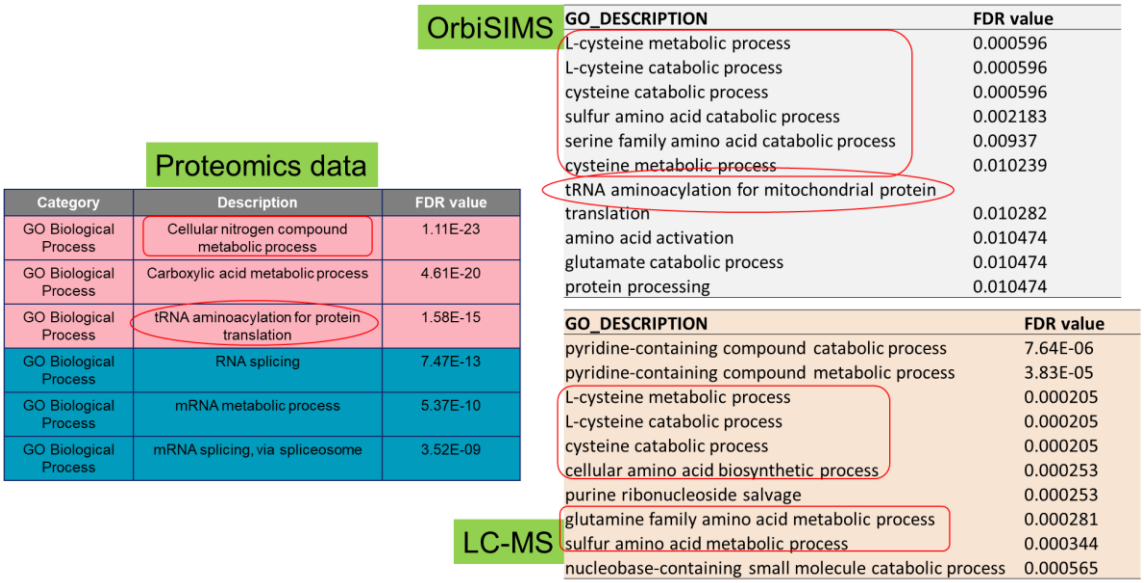

Figure 6. 5. *GO analysis of metabolomics datasets from OrbiSIMS and LC-MS/MS, and comparison with proteomics GO analysis.*

6.4 Conclusion

In conclusion, whilst no studies have yet reported assigning peptides or proteins using OrbiSIMS from complex biological samples, we have successfully assigned peptide fragments induced by a gas cluster ion beam (GCIB) from H4 neuroglioma cell samples. These assignments, based on elemental restrictions, have provided insights into the chemical composition and intensities of peptide fragments. This information suggests that proteins may also be affected by the ApoE4 risk gene. However, the complexity of cellular components and the prevalence of multiple proteins sharing identical peptide sequences mean that our current understanding of OrbiSIMS protein detection remains incomplete. Consequently, further investigation into protein changes through standard proteomics studies is warranted.

Proteomic Gene Ontology (GO) analysis has revealed dysfunctions in organonitrogen compound metabolic processes and RNA splicing, influenced by ApoE4. Gene Ontology analysis, a robust tool in genomics and proteomics, categorises and elucidates the functions of genes and proteins within biological systems. Typically, the biological interpretation of metabolomics data involves pathway analysis and metabolite set enrichment analysis. However, the biological functions of metabolites and metabolic pathways are not fully captured and vary across different databases, potentially leading to misunderstandings and poor biological interpretations.

To bridge proteomics data with metabolomics comprehensively, we also applied GO analysis to our metabolomics studies. Mahajan *et al.* reported an online GO tool for metabolomic datasets, which can identify crucial GO metabolic processes not covered by existing pathway databases. As part of this study, we utilised IDSL.GOA for our metabolomic datasets to obtain deeper biological insights. The overlapping GO analysis of metabolomics and proteomics data further highlighted the significance of amino acids and the tRNA aminoacylation metabolic process in ApoE4 pathology. Overall, this underscores the critical role ApoE4 plays in cellular metabolism and the translation process, contributing to the pathological mechanisms of Alzheimer's disease.

Chapter 7: Conclusion, Limitations and Future Work

Conclusion

Extensive clinical, pathological, epidemiological, and genetic research has demonstrated that ApoE4 is the strongest genetic risk factor for late-onset Alzheimer's Disease (AD) [7]. ApoE4 is associated with multiple AD-related pathologies, including amyloid deposition, tau phosphorylation, innate immune activation, and vascular dysfunction. A deeper understanding of ApoE4-related mechanisms in AD could therefore provide critical insights for developing targeted therapeutic strategies.

Metabolomics and proteomics studies are widely used to investigate gene-related molecular mechanisms. LC-MS-based analyses involve sample extraction, digestion, and separation, all of which require relatively large sample quantities and may result in a loss of spatial information. These limitations reduce the depth of insight that can be obtained from conventional approaches.

To complement and extend existing animal studies and facilitate translational research, there is a need for a screening method that uses smaller sample sizes, requires minimal or non-destructive preparation, and allows for spatially resolved molecular profiling. In this context, OrbiSIMS offers a promising platform for studying ApoE4-mediated molecular alteration in Alzheimer’s disease, owing to its label-free detection, minimal sample requirements and the ability to perform depth profile and imaging analysis compared to other surface mass spectrometry analysis technique.

In this study, H4 neuroglioma cells were used as an initial model to assess the feasibility of OrbiSIMS. Two sample preparation methods-freeze drying and frozen hydration-were evaluated, aiming to optimise the detection of lipids and metabolites. Freeze-dried H4 cells were selected for subsequent experiments based on signal quality.

To establish an ApoE4-relevant disease model, a CRISPR-Cas9 gene editing method was applied to create ApoE4 knock-in (KI) cells. Both control H4 and ApoE4 KI cells

were analysed by OrbiSIMS in their freeze-dried state. A total of 192 metabolites, including lipids and polar metabolites, were detected and assigned using a molecular formula prediction tool. Lipid dye staining and LC-MS/MS-based polar metabolomics were used to validate and complement the OrbiSIMS results. In addition, the capability of OrbiSIMS to detect peptide fragments was explored, and standard proteomics were conducted to further investigate ApoE4-associated protein changes. Gene Ontology (GO) analysis of the metabolomics dataset helped to integrate findings from both metabolomics and proteomics, revealing overlapping biological processes, including nitrogen compound metabolism, amino acids metabolism, and tRNA aminoacylation.

OrbiSIMS enables label-free detection of metabolites and peptide fragments from a single sample with minimal sample preparation. In contrast to LC-MS/MS workflows - which typically require separate extraction and separation processes for lipids, metabolites and peptides – OrbiSIMS offers a streamlined and efficient alternative, particularly suitable for metabolomics screening. While lipids are well detected by OrbiSIMS, polar metabolites such as amino acids can be putatively annotated. However, the fragmentation inherent to SIMS can complicate molecular ion assignment, highlighting the importance of complementary validation using LC/MS/MS.

Pathway analysis revealed that glycerophospholipid biosynthesis was the most affected metabolic pathway in the ApoE4-carried neuroglioma H4 cells, followed by disturbances in alanine, aspartate, and glutamate metabolism, as well as alanine, taurine, and hypotaurine metabolism. These findings shed light on potential metabolic mechanisms of ApoE4-related AD pathology. Moreover, peptide fragments detected in both wild-type and ApoE4-carried cells suggest that protein biosynthesis may be impaired in the presence of ApoE4.

In conclusion, this study presents a novel (Figure 7) combining OrbiSIMS as a label-free metabolomics screening tool with LC-MS/MS as a complementary validation technique. We demonstrated that ApoE4 expression in H4 cells leads to dysregulation of glycerophospholipid metabolism and amino acid hypometabolism, particularly in alanine, aspartate, glutamate, and taurine pathways. We also showed the potential of OrbiSIMS to detect peptide fragments, which could provide further insight into protein

biosynthesis dysfunction. Proteomics analysis revealed the dysfunction of the organonitrogen compound metabolic process and RNA splicing affected by ApoE4. GO analysis confirmed that amino acid metabolism and tRNA aminoacylation are key biological processes affected by ApoE4. Overall, it suggests the key role of ApoE4 played in cellular metabolism and the translation process associated with the pathological mechanism of AD.

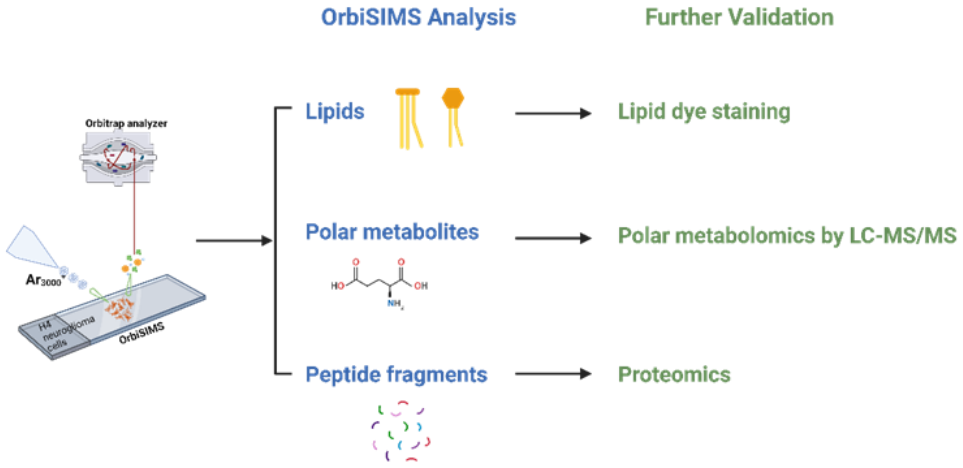

Figure 7.1. The novel workflow of OrbiSIMS as a screening tool suggests further validation methods for each type of metabolite*. Initially, OrbiSIMS depth profile analysis is conducted to obtain spectral information, including lipids, polar metabolites, and peptide fragments. If differentiated levels of lipids are observed under disease or treatment conditions, they are further validated or confirmed through lipid dye staining or lipidomics studies. Similarly, alterations in polar metabolites can be complemented and further explored using LC-MS/MS metabolomics. Finally, the applicability of OrbiSIMS to detect peptide fragments provide initial indications of protein level changes, which can be further investigated by proteomics analysis.*

OrbiSIMS-based depth profiling has been successfully applied to metabolomics and lipidomics in H4 neuroglioma cells. Given the capabilities of SIMS as a mass spectrometry imaging technique, this approach can be extended to spatial analysis of metabolites, lipids, and even proteins. Common surface mass spectrometry imaging techniques are summarised in Table 7.1. These include MALDI (Matrix-Assisted

Laser Desorption/Ionisation), SALDI (Surface-Assisted Laser Desorption/Ionisation), LAESI (Laser Ablation Electrospray Ionisation), DESI (Desorption Electrospray Ionisation), and LESA (Liquid Extraction Surface Analysis) [198, 199].

MALDI is widely used for detecting large biomolecules such as peptides and proteins. However, it requires a matrix, which can introduce background interferences and demands optimisation for specific analytes and sample types. Matrix-derived fragments often dominate the low-mass range, complicating small molecule analysis. SALDI addresses this limitation by using nanostructured substrates, improving the detection of small metabolites and pharmaceutical compounds [200]. LAESI enables ambient ionisation, allowing spatially resolved analysis of metabolic heterogeneity in fresh, water-rich biological samples [201]. Other ambient ionisation techniques such as DESI, LESA, also provide matrix-free surface analysis under atmospheric conditions.

OrbiSIMS presents several advantages, including high sensitivity, minimal sample preparation, no requirement for matrix application, high spatial resolution, and excellent mass resolution. It enables detailed chemical imaging and can detect a broad range of molecular species—including lipids, polar metabolites, and peptide fragments—from biological tissues. However, like all analytical techniques, OrbiSIMS has its limitations. One significant challenge is the presence of isobaric species, which can hinder accurate analyte identification in complex biological samples. Although the MS/MS capability of the Orbitrap analyser can address this issue, it requires sufficient precursor ion intensity for successful fragmentation and detection.

In imaging applications, the high spatial resolution advantage of SIMS is somewhat limited when using argon gas cluster ion beam (GCIB) as the primary ion source. While GCIB induces less fragmentation than a bismuth liquid metal ion gun (LMIG) and C60 ion beam, it sacrifices spatial resolution and acquisition speed. The best achievable spatial resolution for argon GCIB-OrbiSIMS is approximately 2 μm, and image acquisition is significantly slower compared to LMIG-ToF-SIMS imaging.

Table 7.1. Comparison of Surface mass spectrometry approaches

Technique	Ionisation mechanism	Sample Preparation	Spatial Resolution	Key Analyte Types
SIMS (Secondary ion mass spectrometry)	Secondary ions are produced by bombarding the surface with a focused primary ion beam. Hard ionisation under high vacuum.	Samples must be compatible with vacuum; typically dried at room temperature or frozen-hydrated.	~1-10 um ~50 nm nanoSIMS [202]	Small molecules, lipids, polar metabolites, peptides
MALDI (Matrix-assisted laser desorption/ionisation)	Laser irradiates a matrix, which absorbs energy and assists in desorption and ionisation of analytes. High-vacuum condition; Soft ionisation.	A suitable matrix (e.g., CHCA, DHB) must be uniformly applied to the sample surface.	~5-100 um for most commercial instruments ~1.4 um AP-MALDI coupled with optics system [203]. ~600 nm by transmission-mode MALDI with laser post ionization (t-MALDI-2) [204]	Peptides, proteins, lipids
SALDI (Surface assisted laser desorption/ionisation)	No matrix is required; instead, inorganic nanostructured substrates are used to assist in the ionisation of analytes. High-vacuum condition; Soft ionisation.	No matrix required, but samples must tolerate direct laser exposure. Surface should be homogeneous.	~75 nm-100 um [205, 206]	Small molecules, nanomaterials
LAESI (Laser ablation electrospray ionisation)	A focused laser pulse ablates the sample, generating a plume of desorbed molecules, which are subsequently ionised by an electrospray. Atmospheric conditions; Soft ionisation	Samples should be fresh or frozen-hydrated, ideally with high water content.	~100-200 um [207, 208]	Metabolites, lipids
DESI (Desorption electrospray ionisation)	A charged solvent spray desorbs molecules from the surface and ionises them upon impact. Atmospheric conditions; Soft ionisation	Samples must be dry and flat; non-conductive surfaces are preferred.	~35-200 um [209] Down to 7-10 um using nanoDESI [210]	Lipids, metabolites
LESA (Liquid extraction surface analysis)	A solvent droplet extracts analytes from the surface, which are subsequently ionised via electrospray. Atmospheric conditions; Soft ionisation	A flat surface is required; samples can be dried or frozen sections.	Not ideal for imaging; typically ~500–1000 µm [211] But a large number of samples will be ionised which increase sensitivity.	Proteins, peptides, drugs

Limitations

One limitation of this study is the relatively small number of biological replicates within each experimental group. While preliminary or exploratory studies often rely on limited sample sizes due to constraints such as time, cost, or sample availability, a low number of replicates can reduce statistical power and increase the likelihood of both false positives and false negatives [212]. Given the high biological variability of cell samples, a greater number of biological replicates should be considered in experimental design. This includes analysing multiple wells of cells and using cells from different passages to assess whether variations in metabolic profiles occur across different culture conditions. From a technical perspective, SIMS is a surface-sensitive technique, and its performance can be affected by subtle variations in sample handling or instrument stability. Therefore, incorporating technical replicates is crucial to evaluate measurement reproducibility and assess signal consistency across repeated acquisitions [213].

Statistical robustness is further challenged by the high-dimensional nature of untargeted SIMS datasets, which involve thousands of variables per sample. In this context, correcting for multiple hypothesis testing is essential to minimise false discoveries. This study employed False Discovery Rate (FDR) correction methods, such as the Benjamini-Hochberg procedure, to control the proportion of false positives among the list of significant features. However, when the number of replicates is low, FDR control becomes less reliable. Sparse data can lead to unstable variance estimates, resulting in either overcorrection—where true positives are missed—or undercorrection—where false positives are retained. Moreover, when the signal-to-noise ratio is low, FDR-corrected p-values may not adequately distinguish meaningful biological differences from background noise [214]. Ultimately, while FDR correction mitigates some risks of false discovery, it cannot fully compensate for the limitations imposed by small sample sizes and high data dimensionality. As such, the findings of this study should be interpreted with caution, and validation using targeted approaches or larger, statistically supported cohorts will be necessary to confirm the reproducibility and biological relevance of the molecular alterations observed.

Another limitation is the lack of additional cell models to further confirm and validate the impact of ApoE4. Due to budget constraints and the limited time frame of my PhD, other ApoE4 knockout models could not be investigated. Future research should incorporate a broader range of cell types, including microglia, astrocytes, and neurons, to better understand the metabolic pathways affected by ApoE4 in Alzheimer's disease. Given the diverse functions of ApoE4 across different cell types, co-culture models of neurons and astrocytes/microglia may also be necessary. Furthermore, since gene editing can introduce other factors into cells, human-derived stem cells carrying the ApoE4 genotype would provide a better model, as the externally induced risk gene may not fully account for the pathological changes of ApoE4 in the human body.

Moreover, further application of OrbiSIMS in metabolomics and lipidomics studies of biological samples should consider the fragmentation issue, particularly for ions in the low mass range. These ions may originate from, or overlap with, fragments of larger metabolites. Investigating the fragmentation patterns of metabolites in OrbiSIMS will be a valuable direction for future work, enhancing ion annotation and assignment. Conducting OrbiSIMS MS/MS experiments on targeted metabolite, lipid, or peptide ions can be highly beneficial for characterising and confirming the identities of detected ions, as well as for understanding their fragmentation patterns [146]. For example, Suvannapruk *et al.* identified lipid species such as phosphatidylinositol PI (36:2) and PI (38:4) in macrophages using MS/MS [149]. The fragmentation confirmed both the PI head group and the fatty acid side chains, making structural information accessible. However, successful MS/MS experiments require precursor ions with sufficient signal intensity, typically > 0.5 counts per shot. Therefore, it is recommended to perform MS/MS on a targeted list of ions that are of particular interest and have adequate intensity to ensure reliable fragmentation analysis.

Additionally, the use of alternative primary ion beams—such as water cluster ion beams—may improve ion yields from biological samples, thereby enhancing both sensitivity and MS/MS performance [215]. Argon gas clusters have been widely used in recent years for biological analysis due to their advantages of low chemical damage and preservation of intact molecular ions. However, they are still limited by low spatial resolution and low ionisation efficiency. Recent developments by the Vickerman and

Lockyer group have shown that water cluster ion beams can enhance biomolecular ion signals by approximately 100-fold [216]. High-energy (~70 keV) H_2O cluster beams have demonstrated the capability to achieve ~1 μm spatial resolution while delivering higher ionisation yields compared to argon clusters [217]. Notably, Tian *et al.* successfully applied this technique to imaging frozen-hydrated cells and tissues, highlighting its potential in biological surface analysis [218, 219]. Therefore, coupling water cluster ion beams with OrbiSIMS may significantly improve the detection of molecular ions in biological samples. Combined with the MS/MS capabilities of the Orbitrap analyser, this approach could offer more detailed insights into the chemical structures of complex biomolecules.

Future work

This study has demonstrated and validated the capability of OrbiSIMS to detect a wide range of molecular species in biological samples. Notably, OrbiSIMS showed strong potential for identifying lipid alterations associated with disease states, even in small sample volumes—a strategy that could be extended to other biological matrices, including tissues and primary cells. Additionally, ion-specific depth profiling provides valuable insight into molecular distribution across different sample layers.

Despite these advances, the ionisation mechanisms induced by argon gas cluster ion beams (GCIB) remain incompletely understood, particularly due to complex matrix effects. Lipids were among the most readily detected biomolecules in this study and others, likely due to their abundance in cell membranes and their ease of ionisation in both positive and negative modes. To improve metabolite detection in future studies, it will be important to analyse standards of polar metabolites to better understand which physicochemical properties influence ionisation efficiency in OrbiSIMS. A deeper understanding of molecular ionisation behaviours will enhance experimental design and data interpretation in SIMS-based metabolomic and lipidomic research.

OrbiSIMS also demonstrated promising capabilities for peptide detection, suggesting the potential for label-free protein imaging and identification directly from complex biological samples. This would be particularly valuable in studying the spatial

distribution of Alzheimer's disease-related proteins. To improve confidence in protein identification, future work should involve OrbiSIMS analysis of protein standards—particularly those identified as highly abundant in LC-MS/MS datasets of H4 cells. Generating reference spectra from purified proteins would support accurate identification of proteins directly from cell samples and provide insight into OrbiSIMS-specific fragmentation patterns. However, it is important to recognise that standards may not fully replicate the endogenous structures, folding states, or post-translational modifications of native cellular proteins. To bridge this gap, the analysis of H4 cell-derived protein extracts as complex mixtures could offer a more biologically relevant reference. Complementary techniques such as ESI-MS/MS or LESA-MS/MS may also aid in identifying intact proteins and PTMs, as these soft ionisation methods produce less fragmentation than SIMS.

Looking ahead, a major objective is to expand the application of OrbiSIMS as a label-free omics screening tool across a broader range of brain cell types. Future studies will focus on patient-derived, stem cell-differentiated astrocytes and neurons, which more closely reflect the pathophysiological conditions of neurodegenerative diseases. Additionally, the imaging capabilities of OrbiSIMS could be harnessed to investigate cell–cell communication using co-culture systems or 3D cell models. Incorporating diverse cellular models that better represent disease-relevant states will significantly enhance the biological relevance of future investigations.

Chapter 8 References

1. Corder, E.H., A.M. Saunders, W.J. Strittmatter, D.E. Schmechel, P.C. Gaskell, G.W. Small, A.D. Roses, J.L. Haines and M.A. Pericak-Vance, *Gene dose of apolipoprotein E type 4 allele and the risk of Alzheimer's disease in late onset families.* Science, 1993. **261**(5123): p. 921-3.

2. Jackson, R.J., B.T. Hyman and A. Serrano-Pozo, *Multifaceted roles of APOE in Alzheimer disease.* Nat Rev Neurol, 2024. **20**(8): p. 457-474.

3. Sienski, G., P. Narayan, J.M. Bonner, N. Kory, S. Boland, A.A. Arczewska, W.T. Ralvenius, L. Akay, E. Lockshin, L. He, B. Milo, A. Graziosi, V. Baru, C.A. Lewis, M. Kellis, D.M. Sabatini, L.H. Tsai and S. Lindquist, *APOE4 disrupts intracellular lipid homeostasis in human iPSC-derived glia.* Sci Transl Med, 2021. **13**(583).

4. Xiao, J.F., B. Zhou and H.W. Ressom, *Metabolite identification and quantitation in LC-MS/MS-based metabolomics.* Trends Analyt Chem, 2012. **32**: p. 1-14.

5. Karpievitch, Y.V., A.D. Polpitiya, G.A. Anderson, R.D. Smith and A.R. Dabney, *Liquid Chromatography Mass Spectrometry-Based Proteomics: Biological and Technological Aspects.* Ann Appl Stat, 2010. **4**(4): p. 1797-1823.

6. Long, J.M. and D.M. Holtzman, *Alzheimer Disease: An Update on Pathobiology and Treatment Strategies.* Cell, 2019. **179**(2): p. 312-339.

7. Collaborators, G.B.D.D.F., *Estimation of the global prevalence of dementia in 2019 and forecasted prevalence in 2050: an analysis for the Global Burden of Disease Study 2019.* Lancet Public Health, 2022. **7**(2): p. e105-e125.

8. Wimo, A., K. Seeher, R. Cataldi, E. Cyhlarova, J.L. Dielemann, O. Frisell, M. Guerchet, L. Jönsson, A.K. Malaha, E. Nichols, P. Pedroza, M. Prince, M. Knapp and T. Dua, *The worldwide costs of dementia in 2019.* Alzheimer's & Dementia, 2023. **19**(7): p. 2865-2873.

9. Alzheimer's, A., *2019 Alzheimer's disease facts and figures.* Alzheimer's & Dementia, 2019. **15**(3): p. 321-387.

10. Hosoki, S., G.K. Hansra, T. Jayasena, A. Poljak, K.A. Mather, V.S. Catts, R. Rust, A. Sagare, J.C. Kovacic, A. Brodtmann, A. Wallin, B.V. Zlokovic, M. Ihara and P.S. Sachdev, *Molecular biomarkers for vascular cognitive impairment and dementia.* Nature Reviews Neurology, 2023. **19**(12): p. 737-753.

11. Chia, R., M.S. Sabir, S. Bandres-Ciga, S. Saez-Atienzar, R.H. Reynolds, E. Gustavsson, R.L. Walton, S. Ahmed, C. Viollet, J. Ding, M.B. Makarious, M. Diez-Fairen, M.K. Portley, Z. Shah, Y. Abramzon, D.G. Hernandez, C.

Blauwendraat, D.J. Stone, J. Eicher, L. Parkkinen, O. Ansorge, L. Clark, L.S. Honig, K. Marder, A. Lemstra, P. St George-Hyslop, E. Londos, K. Morgan, T. Lashley, T.T. Warner, Z. Jaunmuktane, D. Galasko, I. Santana, P.J. Tienari, L. Myllykangas, M. Oinas, N.J. Cairns, J.C. Morris, G.M. Halliday, V.M. Van Deerlin, J.Q. Trojanowski, M. Grassano, A. Calvo, G. Mora, A. Canosa, G. Floris, R.C. Bohannan, F. Brett, Z. Gan-Or, J.T. Geiger, A. Moore, P. May, R. Krüger, D.S. Goldstein, G. Lopez, N. Tayebi, E. Sidransky, A.R. Sotis, G. Sukumar, C. Alba, N. Lott, E.M. Martinez, M. Tuck, J. Singh, D. Bacikova, X. Zhang, D.N. Hupalo, A. Adeleye, M.D. Wilkerson, H.B. Pollard, L. Norcliffe-Kaufmann, J.-A. Palma, H. Kaufmann, V.G. Shakkottai, M. Perkins, K.L. Newell, T. Gasser, C. Schulte, F. Landi, E. Salvi, D. Cusi, E. Masliah, R.C. Kim, C.A. Caraway, E.S. Monuki, M. Brunetti, T.M. Dawson, L.S. Rosenthal, M.S. Albert, O. Pletnikova, J.C. Troncoso, M.E. Flanagan, Q. Mao, E.H. Bigio, E. Rodríguez-Rodríguez, J. Infante, C. Lage, I. González-Aramburu, P. Sanchez-Juan, B. Ghetti, J. Keith, S.E. Black, M. Masellis, E. Rogaeva, C. Duyckaerts, A. Brice, S. Lesage, G. Xiromerisiou, M.J. Barrett, B.S. Tilley, S. Gentleman, G. Logroscino, G.E. Serrano, T.G. Beach, I.G. McKeith, A.J. Thomas, J. Attems, C.M. Morris, L. Palmer, S. Love, C. Troakes, S. Al-Sarraj, A.K. Hodges, D. Aarsland, G. Klein, S.M. Kaiser, R. Woltjer, P. Pastor, L.M. Bekris, J.B. Leverenz, L.M. Besser, A. Kuzma, A.E. Renton, A. Goate, D.A. Bennett, C.R. Scherzer, H.R. Morris, R. Ferrari, D. Albani, S. Pickering-Brown, K. Faber, W.A. Kukull, E. Morenas-Rodriguez, A. Lleó, J. Fortea, D. Alcolea, J. Clarimon, M.A. Nalls, L. Ferrucci, S.M. Resnick, T. Tanaka, T.M. Foroud, N.R. Graff-Radford, Z.K. Wszolek, T. Ferman, B.F. Boeve, J.A. Hardy, E.J. Topol, A. Torkamani, A.B. Singleton, M. Ryten, D.W. Dickson, A. Chiò, O.A. Ross, J.R. Gibbs, C.L. Dalgard, B.J. Traynor, S.W. Scholz and C. The American Genome, *Genome sequencing analysis identifies new loci associated with Lewy body dementia and provides insights into its genetic architecture.* Nature Genetics, 2021. **53**(3): p. 294-303.

12. Rademakers, R., M. Neumann and I.R. Mackenzie, *Advances in understanding the molecular basis of frontotemporal dementia.* Nature Reviews Neurology, 2012. **8**(8): p. 423-434.

13. Javed, K., V. Reddy and F. Lui, *Neuroanatomy, Cerebral Cortex*, in *StatPearls*. 2025, StatPearls Publishing

14. Catani, M., *Chapter 6 - The anatomy of the human frontal lobe*, in *Handbook of Clinical Neurology*, M. D'Esposito and J.H. Grafman, Editors. 2019, Elsevier. p. 95-122.

15. Freedman, D.J. and G. Ibos, *An Integrative Framework for Sensory, Motor, and Cognitive Functions of the Posterior Parietal Cortex.* Neuron, 2018. **97**(6): p. 1219-1234.

16. Colombari, E., G. Parisi, A. Tafuro, S. Mele, C. Mazzi and S. Savazzi, *Beyond*

primary visual cortex: The leading role of lateral occipital complex in early conscious visual processing. Neuroimage, 2024. **298**: p. 120805.

17. Baxter, M.G., *Involvement of medial temporal lobe structures in memory and perception.* Neuron, 2009. **61**(5): p. 667-77.

18. Garcia, A.D. and E.A. Buffalo, *Anatomy and Function of the Primate Entorhinal Cortex.* Annu Rev Vis Sci, 2020. **6**: p. 411-432.

19. Takehara-Nishiuchi, K., *Entorhinal cortex and consolidated memory.* Neurosci Res, 2014. **84**: p. 27-33.

20. Igarashi, K.M., *Entorhinal cortex dysfunction in Alzheimer's disease.* Trends Neurosci, 2023. **46**(2): p. 124-136.

21. Killiany, R.J., B.T. Hyman, T. Gomez-Isla, M.B. Moss, R. Kikinis, F. Jolesz, R. Tanzi, K. Jones and M.S. Albert, *MRI measures of entorhinal cortex vs hippocampus in preclinical AD.* Neurology, 2002. **58**(8): p. 1188-96.

22. Stouffer, K.M., X. Grande, E. Düzel, M. Johansson, B. Creese, M.P. Witter, M.I. Miller, L.E.M. Wisse and D. Berron, *Amidst an amygdala renaissance in Alzheimer's disease.* Brain, 2023. **147**(3): p. 816-829.

23. Frick, A., G. Besson, E. Salmon and E. Delhaye, *Perirhinal cortex is associated with fine-grained discrimination of conceptually confusable objects in Alzheimer's disease.* Neurobiol Aging, 2023. **130**: p. 1-11.

24. Raslau, F.D., I.T. Mark, A.P. Klein, J.L. Ulmer, V. Mathews and L.P. Mark, *Memory Part 2: The Role of the Medial Temporal Lobe.* American Journal of Neuroradiology, 2015. **36**(5): p. 846-849.

25. Tcw, J. and A.M. Goate, *Genetics of β-Amyloid Precursor Protein in Alzheimer's Disease.* Cold Spring Harbor perspectives in medicine, 2017. **7**(6): p. a024539.

26. Liu, C.-C., T. Kanekiyo, H. Xu and G. Bu, *Apolipoprotein E and Alzheimer disease: risk, mechanisms and therapy.* Nature Reviews Neurology, 2013. **9**(2): p. 106-118.

27. Carmona, S., K. Zahs, E. Wu, K. Dakin, J. Bras and R. Guerreiro, *The role of TREM2 in Alzheimer's disease and other neurodegenerative disorders.* The Lancet Neurology, 2018. **17**(8): p. 721-730.

28. Tagarelli, A., A. Piro, G. Tagarelli, P. Lagonia and A. Quattrone, *Alois Alzheimer: a hundred years after the discovery of the eponymous disorder.* Int J Biomed Sci, 2006. **2**(2): p. 196-204.

29. Cummings, J., Y. Zhou, G. Lee, K. Zhong, J. Fonseca and F. Cheng, *Alzheimer's disease drug development pipeline: 2023.* Alzheimer's & Dementia:

Translational Research & Clinical Interventions, 2023. **9**(2): p. e12385.

30. Li, T., L. Lu, E. Pember, X. Li, B. Zhang and Z. Zhu, *New Insights into Neuroinflammation Involved in Pathogenic Mechanism of Alzheimer’s Disease and Its Potential for Therapeutic Intervention.* Cells, 2022. **11**(12): p. 1925.

31. Alexander, G.C., S. Emerson and A.S. Kesselheim, *Evaluation of Aducanumab for Alzheimer Disease: Scientific Evidence and Regulatory Review Involving Efficacy, Safety, and Futility.* JAMA, 2021. **325**(17): p. 1717-1718.

32. Bellenguez, C., F. Küçükali, I.E. Jansen, L. Kleineidam, S. Moreno-Grau, N. Amin, A.C. Naj, R. Campos-Martin, B. Grenier-Boley, V. Andrade, P.A. Holmans, A. Boland, V. Damotte, S.J. van der Lee, M.R. Costa, T. Kuulasmaa, Q. Yang, I. de Rojas, J.C. Bis, A. Yaqub, I. Prokic, J. Chapuis, S. Ahmad, V. Giedraitis, D. Aarsland, P. Garcia-Gonzalez, C. Abdelnour, E. Alarcón-Martín, D. Alcolea, M. Alegret, I. Alvarez, V. Álvarez, N.J. Armstrong, A. Tsolaki, C. Antúnez, I. Appollonio, M. Arcaro, S. Archetti, A.A. Pastor, B. Arosio, L. Athanasiu, H. Bailly, N. Banaj, M. Baquero, S. Barral, A. Beiser, A.B. Pastor, J.E. Below, P. Benchek, L. Benussi, C. Berr, C. Besse, V. Bessi, G. Binetti, A. Bizarro, R. Blesa, M. Boada, E. Boerwinkle, B. Borroni, S. Boschi, P. Bossù, G. Bråthen, J. Bressler, C. Bresner, H. Brodaty, K.J. Brookes, L.I. Brusco, D. Buiza-Rueda, K. Bûrger, V. Burholt, W.S. Bush, M. Calero, L.B. Cantwell, G. Chene, J. Chung, M.L. Cuccaro, Á. Carracedo, R. Cecchetti, L. Cervera-Carles, C. Charbonnier, H.-H. Chen, C. Chillotti, S. Ciccone, J.A.H.R. Claassen, C. Clark, E. Conti, A. Corma-Gómez, E. Costantini, C. Custodero, D. Daian, M.C. Dalmasso, A. Daniele, E. Dardiotis, J.-F. Dartigues, P.P. de Deyn, K. de Paiva Lopes, L.D. de Witte, S. Debette, J. Deckert, T. del Ser, N. Denning, A. DeStefano, M. Dichgans, J. Diehl-Schmid, M. Diez-Fairen, P.D. Rossi, S. Djurovic, E. Duron, E. Düzel, C. Dufouil, G. Eiriksdottir, S. Engelborghs, V. Escott-Price, A. Espinosa, M. Ewers, K.M. Faber, T. Fabrizio, S.F. Nielsen, D.W. Fardo, L. Farotti, C. Fenoglio, M. Fernández-Fuertes, R. Ferrari, C.B. Ferreira, E. Ferri, B. Fin, P. Fischer, T. Fladby, K. Fließbach, B. Fongang, M. Fornage, J. Fortea, T.M. Foroud, S. Fostinelli, N.C. Fox, E. Franco-Macías, M.J. Bullido, A. Frank-García, L. Froelich, B. Fulton-Howard, D. Galimberti, J.M. García-Alberca, P. García-González, S. Garcia-Madrona, G. Garcia-Ribas, R. Ghidoni, I. Giegling, G. Giorgio, A.M. Goate, O. Goldhardt, D. Gomez-Fonseca, A. González-Pérez, C. Graff, G. Grande, E. Green, T. Grimmer, E. Grünblatt, M. Grunin, V. Gudnason, T. Guetta-Baranes, A. Haapasalo, G. Hadjigeorgiou, J.L. Haines, K.L. Hamilton-Nelson, H. Hampel, O. Hanon, J. Hardy, A.M. Hartmann, L. Hausner, J. Harwood, S. Heilmann-Heimbach, S. Helisalmi, M.T. Heneka, I. Hernández, M.J. Herrmann, P. Hoffmann, C. Holmes, H. Holstege, R.H. Vilas, M. Hulsman, J. Humphrey, G.J. Biessels, X. Jian, C. Johansson, G.R. Jun, Y. Kastumata, J. Kauwe, P.G. Kehoe, L. Kilander, A.K. Ståhlbom, M. Kivipelto, A. Koivisto, J. Kornhuber, M.H. Kosmidis, W.A. Kukull, P.P. Kuksa, B.W. Kunkle, A.B. Kuzma, C. Lage, E.J. Laukka, L. Launer, A. Lauria, C.-Y. Lee, J. Lehtisalo, O. Lerch, A. Lleó, W. Longstreth, O.

Lopez, A.L. de Munain, S. Love, M. Löwemark, L. Luckcuck, K.L. Lunetta, Y. Ma, J. Macías, C.A. MacLeod, W. Maier, F. Mangialasche, M. Spallazzi, M. Marquié, R. Marshall, E.R. Martin, A.M. Montes, C.M. Rodríguez, C. Masullo, R. Mayeux, S. Mead, P. Mecocci, M. Medina, A. Meggy, S. Mehrabian, S. Mendoza, M. Menéndez-González, P. Mir, S. Moebus, M. Mol, L. Molina-Porcel, L. Montrreal, L. Morelli, F. Moreno, K. Morgan, T. Mosley, M.M. Nöthen, C. Muchnik, S. Mukherjee, B. Nacmias, T. Ngandu, G. Nicolas, B.G. Nordestgaard, R. Olaso, A. Orellana, M. Orsini, G. Ortega, A. Padovani, C. Paolo, G. Papenberg, L. Parnetti, F. Pasquier, P. Pastor, G. Peloso, A. Pérez-Cordón, J. Pérez-Tur, P. Pericard, O. Peters, Y.A.L. Pijnenburg, J.A. Pineda, G. Piñol-Ripoll, C. Pisanu, T. Polak, J. Popp, D. Posthuma, J. Priller, R. Puerta, O. Quenez, I. Quintela, J.Q. Thomassen, A. Rábano, I. Rainero, F. Rajabli, I. Ramakers, L.M. Real, M.J.T. Reinders, C. Reitz, D. Reyes-Dumeyer, P. Ridge, S. Riedel-Heller, P. Riederer, N. Roberto, E. Rodriguez-Rodriguez, A. Rongve, I.R. Allende, M. Rosende-Roca, J.L. Royo, E. Rubino, D. Rujescu, M.E. Sáez, P. Sakka, I. Saltvedt, Á. Sanabria and M.B. Sánchez-Arjona, *New insights into the genetic etiology of Alzheimer's disease and related dementias.* Nature Genetics, 2022. **54**(4): p. 412-436.

33. Martens, Y.A., N. Zhao, C.-C. Liu, T. Kanekiyo, A.J. Yang, A.M. Goate, D.M. Holtzman and G. Bu, *ApoE Cascade Hypothesis in the pathogenesis of Alzheimer's disease and related dementias.* Neuron, 2022. **110**(8): p. 1304-1317.

34. Yamazaki, Y., N. Zhao, T.R. Caulfield, C.-C. Liu and G. Bu, *Apolipoprotein E and Alzheimer disease: pathobiology and targeting strategies.* Nature Reviews Neurology, 2019. **15**(9): p. 501-518.

35. Genin, E., D. Hannequin, D. Wallon, K. Sleegers, M. Hiltunen, O. Combarros, M.J. Bullido, S. Engelborghs, P. De Deyn, C. Berr, F. Pasquier, B. Dubois, G. Tognoni, N. Fievet, N. Brouwers, K. Bettens, B. Arosio, E. Coto, M. Del Zompo, I. Mateo, J. Epelbaum, A. Frank-Garcia, S. Helisalmi, E. Porcellini, A. Pilotto, P. Forti, R. Ferri, E. Scarpini, G. Siciliano, V. Solfrizzi, S. Sorbi, G. Spalletta, F. Valdivieso, S. Vepsalainen, V. Alvarez, P. Bosco, M. Mancuso, F. Panza, B. Nacmias, P. Bossu, O. Hanon, P. Piccardi, G. Annoni, D. Seripa, D. Galimberti, F. Licastro, H. Soininen, J.F. Dartigues, M.I. Kamboh, C. Van Broeckhoven, J.C. Lambert, P. Amouyel and D. Campion, *APOE and Alzheimer disease: a major gene with semi-dominant inheritance.* Mol Psychiatry, 2011. **16**(9): p. 903-7.

36. Farrer, L.A., L.A. Cupples, J.L. Haines, B. Hyman, W.A. Kukull, R. Mayeux, R.H. Myers, M.A. Pericak-Vance, N. Risch and C.M. van Duijn, *Effects of Age, Sex, and Ethnicity on the Association Between Apolipoprotein E Genotype and Alzheimer Disease: A Meta-analysis.* JAMA, 1997. **278**(16): p. 1349-1356.

37. Huang, Y. and R.W. Mahley, *Apolipoprotein E: structure and function in lipid metabolism, neurobiology, and Alzheimer's diseases.* Neurobiol Dis, 2014. **72 Pt A**: p. 3-12.

38. Chen, J., Q. Li and J. Wang, *Topology of human apolipoprotein E3 uniquely regulates its diverse biological functions.* Proceedings of the National Academy of Sciences, 2011. **108**(36): p. 14813-14818.

39. Herz, J. and Y. Chen, *Reelin, lipoprotein receptors and synaptic plasticity.* Nature Reviews Neuroscience, 2006. **7**(11): p. 850-859.

40. Zhao, N., C.C. Liu, W. Qiao and G. Bu, *Apolipoprotein E, Receptors, and Modulation of Alzheimer's Disease.* Biol Psychiatry, 2018. **83**(4): p. 347-357.

41. Nguyen, D., P. Dhanasekaran, M. Nickel, R. Nakatani, H. Saito, M.C. Phillips and S. Lund-Katz, *Molecular basis for the differences in lipid and lipoprotein binding properties of human apolipoproteins E3 and E4.* Biochemistry, 2010. **49**(51): p. 10881-9.

42. Corder, E.H., A.M. Saunders, W.J. Strittmatter, D.E. Schmechel, P.C. Gaskell, G.W. Small, A.D. Roses, J.L. Haines and M.A. Pericak-Vance, *Gene dose of apolipoprotein E type 4 allele and the risk of Alzheimer's disease in late onset families.* Science, 1993. **261**(5123): p. 921.

43. Roher, A.E., C.L. Maarouf, L.I. Sue, Y. Hu, J. Wilson and T.G. Beach, *Proteomics-derived cerebrospinal fluid markers of autopsy-confirmed Alzheimer's disease.* Biomarkers, 2009. **14**(7): p. 493-501.

44. Li, X., J. Zhang, D. Li, C. He, K. He, T. Xue, L. Wan, C. Zhang and Q. Liu, *Astrocytic ApoE reprograms neuronal cholesterol metabolism and histone-acetylation-mediated memory.* Neuron, 2021. **109**(6): p. 957-970.e8.

45. Agosta, F., K.A. Vossel, B.L. Miller, R. Migliaccio, S.J. Bonasera, M. Filippi, A.L. Boxer, A. Karydas, K.L. Possin and M.L. Gorno-Tempini, *Apolipoprotein E ε4 is associated with disease-specific effects on brain atrophy in Alzheimer's disease and frontotemporal dementia.* Proceedings of the National Academy of Sciences, 2009. **106**(6): p. 2018-2022.

46. Litvinchuk, A., J.H. Suh, J.L. Guo, K. Lin, S.S. Davis, N. Bien-Ly, E. Tycksen, G.T. Tabor, J. Remolina Serrano, M. Manis, X. Bao, C. Lee, M. Bosch, E.J. Perez, C.M. Yuede, A.G. Cashikar, J.D. Ulrich, G. Di Paolo and D.M. Holtzman, *Amelioration of Tau and ApoE4-linked glial lipid accumulation and neurodegeneration with an LXR agonist.* Neuron, 2024. **112**(3): p. 384-403.e8.

47. Hirsch-Reinshagen, V., B.L. Burgess and C.L. Wellington, *Why lipids are important for Alzheimer disease?* Molecular and Cellular Biochemistry, 2009. **326**(1): p. 121-129.

48. Hardy, J.A. and G.A. Higgins, *Alzheimer's Disease: The Amyloid Cascade Hypothesis.* Science, 1992. **256**(5054): p. 184-185.

49. Bussy, A., B.J. Snider, D. Coble, C. Xiong, A.M. Fagan, C. Cruchaga, T.L.S.

Benzinger, B.A. Gordon, J. Hassenstab, R.J. Bateman and J.C. Morris, *Effect of apolipoprotein E4 on clinical, neuroimaging, and biomarker measures in noncarrier participants in the Dominantly Inherited Alzheimer Network.* Neurobiology of Aging, 2019. **75**: p. 42-50.

50. Liu, C.C., N. Zhao, Y. Fu, N. Wang, C. Linares, C.W. Tsai and G. Bu, *ApoE4 Accelerates Early Seeding of Amyloid Pathology.* Neuron, 2017. **96**(5): p. 1024-1032 e3.

51. Fernandez, C.G., M.E. Hamby, M.L. McReynolds and W.J. Ray, *The Role of APOE4 in Disrupting the Homeostatic Functions of Astrocytes and Microglia in Aging and Alzheimer's Disease.* Frontiers in Aging Neuroscience, 2019. **11**: p. 14.

52. Konings, S.C., E. Nyberg, I. Martinsson, L. Torres-Garcia, O. Klementieva, C.G. Almeida and G.K. Gouras, *Apolipoprotein E intersects with amyloid-β within neurons.* Life Science Alliance, 2023. **6**(8).

53. Shi, Y., K. Yamada, S.A. Liddelow, S.T. Smith, L. Zhao, W. Luo, R.M. Tsai, S. Spina, L.T. Grinberg, J.C. Rojas, G. Gallardo, K. Wang, J. Roh, G. Robinson, M.B. Finn, H. Jiang, P.M. Sullivan, C. Baufeld, M.W. Wood, C. Sutphen, L. McCue, C. Xiong, J.L. Del-Aguila, J.C. Morris, C. Cruchaga, A.M. Fagan, B.L. Miller, A.L. Boxer, W.W. Seeley, O. Butovsky, B.A. Barres, S.M. Paul, D.M. Holtzman and I. Alzheimer's Disease Neuroimaging, *ApoE4 markedly exacerbates tau-mediated neurodegeneration in a mouse model of tauopathy.* Nature, 2017. **549**(7673): p. 523-527.

54. Hashimoto, T., A. Serrano-Pozo, Y. Hori, K.W. Adams, S. Takeda, A.O. Banerji, A. Mitani, D. Joyner, D.H. Thyssen, B.J. Bacskai, M.P. Frosch, T.L. Spires-Jones, M.B. Finn, D.M. Holtzman and B.T. Hyman, *Apolipoprotein E, Especially Apolipoprotein E4, Increases the Oligomerization of Amyloid β Peptide.* Journal of Neuroscience, 2012. **32**(43): p. 15181-15192.

55. Mouchard, A., M.C. Boutonnet, C. Mazzocco, N. Biendon, N. Macrez and C.E.B.N.N. Neuro, *ApoE-fragment/Abeta heteromers in the brain of patients with Alzheimer's disease.* Sci Rep, 2019. **9**(1): p. 3989.

56. Dixit, R., J.L. Ross, Y.E. Goldman and E.L.F. Holzbaur, *Differential Regulation of Dynein and Kinesin Motor Proteins by Tau.* Science, 2008. **319**(5866): p. 1086-1089.

57. Hanseeuw, B.J., R.A. Betensky, H.I.L. Jacobs, A.P. Schultz, J. Sepulcre, J.A. Becker, D.M.O. Cosio, M. Farrell, Y.T. Quiroz, E.C. Mormino, R.F. Buckley, K.V. Papp, R.A. Amariglio, I. Dewachter, A. Ivanoiu, W. Huijbers, T. Hedden, G.A. Marshall, J.P. Chhatwal, D.M. Rentz, R.A. Sperling and K. Johnson, *Association of Amyloid and Tau With Cognition in Preclinical Alzheimer Disease: A Longitudinal Study.* JAMA Neurology, 2019. **76**(8): p. 915-924.

58. Shi, Y. and D.M. Holtzman, *Interplay between innate immunity and Alzheimer disease: APOE and TREM2 in the spotlight.* Nature Reviews Immunology, 2018. **18**(12): p. 759-772.

59. Shi, Y., M. Manis, J. Long, K. Wang, P.M. Sullivan, J. Remolina Serrano, R. Hoyle and D.M. Holtzman, *Microglia drive APOE-dependent neurodegeneration in a tauopathy mouse model.* Journal of Experimental Medicine, 2019. **216**(11): p. 2546-2561.

60. Shi, Y., K. Yamada, S.A. Liddelow, S.T. Smith, L. Zhao, W. Luo, R.M. Tsai, S. Spina, L.T. Grinberg, J.C. Rojas, G. Gallardo, K. Wang, J. Roh, G. Robinson, M.B. Finn, H. Jiang, P.M. Sullivan, C. Baufeld, M.W. Wood, C. Sutphen, L. McCue, C. Xiong, J.L. Del-Aguila, J.C. Morris, C. Cruchaga, I. Alzheimer's Disease Neuroimaging, A.M. Fagan, B.L. Miller, A.L. Boxer, W.W. Seeley, O. Butovsky, B.A. Barres, S.M. Paul and D.M. Holtzman, *ApoE4 markedly exacerbates tau-mediated neurodegeneration in a mouse model of tauopathy.* Nature, 2017. **549**(7673): p. 523-527.

61. Shi, Y., M. Manis, J. Long, K. Wang, P.M. Sullivan, J. Remolina Serrano, R. Hoyle and D.M. Holtzman, *Microglia drive APOE-dependent neurodegeneration in a tauopathy mouse model.* J Exp Med, 2019. **216**(11): p. 2546-2561.

62. Montagne, A., D.A. Nation, A.P. Sagare, G. Barisano, M.D. Sweeney, A. Chakhoyan, M. Pachicano, E. Joe, A.R. Nelson, L.M. D'Orazio, D.P. Buennagel, M.G. Harrington, T.L.S. Benzinger, A.M. Fagan, J.M. Ringman, L.S. Schneider, J.C. Morris, E.M. Reiman, R.J. Caselli, H.C. Chui, J. Tcw, Y. Chen, J. Pa, P.S. Conti, M. Law, A.W. Toga and B.V. Zlokovic, *APOE4 leads to blood–brain barrier dysfunction predicting cognitive decline.* Nature, 2020. **581**(7806): p. 71-76.

63. Heneka, M.T., M.J. Carson, J. El Khoury, G.E. Landreth, F. Brosseron, D.L. Feinstein, A.H. Jacobs, T. Wyss-Coray, J. Vitorica, R.M. Ransohoff, K. Herrup, S.A. Frautschy, B. Finsen, G.C. Brown, A. Verkhratsky, K. Yamanaka, J. Koistinaho, E. Latz, A. Halle, G.C. Petzold, T. Town, D. Morgan, M.L. Shinohara, V.H. Perry, C. Holmes, N.G. Bazan, D.J. Brooks, S. Hunot, B. Joseph, N. Deigendesch, O. Garaschuk, E. Boddeke, C.A. Dinarello, J.C. Breitner, G.M. Cole, D.T. Golenbock and M.P. Kummer, *Neuroinflammation in Alzheimer's disease.* The Lancet. Neurology, 2015. **14**(4): p. 388-405.

64. Reid, M.J., P. Beltran-Lobo, L. Johnson, B.G. Perez-Nievas and W. Noble, *Astrocytes in Tauopathies.* Frontiers in Neurology, 2020. **11**: p. 1119.

65. Colonna, M. and S. Brioschi, *Neuroinflammation and neurodegeneration in human brain at single-cell resolution.* Nature Reviews Immunology, 2020. **20**(2): p. 81-82.

66. Liu, C.C., N. Wang, Y. Chen, Y. Inoue, F. Shue, Y. Ren, M. Wang, W. Qiao, T.C. Ikezu, Z. Li, J. Zhao, Y. Martens, S.V. Doss, C.L. Rosenberg, S. Jeevaratnam, L.

Jia, A.C. Raulin, F. Qi, Y. Zhu, A. Alnobani, J. Knight, Y. Chen, C. Linares, A. Kurti, J.D. Fryer, B. Zhang, L.J. Wu, B.Y.S. Kim and G. Bu, *Cell-autonomous effects of APOE4 in restricting microglial response in brain homeostasis and Alzheimer's disease.* Nat Immunol, 2023. **24**(11): p. 1854-1866.

67. Montagne, A., A.M. Nikolakopoulou, M.T. Huuskonen, A.P. Sagare, E.J. Lawson, D. Lazic, S.V. Rege, A. Grond, E. Zuniga, S.R. Barnes, J. Prince, M. Sagare, C.J. Hsu, M.J. LaDu, R.E. Jacobs and B.V. Zlokovic, *accelerates advanced-stage vascular and neurodegenerative disorder in old Alzheimer's mice via cyclophilin A independently of amyloid-β.* Nature Aging, 2021. **1**(6): p. 506-+.

68. Zhao, J., Y. Fu, Y. Yamazaki, Y. Ren, M.D. Davis, C.-C. Liu, W. Lu, X. Wang, K. Chen, Y. Cherukuri, L. Jia, Y.A. Martens, L. Job, F. Shue, T.T. Nguyen, S.G. Younkin, N.R. Graff-Radford, Z.K. Wszolek, D.A. Brafman, Y.W. Asmann, N. Ertekin-Taner, T. Kanekiyo and G. Bu, *APOE4 exacerbates synapse loss and neurodegeneration in Alzheimer's disease patient iPSC-derived cerebral organoids.* Nature Communications, 2020. **11**(1): p. 5540.

69. Seo, D.O., D. O'Donnell, N. Jain, J.D. Ulrich, J. Herz, Y. Li, M. Lemieux, J. Cheng, H. Hu, J.R. Serrano, X. Bao, E. Franke, M. Karlsson, M. Meier, S. Deng, C. Desai, H. Dodiya, J. Lelwala-Guruge, S.A. Handley, J. Kipnis, S.S. Sisodia, J.I. Gordon and D.M. Holtzman, *ApoE isoform- and microbiota-dependent progression of neurodegeneration in a mouse model of tauopathy.* Science, 2023. **379**(6628): p. eadd1236.

70. Tran, T.T.T., S. Corsini, L. Kellingray, C. Hegarty, G. Le Gall, A. Narbad, M. Muller, N. Tejera, P.W. O'Toole, A.M. Minihane and D. Vauzour, *APOE genotype influences the gut microbiome structure and function in humans and mice: relevance for Alzheimer's disease pathophysiology.* FASEB J, 2019. **33**(7): p. 8221-8231.

71. Wang, C., M. Xiong, M. Gratuze, X. Bao, Y. Shi, P.S. Andhey, M. Manis, C. Schroeder, Z. Yin, C. Madore, O. Butovsky, M. Artyomov, J.D. Ulrich and D.M. Holtzman, *Selective removal of astrocytic APOE4 strongly protects against tau-mediated neurodegeneration and decreases synaptic phagocytosis by microglia.* Neuron, 2021. **109**(10): p. 1657-1674.e7.

72. Zhao, L., A.J. Gottesdiener, M. Parmar, M. Li, S.M. Kaminsky, M.J. Chiuchiolo, D. Sondhi, P.M. Sullivan, D.M. Holtzman, R.G. Crystal and S.M. Paul, *Intracerebral adeno-associated virus gene delivery of apolipoprotein E2 markedly reduces brain amyloid pathology in Alzheimer's disease mouse models.* Neurobiol Aging, 2016. **44**: p. 159-172.

73. Rosenberg, J.B., M.G. Kaplitt, B.P. De, A. Chen, T. Flagiello, C. Salami, E. Pey, L. Zhao, R.J. Ricart Arbona, S. Monette, J.P. Dyke, D.J. Ballon, S.M. Kaminsky, D. Sondhi, G.A. Petsko, S.M. Paul and R.G. Crystal, *AAVrh.10-Mediated APOE2*

Central Nervous System Gene Therapy for APOE4-Associated Alzheimer's Disease. Hum Gene Ther Clin Dev, 2018. **29**(1): p. 24-47.

74. Reiman, E.M., J.F. Arboleda-Velasquez, Y.T. Quiroz, M.J. Huentelman, T.G. Beach, R.J. Caselli, Y. Chen, Y. Su, A.J. Myers, J. Hardy, J. Paul Vonsattel, S.G. Younkin, D.A. Bennett, P.L. De Jager, E.B. Larson, P.K. Crane, C.D. Keene, M.I. Kamboh, J.K. Kofler, L. Duque, J.R. Gilbert, H.E. Gwirtsman, J.D. Buxbaum, D.W. Dickson, M.P. Frosch, B.F. Ghetti, K.L. Lunetta, L.S. Wang, B.T. Hyman, W.A. Kukull, T. Foroud, J.L. Haines, R.P. Mayeux, M.A. Pericak-Vance, J.A. Schneider, J.Q. Trojanowski, L.A. Farrer, G.D. Schellenberg, G.W. Beecham, T.J. Montine and G.R. Jun, *Exceptionally low likelihood of Alzheimer's dementia in APOE2 homozygotes from a 5,000-person neuropathological study.* Nat Commun, 2020. **11**(1): p. 667.

75. Jackson, R.J., M.S. Keiser, J.C. Meltzer, D.P. Fykstra, S.E. Dierksmeier, S. Hajizadeh, J. Kreuzer, R. Morris, A. Melloni, T. Nakajima, L. Tecedor, P.T. Ranum, E. Carrell, Y. Chen, M.A. Nishtar, D.M. Holtzman, W. Haas, B.L. Davidson and B.T. Hyman, *APOE2 gene therapy reduces amyloid deposition and improves markers of neuroinflammation and neurodegeneration in a mouse model of Alzheimer disease.* Mol Ther, 2024.

76. Harach, T., N. Marungruang, N. Duthilleul, V. Cheatham, K.D. Mc Coy, G. Frisoni, J.J. Neher, F. Fåk, M. Jucker, T. Lasser and T. Bolmont, *Reduction of Abeta amyloid pathology in APPPS1 transgenic mice in the absence of gut microbiota.* Sci Rep, 2017. **7**: p. 41802.

77. Wang, X., G. Sun, T. Feng, J. Zhang, X. Huang, T. Wang, Z. Xie, X. Chu, J. Yang, H. Wang, S. Chang, Y. Gong, L. Ruan, G. Zhang, S. Yan, W. Lian, C. Du, D. Yang, Q. Zhang, F. Lin, J. Liu, H. Zhang, C. Ge, S. Xiao, J. Ding and M. Geng, *Sodium oligomannate therapeutically remodels gut microbiota and suppresses gut bacterial amino acids-shaped neuroinflammation to inhibit Alzheimer's disease progression.* Cell Res, 2019. **29**(10): p. 787-803.

78. Xiao, S., P. Chan, T. Wang, Z. Hong, S. Wang, W. Kuang, J. He, X. Pan, Y. Zhou, Y. Ji, L. Wang, Y. Cheng, Y. Peng, Q. Ye, X. Wang, Y. Wu, Q. Qu, S. Chen, S. Li, W. Chen, J. Xu, D. Peng, Z. Zhao, Y. Li, J. Zhang, Y. Du, W. Chen, D. Fan, Y. Yan, X. Liu, W. Zhang, B. Luo, W. Wu, L. Shen, C. Liu, P. Mao, Q. Wang, Q. Zhao, Q. Guo, Y. Zhou, Y. Li, L. Jiang, W. Ren, Y. Ouyang, Y. Wang, S. Liu, J. Jia, N. Zhang, Z. Liu, R. He, T. Feng, W. Lu, H. Tang, P. Gao, Y. Zhang, L. Chen, L. Wang, Y. Yin, Q. Xu, J. Xiao, L. Cong, X. Cheng, H. Zhang, D. Gao, M. Xia, T. Lian, G. Peng, X. Zhang, B. Jiao, H. Hu, X. Chen, Y. Guan, R. Cui, Q. Huang, X. Xin, H. Chen, Y. Ding, J. Zhang, T. Feng, M. Cantillon, K. Chen, J.L. Cummings, J. Ding, M. Geng and Z. Zhang, *A 36-week multicenter, randomized, double-blind, placebo-controlled, parallel-group, phase 3 clinical trial of sodium oligomannate for mild-to-moderate Alzheimer's dementia.* Alzheimers Res Ther, 2021. **13**(1): p. 62.

79. Wang, T., W. Kuang, W. Chen, W. Xu, L. Zhang, Y. Li, H. Li, Y. Peng, Y. Chen, B. Wang, J. Xiao, H. Li, C. Yan, Y. Du, M. Tang, Z. He, H. Chen, W. Li, H. Lin, S. Shi, J. Bi, H. Zhou, Y. Cheng, X. Gao, Y. Guan, Q. Huang, K. Chen, X. Xin, J. Ding, M. Geng and S. Xiao, *A phase II randomized trial of sodium oligomannate in Alzheimer's dementia.* Alzheimers Res Ther, 2020. **12**(1): p. 110.

80. Bosch, M.E., H.B. Dodiya, J. Michalkiewicz, C. Lee, S.M. Shaik, I.Q. Weigle, C. Zhang, J. Osborn, A. Nambiar, P. Patel, S. Parhizkar, X. Zhang, M.L. Laury, P. Mondal, A. Gomm, M.J. Schipma, D. Mallah, O. Butovsky, E.B. Chang, R.E. Tanzi, J.A. Gilbert, D.M. Holtzman and S.S. Sisodia, *Sodium oligomannate alters gut microbiota, reduces cerebral amyloidosis and reactive microglia in a sex-specific manner.* Mol Neurodegener, 2024. **19**(1): p. 18.

81. Hunt, T.J., A. Martinsen, A.-M. Minihane, E. Flanagan, M. Hornberger, P. Mena, D.D. Rio, M. Muller, P. Kroon and D. Vauzour, *Interactions between APOE Genotype, the Gut Microbiome and Polyphenol Metabolism.* Alzheimer's & Dementia, 2023. **19**(S21): p. e079725.

82. Gowda, G.A.N., S. Zhang, H. Gu, V. Asiago, N. Shanaiah and D. Raftery, *Metabolomics-based methods for early disease diagnostics.* Expert review of molecular diagnostics, 2008. **8**(5): p. 617-633.

83. Xie, K., Q. Qin, Z. Long, Y. Yang, C. Peng, C. Xi, L. Li, Z. Wu, V. Daria, Y. Zhao, F. Wang and M. Wang, *High-Throughput Metabolomics for Discovering Potential Biomarkers and Identifying Metabolic Mechanisms in Aging and Alzheimer's Disease.* Frontiers in Cell and Developmental Biology, 2021. **9**.

84. Wightman, D.P., I.E. Jansen, J.E. Savage, A.A. Shadrin, S. Bahrami, D. Holland, A. Rongve, S. Børte, B.S. Winsvold, O.K. Drange, A.E. Martinsen, A.H. Skogholt, C. Willer, G. Bråthen, I. Bosnes, J.B. Nielsen, L.G. Fritsche, L.F. Thomas, L.M. Pedersen, M.E. Gabrielsen, M.B. Johnsen, T.W. Meisingset, W. Zhou, P. Proitsi, A. Hodges, R. Dobson, L. Velayudhan, K. Heilbron, A. Auton, M. Agee, S. Aslibekyan, E. Babalola, R.K. Bell, J. Bielenberg, K. Bryc, E. Bullis, B. Cameron, D. Coker, G.C. Partida, D. Dhamija, S. Das, S.L. Elson, T. Filshtein, K. Fletez-Brant, P. Fontanillas, W. Freyman, P.M. Gandhi, B. Hicks, D.A. Hinds, K.E. Huber, E.M. Jewett, Y. Jiang, A. Kleinman, K. Kukar, V. Lane, K.-H. Lin, M. Lowe, M.K. Luff, J.C. McCreight, M.H. McIntyre, K.F. McManus, S.J. Micheletti, M.E. Moreno, J.L. Mountain, S.V. Mozaffari, P. Nandakumar, E.S. Noblin, J. O'Connell, A.A. Petrakovitz, G.D. Poznik, M. Schumacher, A.J. Shastri, J.F. Shelton, J. Shi, S. Shringarpure, C. Tian, V. Tran, J.Y. Tung, X. Wang, W. Wang, C.H. Weldon, P. Wilton, J.M. Sealock, L.K. Davis, N.L. Pedersen, C.A. Reynolds, I.K. Karlsson, S. Magnusson, H. Stefansson, S. Thordardottir, P.V. Jonsson, J. Snaedal, A. Zettergren, I. Skoog, S. Kern, M. Waern, H. Zetterberg, K. Blennow, E. Stordal, K. Hveem, J.-A. Zwart, L. Athanasiu, P. Selnes, I. Saltvedt, S.B. Sando, I. Ulstein, S. Djurovic, T. Fladby, D. Aarsland, G. Selbæk, S. Ripke, K. Stefansson, O.A. Andreassen, D. Posthuma and T. andMe Research, *A genome-wide association study with 1,126,563 individuals identifies new risk loci for*

Alzheimer's disease. Nature Genetics, 2021. **53**(9): p. 1276-1282.

85. Barisano, G., K. Kisler, B. Wilkinson, A.M. Nikolakopoulou, A.P. Sagare, Y. Wang, W. Gilliam, M.T. Huuskonen, S.-T. Hung, J.K. Ichida, F. Gao, M.P. Coba and B.V. Zlokovic, *A "multi-omics" analysis of blood–brain barrier and synaptic dysfunction in APOE4 mice.* Journal of Experimental Medicine, 2022. **219**(11).

86. Li, B., X. He, W. Jia and H. Li, *Novel Applications of Metabolomics in Personalized Medicine: A Mini-Review.* Molecules, 2017. **22**(7): p. 1173.

87. German, J.B., B.D. Hammock and S.M. Watkins, *Metabolomics: building on a century of biochemistry to guide human health.* Metabolomics : Official journal of the Metabolomic Society, 2005. **1**(1): p. 3-9.

88. Rattray, N.J.W., N.C. Deziel, J.D. Wallach, S.A. Khan, V. Vasiliou, J.P.A. Ioannidis and C.H. Johnson, *Beyond genomics: understanding exposotypes through metabolomics.* Human Genomics, 2018. **12**(1): p. 4.

89. Wishart, D.S., A. Guo, E. Oler, F. Wang, A. Anjum, H. Peters, R. Dizon, Z. Sayeeda, S. Tian, Brian L. Lee, M. Berjanskii, R. Mah, M. Yamamoto, J. Jovel, C. Torres-Calzada, M. Hiebert-Giesbrecht, Vicki W. Lui, D. Varshavi, D. Varshavi, D. Allen, D. Arndt, N. Khetarpal, A. Sivakumaran, K. Harford, S. Sanford, K. Yee, X. Cao, Z. Budinski, J. Liigand, L. Zhang, J. Zheng, R. Mandal, N. Karu, M. Dambrova, Helgi B. Schiöth, R. Greiner and V. Gautam, *HMDB 5.0: the Human Metabolome Database for 2022.* Nucleic Acids Research, 2021. **50**(D1): p. D622-D631.

90. Gu, H., J. Du, F. Carnevale Neto, P.A. Carroll, S.J. Turner, E.G. Chiorean, R.N. Eisenman and D. Raftery, *Metabolomics method to comprehensively analyze amino acids in different domains.* Analyst, 2015. **140**(8): p. 2726-34.

91. Rivas-Ubach, A., Y. Liu, T.S. Bianchi, N. Tolić, C. Jansson and L. Paša-Tolić, *Moving beyond the van Krevelen Diagram: A New Stoichiometric Approach for Compound Classification in Organisms.* Analytical Chemistry, 2018. **90**(10): p. 6152-6160.

92. Johnson, C.H., J. Ivanisevic and G. Siuzdak, *Metabolomics: beyond biomarkers and towards mechanisms.* Nature Reviews Molecular Cell Biology, 2016. **17**(7): p. 451-459.

93. Fan, J., K.A. Krautkramer, J.L. Feldman and J.M. Denu, *Metabolic regulation of histone post-translational modifications.* ACS Chem Biol, 2015. **10**(1): p. 95-108.

94. Diskin, C., T.A.J. Ryan and L.A.J. O'Neill, *Modification of Proteins by Metabolites in Immunity.* Immunity, 2021. **54**(1): p. 19-31.

95. Chen, B., Y. Sun, J. Niu, G.K. Jarugumilli and X. Wu, *Protein Lipidation in Cell Signaling and Diseases: Function, Regulation, and Therapeutic Opportunities.* Cell Chem Biol, 2018. **25**(7): p. 817-831.

96. Jiang, H., X. Zhang, X. Chen, P. Aramsangtienchai, Z. Tong and H. Lin, *Protein Lipidation: Occurrence, Mechanisms, Biological Functions, and Enabling Technologies.* Chemical Reviews, 2018. **118**(3): p. 919-988.

97. Di Paolo, G. and T.-W. Kim, *Linking lipids to Alzheimer's disease: cholesterol and beyond.* Nature Reviews Neuroscience, 2011. **12**(5): p. 284-296.

98. Fahy, E., S. Subramaniam, H.A. Brown, C.K. Glass, A.H. Merrill, Jr., R.C. Murphy, C.R. Raetz, D.W. Russell, Y. Seyama, W. Shaw, T. Shimizu, F. Spener, G. van Meer, M.S. VanNieuwenhze, S.H. White, J.L. Witztum and E.A. Dennis, *A comprehensive classification system for lipids.* J Lipid Res, 2005. **46**(5): p. 839-61.

99. Fahy, E., S. Subramaniam, R.C. Murphy, M. Nishijima, C.R. Raetz, T. Shimizu, F. Spener, G. van Meer, M.J. Wakelam and E.A. Dennis, *Update of the LIPID MAPS comprehensive classification system for lipids.* J Lipid Res, 2009. **50 Suppl**(Suppl): p. S9-14.

100. Foley, P., *Lipids in Alzheimer's disease: A century-old story.* Biochimica et Biophysica Acta (BBA) - Molecular and Cell Biology of Lipids, 2010. **1801**(8): p. 750-753.

101. Hartmann, T., J. Kuchenbecker and M.O.W. Grimm, *Alzheimer's disease: the lipid connection.* Journal of Neurochemistry, 2007. **103**(s1): p. 159-170.

102. Dietschy, J.M. and S.D. Turley, *Cholesterol metabolism in the brain.* Current Opinion in Lipidology, 2001. **12**(2).

103. Schrimpe-Rutledge, A.C., S.G. Codreanu, S.D. Sherrod and J.A. McLean, *Untargeted Metabolomics Strategies—Challenges and Emerging Directions.* Journal of the American Society for Mass Spectrometry, 2016. **27**(12): p. 1897-1905.

104. Roberts, L.D., A.L. Souza, R.E. Gerszten and C.B. Clish, *Targeted metabolomics.* Curr Protoc Mol Biol, 2012. **Chapter 30**: p. Unit 30.2.1-24.

105. Dubois, B., H. Hampel, H.H. Feldman, P. Scheltens, P. Aisen, S. Andrieu, H. Bakardjian, H. Benali, L. Bertram, K. Blennow, K. Broich, E. Cavedo, S. Crutch, J.-F. Dartigues, C. Duyckaerts, S. Epelbaum, G.B. Frisoni, S. Gauthier, R. Genthon, A.A. Gouw, M.-O. Habert, D.M. Holtzman, M. Kivipelto, S. Lista, J.-L. Molinuevo, S.E. O'Bryant, G.D. Rabinovici, C. Rowe, S. Salloway, L.S. Schneider, R. Sperling, M. Teichmann, M.C. Carrillo, J. Cummings, C.R. Jack, Jr., G. Proceedings of the Meeting of the International Working, A. the American

Alzheimer's Association on “The Preclinical State of, July and U.S.A. Washington Dc, *Preclinical Alzheimer's disease: Definition, natural history, and diagnostic criteria.* Alzheimer's & dementia : the journal of the Alzheimer's Association, 2016. **12**(3): p. 292-323.

106. Trushina, E. and M.M. Mielke, *Recent advances in the application of metabolomics to Alzheimer's Disease.* Biochimica et Biophysica Acta (BBA) - Molecular Basis of Disease, 2014. **1842**(8): p. 1232-1239.

107. Cuperlovic-Culf, M. and A. Badhwar, *Recent advances from metabolomics and lipidomics application in alzheimer's disease inspiring drug discovery.* Expert Opin Drug Discov, 2020. **15**(3): p. 319-331.

108. Jagust, W.J., S.M. Landau and I. Alzheimer's Disease Neuroimaging, *Apolipoprotein E, not fibrillar beta-amyloid, reduces cerebral glucose metabolism in normal aging.* J Neurosci, 2012. **32**(50): p. 18227-33.

109. Reiman, E.M., K. Chen, G.E. Alexander, R.J. Caselli, D. Bandy, D. Osborne, A.M. Saunders and J. Hardy, *Functional brain abnormalities in young adults at genetic risk for late-onset Alzheimer's dementia.* Proc Natl Acad Sci U S A, 2004. **101**(1): p. 284-9.

110. Purandare, N., M. Zubair, Y. Xu, D. Broadhurst, W.B. Dunn, P. Begley, S. Francis-McIntyre, S. Chew-Graham, A. Halsall, H. Consortium, A. Burns, D.B. Kell and R. Goodacre, *P4-310: Serum Metabolite Biomarkers In Alzheimer's Disease.* Alzheimer's & Dementia, 2009. **5**(4S_Part_17): p. e21-e21.

111. An, Y., V.R. Varma, S. Varma, R. Casanova, E. Dammer, O. Pletnikova, C.W. Chia, J.M. Egan, L. Ferrucci, J. Troncoso, A.I. Levey, J. Lah, N.T. Seyfried, C. Legido-Quigley, R. O'Brien and M. Thambisetty, *Evidence for brain glucose dysregulation in Alzheimer's disease.* Alzheimers Dement, 2018. **14**(3): p. 318-329.

112. Liu, Y., A. Thalamuthu, K.A. Mather, J. Crawford, M. Ulanova, M.W.K. Wong, R. Pickford, P.S. Sachdev and N. Braidy, *Plasma lipidome is dysregulated in Alzheimer’s disease and is associated with disease risk genes.* Translational Psychiatry, 2021. **11**(1): p. 344.

113. Yin, F., *Lipid metabolism and Alzheimer's disease: clinical evidence, mechanistic link and therapeutic promise.* Febs j, 2022.

114. Wu, L., X. Zhang and L. Zhao, *Human ApoE Isoforms Differentially Modulate Brain Glucose and Ketone Body Metabolism: Implications for Alzheimer's Disease Risk Reduction and Early Intervention.* J Neurosci, 2018. **38**(30): p. 6665-6681.

115. Lee, S., N.A. Devanney, L.R. Golden, C.T. Smith, J.L. Schwartz, A.E. Walsh, H.A.

Clarke, D.S. Goulding, E.J. Allenger, G. Morillo-Segovia, C.M. Friday, A.A. Gorman, T.R. Hawkinson, S.M. MacLean, H.C. Williams, R.C. Sun, J.M. Morganti and L.A. Johnson, *APOE modulates microglial immunometabolism in response to age, amyloid pathology, and inflammatory challenge.* Cell Rep, 2023. **42**(3): p. 112196.

116. Qi, G., Y. Mi, X. Shi, H. Gu, R.D. Brinton and F. Yin, *ApoE4 Impairs Neuron-Astrocyte Coupling of Fatty Acid Metabolism.* Cell Rep, 2021. **34**(1): p. 108572.

117. Fitz, N.F., K.N. Nam, C.M. Wolfe, F. Letronne, B.E. Playso, B.E. Iordanova, T.D.Y. Kozai, R.J. Biedrzycki, V.E. Kagan, Y.Y. Tyurina, X. Han, I. Lefterov and R. Koldamova, *Phospholipids of APOE lipoproteins activate microglia in an isoform-specific manner in preclinical models of Alzheimer's disease.* Nature Communications, 2021. **12**(1): p. 3416.

118. Blanchard, J.W., L.A. Akay, J. Davila-Velderrain, D. von Maydell, H. Mathys, S.M. Davidson, A. Effenberger, C.-Y. Chen, K. Maner-Smith, I. Hajjar, E.A. Ortlund, M. Bula, E. Agbas, A. Ng, X. Jiang, M. Kahn, C. Blanco-Duque, N. Lavoie, L. Liu, R. Reyes, Y.-T. Lin, T. Ko, L. R'Bibo, W.T. Ralvenius, D.A. Bennett, H.P. Cam, M. Kellis and L.-H. Tsai, *APOE4 impairs myelination via cholesterol dysregulation in oligodendrocytes.* Nature, 2022. **611**(7937): p. 769-779.

119. Miranda, A.M., A. Ashok, R.B. Chan, B. Zhou, Y. Xu, L.B. McIntire, E. Area-Gomez, G. Di Paolo, K.E. Duff, T.G. Oliveira and T. Nuriel, *Effects of APOE4 allelic dosage on lipidomic signatures in the entorhinal cortex of aged mice.* Translational Psychiatry, 2022. **12**(1): p. 129.

120. Balu, D., A.J. Karstens, E. Loukenas, J. Maldonado Weng, J.M. York, A.C. Valencia-Olvera and M.J. LaDu, *The role of APOE in transgenic mouse models of AD.* Neurosci Lett, 2019. **707**: p. 134285.

121. Shuken, S.R., *An Introduction to Mass Spectrometry-Based Proteomics.* J Proteome Res, 2023. **22**(7): p. 2151-2171.

122. Sung, Y.J., C. Yang, J. Norton, M. Johnson, A. Fagan, R.J. Bateman, R.J. Perrin, J.C. Morris, M.R. Farlow, J.P. Chhatwal, P.R. Schofield, H. Chui, F. Wang, B. Novotny, A. Eteleeb, C. Karch, S.E. Schindler, H. Rhinn, E.C.B. Johnson, H.S. Oh, J.E. Rutledge, E.B. Dammer, N.T. Seyfried, T. Wyss-Coray, O. Harari and C. Cruchaga, *Proteomics of brain, CSF, and plasma identifies molecular signatures for distinguishing sporadic and genetic Alzheimer's disease.* Sci Transl Med, 2023. **15**(703): p. eabq5923.

123. Johnson, E.C.B., S. Bian, R.U. Haque, E.K. Carter, C.M. Watson, B.A. Gordon, L. Ping, D.M. Duong, M.P. Epstein, E. McDade, N.R. Barthélemy, C.M. Karch, C. Xiong, C. Cruchaga, R.J. Perrin, A.P. Wingo, T.S. Wingo, J.P. Chhatwal, G.S. Day, J.M. Noble, S.B. Berman, R. Martins, N.R. Graff-Radford, P.R. Schofield, T. Ikeuchi, H. Mori, J. Levin, M. Farlow, J.J. Lah, C. Haass, M. Jucker, J.C. Morris,

T.L.S. Benzinger, B.R. Roberts, R.J. Bateman, A.M. Fagan, N.T. Seyfried, A.I. Levey, J. Vöglein, R. Allegri, P.C. Mendez, E. Surace, S.B. Berman, S. Ikonomovic, N. Nadkarni, F. Lopera, L. Ramirez, D. Aguillon, Y. Leon, C. Ramos, D. Alzate, A. Baena, N. Londono, S. Moreno, C. Laske, E. Kuder-Buletta, S. Graber-Sultan, O. Preische, A. Hofmann, K. Kasuga, Y. Niimi, K. Ishii, M. Senda, R. Sanchez-Valle, P. Rosa-Neto, N. Fox, D. Cash, J.-H. Lee, J.H. Roh, M. Riddle, W. Menard, C. Bodge, M. Surti, L.T. Takada, V.J. Sanchez-Gonzalez, M. Orozco-Barajas, A. Goate, A. Renton, B. Esposito, J. Marsh, C. Cruchaga, V. Fernandez, G. Jerome, E. Herries, J. Llibre-Guerra, W. Brooks, J. Bechara, J. Hassenstab, E. Franklin, A. Chen, C. Chen, S. Flores, N. Friedrichsen, N. Hantler, R. Hornbeck, S. Jarman, S. Keefe, D. Koudelis, P. Massoumzadeh, A. McCullough, N. McKay, J. Nicklaus, C. Pulizos, Q. Wang, S. Mishall, E. Sabaredzovic, E. Deng, M. Candela, H. Smith, D. Hobbs, J. Scott, P. Wang, X. Xu, Y. Li, E. Gremminger, Y. Ma, R. Bui, R. Lu, A.L.S. Ortiz, A. Daniels, L. Courtney, C. Supnet-Bell, J. Xu, J. Ringman and N. the Dominantly Inherited Alzheimer, *Cerebrospinal fluid proteomics define the natural history of autosomal dominant Alzheimer's disease.* Nature Medicine, 2023. **29**(8): p. 1979-1988.

124. Higginbotham, L., L. Ping, E.B. Dammer, D.M. Duong, M. Zhou, M. Gearing, C. Hurst, J.D. Glass, S.A. Factor, E.C.B. Johnson, I. Hajjar, J.J. Lah, A.I. Levey and N.T. Seyfried, *Integrated proteomics reveals brain-based cerebrospinal fluid biomarkers in asymptomatic and symptomatic Alzheimer's disease.* Science Advances, 2020. **6**(43): p. eaaz9360.

125. Gowda, G.A. and D. Djukovic, *Overview of mass spectrometry-based metabolomics: opportunities and challenges.* Methods Mol Biol, 2014. **1198**: p. 3-12.

126. Wang, J.H., J. Byun and S. Pennathur, *Analytical approaches to metabolomics and applications to systems biology.* Seminars in nephrology, 2010. **30**(5): p. 500-511.

127. Doğan, H.O., *Metabolomics: a review of liquid chromatography mass spectrometry-based methods and clinical applications.* Turkish Journal of Biochemistry, 2024. **49**(1): p. 1-14.

128. Alseekh, S., A. Aharoni, Y. Brotman, K. Contrepois, J. D'Auria, J. Ewald, J. C. Ewald, P.D. Fraser, P. Giavalisco, R.D. Hall, M. Heinemann, H. Link, J. Luo, S. Neumann, J. Nielsen, L. Perez de Souza, K. Saito, U. Sauer, F.C. Schroeder, S. Schuster, G. Siuzdak, A. Skirycz, L.W. Sumner, M.P. Snyder, H. Tang, T. Tohge, Y. Wang, W. Wen, S. Wu, G. Xu, N. Zamboni and A.R. Fernie, *Mass spectrometry-based metabolomics: a guide for annotation, quantification and best reporting practices.* Nature Methods, 2021. **18**(7): p. 747-756.

129. Zhou, B., J.F. Xiao, L. Tuli and H.W. Ressom, *LC-MS-based metabolomics.* Molecular bioSystems, 2012. **8**(2): p. 470-481.

130. Tobolkina, E., V. González-Ruiz, I. Meister, M. De Figueiredo, D. Guillarme, J. Boccard and S. Rudaz, *Challenges in ESI-MS-based Untargeted Metabolomics.* Chimia (Aarau), 2022. **76**(1-2): p. 90-100.

131. Chetwynd, A.J. and A. David, *A review of nanoscale LC-ESI for metabolomics and its potential to enhance the metabolome coverage.* Talanta, 2018. **182**: p. 380-390.

132. Lu, W., X. Su, M.S. Klein, I.A. Lewis, O. Fiehn and J.D. Rabinowitz, *Metabolite Measurement: Pitfalls to Avoid and Practices to Follow.* Annu Rev Biochem, 2017. **86**: p. 277-304.

133. Commisso, M., A. Anesi, S. Dal Santo and F. Guzzo, *Performance comparison of electrospray ionization and atmospheric pressure chemical ionization in untargeted and targeted liquid chromatography/mass spectrometry based metabolomics analysis of grapeberry metabolites.* Rapid Commun Mass Spectrom, 2017. **31**(3): p. 292-300.

134. Gika, H. and G. Theodoridis, *Sample preparation prior to the LC-MS-based metabolomics/metabonomics of blood-derived samples.* Bioanalysis, 2011. **3**(14): p. 1647-61.

135. Sitnikov, D.G., C.S. Monnin and D. Vuckovic, *Systematic Assessment of Seven Solvent and Solid-Phase Extraction Methods for Metabolomics Analysis of Human Plasma by LC-MS.* Scientific Reports, 2016. **6**(1): p. 38885.

136. Jia, F., X. Zhao and Y. Zhao, *Advancements in ToF-SIMS imaging for life sciences.* Front Chem, 2023. **11**: p. 1237408.

137. Vickerman, J.C., *Secondary ion mass spectrometry–basic concepts, instrumental aspects, applications and trends. A. BENNINGHOVEN, F. G. RUDENAUER and H. W. WERNER, Wiley, New York, 1987, 1277 pages.* Surface and Interface Analysis, 1987. **10**(8): p. 435-435.

138. Honig, R.E., *Sputtering of Surfaces by Positive Ion Beams of Low Energy.* Journal of Applied Physics, 1958. **29**(3): p. 549-555.

139. Finšgar, M., *From surface to core: Comprehensive ToF-SIMS insights into pharmaceutical tablet analysis.* Microchemical Journal, 2024. **202**: p. 110835.

140. Muramoto, S. and D. Graham, *Deep depth profiling using gas cluster secondary ion mass spectrometry: Micrometer topography development and effects on depth resolution.* Surf Interface Anal, 2021. **53**(9): p. 814-823.

141. Dimovska Nilsson, K., A. Karagianni, I. Kaya, M. Henricsson and J.S. Fletcher, *(CO2)n+, (H2O)n+, and (H2O)n+ (CO2) gas cluster ion beam secondary ion mass spectrometry: analysis of lipid extracts, cells, and Alzheimer's model mouse brain tissue.* Analytical and Bioanalytical Chemistry, 2021. **413**(16): p.

4181-4194.

142. Ho, C.S., C.W. Lam, M.H. Chan, R.C. Cheung, L.K. Law, L.C. Lit, K.F. Ng, M.W. Suen and H.L. Tai, *Electrospray ionisation mass spectrometry: principles and clinical applications.* Clin Biochem Rev, 2003. **24**(1): p. 3-12.

143. Luxembourg, S.L. and R.M.A. Heeren, *Fragmentation at and above surfaces in SIMS: Effects of biomolecular yield enhancing surface modifications.* International Journal of Mass Spectrometry, 2006. **253**(3): p. 181-192.

144. Shard, A.G., S.J. Spencer, S.A. Smith, R. Havelund and I.S. Gilmore, *The matrix effect in organic secondary ion mass spectrometry.* International Journal of Mass Spectrometry, 2015. **377**: p. 599-609.

145. Youn, S.C., L.Y. Chen, R.J. Chiou, T.J. Lai, W.C. Liao, F.D. Mai and H.M. Chang, *Comprehensive Application of Time-of-flight Secondary Ion Mass Spectrometry (TOF-SIMS) for Ionic Imaging and Bio-energetic Analysis of Club Drug-induced Cognitive Deficiency.* Sci Rep, 2015. **5**: p. 18420.

146. Passarelli, M.K., A. Pirkl, R. Moellers, D. Grinfeld, F. Kollmer, R. Havelund, C.F. Newman, P.S. Marshall, H. Arlinghaus, M.R. Alexander, A. West, S. Horning, E. Niehuis, A. Makarov, C.T. Dollery and I.S. Gilmore, *The 3D OrbiSIMS-label-free metabolic imaging with subcellular lateral resolution and high mass-resolving power.* Nat Methods, 2017. **14**(12): p. 1175-1183.

147. Zubarev, R.A. and A. Makarov, *Orbitrap Mass Spectrometry.* Analytical Chemistry, 2013. **85**(11): p. 5288-5296.

148. Matjacic, L., M.P. Seah, G.F. Trindade, A. Pirkl, R. Havelund, J.-L. Vorng, E. Niehuis and I.S. Gilmore, *OrbiSIMS metrology Part I: Optimisation of the target potential and collision cell pressure.* Surface and Interface Analysis, 2022. **54**(4): p. 331-340.

149. Suvannapruk, W., M.K. Edney, D.H. Kim, D.J. Scurr, A.M. Ghaemmaghami and M.R. Alexander, *Single-Cell Metabolic Profiling of Macrophages Using 3D OrbiSIMS: Correlations with Phenotype.* Anal Chem, 2022. **94**(26): p. 9389-9398.

150. Linke, F., J.E.C. Johnson, S. Kern, C.D. Bennett, A. Lourdusamy, D. Lea, S.C. Clifford, C.L.R. Merry, S. Stolnik, M.R. Alexander, A.C. Peet, D.J. Scurr, R.L. Griffiths, A.M. Grabowska, I.D. Kerr and B. Coyle, *Identifying new biomarkers of aggressive Group 3 and SHH medulloblastoma using 3D hydrogel models, single cell RNA sequencing and 3D OrbiSIMS imaging.* Acta Neuropathol Commun, 2023. **11**(1): p. 6.

151. Graham, D.J. and L.J. Gamble, *Back to the basics of time-of-flight secondary ion mass spectrometry of bio-related samples. I. Instrumentation and data*

collection. Biointerphases, 2023. **18**(2): p. 021201.

152. Malm, J., D. Giannaras, M.O. Riehle, N. Gadegaard and P. Sjövall, *Fixation and Drying Protocols for the Preparation of Cell Samples for Time-of-Flight Secondary Ion Mass Spectrometry Analysis.* Analytical Chemistry, 2009. **81**(17): p. 7197-7205.

153. Zhang, J., J. Brown, D.J. Scurr, A. Bullen, K. MacLellan-Gibson, P. Williams, M.R. Alexander, K.R. Hardie, I.S. Gilmore and P.D. Rakowska, *Cryo-OrbiSIMS for 3D Molecular Imaging of a Bacterial Biofilm in Its Native State.* Anal Chem, 2020. **92**(13): p. 9008-9015.

154. Starr, N.J., M.H. Khan, M.K. Edney, G.F. Trindade, S. Kern, A. Pirkl, M. Kleine-Boymann, C. Elms, M.M. O'Mahony, M. Bell, M.R. Alexander and D.J. Scurr, *Elucidating the molecular landscape of the stratum corneum.* Proc Natl Acad Sci U S A, 2022. **119**(12): p. e2114380119.

155. Vorng, J.L., A.M. Kotowska, M.K. Passarelli, A. West, P.S. Marshall, R. Havelund, M.P. Seah, C.T. Dollery, P.D. Rakowska and I.S. Gilmore, *Semiempirical Rules To Determine Drug Sensitivity and Ionization Efficiency in Secondary Ion Mass Spectrometry Using a Model Tissue Sample.* Anal Chem, 2016. **88**(22): p. 11028-11036.

156. Edney, M.K., A.M. Kotowska, M. Spanu, G.F. Trindade, E. Wilmot, J. Reid, J. Barker, J.W. Aylott, A.G. Shard, M.R. Alexander, C.E. Snape and D.J. Scurr, *Molecular Formula Prediction for Chemical Filtering of 3D OrbiSIMS Datasets.* Analytical Chemistry, 2022. **94**(11): p. 4703-4711.

157. Kind, T. and O. Fiehn, *Seven Golden Rules for heuristic filtering of molecular formulas obtained by accurate mass spectrometry.* BMC Bioinformatics, 2007. **8**(1): p. 105.

158. Passarelli, M.K., A. Pirkl, R. Moellers, D. Grinfeld, F. Kollmer, R. Havelund, C.F. Newman, P.S. Marshall, H. Arlinghaus, M.R. Alexander, A. West, S. Horning, E. Niehuis, A. Makarov, C.T. Dollery and I.S. Gilmore, *The 3D OrbiSIMS—label-free metabolic imaging with subcellular lateral resolution and high mass-resolving power.* Nature Methods, 2017. **14**(12): p. 1175-1183.

159. Meurs, J., D.J. Scurr, A. Lourdusamy, L.C.D. Storer, R.G. Grundy, M.R. Alexander, R. Rahman and D.-H. Kim, *Sequential Orbitrap Secondary Ion Mass Spectrometry and Liquid Extraction Surface Analysis-Tandem Mass Spectrometry-Based Metabolomics for Prediction of Brain Tumor Relapse from Sample-Limited Primary Tissue Archives.* Analytical Chemistry, 2021. **93**(18): p. 6947-6954.

160. Suvannapruk, W., M.K. Edney, D.-H. Kim, D.J. Scurr, A.M. Ghaemmaghami and M.R. Alexander, *Single-Cell Metabolic Profiling of Macrophages Using 3D*

OrbiSIMS: Correlations with Phenotype. Analytical Chemistry, 2022.

161. Linke, F., J.E.C. Johnson, S. Kern, C.D. Bennett, A. Lourdusamy, D. Lea, S.C. Clifford, C.L.R. Merry, S. Stolnik, M.R. Alexander, A.C. Peet, D.J. Scurr, R.L. Griffiths, A.M. Grabowska, I.D. Kerr and B. Coyle, *Identifying new biomarkers of aggressive Group 3 and SHH medulloblastoma using 3D hydrogel models, single cell RNA sequencing and 3D OrbiSIMS imaging.* Acta Neuropathologica Communications, 2023. **11**(1): p. 6.

162. Kotowska, A.M., G.F. Trindade, P.M. Mendes, P.M. Williams, J.W. Aylott, A.G. Shard, M.R. Alexander and D.J. Scurr, *Protein identification by 3D OrbiSIMS to facilitate in situ imaging and depth profiling.* Nature Communications, 2020. **11**(1): p. 5832.

163. Malm, J., D. Giannaras, M.O. Riehle, N. Gadegaard and P. Sjovall, *Fixation and drying protocols for the preparation of cell samples for time-of-flight secondary ion mass spectrometry analysis.* Anal Chem, 2009. **81**(17): p. 7197-205.

164. Piwowar, A.M., J.S. Fletcher, J. Kordys, N.P. Lockyer, N. Winograd and J.C. Vickerman, *Effects of cryogenic sample analysis on molecular depth profiles with TOF-secondary ion mass spectrometry.* Anal Chem, 2010. **82**(19): p. 8291-9.

165. Newell, C.L., J.L. Vorng, J.I. MacRae, I.S. Gilmore and A.P. Gould, *Cryogenic OrbiSIMS Localizes Semi-Volatile Molecules in Biological Tissues.* Angew Chem Int Ed Engl, 2020. **59**(41): p. 18194-18200.

166. Vance, J.E., *Phospholipid Synthesis and Transport in Mammalian Cells.* Traffic, 2015. **16**(1): p. 1-18.

167. Bhattacharya, A., R.J. Brea, H. Niederholtmeyer and N.K. Devaraj, *A minimal biochemical route towards de novo formation of synthetic phospholipid membranes.* Nature Communications, 2019. **10**(1): p. 300.

168. Mukherjee, P.K., S. Biswas, A. Kar, N. Sharma and P.K. Haldar, *Chapter 4 - Phospholipid complexation: A versatile technique for delivery of phytomedicine*, in *Evidence-Based Validation of Herbal Medicine (Second Edition)*, P.K. Mukherjee, Editor. 2022, Elsevier. p. 65-108.

169. Xia, J., N. Psychogios, N. Young and D.S. Wishart, *MetaboAnalyst: a web server for metabolomic data analysis and interpretation.* Nucleic Acids Research, 2009. **37**(suppl_2): p. W652-W660.

170. Kawecki, M. and L. Bernard, *Database of proteinogenic amino acid reference spectra for Bismuth-cluster ToF-SIMS. I. Negative polarity.* Surface Science Spectra, 2018. **25**(1).

171. Liang, Y., P. Neta, X. Yang and S.E. Stein, *Collision-Induced Dissociation of Deprotonated Peptides. Relative Abundance of Side-Chain Neutral Losses, Residue-Specific Product Ions, and Comparison with Protonated Peptides.* Journal of The American Society for Mass Spectrometry, 2018. **29**(3): p. 463-469.

172. Okamoto, S., Y. Amaishi, I. Maki, T. Enoki and J. Mineno, *Highly efficient genome editing for single-base substitutions using optimized ssODNs with Cas9-RNPs.* Scientific Reports, 2019. **9**(1): p. 4811.

173. Leal, A.F., A.M. Herreno-Pachón, E. Benincore-Flórez, A. Karunathilaka and S. Tomatsu, *Current Strategies for Increasing Knock-In Efficiency in CRISPR/Cas9-Based Approaches.* Int J Mol Sci, 2024. **25**(5).

174. Ghetti, S., M. Burigotto, A. Mattivi, G. Magnani, A. Casini, A. Bianchi, A. Cereseto and L.L. Fava, *CRISPR/Cas9 ribonucleoprotein-mediated knockin generation in hTERT-RPE1 cells.* STAR Protoc, 2021. **2**(2): p. 100407.

175. Verghese, P.B., J.M. Castellano, K. Garai, Y. Wang, H. Jiang, A. Shah, G. Bu, C. Frieden and D.M. Holtzman, *ApoE influences amyloid-β (Aβ) clearance despite minimal apoE/Aβ association in physiological conditions.* Proceedings of the National Academy of Sciences, 2013. **110**(19): p. E1807-E1816.

176. DeTure, M., L.-W. Ko, C. Easson, M. Hutton and S.-H. Yen, *Inducible Transgenic Expression of Wild-Type tau in H4 Neuroglioma Cells*, in *Alzheimer's Disease*. 2001. p. 651-660.

177. Mondragón-Rodríguez, S., G. Perry, J. Luna-Muñoz, M.C. Acevedo-Aquino and S. Williams, *Phosphorylation of tau protein at sites Ser396–404 is one of the earliest events in Alzheimer's disease and Down syndrome.* Neuropathology and Applied Neurobiology, 2014. **40**(2): p. 121-135.

178. Fayed, N., P.J. Modrego, G. Rojas-Salinas and K. Aguilar, *Brain glutamate levels are decreased in Alzheimer's disease: a magnetic resonance spectroscopy study.* Am J Alzheimers Dis Other Demen, 2011. **26**(6): p. 450-6.

179. Schousboe, A., S. Scafidi, L.K. Bak, H.S. Waagepetersen and M.C. McKenna, *Glutamate metabolism in the brain focusing on astrocytes.* Adv Neurobiol, 2014. **11**: p. 13-30.

180. Xu, J., P. Begley, S.J. Church, S. Patassini, K.A. Hollywood, M. Jüllig, M.A. Curtis, H.J. Waldvogel, R.L.M. Faull, R.D. Unwin and G.J.S. Cooper, *Graded perturbations of metabolism in multiple regions of human brain in Alzheimer's disease: Snapshot of a pervasive metabolic disorder.* Biochimica et Biophysica Acta (BBA) - Molecular Basis of Disease, 2016. **1862**(6): p. 1084-1092.

181. Lau, C.G. and R.S. Zukin, *NMDA receptor trafficking in synaptic plasticity and*

neuropsychiatric disorders. Nature Reviews Neuroscience, 2007. **8**(6): p. 413-426.

182. D'Aniello, A., A. Vetere, G.H. Fisher, G. Cusano, M. Chavez and L. Petrucelli, *Presence of d-alanine in proteins of normal and Alzheimer human brain.* Brain Research, 1992. **592**(1): p. 44-48.

183. Lin, C.-H., H.-T. Yang and H.-Y. Lane, *D-glutamate, D-serine, and D-alanine differ in their roles in cognitive decline in patients with Alzheimer's disease or mild cognitive impairment.* Pharmacology Biochemistry and Behavior, 2019. **185**: p. 172760.

184. Bröer, S., A. Bröer, J.T. Hansen, W.A. Bubb, V.J. Balcar, F.A. Nasrallah, B. Garner and C. Rae, *Alanine metabolism, transport, and cycling in the brain.* J Neurochem, 2007. **102**(6): p. 1758-1770.

185. Pereira, A.C. and S. Saroja, *Apolipoprotein E4 drives tau propagation through astrocyte-secreted glypican-4.* Alzheimer's & Dementia, 2021. **17**(S3): p. e054243.

186. Chiang, G.C., P.S. Insel, D. Tosun, N. Schuff, D. Truran-Sacrey, S.T. Raptentsetsang, P.M. Thompson, E.M. Reiman, C.R. Jack Jr., N.C. Fox, W.J. Jagust, D.J. Harvey, L.A. Beckett, A. Gamst, P.S. Aisen, R.C. Petersen and M.W. Weiner, *Impact of apolipoprotein ε4–cerebrospinal fluid beta-amyloid interaction on hippocampal volume loss over 1 year in mild cognitive impairment.* Alzheimer's & Dementia, 2011. **7**(5): p. 514-520.

187. Deane, R., A. Sagare, K. Hamm, M. Parisi, S. Lane, M.B. Finn, D.M. Holtzman and B.V. Zlokovic, *apoE isoform-specific disruption of amyloid beta peptide clearance from mouse brain.* J Clin Invest, 2008. **118**(12): p. 4002-13.

188. Dunn, W.B., D. Broadhurst, P. Begley, E. Zelena, S. Francis-McIntyre, N. Anderson, M. Brown, J.D. Knowles, A. Halsall, J.N. Haselden, A.W. Nicholls, I.D. Wilson, D.B. Kell, R. Goodacre and C. The Human Serum Metabolome, *Procedures for large-scale metabolic profiling of serum and plasma using gas chromatography and liquid chromatography coupled to mass spectrometry.* Nature Protocols, 2011. **6**(7): p. 1060-1083.

189. Broadhurst, D., R. Goodacre, S.N. Reinke, J. Kuligowski, I.D. Wilson, M.R. Lewis and W.B. Dunn, *Guidelines and considerations for the use of system suitability and quality control samples in mass spectrometry assays applied in untargeted clinical metabolomic studies.* Metabolomics, 2018. **14**(6): p. 72.

190. Sumner, L.W., A. Amberg, D. Barrett, M.H. Beale, R. Beger, C.A. Daykin, T.W. Fan, O. Fiehn, R. Goodacre, J.L. Griffin, T. Hankemeier, N. Hardy, J. Harnly, R. Higashi, J. Kopka, A.N. Lane, J.C. Lindon, P. Marriott, A.W. Nicholls, M.D. Reily, J.J. Thaden and M.R. Viant, *Proposed minimum reporting standards for*

chemical analysis Chemical Analysis Working Group (CAWG) Metabolomics Standards Initiative (MSI). Metabolomics, 2007. **3**(3): p. 211-221.

191. Huxtable, R.J., *Taurine in the central nervous system and the mammalian actions of taurine.* Progress in Neurobiology, 1989. **32**(6): p. 471-533.

192. Muthuraman, A., M. Ramesh, S.A. Shaikh, S. Aswinprakash and D. Jagadeesh, *Physiological and Pathophysiological Role of Cysteine Metabolism in Human Metabolic Syndrome.* Drug Metab Lett, 2021. **14**(3): p. 177-192.

193. Doncheva, N.T., J.H. Morris, J. Gorodkin and L.J. Jensen, *Cytoscape StringApp: Network Analysis and Visualization of Proteomics Data.* Journal of Proteome Research, 2019. **18**(2): p. 623-632.

194. Ramakrishna, S., V. Jhaveri, S.C. Konings, B. Nawalpuri, S. Chakraborty, B. Holst, B. Schmid, G.K. Gouras, K.K. Freude and R.S. Muddashetty, *APOE4 Affects Basal and NMDAR-Mediated Protein Synthesis in Neurons by Perturbing Calcium Homeostasis.* The Journal of Neuroscience, 2021. **41**(42): p. 8686-8709.

195. Raj, T., Y.I. Li, G. Wong, J. Humphrey, M. Wang, S. Ramdhani, Y.-C. Wang, B. Ng, I. Gupta, V. Haroutunian, E.E. Schadt, T. Young-Pearse, S. Mostafavi, B. Zhang, P. Sklar, D.A. Bennett and P.L. De Jager, *Integrative transcriptome analyses of the aging brain implicate altered splicing in Alzheimer's disease susceptibility.* Nature Genetics, 2018. **50**(11): p. 1584-1592.

196. Chen, P.-C., X. Han, T.I. Shaw, Y. Fu, H. Sun, M. Niu, Z. Wang, Y. Jiao, B.J.W. Teubner, D. Eddins, L.N. Beloate, B. Bai, J. Mertz, Y. Li, J.-H. Cho, X. Wang, Z. Wu, D. Liu, S. Poudel, Z.-F. Yuan, A. Mancieri, J. Low, H.-M. Lee, M.H. Patton, L.R. Earls, E. Stewart, P. Vogel, Y. Hui, S. Wan, D.A. Bennett, G.E. Serrano, T.G. Beach, M.A. Dyer, R.J. Smeyne, T. Moldoveanu, T. Chen, G. Wu, S.S. Zakharenko, G. Yu and J. Peng, *Alzheimer's disease-associated U1 snRNP splicing dysfunction causes neuronal hyperexcitability and cognitive impairment.* Nature Aging, 2022. **2**(10): p. 923-940.

197. Mahajan, P., O. Fiehn and D. Barupal, *IDSL.GOA: Gene Ontology Analysis for Metabolomics.* bioRxiv, 2023.

198. Zhang, H., D.G. Delafield and L. Li, *Mass spectrometry imaging: the rise of spatially resolved single-cell omics.* Nature Methods, 2023. **20**(3): p. 327-330.

199. Zhang, H., K.H. Lu, M. Ebbini, P. Huang, H. Lu and L. Li, *Mass spectrometry imaging for spatially resolved multi-omics molecular mapping.* npj Imaging, 2024. **2**(1): p. 20.

200. Chu, H.-W., B. Unnikrishnan, A. Anand, J.-Y. Mao and C.-C. Huang, *Nanoparticle-based laser desorption/ionization mass spectrometric analysis*

of drugs and metabolites. Journal of Food and Drug Analysis, 2018. **26**(4): p. 1215-1228.

201. Etalo, D.W., C. Díez-Simón, R.C.H. de Vos and R.D. Hall, *Laser Ablation Electrospray Ionization-Mass Spectrometry Imaging (LAESI-MS) for Spatially Resolved Plant Metabolomics*, in *Plant Metabolomics: Methods and Protocols*, C. António, Editor. 2018, Springer New York: New York, NY. p. 253-267.

202. Brunet, M.A. and M.L. Kraft, *Toward Understanding the Subcellular Distributions of Cholesterol and Sphingolipids Using High-Resolution NanoSIMS Imaging.* Acc Chem Res, 2023. **56**(7): p. 752-762.

203. Kompauer, M., S. Heiles and B. Spengler, *Atmospheric pressure MALDI mass spectrometry imaging of tissues and cells at 1.4-μm lateral resolution.* Nature Methods, 2017. **14**(1): p. 90-96.

204. Niehaus, M., J. Soltwisch, M.E. Belov and K. Dreisewerd, *Transmission-mode MALDI-2 mass spectrometry imaging of cells and tissues at subcellular resolution.* Nat Methods, 2019. **16**(9): p. 925-931.

205. Kuznetsov, I., J. Filevich, F. Dong, M. Woolston, W. Chao, E.H. Anderson, E.R. Bernstein, D.C. Crick, J.J. Rocca and C.S. Menoni, *Three-dimensional nanoscale molecular imaging by extreme ultraviolet laser ablation mass spectrometry.* Nature Communications, 2015. **6**(1): p. 6944.

206. Li, X., L. Hang, T. Wang, Y. Leng, H. Zhang, Y. Meng, Z. Yin and W. Hang, *Nanoscale Three-Dimensional Imaging of Drug Distributions in Single Cells via Laser Desorption Post-Ionization Mass Spectrometry.* J Am Chem Soc, 2021. **143**(51): p. 21648-21656.

207. Kulkarni, P., R.A. Wilschut, K.J.F. Verhoeven, W.H. van der Putten and P. Garbeva, *LAESI mass spectrometry imaging as a tool to differentiate the root metabolome of native and range-expanding plant species.* Planta, 2018. **248**(6): p. 1515-1523.

208. Taylor, M.J., A. Liyu, A. Vertes and C.R. Anderton, *Ambient Single-Cell Analysis and Native Tissue Imaging Using Laser-Ablation Electrospray Ionization Mass Spectrometry with Increased Spatial Resolution.* Journal of the American Society for Mass Spectrometry, 2021. **32**(9): p. 2490-2494.

209. Campbell, D.I., C.R. Ferreira, L.S. Eberlin and R.G. Cooks, *Improved spatial resolution in the imaging of biological tissue using desorption electrospray ionization.* Anal Bioanal Chem, 2012. **404**(2): p. 389-98.

210. Yin, R., K.E. Burnum-Johnson, X. Sun, S.K. Dey and J. Laskin, *High spatial resolution imaging of biological tissues using nanospray desorption electrospray ionization mass spectrometry.* Nat Protoc, 2019. **14**(12): p. 3445-

3470.

211. Swales, J.G., N. Strittmatter, J.W. Tucker, M.R. Clench, P.J.H. Webborn and R.J.A. Goodwin, *Spatial Quantitation of Drugs in tissues using Liquid Extraction Surface Analysis Mass Spectrometry Imaging.* Scientific Reports, 2016. **6**(1): p. 37648.

212. Blainey, P., M. Krzywinski and N. Altman, *Replication.* Nature Methods, 2014. **11**(9): p. 879-880.

213. Ghosh, T., D. Philtron, W. Zhang, K. Kechris and D. Ghosh, *Reproducibility of mass spectrometry based metabolomics data.* BMC Bioinformatics, 2021. **22**(1): p. 423.

214. Scheubert, K., F. Hufsky, D. Petras, M. Wang, L.-F. Nothias, K. Dührkop, N. Bandeira, P.C. Dorrestein and S. Böcker, *Significance estimation for large scale metabolomics annotations by spectral matching.* Nature Communications, 2017. **8**(1): p. 1494.

215. Sheraz, S., H. Tian, J.C. Vickerman, P. Blenkinsopp, N. Winograd and P. Cumpson, *Enhanced Ion Yields Using High Energy Water Cluster Beams for Secondary Ion Mass Spectrometry Analysis and Imaging.* Analytical Chemistry, 2019. **91**(14): p. 9058-9068.

216. Sheraz née Rabbani, S., I. Berrueta Razo, T. Kohn, N.P. Lockyer and J.C. Vickerman, *Enhancing Ion Yields in Time-of-Flight-Secondary Ion Mass Spectrometry: A Comparative Study of Argon and Water Cluster Primary Beams.* Analytical Chemistry, 2015. **87**(4): p. 2367-2374.

217. Tian, H., L.J. Sparvero, P. Blenkinsopp, A.A. Amoscato, S.C. Watkins, H. Bayır, V.E. Kagan and N. Winograd, *Secondary-Ion Mass Spectrometry Images Cardiolipins and Phosphatidylethanolamines at the Subcellular Level.* Angewandte Chemie International Edition, 2019. **58**(10): p. 3156-3161.

218. Tian, H., S. Sheraz née Rabbani, J.C. Vickerman and N. Winograd, *Multiomics Imaging Using High-Energy Water Gas Cluster Ion Beam Secondary Ion Mass Spectrometry [(H2O)n-GCIB-SIMS] of Frozen-Hydrated Cells and Tissue.* Analytical Chemistry, 2021. **93**(22): p. 7808-7814.

219. Tian, H., L.J. Sparvero, T.S. Anthonymuthu, W.-Y. Sun, A.A. Amoscato, R.-R. He, H. Bayır, V.E. Kagan and N. Winograd, *Successive High-Resolution (H2O)n-GCIB and C60-SIMS Imaging Integrates Multi-Omics in Different Cell Types in Breast Cancer Tissue.* Analytical Chemistry, 2021. **93**(23): p. 8143-8151.

Chapter 9 Appendix

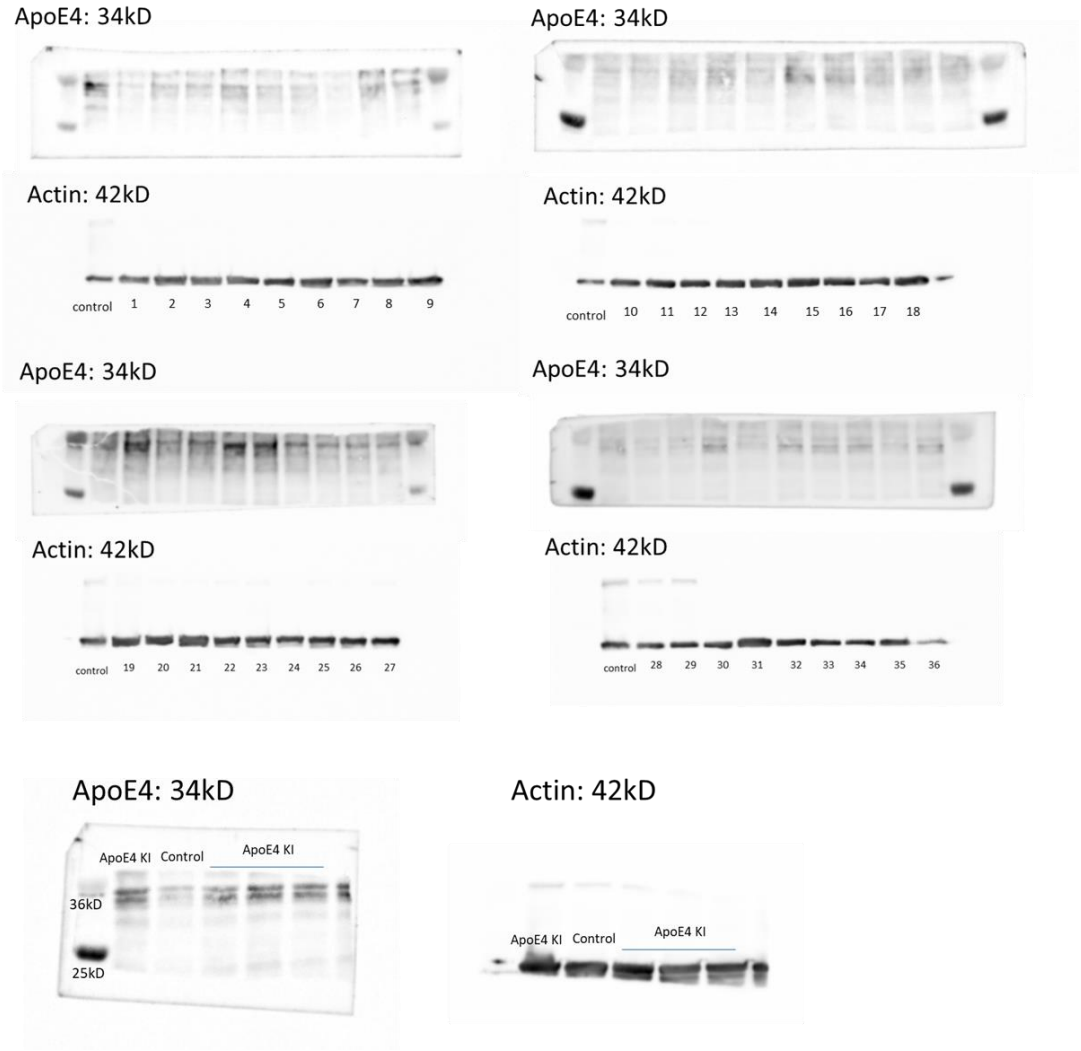

Figure S1. Original Western blot gel image used for selecting monoclonal cell lines (1–36). Two proteins were detected: actin (42 kDa) as the reference protein and ApoE4 (34 kDa) as the target protein.

Table S 1. Peptide assignments from each of Control H4 samples.

Control1			**Control2**			**Control3**		
Mass	Normalized intensity	Chemical formula	Mass	Normalized intensity	Chemical formula	Mass	Normalized intensity	Chemical formula
98.0611	0.000204	C_5H_8NO-	98.0611	0.000204	C_5H_8NO-	98.0611	0.000178	C_5H_8NO-
141.067	0.000676	$C_6H_9N_2O_2$-	141.06	0.000676	$C_6H_9N_2O_2$-	141.067	0.00051	$C_6H_9N_2O_2$-

			7					
145.0982	4.29E-06	$C_6H_{13}N_2O_2$-	145.098	4.29E-06	$C_6H_{13}N_2O_2$-	145.0982	4.43E-06	$C_6H_{13}N_2O_2$-
153.0669	0.00149	$C_7H_9N_2O_2$-	153.067	0.00149	$C_7H_9N_2O_2$-	153.0669	0.00114	$C_7H_9N_2O_2$-
155.0826	0.000683	$C_7H_{11}N_2O_2$-	155.083	0.000683	$C_7H_{11}N_2O_2$-	155.0826	0.000509	$C_7H_{11}N_2O_2$-
166.0748	8.89E-06	$C_8H_{10}N_2O_2$-	166.075	8.89E-06	$C_8H_{10}N_2O_2$-	166.0748	5.26E-06	$C_8H_{10}N_2O_2$-
167.0826	0.000592	$C_8H_{11}N_2O_2$-	167.083	0.000592	$C_8H_{11}N_2O_2$-	167.0826	0.000451	$C_8H_{11}N_2O_2$-
169.0982	0.000352	$C_8H_{13}N_2O_2$-	169.098	0.000352	$C_8H_{13}N_2O_2$-	169.0983	0.000235	$C_8H_{13}N_2O_2$-
181.0983	0.000385	$C_9H_{13}N_2O_2$-	181.098	0.000385	$C_9H_{13}N_2O_2$-	181.0983	0.000271	$C_9H_{13}N_2O_2$-
183.1139	5.84E-05	$C_9H_{15}N_2O_2$-	183.114	5.84E-05	$C_9H_{15}N_2O_2$-	183.1139	3.85E-05	$C_9H_{15}N_2O_2$-
191.0826	3.38E-05	$C_{10}H_{11}N_2O_2$-	191.083	3.38E-05	$C_{10}H_{11}N_2O_2$-	191.0827	1.79E-05	$C_{10}H_{11}N_2O_2$-
193.0982	2.25E-05	$C_{10}H_{13}N_2O_2$-	193.098	2.25E-05	$C_{10}H_{13}N_2O_2$-	193.0983	1.30E-05	$C_{10}H_{13}N_2O_2$-
194.0935	9.98E-05	$C_9H_{12}N_3O_2$-	194.094	9.98E-05	$C_9H_{12}N_3O_2$-	194.0935	5.39E-05	$C_9H_{12}N_3O_2$-
195.0775	3.00E-05	$C_9H_{11}N_2O_3$-	195.078	3.00E-05	$C_9H_{11}N_2O_3$-	195.0775	1.81E-05	$C_9H_{11}N_2O_3$-
195.1139	0.000148	$C_{10}H_{15}N_2O_2$-	195.114	0.000148	$C_{10}H_{15}N_2O_2$-	195.1139	9.61E-05	$C_{10}H_{15}N_2O_2$-
196.1092	9.37E-05	$C_9H_{14}N_3O_2$-	196.109	9.37E-05	$C_9H_{14}N_3O_2$-	196.1092	5.95E-05	$C_9H_{14}N_3O_2$-
197.1296	8.93E-06	$C_{10}H_{17}N_2O_2$-	197.13	8.93E-06	$C_{10}H_{17}N_2O_2$-	197.1296	6.08E-06	$C_{10}H_{17}N_2O_2$-
198.1249	4.47E-05	$C_9H_{16}N_3O_2$-	198.125	4.47E-05	$C_9H_{16}N_3O_2$-	198.1249	3.26E-05	$C_9H_{16}N_3O_2$-
200.1405	9.69E-06	$C_9H_{18}N_3O_2$-	200.141	9.69E-06	$C_9H_{18}N_3O_2$-	200.1406	5.28E-06	$C_9H_{18}N_3O_2$-
207.0776	8.21E-06	$C_{10}H_{11}N_2O_3$-	207.078	8.21E-06	$C_{10}H_{11}N_2O_3$-	207.0775	4.79E-06	$C_{10}H_{11}N_2O_3$-
208.1092	9.96E-05	$C_{10}H_{14}N_3O_2$-	208.109	9.96E-05	$C_{10}H_{14}N_3O_2$-	208.1092	6.84E-05	$C_{10}H_{14}N_3O_2$-
209.0932	1.10E-05	$C_{10}H_{13}N_2O_3$-	209.093	1.10E-05	$C_{10}H_{13}N_2O_3$-	209.0932	9.45E-06	$C_{10}H_{13}N_2O_3$-
210.0885	0.000123	$C_9H_{12}N_3O_3$-	210.089	0.000123	$C_9H_{12}N_3O_3$-	210.0885	9.18E-05	$C_9H_{12}N_3O_3$-
210.1249	4.15E-05	$C_{10}H_{16}N_3O_2$-	210.125	4.15E-05	$C_{10}H_{16}N_3O_2$-	210.1249	3.12E-05	$C_{10}H_{16}N_3O_2$-
212.1041	3.63E-05	$C_9H_{14}N_3O_3$-	212.104	3.63E-05	$C_9H_{14}N_3O_3$-	212.1042	2.14E-05	$C_9H_{14}N_3O_3$-
212.1405	3.13E-05	$C_{10}H_{18}N_3O_2$-	212.141	3.13E-05	$C_{10}H_{18}N_3O_2$-	212.1406	1.89E-05	$C_{10}H_{18}N_3O_2$-
224.1042	5.48E-05	$C_{10}H_{14}N_3O_3$-	224.104	5.48E-05	$C_{10}H_{14}N_3O_3$-	224.1042	2.81E-05	$C_{10}H_{14}N_3O_3$-
226.1199	2.18E-05	$C_{10}H_{16}N_3O_3$-	226.12	2.18E-05	$C_{10}H_{16}N_3O_3$-	226.1199	1.68E-05	$C_{10}H_{16}N_3O_3$-
238.1199	2.22E-05	$C_{11}H_{16}N_3O_3$-	238.12	2.22E-05	$C_{11}H_{16}N_3O_3$-	238.1199	1.35E-05	$C_{11}H_{16}N_3O_3$-
240.1355	2.28E-05	$C_{11}H_{18}N_3O_3$-	240.136	2.28E-05	$C_{11}H_{18}N_3O_3$-	240.1356	1.58E-05	$C_{11}H_{18}N_3O_3$-

252.1356	7.35E-06	$C_{12}H_{18}N_3O_3$-	252.136	7.35E-06	$C_{12}H_{18}N_3O_3$-	252.1356	5.89E-06	$C_{12}H_{18}N_3O_3$-
266.1512	5.31E-06	$C_{13}H_{20}N_3O_3$-	266.151	5.31E-06	$C_{13}H_{20}N_3O_3$-	266.1513	3.81E-06	$C_{13}H_{20}N_3O_3$-
267.1465	3.09E-06	$C_{12}H_{19}N_4O_3$-	267.147	3.09E-06	$C_{12}H_{19}N_4O_3$-	267.1465	2.24E-06	$C_{12}H_{19}N_4O_3$-
297.1571	3.31E-06	$C_{13}H_{21}N_4O_4$-	297.157	3.31E-06	$C_{13}H_{21}N_4O_4$-	297.1569	1.98E-06	$C_{13}H_{21}N_4O_4$-
553.2786	1.69E-05	$C_{28}H_{37}N_6O_6$-	553.279	1.69E-05	$C_{28}H_{37}N_6O_6$-	553.2786	1.41E-05	$C_{28}H_{37}N_6O_6$-
562.2556	5.68E-06	$C_{29}H_{34}N_6O_6$-	562.256	5.68E-06	$C_{29}H_{34}N_6O_6$-	562.2555	5.66E-06	$C_{29}H_{34}N_6O_6$-
571.2891	5.19E-06	$C_{28}H_{39}N_6O_7$-	571.289	5.19E-06	$C_{28}H_{39}N_6O_7$-	571.2888	2.54E-06	$C_{28}H_{39}N_6O_7$-
579.2943	5.70E-05	$C_{30}H_{39}N_6O_6$-	579.294	5.70E-05	$C_{30}H_{39}N_6O_6$-	579.2942	4.58E-05	$C_{30}H_{39}N_6O_6$-
580.2976	1.13E-05	$C_{25}H_{40}N_8O_8$-	580.298	1.13E-05	$C_{25}H_{40}N_8O_8$-	580.2977	8.05E-06	$C_{25}H_{40}N_8O_8$-
581.3098	9.60E-05	$C_{30}H_{41}N_6O_6$-	581.31	9.60E-05	$C_{30}H_{41}N_6O_6$-	581.3099	8.87E-05	$C_{30}H_{41}N_6O_6$-
582.3133	2.04E-05	$C_{25}H_{42}N_8O_8$-	582.313	2.04E-05	$C_{25}H_{42}N_8O_8$-	582.3134	2.08E-05	$C_{25}H_{42}N_8O_8$-
597.3051	1.33E-05	$C_{30}H_{41}N_6O_7$-	597.305	1.33E-05	$C_{30}H_{41}N_6O_7$-	597.3048	1.16E-05	$C_{30}H_{41}N_6O_7$-
599.3205	3.20E-05	$C_{30}H_{43}N_6O_7$-	599.321	3.20E-05	$C_{30}H_{43}N_6O_7$-	599.3206	3.08E-05	$C_{30}H_{43}N_6O_7$-
834.5221	5.85E-06	$C_{39}H_{68}N_{11}O_9$-	834.522	5.85E-06	$C_{39}H_{68}N_{11}O_9$-	834.5223	2.95E-06	$C_{39}H_{68}N_{11}O_9$-
836.5379	2.85E-05	$C_{39}H_{70}N_{11}O_9$-	836.538	2.85E-05	$C_{39}H_{70}N_{11}O_9$-	836.5378	2.48E-05	$C_{39}H_{70}N_{11}O_9$-
860.5383	4.04E-06	$C_{41}H_{70}N_{11}O_9$-	860.538	4.04E-06	$C_{41}H_{70}N_{11}O_9$-	860.5378	5.70E-06	$C_{41}H_{70}N_{11}O_9$-
862.5535	6.67E-05	$C_{41}H_{72}N_{11}O_9$-	862.554	6.67E-05	$C_{41}H_{72}N_{11}O_9$-	862.5533	4.39E-05	$C_{41}H_{72}N_{11}O_9$-
864.569	5.27E-05	$C_{41}H_{74}N_{11}O_9$-	864.569	5.27E-05	$C_{41}H_{74}N_{11}O_9$-	864.569	5.02E-05	$C_{41}H_{74}N_{11}O_9$-
884.5378	1.04E-05	$C_{43}H_{70}N_{11}O_9$-	884.538	1.04E-05	$C_{43}H_{70}N_{11}O_9$-	884.538	9.11E-06	$C_{43}H_{70}N_{11}O_9$-
886.5534	5.72E-05	$C_{43}H_{72}N_{11}O_9$-	886.553	5.72E-05	$C_{43}H_{72}N_{11}O_9$-	886.5533	4.84E-05	$C_{43}H_{72}N_{11}O_9$-
1063.689	7.41E-06	$C_{51}H_{91}N_{12}O_{12}$-	1063.69	7.41E-06	$C_{51}H_{91}N_{12}O_{12}$-	1063.6891	9.49E-06	$C_{51}H_{91}N_{12}O_{12}$-
1064.693	4.45E-06	$C_{46}H_{92}N_{14}O_{14}$-	1064.69	4.45E-06	$C_{46}H_{92}N_{14}O_{14}$-	1064.6929	6.38E-06	$C_{46}H_{92}N_{14}O_{14}$-
86.0609	7.24E-06	C_4H_8NO-	86.0609	7.24E-06	C_4H_8NO-	86.0609	4.44E-06	C_4H_8NO-
100.0768	6.33E-06	$C_5H_{10}NO$-	100.077	6.33E-06	$C_5H_{10}NO$-	100.0768	5.04E-06	$C_5H_{10}NO$-
168.0905	4.80E-06	$C_8H_{12}N_2O_2$-	168.091	4.80E-06	$C_8H_{12}N_2O_2$-	168.0904	2.90E-06	$C_8H_{12}N_2O_2$-
179.0826	9.86E-05	$C_9H_{11}N_2O_2$-	179.083	9.86E-05	$C_9H_{11}N_2O_2$-	179.0826	6.70E-05	$C_9H_{11}N_2O_2$-
206.0935	2.79E-05	$C_{10}H_{12}N_3O_2$-	206.094	2.79E-05	$C_{00}H_{32}N_3O_2S$-	206.0935	1.96E-05	$C_{10}H_{12}N_3O_2$-
222.0885	3.95E-06	$C_{10}H_{12}N_3O_3$-	222.08	3.95E-06	$C_{10}H_{12}N_3O_3$-	222.0886	4.59E-06	$C_{10}H_{12}N_3O_3$-

			9					
236.1041	4.62E-06	$C_{11}H_{14}N_3O_3$-	236.104	4.62E-06	$C_{11}H_{14}N_3O_3$-	236.1042	3.05E-06	$C_{11}H_{14}N_3O_3$-
389.2099	4.38E-06	$C_{16}H_{31}N_5O_4$-	389.21	4.38E-06	$C_{16}H_{31}N_5O_4S$-	389.21	3.83E-06	$C_{16}H_{31}N_5O_4S$-
391.2257	5.78E-05	$C_{16}H_{33}N_5O_4$-	391.226	5.78E-05	$C_{16}H_{33}N_5O_4S$-	391.2257	5.62E-05	$C_{16}H_{33}N_5O_4S$-
405.2412	2.56E-06	$C_{17}H_{35}N_5O_4$-	405.241	2.56E-06	$C_{17}H_{35}N_5O_4S$-	405.2412	3.99E-06	$C_{17}H_{35}N_5O_4S$-
417.2413	0.000107	$C_{18}H_{35}N_5O_4$-	417.241	0.000107	$C_{18}H_{35}N_5O_4S$-	417.2413	8.75E-05	$C_{18}H_{35}N_5O_4S$-
575.2234	2.14E-06	$C_{27}H_{29}N_9O_6$-	575.223	2.14E-06	$C_{27}H_{29}N_9O_6$-	575.2252	2.03E-06	$C_{29}H_{31}N_6O_7$-
764.5165	9.58E-06	$C_{38}H_{68}N_8O_8$-	764.517	9.58E-06	$C_{38}H_{68}N_8O_8$-	575.2252	2.03E-06	$C_{27}H_{29}N_9O_6$-
772.53	1.10E-05	$C_{36}H_{70}N_9O_9$-	772.53	1.10E-05	$C_{36}H_{70}N_9O_9$-	764.517	2.02E-06	$C_{38}H_{68}N_8O_8$-
790.5202	2.99E-06	$C_{39}H_{68}N_9O_8$-	790.52	2.99E-06	$C_{39}H_{68}N_9O_8$-	772.5303	3.91E-06	$C_{36}H_{70}N_9O_9$-
798.5342	2.86E-06	$C_{37}H_{70}N_{10}O_9$-	798.534	2.86E-06	$C_{37}H_{70}N_{10}O_9$-	798.5343	2.70E-06	$C_{37}H_{70}N_{10}O_9$-
804.4966	1.32E-05	$C_{37}H_{64}N_{12}O_8$-	804.497	1.32E-05	$C_{37}H_{64}N_{12}O_8$-	804.4968	4.04E-06	$C_{37}H_{64}N_{12}O_8$-
804.4966	1.32E-05	$C_{36}H_{68}N_8O_{12}$-	804.497	1.32E-05	$C_{36}H_{68}N_8O_{12}$-	804.4968	4.04E-06	$C_{36}H_{68}N_8O_{12}$-
804.4966	1.32E-05	$C_{34}H_{66}N_{11}O_{11}$-	804.497	1.32E-05	$C_{34}H_{66}N_{11}O_{11}$-	804.4968	4.04E-06	$C_{34}H_{66}N_{11}O_{11}$-
806.4942	3.96E-06	$C_{34}H_{68}N_{11}O_9$-	806.494	3.96E-06	$C_{34}H_{68}N_{11}O_9S$-	810.5819	4.82E-05	$C_{40}H_{76}N_9O_8$-
810.5815	1.06E-05	$C_{40}H_{76}N_9O_8$-	810.582	1.06E-05	$C_{40}H_{76}N_9O_8$-	812.523	3.99E-06	$C_{36}H_{68}N_{12}O_9$-
812.5227	1.19E-05	$C_{36}H_{68}N_{12}O_9$-	812.523	1.19E-05	$C_{36}H_{68}N_{12}O_9$-	813.5102	2.55E-06	$C_{38}H_{69}N_8O_{11}$-
813.5111	3.09E-06	$C_{38}H_{69}N_8O_{11}$-	813.511	3.09E-06	$C_{38}H_{69}N_8O_{11}$-	814.5084	9.23E-06	$C_{40}H_{66}N_{10}O_8$-
814.508	1.56E-05	$C_{40}H_{66}N_{10}O_8$-	814.508	1.56E-05	$C_{40}H_{66}N_{10}O_8$-	814.5084	9.23E-06	$C_{37}H_{70}N_{10}O_8S$-
814.521	3.68E-06	$C_{38}H_{72}N_9O_8$-	814.521	3.68E-06	$C_{38}H_{72}N_9O_8S$-	814.5214	3.29E-06	$C_{38}H_{72}N_9O_8S$-
828.4966	2.39E-05	$C_{39}H_{64}N_{12}O_8$-	828.497	2.39E-05	$C_{39}H_{64}N_{12}O_8$-	828.4969	7.99E-06	$C_{41}H_{66}N_9O_9$-
828.4966	2.39E-05	$C_{38}H_{68}N_8O_{12}$-	828.497	2.39E-05	$C_{38}H_{68}N_8O_{12}$-	828.4969	7.99E-06	$C_{39}H_{64}N_{12}O_8$-
828.4966	2.39E-05	$C_{36}H_{66}N_{11}O_{11}$-	828.497	2.39E-05	$C_{36}H_{66}N_{11}O_{11}$-	828.4969	7.99E-06	$C_{38}H_{68}N_8O_{12}$-
830.4942	6.65E-06	$C_{38}H_{70}N_8O_{10}$-	830.494	6.65E-06	$C_{38}H_{70}N_8O_{10}S$-	828.4969	7.99E-06	$C_{36}H_{66}N_{11}O_{11}$-
830.4942	6.65E-06	$C_{36}H_{68}N_{11}O_9$-	830.494	6.65E-06	$C_{36}H_{68}N_{11}O_9S$-	830.494	3.75E-06	$C_{38}H_{70}N_8O_{10}S$-
833.5188	1.55E-05	$C_{38}H_{73}N_8O_{10}$-	833.519	1.55E-05	$C_{38}H_{73}N_8O_{10}S$-	830.494	3.75E-06	$C_{36}H_{68}N_{11}O_9S$-
834.5221	5.85E-06	$C_{36}H_{72}N_{11}O_9$-	834.522	5.85E-06	$C_{36}H_{72}N_{11}O_9S$-	830.5212	2.86E-06	$C_{37}H_{70}N_{10}O_{11}$-
850.4787	2.77E-05	$C_{40}H_{66}N_8O_{12}$-	850.479	2.77E-05	$C_{40}H_{66}N_8O_{12}$-	833.5186	7.26E-06	$C_{38}H_{73}N_8O_{10}S$-
850.4787	2.77E-05	$C_{38}H_{64}N_{11}O_{11}$-	850.479	2.77E-05	$C_{38}H_{64}N_{11}O_{11}$-	834.5223	2.95E-06	$C_{36}H_{72}N_{11}O_9S$-

852.4765	1.04E-05	$C_{40}H_{68}N_8O_{10}$-	852.477	1.04E-05	$C_{40}H_{68}N_8O_{10}S$-	850.4793	7.97E-06	$C_{40}H_{66}N_8O_{12}$-
852.4765	1.04E-05	$C_{38}H_{66}N_{11}O_9$-	852.477	1.04E-05	$C_{38}H_{66}N_{11}O_9S$-	850.4793	7.97E-06	$C_{38}H_{64}N_{11}O_{11}$-
857.5186	5.15E-06	$C_{40}H_{73}N_8O_{10}$-	857.519	5.15E-06	$C_{40}H_{73}N_8O_{10}S$-	852.4766	4.00E-06	$C_{40}H_{68}N_8O_{10}S$-
858.5216	1.88E-06	$C_{41}H_{68}N_{11}O_9$-	858.522	1.88E-06	$C_{41}H_{68}N_{11}O_9$-	852.4766	4.00E-06	$C_{38}H_{66}N_{11}O_9S$-
859.5344	1.56E-05	$C_{40}H_{75}N_8O_{10}$-	859.534	1.56E-05	$C_{40}H_{75}N_8O_{10}S$-	857.5188	4.26E-06	$C_{40}H_{73}N_8O_{10}S$-
860.5383	4.04E-06	$C_{38}H_{74}N_{11}O_9$-	860.538	4.04E-06	$C_{38}H_{74}N_{11}O_9S$-	858.5225	2.14E-06	$C_{41}H_{68}N_{11}O_9$-
862.5535	6.67E-05	$C_{38}H_{76}N_{11}O_9$-	862.554	6.67E-05	$C_{38}H_{76}N_{11}O_9S$-	858.5225	2.14E-06	$C_{38}H_{72}N_{11}O_9S$-
866.4528	1.72E-05	$C_{41}H_{60}N_{11}O_{10}$-	866.453	1.72E-05	$C_{41}H_{60}N_{11}O_{10}$-	859.5347	1.07E-05	$C_{40}H_{75}N_8O_{10}S$-
868.4772	6.53E-06	$C_{39}H_{66}N_9O_{13}$-	868.477	6.53E-06	$C_{39}H_{66}N_9O_{13}$-	860.5378	5.70E-06	$C_{38}H_{74}N_{11}O_9S$-
868.4772	6.53E-06	$C_{37}H_{64}N_{12}O_{12}$-	868.477	6.53E-06	$C_{37}H_{64}N_{12}O_{12}$-	862.5533	4.39E-05	$C_{38}H_{76}N_{11}O_9S$-
870.475	3.78E-06	$C_{42}H_{64}N_9O_{11}$-	870.475	3.78E-06	$C_{42}H_{64}N_9O_{11}$-	866.4526	6.51E-06	$C_{41}H_{60}N_{11}O_{10}$-
870.475	3.78E-06	$C_{39}H_{68}N_9O_{11}$-	870.475	3.78E-06	$C_{39}H_{68}N_9O_{11}S$-	868.4768	3.72E-06	$C_{39}H_{66}N_9O_{13}$-
870.475	3.78E-06	$C_{37}H_{66}N_{12}O_{10}$-	870.475	3.78E-06	$C_{37}H_{66}N_{12}O_{10}S$-	868.4768	3.72E-06	$C_{37}H_{64}N_{12}O_{12}$-
872.5005	4.61E-06	$C_{41}H_{66}N_{11}O_{10}$-	872.501	4.61E-06	$C_{41}H_{66}N_{11}O_{10}$-	870.4731	3.96E-06	$C_{42}H_{64}N_9O_{11}$-
873.549	5.52E-06	$C_{39}H_{75}N_{11}O_9$-	873.549	5.52E-06	$C_{39}H_{75}N_{11}O_9S$-	870.4731	3.96E-06	$C_{40}H_{62}N_{12}O_{10}$-
875.5662	8.44E-06	$C_{38}H_{75}N_{12}O_{11}$-	875.566	8.44E-06	$C_{38}H_{75}N_{12}O_{11}$-	870.4731	3.96E-06	$C_{37}H_{66}N_{12}O_{10}S$-
883.5339	2.72E-05	$C_{40}H_{73}N_{11}O_9$-	883.534	2.72E-05	$C_{40}H_{73}N_{11}O_9S$-	872.503	1.46E-06	$C_{40}H_{72}N_8O_{11}S$-
884.5378	1.04E-05	$C_{40}H_{74}N_{11}O_9$-	884.538	1.04E-05	$C_{40}H_{74}N_{11}O_9S$-	872.503	1.46E-06	$C_{38}H_{70}N_{11}O_{10}S$-
886.5534	5.72E-05	$C_{40}H_{76}N_{11}O_9$-	886.553	5.72E-05	$C_{40}H_{76}N_{11}O_9S$-	873.5481	4.32E-06	$C_{39}H_{75}N_{11}O_9S$-
888.5693	6.03E-05	$C_{43}H_{74}N_{11}O_9$-	888.569	6.03E-05	$C_{43}H_{74}N_{11}O_9$-	875.5681	1.15E-05	$C_{40}H_{77}N_9O_{12}$-
888.5693	6.03E-05	$C_{40}H_{78}N_{11}O_9$-	888.569	6.03E-05	$C_{40}H_{78}N_{11}O_9S$-	875.5681	1.15E-05	$C_{38}H_{75}N_{12}O_{11}$-
890.4579	5.24E-06	$C_{40}H_{64}N_{11}O_{10}$-	890.458	5.24E-06	$C_{40}H_{64}N_{11}O_{10}S$-	884.538	9.11E-06	$C_{40}H_{74}N_{11}O_9S$-
890.585	2.33E-05	$C_{43}H_{76}N_{11}O_9$-	890.585	2.33E-05	$C_{43}H_{76}N_{11}O_9$-	886.5533	4.84E-05	$C_{40}H_{76}N_{11}O_9S$-
906.4323	3.57E-06	$C_{43}H_{60}N_{11}O_9$-	906.432	3.57E-06	$C_{43}H_{60}N_{11}O_9S$-	888.5701	7.92E-05	$C_{40}H_{78}N_{11}O_9S$-
911.5663	1.35E-05	$C_{41}H_{75}N_{12}O_{11}$-	911.566	1.35E-05	$C_{41}H_{75}N_{12}O_{11}$-	890.4553	1.10E-06	$C_{40}H_{64}N_{11}O_{10}S$-
912.5689	6.77E-06	$C_{45}H_{74}N_{11}O_9$-	912.569	6.77E-06	$C_{45}H_{74}N_{11}O_9$-	890.5842	4.96E-05	$C_{43}H_{76}N_{11}O_9$-
912.5689	6.77E-06	$C_{42}H_{78}N_{11}O_9$-	912.569	6.77E-06	$C_{42}H_{78}N_{11}O_9S$-	901.5821	5.61E-06	$C_{40}H_{77}N_{12}O_{11}$-

913.5809	1.38E-05	$C_{42}H_{79}N_{11}O_{9}$-	913.581	1.38E-05	$C_{42}H_{79}N_{11}O_{9}S$-	906.4315	1.77E-06	$C_{43}H_{60}N_{11}O_{9}S$-
914.5843	6.01E-06	$C_{45}H_{76}N_{11}O_{9}$-	914.584	6.01E-06	$C_{45}H_{76}N_{11}O_{9}$-	911.5667	1.85E-05	$C_{41}H_{75}N_{12}O_{11}$-
916.4588	1.65E-06	$C_{43}H_{66}N_{9}O_{11}$-	916.459	1.65E-06	$C_{43}H_{66}N_{9}O_{11}S$-	912.5715	1.77E-05	$C_{42}H_{78}N_{11}O_{9}S$-
916.4588	1.65E-06	$C_{41}H_{64}N_{12}O_{10}$-	916.459	1.65E-06	$C_{41}H_{64}N_{12}O_{10}S$-	913.581	1.63E-05	$C_{42}H_{79}N_{11}O_{9}S$-
930.4337	8.97E-06	$C_{44}H_{58}N_{12}O_{11}$-	930.434	8.97E-06	$C_{44}H_{58}N_{12}O_{11}$-	914.4594	2.30E-06	$C_{41}H_{62}N_{12}O_{12}$-
932.4315	5.94E-06	$C_{44}H_{60}N_{12}O_{9}$-	932.432	5.94E-06	$C_{44}H_{60}N_{12}O_{9}S$-	914.5857	8.52E-06	$C_{42}H_{80}N_{11}O_{9}S$-
932.4315	5.94E-06	$C_{41}H_{62}N_{11}O_{12}$-	932.432	5.94E-06	$C_{41}H_{62}N_{11}O_{12}S$-	916.4589	2.06E-06	$C_{43}H_{66}N_{9}O_{11}S$-
946.4135	3.39E-06	$C_{44}H_{58}N_{12}O_{10}$-	946.414	3.39E-06	$C_{44}H_{58}N_{12}O_{10}S$-	916.4589	2.06E-06	$C_{41}H_{64}N_{12}O_{10}S$-
968.4004	6.15E-06	$C_{45}H_{54}N_{13}O_{12}$-	968.4	6.15E-06	$C_{45}H_{54}N_{13}O_{12}$-	930.4336	4.72E-06	$C_{44}H_{58}N_{12}O_{11}$-
970.3986	3.12E-06	$C_{50}H_{54}N_{10}O_{11}$-	970.399	3.12E-06	$C_{50}H_{54}N_{10}O_{11}$-	932.4325	3.40E-06	$C_{44}H_{60}N_{12}O_{9}S$-
970.3986	3.12E-06	$C_{48}H_{52}N_{13}O_{10}$-	970.399	3.12E-06	$C_{48}H_{52}N_{13}O_{10}$-	932.4325	3.40E-06	$C_{41}H_{62}N_{11}O_{12}S$-
970.3986	3.12E-06	$C_{45}H_{56}N_{13}O_{10}$-	970.399	3.12E-06	$C_{45}H_{56}N_{13}O_{10}S$-	946.4167	1.35E-06	$C_{45}H_{58}N_{10}O_{13}$-
970.3986	3.12E-06	$C_{44}H_{60}N_{9}O_{14}$-	970.399	3.12E-06	$C_{44}H_{60}N_{9}O_{14}S$-	946.4167	1.35E-06	$C_{43}H_{56}N_{13}O_{12}$-
970.3986	3.12E-06	$C_{42}H_{58}N_{12}O_{13}$-	970.399	3.12E-06	$C_{42}H_{58}N_{12}O_{13}S$-	968.4005	3.23E-06	$C_{45}H_{54}N_{13}O_{12}$-
984.3753	3.16E-06	$C_{50}H_{52}N_{10}O_{12}$-	984.375	3.16E-06	$C_{50}H_{52}N_{10}O_{12}$-	970.3985	1.11E-06	$C_{50}H_{54}N_{10}O_{11}$-
984.3753	3.16E-06	$C_{48}H_{50}N_{13}O_{11}$-	984.375	3.16E-06	$C_{48}H_{50}N_{13}O_{11}$-	970.3985	1.11E-06	$C_{48}H_{52}N_{13}O_{10}$-
984.3753	3.16E-06	$C_{45}H_{52}N_{12}O_{14}$-	984.375	3.16E-06	$C_{45}H_{52}N_{12}O_{14}$-	970.3985	1.11E-06	$C_{45}H_{56}N_{13}O_{10}S$-
984.3753	3.16E-06	$C_{42}H_{56}N_{12}O_{14}$-	984.375	3.16E-06	$C_{42}H_{56}N_{12}O_{14}S$-	970.3985	1.11E-06	$C_{44}H_{60}N_{9}O_{14}S$-
1063.689	7.41E-06	$C_{49}H_{89}N_{15}O_{11}$-	1063.69	7.41E-06	$C_{49}H_{89}N_{15}O_{11}$-	970.3985	1.11E-06	$C_{42}H_{58}N_{12}O_{13}S$-
1063.689	7.41E-06	$C_{46}H_{93}N_{15}O_{11}$-	1063.69	7.41E-06	$C_{46}H_{93}N_{15}O_{11}S$-	984.3744	1.99E-06	$C_{48}H_{50}N_{13}O_{11}$-
1064.693	4.45E-06	$C_{49}H_{90}N_{15}O_{11}$-	1064.69	4.45E-06	$C_{49}H_{90}N_{15}O_{11}$-	984.3744	1.99E-06	$C_{45}H_{52}N_{12}O_{14}$-
						984.3744	1.99E-06	$C_{42}H_{56}N_{12}O_{14}S$-
						1063.6891	9.49E-06	$C_{49}H_{89}N_{15}O_{11}$-
						1063.6891	9.49E-06	$C_{46}H_{93}N_{15}O_{11}S$-
						1064.6929	6.38E-06	$C_{49}H_{90}N_{15}O_{11}$-

Table S 2. Peptide assignments from each of ApoE4 KI H4 samples.

ApoE4 KI1			ApoE4 KI2			ApoE4 KI3		
Mass	Normalized intensity	Chemical formula	Mass	Normalized intensity	Chemical formula	Mass	Normalized intensity	Chemical formula
98.0611	8.52E-05	$C_5H_8NO^-$	98.061	6.07E-05	$C_5H_8NO^-$	98.061	7.15E-05	$C_5H_8NO^-$
141.067	1.91E-04	$C_6H_9N_2O_2^-$	141.067	1.37E-04	$C_6H_9N_2O_2^-$	141.067	1.47E-04	$C_6H_9N_2O_2^-$
145.098	3.91E-06	$C_6H_{13}N_2O_2^-$	145.098	2.43E-06	$C_6H_{13}N_2O_2^-$	145.098	2.39E-06	$C_6H_{13}N_2O_2^-$
153.067	4.78E-04	$C_7H_9N_2O_2^-$	153.067	3.39E-04	$C_7H_9N_2O_2^-$	153.067	3.69E-04	$C_7H_9N_2O_2^-$
155.083	1.62E-04	$C_7H_{11}N_2O_2^-$	155.083	1.21E-04	$C_7H_{11}N_2O_2^-$	155.082	1.26E-04	$C_7H_{11}N_2O_2^-$
166.075	2.12E-06	$C_8H_{10}N_2O_2^-$	166.075	1.48E-06	$C_8H_{10}N_2O_2^-$	166.075	1.32E-06	$C_8H_{10}N_2O_2^-$
167.083	1.58E-04	$C_8H_{11}N_2O_2^-$	167.082	1.22E-04	$C_8H_{11}N_2O_2^-$	167.082	1.27E-04	$C_8H_{11}N_2O_2^-$
169.098	7.72E-05	$C_8H_{13}N_2O_2^-$	169.098	5.51E-05	$C_8H_{13}N_2O_2^-$	169.098	5.75E-05	$C_8H_{13}N_2O_2^-$
181.098	8.44E-05	$C_9H_{13}N_2O_2^-$	181.098	6.35E-05	$C_9H_{13}N_2O_2^-$	181.098	6.63E-05	$C_9H_{13}N_2O_2^-$
183.114	1.82E-05	$C_9H_{15}N_2O_2^-$	183.114	1.49E-05	$C_9H_{15}N_2O_2^-$	183.114	1.28E-05	$C_9H_{15}N_2O_2^-$
191.083	9.02E-06	$C_{10}H_{11}N_2O_2^-$	191.083	6.69E-06	$C_{10}H_{11}N_2O_2^-$	191.083	6.02E-06	$C_{10}H_{11}N_2O_2^-$
193.098	6.94E-06	$C_{10}H_{13}N_2O_2^-$	193.098	4.09E-06	$C_{10}H_{13}N_2O_2^-$	193.098	4.38E-06	$C_{10}H_{13}N_2O_2^-$
194.093	2.49E-05	$C_9H_{12}N_3O_2^-$	194.093	1.64E-05	$C_9H_{12}N_3O_2^-$	194.093	1.72E-05	$C_9H_{12}N_3O_2^-$
195.077	1.11E-05	$C_9H_{11}N_2O_3^-$	195.077	8.09E-06	$C_9H_{11}N_2O_3^-$	195.077	7.25E-06	$C_9H_{11}N_2O_3^-$
195.114	3.29E-05	$C_{10}H_{15}N_2O_2^-$	195.114	2.31E-05	$C_{10}H_{15}N_2O_2^-$	195.114	2.46E-05	$C_{10}H_{15}N_2O_2^-$
196.109	2.29E-05	$C_9H_{14}N_3O_2^-$	196.109	1.67E-05	$C_9H_{14}N_3O_2^-$	196.109	1.73E-05	$C_9H_{14}N_3O_2^-$
197.13	3.41E-06	$C_{10}H_{17}N_2O_2^-$	197.13	2.87E-06	$C_{10}H_{17}N_2O_2^-$	197.13	2.10E-06	$C_{10}H_{17}N_2O_2^-$
198.125	1.42E-05	$C_9H_{16}N_3O_2^-$	198.125	1.01E-05	$C_9H_{16}N_3O_2^-$	198.125	9.10E-06	$C_9H_{16}N_3O_2^-$
200.14	3.66E-06	$C_9H_{18}N_3O_2^-$	200.14	1.79E-06	$C_9H_{18}N_3O_2^-$	200.141	2.47E-06	$C_9H_{18}N_3O_2^-$
207.078	2.64E-06	$C_{10}H_{11}N_2O_3^-$	207.077	1.20E-06	$C_{10}H_{11}N_2O_3^-$	207.078	1.09E-06	$C_{10}H_{11}N_2O_3^-$
208.109	2.21E-05	$C_{10}H_{14}N_3O_2^-$	208.109	1.81E-05	$C_{10}H_{14}N_3O_2^-$	208.109	1.66E-05	$C_{10}H_{14}N_3O_2^-$
209.093	4.37E-06	$C_{10}H_{13}N_2O_3^-$	209.093	4.34E-06	$C_{10}H_{13}N_2O_3^-$	209.093	3.66E-06	$C_{10}H_{13}N_2O_3^-$
210.088	6.37E-05	$C_9H_{12}N_3O_3^-$	210.088	5.04E-05	$C_9H_{12}N_3O_3^-$	210.088	4.59E-05	$C_9H_{12}N_3O_3^-$
210.125	1.10E-05	$C_{10}H_{16}N_3O_2^-$	210.125	7.44E-06	$C_{10}H_{16}N_3O_2^-$	210.125	7.11E-06	$C_{10}H_{16}N_3O_2^-$
212.104	1.34E-05	$C_9H_{14}N_3O_3^-$	212.104	9.88E-06	$C_9H_{14}N_3O_3^-$	212.104	9.78E-06	$C_9H_{14}N_3O_3^-$
212.14	1.08E-05	$C_{10}H_{18}N_3O_2^-$	212.14	6.35E-06	$C_{10}H_{18}N_3O_2^-$	212.14	6.83E-06	$C_{10}H_{18}N_3O_2^-$
224.104	1.60E-05	$C_{10}H_{14}N_3O_3^-$	224.104	1.18E-05	$C_{10}H_{14}N_3O_3^-$	224.104	1.14E-05	$C_{10}H_{14}N_3O_3^-$
226.12	1.03E-05	$C_{10}H_{16}N_3O_3^-$	226.12	8.98E-06	$C_{10}H_{16}N_3O_3^-$	226.12	6.97E-06	$C_{10}H_{16}N_3O_3^-$
238.12	6.86E-06	$C_{11}H_{16}N_3O_3^-$	238.12	4.11E-06	$C_{11}H_{16}N_3O_3^-$	238.12	5.08E-06	$C_{11}H_{16}N_3O_3^-$
240.135	1.05E-05	$C_{11}H_{18}N_3O_3^-$	240.135	8.98E-06	$C_{11}H_{18}N_3O_3^-$	240.135	7.52E-06	$C_{11}H_{18}N_3O_3^-$
252.136	3.13E-06	$C_{12}H_{18}N_3O_3^-$	252.135	1.98E-06	$C_{12}H_{18}N_3O_3^-$	252.135	1.95E-06	$C_{12}H_{18}N_3O_3^-$
266.151	1.81E-06	$C_{13}H_{20}N_3O_3^-$	266.151	2.11E-06	$C_{13}H_{20}N_3O_3^-$	266.151	1.50E-06	$C_{13}H_{20}N_3O_3^-$
267.146	9.75E-07	$C_{12}H_{19}N_4O_3^-$	267.146	4.35E-07	$C_{12}H_{19}N_4O_3^-$	267.146	7.25E-07	$C_{12}H_{19}N_4O_3^-$
297.157	1.55E-06	$C_{13}H_{21}N_4O_4^-$	297.157	1.59E-06	$C_{13}H_{21}N_4O_4^-$	297.157	1.14E-06	$C_{13}H_{21}N_4O_4^-$
553.279	6.13E-06	$C_{28}H_{37}N_6O_6^-$	553.279	8.60E-06	$C_{28}H_{37}N_6O_6^-$	553.279	4.34E-06	$C_{28}H_{37}N_6O_6^-$
562.255	1.76E-06	$C_{29}H_{34}N_6O_6^-$	562.255	9.41E-07	$C_{29}H_{34}N_6O_6^-$	562.255	1.25E-06	$C_{29}H_{34}N_6O_6^-$
571.289	1.23E-06	$C_{28}H_{39}N_6O_7^-$	571.289	1.71E-06	$C_{28}H_{39}N_6O_7^-$	571.289	9.82E-07	$C_{28}H_{39}N_6O_7^-$
579.294	2.27E-05	$C_{30}H_{39}N_6O_6^-$	579.294	3.85E-05	$C_{30}H_{39}N_6O_6^-$	579.294	1.44E-05	$C_{30}H_{39}N_6O_6^-$
580.298	3.89E-06	$C_{25}H_{40}N_8O_8^-$	580.298	6.45E-06	$C_{25}H_{40}N_8O_8^-$	580.298	2.53E-06	$C_{25}H_{40}N_8O_8^-$
581.31	4.61E-05	$C_{30}H_{41}N_6O_6^-$	581.31	5.67E-05	$C_{30}H_{41}N_6O_6^-$	581.31	3.35E-05	$C_{30}H_{41}N_6O_6^-$
582.313	8.25E-06	$C_{25}H_{42}N_8O_8^-$	582.313	1.09E-05	$C_{25}H_{42}N_8O_8^-$	582.313	6.59E-06	$C_{25}H_{42}N_8O_8^-$
597.305	4.68E-06	$C_{30}H_{41}N_6O_7^-$	597.305	7.61E-06	$C_{30}H_{41}N_6O_7^-$	597.305	3.09E-06	$C_{30}H_{41}N_6O_7^-$

599.321	1.30E-05	$C_{30}H_{43}N_6O_7^-$	599.32	1.72E-05	$C_{30}H_{43}N_6O_7^-$	599.321	1.05E-05	$C_{30}H_{43}N_6O_7^-$
834.522	8.78E-07	$C_{39}H_{68}N_{11}O_9^-$	834.522	1.31E-06	$C_{39}H_{68}N_{11}O_9^-$	834.522	5.53E-07	$C_{39}H_{68}N_{11}O_9^-$
836.538	6.23E-06	$C_{39}H_{70}N_{11}O_9^-$	836.538	9.25E-06	$C_{39}H_{70}N_{11}O_9^-$	836.538	4.63E-06	$C_{39}H_{70}N_{11}O_9^-$
860.538	1.05E-06	$C_{41}H_{70}N_{11}O_9^-$	860.538	9.51E-07	$C_{41}H_{70}N_{11}O_9^-$	860.537	1.14E-06	$C_{41}H_{70}N_{11}O_9^-$
862.554	1.52E-05	$C_{41}H_{72}N_{11}O_9^-$	862.554	2.97E-05	$C_{41}H_{72}N_{11}O_9^-$	862.554	8.61E-06	$C_{41}H_{72}N_{11}O_9^-$
864.57	1.47E-05	$C_{41}H_{74}N_{11}O_9^-$	864.569	2.20E-05	$C_{41}H_{74}N_{11}O_9^-$	864.57	9.45E-06	$C_{41}H_{74}N_{11}O_9^-$
884.538	3.34E-06	$C_{43}H_{70}N_{11}O_9^-$	884.538	3.80E-06	$C_{43}H_{70}N_{11}O_9^-$	884.538	3.66E-06	$C_{43}H_{70}N_{11}O_9^-$
886.554	1.74E-05	$C_{43}H_{72}N_{11}O_9^-$	886.553	1.94E-05	$C_{43}H_{72}N_{11}O_9^-$	886.554	1.57E-05	$C_{43}H_{72}N_{11}O_9^-$
1063.69	3.03E-06	$C_{51}H_{91}N_{12}O_{12}^-$	1063.69	2.49E-06	$C_{51}H_{91}N_{12}O_{12}^-$	1063.69	2.72E-06	$C_{51}H_{91}N_{12}O_{12}^-$
1064.69	1.57E-06	$C_{46}H_{92}N_{14}O_{14}^-$	1064.69	1.25E-06	$C_{46}H_{92}N_{14}O_{14}^-$	1064.69	9.02E-07	$C_{46}H_{92}N_{14}O_{14}^-$
86.0609	3.33E-06	$C_4H_8NO^-$	86.0609	1.82E-06	$C_4H_8N_1O_1^-$	86.0609	1.70E-06	$C_4H_8NO^-$
100.077	3.05E-06	$C_5H_{10}NO^-$	100.077	2.06E-06	$C_5H_{10}N_1O_1^-$	100.077	2.20E-06	$C_5H_{10}NO^-$
143.083	1.73E-06	$C_6H_{11}N_2O_2^-$	140.059	4.02E-07	$C_6H_8N_2O_2^-$	143.083	1.06E-06	$C_6H_{11}N_2O_2^-$
154.075	6.91E-07	$C_7H_{10}N_2O_2^-$	143.083	1.30E-06	$C_6H_{11}N_2O_2^-$	154.075	4.82E-07	$C_7H_{10}N_2O_2^-$
157.098	1.95E-06	$C_7H_{13}N_2O_2^-$	154.075	4.02E-07	$C_7H_{10}N_2O_2^-$	157.098	1.21E-06	$C_7H_{13}N_2O_2^-$
168.09	1.06E-06	$C_8H_{12}N_2O_2^-$	157.098	1.24E-06	$C_7H_{13}N_2O_2^-$	168.09	8.22E-07	$C_8H_{12}N_2O_2^-$
171.114	1.63E-06	$C_8H_{15}N_2O_2^-$	171.114	8.12E-07	$C_8H_{15}N_2O_2^-$	171.114	9.05E-07	$C_8H_{15}N_2O_2^-$
173.039	1.02E-06	$C_6H_9N_2O_2S^-$	173.039	5.46E-07	$C_6H_9N_2O_2S^-$	173.039	7.16E-07	$C_6H_9N_2O_2S^-$
179.083	2.44E-05	$C_9H_{11}N_2O_2^-$	179.082	1.86E-05	$C_9H_{11}N_2O_2S^-$	179.083	1.84E-05	$C_9H_{11}N_2O_2^-$
180.09	5.37E-07	$C_9H_{12}N_2O_2^-$	185.039	4.50E-07	$C_7H_9N_2O_2S^-$	180.09	4.53E-07	$C_9H_{12}N_2O_2^-$
185.039	1.02E-06	$C_7H_9N_2O_2S^-$	197.093	6.04E-07	$C_9H_{13}N_2O_3^-$	185.039	1.02E-06	$C_7H_9N_2O_2S^-$
197.093	9.39E-07	$C_9H_{13}N_2O_3^-$	206.093	4.55E-06	$C_{10}H_{12}N_3O_2^-$	197.093	7.50E-07	$C_9H_{13}N_2O_3^-$
206.093	6.80E-06	$C_{10}H_{12}N_3O_2^-$	211.109	6.20E-07	$C_{10}H_{15}N_2O_3^-$	206.093	4.68E-06	$C_{10}H_{12}N_3O_2^-$
211.109	5.58E-07	$C_{10}H_{15}N_2O_3^-$	222.088	1.22E-06	$C_{10}H_{12}N_3O_3S^-$	211.096	5.93E-07	$C_9H_{13}N_3O_3^-$
214.12	5.51E-07	$C_9H_{16}N_3O_3^-$	230.073	6.69E-07	$C_9H_{14}N_2O_3S^-$	214.156	4.67E-07	$C_{10}H_{20}N_3O_2^-$
214.156	5.27E-07	$C_{10}H_{20}N_3O_2^-$	236.104	9.24E-07	$C_{11}H_{14}N_3O_3S^-$	222.088	1.66E-06	$C_{10}H_{12}N_3O_3^-$
222.088	1.76E-06	$C_{10}H_{12}N_3O_3^-$	240.082	8.31E-07	$C_{10}H_{14}N_3O_2S^-$	236.104	8.20E-07	$C_{11}H_{14}N_3O_3^-$
236.104	1.38E-06	$C_{11}H_{14}N_3O_3^-$	242.061	4.99E-07	$C_9H_{12}N_3O_3S^-$	240.082	9.45E-07	$C_{10}H_{14}N_3O_2S^-$
240.057	6.79E-07	$C_{10}H_{12}N_2O_3S^-$	244.077	8.31E-07	$C_9H_{14}N_3O_3S^-$	254.151	1.05E-06	$C_{12}H_{20}N_3O_3^-$
240.082	1.12E-06	$C_{10}H_{14}N_3O_2S^-$	250.12	6.37E-07	$C_{12}H_{16}N_3O_3^-$	269.162	7.91E-07	$C_{12}H_{21}N_4O_3^-$
244.077	6.09E-07	$C_9H_{14}N_3O_3S^-$	254.151	1.15E-06	$C_{12}H_{20}N_3O_3^-$	281.126	5.30E-07	$C_{12}H_{17}N_4O_4^-$
250.12	7.38E-07	$C_{12}H_{16}N_3O_3^-$	260.104	4.41E-07	$C_{13}H_{14}N_3O_3^-$	281.162	6.37E-07	$C_{13}H_{21}N_4O_3^-$
254.151	9.64E-07	$C_{12}H_{20}N_3O_3^-$	265.131	4.01E-07	$C_{12}H_{17}N_4O_3^-$	283.141	7.90E-07	$C_{12}H_{19}N_4O_4^-$
258.092	6.22E-07	$C_{10}H_{16}N_3O_3S^-$	269.162	6.16E-07	$C_{12}H_{21}N_4O_3^-$	283.178	6.59E-07	$C_{13}H_{23}N_4O_3^-$
269.162	8.58E-07	$C_{12}H_{21}N_4O_3^-$	280.167	4.43E-07	$C_{14}H_{22}N_3O_3^-$	295.141	5.41E-07	$C_{13}H_{19}N_4O_4^-$
274.12	9.27E-07	$C_{14}H_{16}N_3O_3^-$	281.126	4.21E-07	$C_{12}H_{17}N_4O_4^-$	328.236	6.57E-07	$C_{15}H_{30}N_5O_3^-$
279.146	5.53E-07	$C_{13}H_{19}N_4O_3^-$	281.162	8.73E-07	$C_{13}H_{21}N_4O_3^-$	389.21	1.17E-06	$C_{16}H_{31}N_5O_4S^-$
280.167	6.12E-07	$C_{14}H_{22}N_3O_3^-$	283.141	1.07E-06	$C_{12}H_{19}N_4O_4^-$	391.226	1.49E-05	$C_{16}H_{33}N_5O_4S^-$
281.126	8.59E-07	$C_{12}H_{17}N_4O_4^-$	283.178	7.33E-07	$C_{13}H_{23}N_4O_3^-$	405.241	1.26E-06	$C_{17}H_{35}N_5O_4S^-$
281.162	8.02E-07	$C_{13}H_{21}N_4O_3^-$	295.141	6.08E-07	$C_{13}H_{19}N_4O_4^-$	415.226	9.31E-07	$C_{18}H_{33}N_5O_4S^-$
283.141	1.30E-06	$C_{12}H_{19}N_4O_4^-$	311.173	7.26E-07	$C_{14}H_{23}N_4O_4^-$	417.241	3.11E-05	$C_{18}H_{35}N_5O_4S^-$
283.178	1.32E-06	$C_{13}H_{23}N_4O_3^-$	323.173	4.21E-07	$C_{15}H_{23}N_4O_4^-$	436.256	4.59E-07	$C_{21}H_{34}N_5O_5^-$
295.141	7.53E-07	$C_{13}H_{19}N_4O_4^-$	328.236	8.62E-07	$C_{15}H_{30}N_5O_3^-$	439.187	6.40E-07	$C_{22}H_{25}N_5O_5^-$
309.157	5.79E-07	$C_{14}H_{21}N_4O_4^-$	389.21	2.42E-06	$C_{16}H_{31}N_5O_4S^-$	439.226	6.29E-07	$C_{20}H_{33}N_5O_4S^-$
311.173	6.42E-07	$C_{14}H_{23}N_4O_4^-$	391.226	2.42E-05	$C_{16}H_{33}N_5O_4S^-$	445.273	5.21E-07	$C_{20}H_{39}N_5O_4S^-$
323.173	5.56E-07	$C_{15}H_{23}N_4O_4^-$	405.241	1.21E-06	$C_{17}H_{35}N_5O_4S^-$	465.167	6.61E-07	$C_{23}H_{23}N_5O_6^-$
389.21	1.57E-06	$C_{16}H_{31}N_5O_4S^-$	410.24	4.01E-07	$C_{19}H_{32}N_5O_5^-$	583.316	7.35E-07	$C_{26}H_{45}N_7O_6S^-$

391.226	1.96E-05	$C_{16}H_{33}N_5O_4S^-$	415.226	1.60E-06	$C_{18}H_{33}N_5O_4S^-$	655.221	5.74E-07	$C_{30}H_{35}N_6O_9S^-$
405.241	1.39E-06	$C_{17}H_{35}N_5O_4S^-$	417.241	6.56E-05	$C_{18}H_{35}N_5O_4S^-$	673.232	1.95E-06	$C_{33}H_{35}N_7O_7S^-$
415.226	8.67E-07	$C_{18}H_{33}N_5O_4S^-$	431.257	4.03E-07	$C_{19}H_{37}N_5O_4S^-$	812.514	7.39E-07	$C_{37}H_{68}N_{10}O_{10}^-$
417.241	4.68E-05	$C_{18}H_{35}N_5O_4S^-$	437.171	5.49E-07	$C_{22}H_{23}N_5O_5^-$	833.519	1.41E-06	$C_{38}H_{73}N_8O_{10}S^-$
436.256	7.95E-07	$C_{21}H_{34}N_5O_5^-$	439.225	6.09E-07	$C_{20}H_{33}N_5O_4S^-$	834.522	5.53E-07	$C_{36}H_{72}N_{11}O_9S^-$
438.271	2.99E-06	$C_{21}H_{36}N_5O_5^-$	441.241	4.56E-07	$C_{20}H_{35}N_5O_4S^-$	835.284	8.77E-07	$C_{37}H_{43}N_{10}O_{11}S^-$
441.241	8.12E-07	$C_{20}H_{35}N_5O_4S^-$	445.272	1.07E-06	$C_{20}H_{39}N_5O_4S^-$	847.43	7.01E-07	$C_{38}H_{59}N_{10}O_{12}^-$
445.273	5.66E-07	$C_{20}H_{39}N_5O_4S^-$	575.23	4.40E-07	$C_{26}H_{35}N_6O_7S^-$	857.519	1.12E-06	$C_{40}H_{73}N_8O_{10}S^-$
575.214	5.54E-07	$C_{28}H_{29}N_7O_7^-$	583.316	1.09E-06	$C_{26}H_{45}N_7O_6S^-$	858.521	6.17E-07	$C_{41}H_{68}N_{11}O_9^-$
583.316	1.17E-06	$C_{26}H_{45}N_7O_6S^-$	583.325	4.67E-07	$C_{30}H_{43}N_6O_6^-$	859.535	2.14E-06	$C_{40}H_{75}N_8O_{10}S^-$
601.278	1.19E-06	$C_{24}H_{41}N_8O_8S^-$	601.278	1.22E-06	$C_{24}H_{41}N_8O_8S^-$	859.535	2.14E-06	$C_{37}H_{71}N_{12}O_{11}^-$
603.294	8.00E-07	$C_{24}H_{43}N_8O_8S^-$	603.294	7.74E-07	$C_{24}H_{43}N_8O_8S^-$	860.339	4.21E-07	$C_{44}H_{46}N_9O_{10}^-$
671.216	6.68E-07	$C_{33}H_{33}N_7O_7S^-$	605.31	4.34E-07	$C_{24}H_{45}N_8O_8S^-$	860.339	4.21E-07	$C_{41}H_{50}N_9O_{10}S^-$
671.216	6.68E-07	$C_{30}H_{35}N_6O_{10}S^-$	607.326	4.43E-07	$C_{24}H_{47}N_8O_8S^-$	860.339	4.21E-07	$C_{39}H_{48}N_{12}O_9S^-$
673.232	1.93E-06	$C_{33}H_{35}N_7O_7S^-$	673.231	1.79E-06	$C_{33}H_{35}N_7O_7S^-$	860.357	1.51E-06	$C_{41}H_{50}N_9O_{12}^-$
729.257	4.93E-07	$C_{34}H_{37}N_{10}O_7S^-$	673.231	1.79E-06	$C_{30}H_{37}N_6O_{10}S^-$	860.357	1.51E-06	$C_{39}H_{48}N_{12}O_{11}^-$
826.502	8.79E-07	$C_{36}H_{66}N_{12}O_{10}^-$	812.511	4.63E-07	$C_{37}H_{68}N_{10}O_{10}^-$	860.38	1.29E-06	$C_{39}H_{50}N_{13}O_{10}^-$
833.519	2.28E-06	$C_{38}H_{73}N_8O_{10}S^-$	812.525	4.86E-07	$C_{38}H_{70}N_9O_{10}^-$	860.397	7.00E-07	$C_{42}H_{54}N_9O_{11}^-$
834.522	8.78E-07	$C_{36}H_{72}N_{11}O_9S^-$	812.525	4.86E-07	$C_{36}H_{68}N_{12}O_9^-$	860.397	7.00E-07	$C_{39}H_{58}N_9O_{11}S^-$
835.284	8.81E-07	$C_{37}H_{43}N_{10}O_{11}S^-$	833.519	3.79E-06	$C_{38}H_{73}N_8O_{10}S^-$	860.397	7.00E-07	$C_{37}H_{56}N_{12}O_{10}S^-$
840.494	7.21E-07	$C_{37}H_{66}N_{11}O_{11}^-$	834.522	1.31E-06	$C_{36}H_{72}N_{11}O_9S^-$	860.431	8.01E-07	$C_{43}H_{58}N_9O_{10}^-$
840.527	9.01E-07	$C_{39}H_{72}N_{10}O_8S^-$	835.284	8.20E-07	$C_{37}H_{43}N_{10}O_{11}S^-$	860.431	8.01E-07	$C_{41}H_{56}N_{12}O_9^-$
847.431	7.98E-07	$C_{38}H_{59}N_{10}O_{12}^-$	845.415	4.29E-07	$C_{38}H_{57}N_{10}O_{12}^-$	861.43	4.88E-07	$C_{39}H_{61}N_{10}O_{10}S^-$
849.551	1.10E-06	$C_{36}H_{73}N_{12}O_{11}^-$	847.43	9.34E-07	$C_{38}H_{59}N_{10}O_{12}^-$	862.554	8.61E-06	$C_{38}H_{76}N_{11}O_9S^-$
857.52	1.91E-06	$C_{40}H_{73}N_8O_{10}S^-$	850.552	4.86E-07	$C_{40}H_{72}N_{11}O_9^-$	873.549	5.72E-07	$C_{39}H_{75}N_{11}O_9S^-$
857.52	1.91E-06	$C_{37}H_{69}N_{12}O_{11}^-$	857.519	1.48E-06	$C_{40}H_{73}N_8O_{10}S^-$	876.569	4.48E-07	$C_{42}H_{74}N_{11}O_9^-$
858.524	8.02E-07	$C_{40}H_{74}N_8O_{10}S^-$	858.523	5.09E-07	$C_{41}H_{68}N_{11}O_9^-$	884.538	3.66E-06	$C_{40}H_{74}N_{11}O_9S^-$
858.524	8.02E-07	$C_{38}H_{72}N_{11}O_9S^-$	858.523	5.09E-07	$C_{38}H_{72}N_{11}O_9S^-$	886.554	1.57E-05	$C_{40}H_{76}N_{11}O_9S^-$
859.535	2.30E-06	$C_{40}H_{75}N_8O_{10}S^-$	859.534	3.93E-06	$C_{40}H_{75}N_8O_{10}S^-$	887.566	1.88E-05	$C_{39}H_{75}N_{12}O_{11}^-$
859.535	2.30E-06	$C_{37}H_{71}N_{12}O_{11}^-$	860.538	9.51E-07	$C_{38}H_{74}N_{11}O_9S^-$	888.569	8.29E-06	$C_{43}H_{74}N_{11}O_9^-$
860.538	1.05E-06	$C_{38}H_{74}N_{11}O_9S^-$	862.554	2.97E-05	$C_{38}H_{76}N_{11}O_9S^-$	888.569	8.29E-06	$C_{40}H_{78}N_{11}O_9S^-$
862.554	1.52E-05	$C_{38}H_{76}N_{11}O_9S^-$	871.43	4.68E-07	$C_{40}H_{59}N_{10}O_{12}^-$	889.571	3.99E-07	$C_{40}H_{77}N_{10}O_{12}^-$
873.551	6.13E-07	$C_{38}H_{73}N_{12}O_{11}^-$	871.57	7.06E-07	$C_{40}H_{77}N_{11}O_8S^-$	889.582	3.57E-06	$C_{39}H_{77}N_{12}O_{11}^-$
876.57	6.60E-07	$C_{42}H_{74}N_{11}O_9^-$	875.565	2.38E-06	$C_{39}H_{77}N_{11}O_9S^-$	892.6	4.96E-07	$C_{43}H_{78}N_{11}O_9^-$
884.538	3.34E-06	$C_{40}H_{74}N_{11}O_9S^-$	876.57	1.14E-06	$C_{42}H_{74}N_{11}O_9^-$	901.582	8.88E-07	$C_{40}H_{77}N_{12}O_{11}^-$
886.554	1.74E-05	$C_{40}H_{76}N_{11}O_9S^-$	884.538	3.80E-06	$C_{40}H_{74}N_{11}O_9S^-$	902.585	6.09E-07	$C_{44}H_{76}N_{11}O_9^-$
887.566	2.36E-05	$C_{39}H_{75}N_{12}O_{11}^-$	886.553	1.94E-05	$C_{40}H_{76}N_{11}O_9S^-$	902.585	6.09E-07	$C_{41}H_{80}N_{11}O_9S^-$
888.57	1.01E-05	$C_{43}H_{74}N_{11}O_9^-$	888.569	1.22E-05	$C_{43}H_{74}N_{11}O_9^-$	909.551	3.23E-06	$C_{41}H_{73}N_{12}O_{11}^-$
888.57	1.01E-05	$C_{40}H_{78}N_{11}O_9S^-$	888.569	1.22E-05	$C_{40}H_{78}N_{11}O_9S^-$	910.554	1.40E-06	$C_{45}H_{72}N_{11}O_9^-$
889.582	6.45E-06	$C_{39}H_{77}N_{12}O_{11}^-$	890.585	6.10E-06	$C_{43}H_{76}N_{11}O_9^-$	910.554	1.40E-06	$C_{42}H_{76}N_{11}O_9S^-$
890.585	3.36E-06	$C_{43}H_{76}N_{11}O_9^-$	892.6	8.78E-07	$C_{43}H_{78}N_{11}O_9^-$	911.566	4.74E-06	$C_{41}H_{75}N_{12}O_{11}^-$
892.6	4.88E-07	$C_{43}H_{78}N_{11}O_9^-$	902.584	6.42E-07	$C_{44}H_{76}N_{11}O_9^-$	912.57	2.44E-06	$C_{45}H_{74}N_{11}O_9^-$
901.582	7.63E-07	$C_{40}H_{77}N_{12}O_{11}^-$	907.535	4.25E-07	$C_{41}H_{71}N_{12}O_{11}^-$	912.57	2.44E-06	$C_{42}H_{78}N_{11}O_9S^-$
902.585	5.49E-07	$C_{44}H_{76}N_{11}O_9^-$	910.553	2.36E-06	$C_{45}H_{72}N_{11}O_9^-$	914.584	1.24E-06	$C_{45}H_{76}N_{11}O_9^-$
902.585	5.49E-07	$C_{41}H_{80}N_{11}O_9S^-$	912.569	2.99E-06	$C_{45}H_{74}N_{11}O_9^-$	915.596	5.93E-07	$C_{42}H_{81}N_{11}O_9S^-$
910.554	1.99E-06	$C_{42}H_{76}N_{11}O_9S^-$	912.569	2.99E-06	$C_{42}H_{78}N_{11}O_9S^-$	1063.69	2.72E-06	$C_{46}H_{93}N_{15}O_{11}S^-$

911.566	5.91E-06	$C_{41}H_{75}N_{12}O_{11}^-$	914.585	1.84E-06	$C_{45}H_{76}N_{11}O_9^-$	1064.69	9.02E-07	$C_{49}H_{90}N_{15}O_{11}^-$
912.57	2.52E-06	$C_{45}H_{74}N_{11}O_9^-$	914.585	1.84E-06	$C_{42}H_{80}N_{11}O_9S^-$	1123.72	1.32E-06	$C_{53}H_{97}N_{13}O_{11}S^-$
912.57	2.52E-06	$C_{42}H_{78}N_{11}O_9S^-$	915.596	8.05E-07	$C_{42}H_{81}N_{11}O_9S^-$	1124.34	6.12E-07	$C_{54}H_{50}N_{11}O_{17}^-$
914.585	1.61E-06	$C_{45}H_{76}N_{11}O_9^-$	1063.69	2.49E-06	$C_{49}H_{89}N_{15}O_{11}^-$	1124.34	6.12E-07	$C_{49}H_{52}N_{14}O_{16}S^-$
914.585	1.61E-06	$C_{42}H_{80}N_{11}O_9S^-$	1063.69	2.49E-06	$C_{46}H_{93}N_{15}O_{11}S^-$	1124.4	4.70E-07	$C_{58}H_{54}N_{13}O_{12}^-$
915.595	7.83E-07	$C_{42}H_{81}N_{11}O_9S^-$				1124.4	4.70E-07	$C_{55}H_{56}N_{12}O_{15}^-$
1063.69	3.03E-06	$C_{49}H_{89}N_{15}O_{11}^-$				1124.4	4.70E-07	$C_{53}H_{54}N_{15}O_{14}^-$
1063.69	3.03E-06	$C_{46}H_{93}N_{15}O_{11}S^-$				1124.4	4.70E-07	$C_{52}H_{60}N_{12}O_{15}S^-$
1064.69	1.57E-06	$C_{49}H_{90}N_{15}O_{11}^-$				1124.4	4.70E-07	$C_{50}H_{58}N_{15}O_{14}S^-$

Table S 3. The enrichment analysis of up-regulated proteins:

category	description	FDR value
GO Biological Process	Organonitrogen compound biosynthetic process	1.47E-25
GO Biological Process	Amide biosynthetic process	2.37E-25
GO Biological Process	Cellular nitrogen compound metabolic process	1.11E-23
GO Biological Process	Cellular nitrogen compound biosynthetic process	1.11E-23
GO Biological Process	Translation	1.28E-23
GO Biological Process	Cellular amide metabolic process	1.71E-23
GO Biological Process	Cellular amino acid metabolic process	3.30E-20
GO Biological Process	tRNA metabolic process	4.61E-20
GO Biological Process	Carboxylic acid metabolic process	4.61E-20
GO Biological Process	Organic substance biosynthetic process	4.61E-20
GO Biological Process	Oxoacid metabolic process	8.57E-20
GO Biological Process	Cellular biosynthetic process	1.96E-19
GO Biological Process	Cellular metabolic process	3.99E-19
GO Biological Process	Small molecule metabolic process	8.60E-18
GO Biological Process	Metabolic process	9.69E-18
GO Biological Process	Primary metabolic process	3.05E-17
GO Biological Process	tRNA aminoacylation for protein translation	1.58E-15
GO Biological Process	ncRNA metabolic process	1.58E-15
GO Biological Process	Organic substance metabolic process	1.58E-15
GO Biological Process	Organic cyclic compound metabolic process	1.76E-14
GO Biological Process	Heterocycle metabolic process	6.16E-14
GO Biological Process	Mitochondrial gene expression	6.28E-14
GO Biological Process	Nitrogen compound metabolic process	1.01E-13
GO Biological Process	Gene expression	3.72E-13
GO Biological Process	Cellular aromatic compound metabolic process	5.43E-13
GO Biological Process	Nucleobase-containing compound metabolic process	1.89E-11
GO Biological Process	Mitochondrial translation	3.57E-11
GO Biological Process	Cellular macromolecule biosynthetic process	1.54E-10
GO Biological Process	Organonitrogen compound metabolic process	6.16E-10
GO Biological Process	Alpha-amino acid metabolic process	1.40E-08
GO Biological Process	RNA metabolic process	4.24E-07
GO Biological Process	Mitochondrial translational elongation	6.56E-07

GO Biological Process	Mitochondrial translational termination	7.00E-07
GO Biological Process	tRNA processing	7.11E-07
GO Biological Process	Nucleotide biosynthetic process	1.56E-06
GO Biological Process	Nucleotide metabolic process	1.78E-06
GO Biological Process	Organic cyclic compound biosynthetic process	2.90E-06
GO Biological Process	ncRNA processing	3.73E-06
GO Biological Process	Heterocycle biosynthetic process	5.77E-06
GO Biological Process	Alpha-amino acid biosynthetic process	1.01E-05
GO Biological Process	Tricarboxylic acid cycle	1.25E-05
GO Biological Process	Nucleobase metabolic process	1.86E-05
GO Biological Process	Nucleic acid metabolic process	2.32E-05
GO Biological Process	Glutamine family amino acid metabolic process	2.72E-05
GO Biological Process	Ribose phosphate biosynthetic process	6.83E-05
GO Biological Process	Aromatic compound biosynthetic process	1.20E-04
GO Biological Process	Dicarboxylic acid metabolic process	1.70E-04
GO Biological Process	Regulation of translation	2.60E-04
GO Biological Process	Purine nucleotide metabolic process	2.80E-04
GO Biological Process	Ribose phosphate metabolic process	2.80E-04
GO Biological Process	Oxidation-reduction process	3.10E-04
GO Biological Process	Small molecule biosynthetic process	3.30E-04
GO Biological Process	Posttranscriptional regulation of gene expression	3.40E-04
GO Biological Process	Purine nucleotide biosynthetic process	4.10E-04
GO Biological Process	Organophosphate metabolic process	4.60E-04
GO Biological Process	Cellular protein metabolic process	5.80E-04
GO Biological Process	Carboxylic acid biosynthetic process	5.80E-04
GO Biological Process	Macromolecule metabolic process	6.10E-04
GO Biological Process	Mitochondrial RNA metabolic process	6.20E-04
GO Biological Process	Organophosphate biosynthetic process	8.00E-04
GO Biological Process	Nucleobase biosynthetic process	0.001
GO Biological Process	tRNA modification	0.0014
GO Biological Process	Cellular macromolecule metabolic process	0.0015
GO Biological Process	Cellular process	0.0021
GO Biological Process	Nucleobase-containing compound biosynthetic process	0.0022
GO Biological Process	Ribonucleotide biosynthetic process	0.0036
GO Biological Process	RNA processing	0.0052
GO Biological Process	Ribonucleotide metabolic process	0.0068
GO Biological Process	Serine family amino acid metabolic process	0.0081
GO Biological Process	Mitochondrial tRNA processing	0.0098
GO Biological Process	Carboxylic acid catabolic process	0.01
GO Biological Process	Tricarboxylic acid metabolic process	0.0115
GO Biological Process	Translational initiation	0.0147
GO Biological Process	Pyrimidine nucleobase metabolic process	0.0157
GO Biological Process	Arginine metabolic process	0.0157
GO Biological Process	Glutamine family amino acid biosynthetic process	0.0157
GO Biological Process	glutaminyl-tRNA aminoacylation	0.0196
GO Biological Process	isoleucyl-tRNA aminoacylation	0.0196
GO Biological Process	Ribosome biogenesis	0.0196
GO Biological Process	Tetrahydrofolate metabolic process	0.02
GO Biological Process	Glutamine metabolic process	0.0292

GO Biological Process	Alpha-amino acid catabolic process	0.0292
GO Biological Process	Purine nucleobase metabolic process	0.0322
GO Biological Process	Small molecule catabolic process	0.0443
GO Biological Process	CUT catabolic process	0.0443
KEGG Pathways	Aminoacyl-tRNA biosynthesis	5.31E-16
KEGG Pathways	Metabolic pathways	1.70E-10
KEGG Pathways	Citrate cycle (TCA cycle)	6.31E-08
KEGG Pathways	Biosynthesis of amino acids	1.50E-05
KEGG Pathways	Carbon metabolism	2.40E-04
KEGG Pathways	2-Oxocarboxylic acid metabolism	0.0092
KEGG Pathways	One carbon pool by folate	0.0104
KEGG Pathways	RNA transport	0.0104
KEGG Pathways	Antifolate resistance	0.0247
KEGG Pathways	Ribosome	0.0247
KEGG Pathways	Alanine, aspartate and glutamate metabolism	0.0321

Table S 4. The enrichment analysis of down-regulated proteins:

category	description	FDR value
GO Biological Process	RNA splicing	7.47E-13
GO Biological Process	RNA processing	5.59E-12
GO Biological Process	Gene expression	1.59E-11
GO Biological Process	mRNA processing	2.33E-11
GO Biological Process	mRNA metabolic process	2.33E-11
GO Biological Process	RNA splicing, via transesterification reactions	1.91E-10
GO Biological Process	RNA metabolic process	5.37E-10
GO Biological Process	Heterocycle metabolic process	3.11E-09
GO Biological Process	Nucleobase-containing compound metabolic process	3.49E-09
GO Biological Process	mRNA splicing, via spliceosome	3.52E-09
GO Biological Process	Macromolecule metabolic process	9.00E-09
GO Biological Process	Cellular aromatic compound metabolic process	1.09E-08
GO Biological Process	Cellular nitrogen compound metabolic process	1.09E-08
GO Biological Process	Nucleic acid metabolic process	1.14E-08
GO Biological Process	Cellular metabolic process	2.07E-08
GO Biological Process	Organic cyclic compound metabolic process	9.36E-08
GO Biological Process	Nitrogen compound metabolic process	1.14E-07
GO Biological Process	Metabolic process	4.16E-07
GO Biological Process	Organic substance metabolic process	1.20E-06
GO Biological Process	Primary metabolic process	2.84E-06
GO Biological Process	Regulation of mRNA processing	9.87E-05
GO Biological Process	Cellular component organization or biogenesis	2.60E-04
GO Biological Process	Establishment of localization in cell	2.60E-04
GO Biological Process	Ribonucleoprotein complex export from nucleus	5.40E-04
GO Biological Process	Cellular process	5.40E-04
GO Biological Process	Cellular localization	6.30E-04
GO Biological Process	Cellular macromolecule metabolic process	6.30E-04

GO Biological Process	Establishment of protein localization	6.30E-04
GO Biological Process	Intracellular transport	6.30E-04
GO Biological Process	Nucleus organization	7.00E-04
GO Biological Process	mRNA export from nucleus	7.20E-04
GO Biological Process	Protein transport	0.0016
GO Biological Process	Organelle organization	0.0017
GO Biological Process	mRNA transport	0.0018
GO Biological Process	Intracellular protein transport	0.0019
GO Biological Process	RNA localization	0.0023
GO Biological Process	Regulation of mRNA metabolic process	0.0023
GO Biological Process	Cellular component organization	0.0023
GO Biological Process	Nucleobase-containing compound transport	0.0032
GO Biological Process	RNA transport	0.0033
GO Biological Process	Vesicle-mediated transport	0.0037
GO Biological Process	Cellular protein localization	0.0037
GO Biological Process	Positive regulation of organelle organization	0.0049
GO Biological Process	Nucleocytoplasmic transport	0.0049
GO Biological Process	Protein localization	0.0052
GO Biological Process	Regulation of organelle organization	0.0056
GO Biological Process	Transcription elongation from RNA polymerase II promoter	0.0068
GO Biological Process	Vesicle organization	0.007
GO Biological Process	Regulation of RNA splicing	0.0075
GO Biological Process	Cellular protein metabolic process	0.0075
GO Biological Process	Nitrogen compound transport	0.0079
GO Biological Process	Protein-containing complex localization	0.0125
GO Biological Process	Viral life cycle	0.019
GO Biological Process	Regulation of mRNA 3-end processing	0.0237
GO Biological Process	ncRNA metabolic process	0.0266
GO Biological Process	Regulation of histone H3-K4 methylation	0.0266
GO Biological Process	Regulation of histone methylation	0.0281
GO Biological Process	Golgi vesicle transport	0.0325
GO Biological Process	Regulation of intracellular transport	0.033
GO Biological Process	Symbiotic process	0.033
GO Biological Process	Protein-containing complex subunit organization	0.0337
GO Biological Process	Multivesicular body organization	0.0365
GO Biological Process	Endosome organization	0.0384
GO Biological Process	Protein K48-linked ubiquitination	0.0411
GO Biological Process	Regulation of protein transport	0.0434
GO Biological Process	Intracellular transport of virus	0.0439
KEGG Pathways	Spliceosome	6.00E-04
KEGG Pathways	Endocytosis	0.0054
KEGG Pathways	RNA transport	0.0062

Table S 5. The GO analysis for OrbiSIMS signatures.

GO_ID	GO_DESCRIPTION	GO_LINKED_COMPOUNDS	GO_LINKED_COMPOUNDS_TOTAL	INPUT_COMPOUNDS	OVERLAP	PVALUE_HYPER_RAW	PVALUE_ADJ_FDR
GO:0046439	L-cysteine metabolic process	23	2212	15	4	1.126E-05	0.00059592
GO:0019448	L-cysteine catabolic process	23	2212	15	4	1.126E-05	0.00059592
GO:0009093	cysteine catabolic process	23	2212	15	4	1.126E-05	0.00059592
GO:0000098	sulfur amino acid catabolic process	35	2212	15	4	6.3452E-05	0.00218276
GO:0009071	serine family amino acid catabolic process	55	2212	15	4	0.00038133	0.0093697
GO:0006534	cysteine metabolic process	59	2212	15	4	0.00050071	0.01023947
GO:0070127	tRNA aminoacylation for mitochondrial protein translation	26	2212	15	3	0.00059779	0.01028206
GO:0043038	amino acid activation	69	2212	15	4	0.00091342	0.01047384
GO:0006538	glutamate catabolic process	29	2212	15	3	0.00082988	0.01047384
GO:0016485	protein processing	67	2212	15	4	0.00081643	0.01047384
GO:0043039	tRNA aminoacylation	69	2212	15	4	0.00091342	0.01047384
GO:0006418	tRNA aminoacylation for protein translation	64	2212	15	4	0.00068504	0.01047384
GO:0006497	protein lipidation	37	2212	15	3	0.00170785	0.01546057
GO:0019363	pyridine nucleotide biosynthetic process	50	2212	15	3	0.00408472	0.02509188
GO:0009435	NAD biosynthetic	50	2212	15	3	0.00408472	0.02509188

	process						
GO:0019359	nicotinamide nucleotide biosynthetic process	50	2212	15	3	0.00408472	0.02509188
GO:0019370	leukotriene biosynthetic process	49	2212	15	3	0.00385541	0.02509188

Table S 6. The GO analysis for LC-MS signatures.

GO_ID	GO_DESCRIPTION	GO_LINKED_COMPOUNDS	GO_LINKED_COMPOUNDS_TOTAL	INPUT_COMPOUNDS	OVERLAP	PVALUE_HYPER_RAW	PVALUE_ADJ_FDR
GO:0072526	pyridine-containing compound catabolic process	34	2212	28	7	9.9703E-08	7.6373E-06
GO:0072524	pyridine-containing compound metabolic process	181	2212	28	12	6.001E-07	3.8307E-05
GO:0046439	L-cysteine metabolic process	23	2212	28	5	6.4327E-06	0.00020531
GO:0019448	L-cysteine catabolic process	23	2212	28	5	6.4327E-06	0.00020531
GO:0009093	cysteine catabolic process	23	2212	28	5	6.4327E-06	0.00020531
GO:0008652	cellular amino acid biosynthetic process	234	2212	28	12	9.697E-06	0.00025306
GO:0006166	purine ribonucleoside salvage	43	2212	28	6	1.0333E-05	0.00025306
GO:0009064	glutamine family amino acid metabolic process	161	2212	28	10	1.3214E-05	0.00028116
GO:0000096	sulfur amino acid metabolic process	99	2212	28	8	1.7958E-05	0.0003439
GO:0034656	nucleobase-containing small molecule catabolic process	80	2212	28	7	3.9862E-05	0.00056545
GO:0043101	purine-containing compound salvage	55	2212	28	6	4.4283E-05	0.00060573
GO:0000098	sulfur amino acid catabolic process	35	2212	28	5	5.5875E-05	0.00069032
GO:0006534	cysteine metabolic process	59	2212	28	6	6.648E-05	0.000724
GO:0046090	deoxyadenosine metabolic process	37	2212	28	5	7.3723E-05	0.000724

GO:0046094	deoxyinosine metabolic process	37	2212	28	5	7.3723E-05	0.000724
GO:0046102	inosine metabolic process	37	2212	28	5	7.3723E-05	0.000724
GO:0046124	purine deoxyribonucleoside catabolic process	37	2212	28	5	7.3723E-05	0.000724
GO:0006148	inosine catabolic process	37	2212	28	5	7.3723E-05	0.000724
GO:0006149	deoxyinosine catabolic process	37	2212	28	5	7.3723E-05	0.000724
GO:0006157	deoxyadenosine catabolic process	37	2212	28	5	7.3723E-05	0.000724
GO:0043174	nucleoside salvage	61	2212	28	6	8.0515E-05	0.00075213
GO:0043096	purine nucleobase salvage	20	2212	28	4	8.6711E-05	0.00079073
GO:0006536	glutamate metabolic process	93	2212	28	7	0.00010638	0.00083152
GO:0042451	purine nucleoside biosynthetic process	64	2212	28	6	0.00010592	0.00083152
GO:0042455	ribonucleoside biosynthetic process	64	2212	28	6	0.00010592	0.00083152
GO:0046129	purine ribonucleoside biosynthetic process	64	2212	28	6	0.00010592	0.00083152
GO:0046130	purine ribonucleoside catabolic process	39	2212	28	5	9.5687E-05	0.00083152
GO:0043094	cellular metabolic compound salvage	95	2212	28	7	0.00012198	0.00090138
GO:0006152	purine nucleoside catabolic process	41	2212	28	5	0.00012238	0.00090138
GO:0046122	purine deoxyribonucleoside metabolic process	41	2212	28	5	0.00012238	0.00090138
GO:0032263	GMP salvage	22	2212	28	4	0.00012865	0.00092087
GO:0009164	nucleoside catabolic process	67	2212	28	6	0.00013736	0.00095652
GO:0009113	purine nucleobase biosynthetic process	43	2212	28	5	0.00015447	0.00103791
GO:0006177	GMP biosynthetic process	45	2212	28	5	0.00019265	0.00125058
GO:0046128	purine ribonucleoside metabolic process	105	2212	28	7	0.00023061	0.00147208
GO:0046110	xanthine metabolic process	26	2212	28	4	0.0002539	0.00154356

GO:0006154	adenosine catabolic process	26	2212	28	4	0.0002539	0.00154356
GO:0042454	ribonucleoside catabolic process	48	2212	28	5	0.00026299	0.00154961
GO:0046121	deoxyribonucleoside catabolic process	48	2212	28	5	0.00026299	0.00154961
GO:0046083	adenine metabolic process	27	2212	28	4	0.00029547	0.00164116
GO:0106380	purine ribonucleotide salvage	27	2212	28	4	0.00029547	0.00164116
GO:0044209	AMP salvage	27	2212	28	4	0.00029547	0.00164116
GO:0009119	ribonucleoside metabolic process	110	2212	28	7	0.00030887	0.00168997
GO:0009155	purine deoxyribonucleotide catabolic process	78	2212	28	6	0.00032127	0.00170895
GO:0006167	AMP biosynthetic process	50	2212	28	5	0.00031976	0.00170895
GO:0042278	purine nucleoside metabolic process	111	2212	28	7	0.00032684	0.0017148
GO:0034404	nucleobase-containing small molecule biosynthetic process	81	2212	28	6	0.00039546	0.0019929
GO:0009163	nucleoside biosynthetic process	81	2212	28	6	0.00039546	0.0019929
GO:0009168	purine ribonucleoside monophosphate biosynthetic process	53	2212	28	5	0.00042184	0.00207133
GO:0009071	serine family amino acid catabolic process	55	2212	28	5	0.00050248	0.00241037
GO:0016226	iron-sulfur cluster assembly	32	2212	28	4	0.00057955	0.00269839
GO:0009151	purine deoxyribonucleotide metabolic process	88	2212	28	6	0.00062125	0.0028326
GO:0046112	nucleobase biosynthetic process	59	2212	28	5	0.00069818	0.00314592
GO:1901659	glycosyl compound biosynthetic process	91	2212	28	6	0.00074437	0.00321292
GO:0009127	purine nucleoside monophosphate	60	2212	28	5	0.00075499	0.00321292

	biosynthetic process						
GO:0046059	dAMP catabolic process	60	2212	28	5	0.00075499	0.00321292
GO:0009172	purine deoxyribonucleoside monophosphate catabolic process	60	2212	28	5	0.00075499	0.00321292
GO:0009162	deoxyribonucleoside monophosphate metabolic process	93	2212	28	6	0.00083649	0.00344489
GO:0046040	IMP metabolic process	93	2212	28	6	0.00083649	0.00344489
GO:0006204	IMP catabolic process	62	2212	28	5	0.00087897	0.00358135
GO:0009394	2'-deoxyribonucleotide metabolic process	131	2212	28	7	0.000904	0.0035828
GO:0032261	purine nucleotide salvage	36	2212	28	4	0.00091675	0.0035828
GO:0009262	deoxyribonucleotide metabolic process	134	2212	28	7	0.00103601	0.00385234
GO:0019692	deoxyribose phosphate metabolic process	134	2212	28	7	0.00103601	0.00385234
GO:0046053	dAMP metabolic process	64	2212	28	5	0.00101763	0.00385234
GO:0000255	allantoin metabolic process	65	2212	28	5	0.00109279	0.00398608
GO:0006188	IMP biosynthetic process	38	2212	28	4	0.00112891	0.00407898
GO:0009170	purine deoxyribonucleoside monophosphate metabolic process	66	2212	28	5	0.00117202	0.00416796
GO:0009120	deoxyribonucleoside metabolic process	67	2212	28	5	0.00125546	0.00437129
GO:0046100	hypoxanthine metabolic process	39	2212	28	4	0.00124699	0.00437129
GO:0009264	deoxyribonucleotide catabolic process	103	2212	28	6	0.00143778	0.00483042
GO:0046386	deoxyribose phosphate catabolic process	103	2212	28	6	0.00143778	0.00483042
GO:0009128	purine nucleoside monophosphate catabolic process	69	2212	28	5	0.00143552	0.00483042
GO:0009169	purine ribonucleoside monophosphate catabolic process	69	2212	28	5	0.00143552	0.00483042

GO:0009449	gamma-aminobutyric acid biosynthetic process	72	2212	28	5	0.00174067	0.00560234
GO:0042136	neurotransmitter biosynthetic process	73	2212	28	5	0.00185231	0.00581505
GO:0009167	purine ribonucleoside monophosphate metabolic process	108	2212	28	6	0.00184179	0.00581505
GO:0009126	purine nucleoside monophosphate metabolic process	110	2212	28	6	0.00202573	0.00630775
GO:0009159	deoxyribonucleoside monophosphate catabolic process	77	2212	28	5	0.00235235	0.00701951
GO:0043605	cellular amide catabolic process	114	2212	28	6	0.00243546	0.00712048
GO:0006147	guanine catabolic process	23	2212	28	3	0.00271683	0.00776528
GO:0042453	deoxyguanosine metabolic process	23	2212	28	3	0.00271683	0.00776528
GO:0006161	deoxyguanosine catabolic process	23	2212	28	3	0.00271683	0.00776528
GO:0042219	cellular modified amino acid catabolic process	80	2212	28	5	0.00278766	0.00790869
GO:0009448	gamma-aminobutyric acid metabolic process	81	2212	28	5	0.00294504	0.00823322
GO:0043173	nucleotide salvage	51	2212	28	4	0.00341188	0.00938791
GO:0043649	dicarboxylic acid catabolic process	84	2212	28	5	0.00345612	0.00938791
GO:0009156	ribonucleoside monophosphate biosynthetic process	84	2212	28	5	0.00345612	0.00938791
GO:0009158	ribonucleoside monophosphate catabolic process	84	2212	28	5	0.00345612	0.00938791
GO:0009125	nucleoside monophosphate catabolic process	86	2212	28	5	0.0038308	0.01011859
GO:0046055	dGMP catabolic process	55	2212	28	4	0.00449668	0.0112564
GO:0046037	GMP metabolic process	90	2212	28	5	0.00466708	0.0116071
GO:0006196	AMP catabolic process	56	2212	28	4	0.00480051	0.01186191
GO:0046054	dGMP metabolic process	57	2212	28	4	0.00511796	0.01225113
GO:0006750	glutathione biosynthetic	31	2212	28	3	0.00644346	0.01451674

	process						
GO:00 46487	glyoxylate metabolic process	31	2212	28	3	0.00644346	0.01451674
GO:00 06145	purine nucleobase catabolic process	31	2212	28	3	0.00644346	0.01451674
GO:00 46038	GMP catabolic process	31	2212	28	3	0.00644346	0.01451674
GO:00 46033	AMP metabolic process	98	2212	28	5	0.00672116	0.01505383
GO:00 72525	pyridine-containing compound biosynthetic process	62	2212	28	4	0.00691926	0.01531835
GO:00 46098	guanine metabolic process	34	2212	28	3	0.00836279	0.01789357
GO:00 00097	sulfur amino acid biosynthetic process	66	2212	28	4	0.008633	0.0182677
GO:00 16485	protein processing	67	2212	28	4	0.00910141	0.01884239
GO:00 19184	nonribosomal peptide biosynthetic process	35	2212	28	3	0.00906974	0.01884239
GO:00 09065	glutamine family amino acid catabolic process	70	2212	28	4	0.0106064	0.02115755
GO:00 09226	nucleotide-sugar biosynthetic process	38	2212	28	3	0.01139735	0.02238556
GO:00 46085	adenosine metabolic process	72	2212	28	4	0.01169508	0.02273714
GO:00 46113	nucleobase catabolic process	39	2212	28	3	0.01224321	0.02356357
GO:00 46184	aldehyde biosynthetic process	41	2212	28	3	0.01404157	0.02649223
GO:00 97052	L-kynurenine metabolic process	42	2212	28	3	0.01499454	0.02815151
GO:00 19674	NAD metabolic process	79	2212	28	4	0.01606937	0.03002228
GO:00 06555	methionine metabolic process	45	2212	28	3	0.0180708	0.03343535
GO:00 46073	dTMP metabolic process	48	2212	28	3	0.02147605	0.03843611
GO:00 09225	nucleotide-sugar metabolic process	50	2212	28	3	0.02393018	0.04092556
GO:00 19363	pyridine nucleotide biosynthetic process	50	2212	28	3	0.02393018	0.04092556
GO:00 09435	NAD biosynthetic process	50	2212	28	3	0.02393018	0.04092556

GO:0019359	nicotinamide nucleotide biosynthetic process	50	2212	28	3	0.02393018	0.04092556
GO:0070189	kynurenine metabolic process	53	2212	28	3	0.02788806	0.04603934
GO:0006586	indolalkylamine metabolic process	55	2212	28	3	0.03071098	0.04861123
GO:0006103	2-oxoglutarate metabolic process	55	2212	28	3	0.03071098	0.04861123